

TEXTURE CHARACTERIZATION OF ROLLER COMPACTED CONCRETE
PAVEMENTS BY AN IN-HOUSE DEVELOPED OPTICAL SURFACE
PROFILER

A THESIS SUBMITTED TO
THE GRADUATE SCHOOL OF NATURAL AND APPLIED SCIENCES
OF
MIDDLE EAST TECHNICAL UNIVERSITY

BY

MAHDI MAHYAR

IN PARTIAL FULFILLMENT OF THE REQUIREMENTS
FOR
THE DEGREE OF DOCTOR OF PHILOSOPHY
IN
CIVIL ENGINEERING

FEBRUARY 2021

Approval of the thesis:

**TEXTURE CHARACTERIZATION OF ROLLER COMPACTED
CONCRETE PAVEMENTS BY AN IN-HOUSE DEVELOPED OPTICAL
SURFACE PROFILER**

submitted by **MAHDI MAHYAR** in partial fulfillment of the requirements for the degree of **Doctor of Philosophy in Civil Engineering Department, Middle East Technical University** by,

Prof. Dr. Halil Kalıpçılar _____
Dean, Graduate School of **Natural and Applied Sciences**

Prof. Dr. Ahmet Türer _____
Head of Department, **Civil Engineering**

Prof. Dr. İsmail Özgür Yaman _____
Supervisor, **Civil Engineering Dept., METU**

Dr. Burhan Aleessa Alam _____
Co-Supervisor, **Civil Engineering Dept., METU**

Examining Committee Members:

Prof. Dr. Murat Güler _____
Civil Engineering Dept., METU

Prof. Dr. İsmail Özgür Yaman _____
Civil Engineering Dept., METU

Prof. Dr. Mustafa Şahmaran _____
Civil Engineering Dept., Hacettepe University

Assoc. Prof. Dr. Can Baran Aktaş _____
Civil Engineering Dept., TED University

Assist. Prof. Dr. Hande Işık Öztürk _____
Civil Engineering Dept., METU

Date: 15.02.2021

I hereby declare that all information in this document has been obtained and presented in accordance with academic rules and ethical conduct. I also declare that, as required by these rules and conduct, I have fully cited and referenced all material and results that are not original to this work.

Name, Last name : Mahdi Mahyar

Signature :

ABSTRACT

TEXTURE CHARACTERIZATION OF ROLLER COMPACTED CONCRETE PAVEMENTS BY AN IN-HOUSE DEVELOPED OPTICAL SURFACE PROFILER

Mahyar, Mahdi

Doctor of Philosophy, Department of Civil Engineering

Supervisor: Prof. Dr. İsmail Özgür Yaman

Co-Supervisor: Dr. Burhan Aleessa Alam

February 2021, 173 pages

The use of concrete instead of traditional asphalt in road construction has been a challenge in the last century for road owners looking for a safe and sustainable solution. Very heavy expenditures of asphalt pavement rehabilitation during its lifetime, have made concrete the best choice for substitution. However, it is generally accepted that the initial construction costs of conventional concrete pavements are high. In concrete pavement construction, a competitive method for decreasing initial cost of construction is the application of roller compacted concrete (RCC) paving technology which carries the advantages of both methods in terms of costs; low construction costs similar to asphalt pavement and low rehabilitation costs similar to conventional concrete pavements.

RCC is a zero-slump concrete consisting of densely graded aggregates. Because of its poor workability, it is usually placed with an asphalt paver, and compacted by a vibrating roller. The most common disadvantages of RCC pavements are due to the uncertainties in the unevenness and the skid resistance which are both related to its surface texture. Hence, it is commonly recommended for heavy load carrying lots and urban streets with lower traffic speeds. However, unlike mechanical properties

of RCC pavements, which is almost well-understood in literature, there is not any adequate evidence of its surface texture characteristics.

Within the framework of this study, a high accuracy 3D laser beam scanner is developed at the METU Materials of Construction Laboratory. It has a capacity of scanning 500x500 mm samples with a 0.010 mm accuracy in depth and MATLAB is used for the surface texture analysis using the ISO 25178-2 international standard. The standard defines various roughness parameters as quantitative parameters computed from the measured 3D surface textures.

This study intended to investigate the roughness parameters of various RCC samples prepared using different compaction methods. Superpave gyratory compactor, and a double drum a double drum vibratory hand roller (DDVHR) to better simulate the field compaction procedures of RCC were the two compaction procedures utilized. Besides RCC, hot mix asphalt (HMA) specimens were also utilized. It was shown that, super-pave gyratory compactor cannot represent the vibratory rollers in terms of surface texture. Furthermore, it was observed that the generated texture of RCC and HMA surface, utilizing identical aggregate gradation, type and content, is not identical as demonstrated with 3D scanning of textures and comparing computed roughness parameters based on ISO 25178-2. It is found that HMA texture provides higher degree of contact with 4 to 7 times more contact points compared to RCC texture. Shape of the contact points for the asphalt samples are 3 times pointier than the RCC samples. As a summary, RCC suffers from producing a uniform texture and it is prone to get waviness from compaction. However, comparisons also showed that RCC can provide equal and greater macro-texture to HMA.

Additionally, potential correlations between micro-texture and skid resistance of the surfaces and the surface-scaling durability of the RCC pavement samples subjected to chemical deicers under freeze and thaw cycling was determined. Finally, two texture modification techniques were applied on the RCC pavements and their influence on macro-texture and micro-texture were also determined.

Keywords: Roller Compacted Concrete Pavement, Micro- and Macro-Texture Parameters, Skid Resistance, Optical Surface Profiler

ÖZ

KURUM İÇİ GELİŞTİRİLEN OPTİK YÜZEY PÜRÜZLÜLÜKÖLÇER İLE SİLİNDİRLE SIKIŞTIRILMIŞ BETON KAPLAMALARIN YÜZEY DOKU KARAKTERİZASYONU

Mahyar, Mahdi
Doktora, İnşaat Mühendisliği
Tez Danışmanı: Prof. Dr. İsmail Özgür Yaman
Ortak Tez Danışmanı: Dr. Burhan Aleessa Alam

Şubat 2021, 173 sayfa

Yol yapımında, geleneksel asfalt yerine beton kullanımı, güvenli ve sürdürülebilir bir çözüm arayan yol sahipleri için son yüzyılda bir zorluk olmuştur. Kullanım ömrü boyunca çok ağır asfalt kaplama rehabilitasyonu harcamaları, betonu ikame için en iyi seçenek haline getirmiştir. Ancak geleneksel beton kaplamaların genel olarak ilk yapım maliyetlerinin yüksek olduğu bilinmektedir. Beton yol yapımında, maliyet açısından her iki yöntemin avantajlarını da taşıyan silindire sıkıştırılmış beton (SSB) kaplama teknolojisinin uygulanması, ilk yapım maliyetini düşürmenin rekabetçi bir yöntemidir. Başka bir ifade ile; inşa maliyeti asfalt yollar gibi az olmasına karşın, onarım maliyeti de beton yollar gibi düşüktür.

SSB, yoğun agrega gradasyonu içeren sıfır çökme değerine sahip bir betondur. Kötü işlenebilirliği nedeniyle, genellikle bir asfalt serici ile yerleştirilir ve bir titreşimli silindire sıkıştırılır. SSB kaplamaların en yaygın dezavantajı, her ikisi de yüzey dokusuyla ilgili olan düzgünlük ve kayma direncindeki belirsizliklerden kaynaklanmaktadır. Bu nedenle, genellikle ağır yük taşıyan bölgelerde ve düşük trafik hızına sahip şehir içi caddeler için önerilmektedir. Bununla birlikte, SSB kaplamaların, literatürde hemen hemen iyi anlaşılan mekanik özelliklerinden farklı olarak, yüzey dokusu özelliklerine ilişkin yeterli kanıt yoktur.

Bu çalışma çerçevesinde ODTÜ Yapı Malzemeleri Laboratuvarında yüksek hassasiyetli bir 3D lazer ışın tarayıcı geliştirilmiştir. Geliştirilen bu tarayıcının 500x500 mm büyüklüğündeki numuneleri 0,010 mm hassasiyetle tarama kapasitesine sahiptir ve ISO 25178-2 uluslararası standardı kullanılarak yüzey dokusu analizi için MATLAB kullanılmaktadır. Standart, çeşitli pürüzlülük parametrelerini, ölçülen 3-boyutlu yüzey dokularından hesaplanan nicel parametreler olarak tanımlamaktadır.

Bu çalışma, farklı sıkıştırma yöntemleri kullanılarak hazırlanan çeşitli SSB numunelerinin pürüzlülük parametrelerini incelemeyi amaçlamıştır. Superpave yoğurmalı sıkıştırıcı ve SSB'nin sahada sıkıştırma prosedürlerini daha iyi benzetmek için çift tamburlu titreşimli el silindiri (ÇTTES), kullanılan iki sıkıştırma prosedürüdür. SSB'nin yanı sıra, sıcak karışım asfalt (HMA) numuneleri de kullanılmıştır. Süperpave yoğurmalı sıkıştırıcının yüzey dokusu açısından ÇTTES'ni temsil edemediği gösterilmiştir. Ayrıca, aynı agrega gradasyonu, türü ve içeriği kullanılarak oluşturulan SSB ve HMA yüzey dokusunun aynı olmadığı ISO 25178-2'ye dayalı hesaplanmış pürüzlülük parametrelerinin karşılaştırılmasıyla görülmüştür. Asfalt dokusunun, SSB dokusuna kıyasla 4 ila 7 kat daha fazla temas noktasıyla daha yüksek derecede temas sağladığı bulunmuştur. Asfalt numuneleri için temas noktalarının şekli, SSB numunelerine göre 3 kat daha sivridir. Özet olarak, SSB tek tip yüzey dokusu üretmekten muzdariptir ve sıkışmadan dolayı düzensizlik gösterme eğilimindedir. Bununla birlikte, RCC'nin asfalt'a eşit ve daha büyük makro doku sağlayabileceği de gözlenmiştir.

Ek olarak, yüzeylerin mikro doku ve kayma direnci arasındaki potansiyel korelasyonlar ile donma ve çözülme döngüsü altında kimyasal çözücülere tabi tutulan SSB kaplama örneklerinin yüzey pullanma dayanıklılığı belirlendi. Son olarak, SSB kaplamalara iki doku modifikasyon tekniği uygulanmış ve bunların makro doku ve mikro doku üzerindeki etkileri de belirlenmiştir.

Anahtar Kelimeler: Silindirle Sıkıştırılmış Beton Kaplama, Mikro ve Makro Doku Parametreleri, Kayma Direnci, Optik Yüzey Pürüzlülükölçer

To my wife,

Nasim

ACKNOWLEDGMENTS

I wish to express my gratitude towards my advisor, Prof. Dr. İsmail Özgür Yaman from METU for supervising my work. Thanks to his sincere care, trust and guidance, understanding, motivation and support from the beginning of my Ph. D program and during the time I worked on this thesis. I am also grateful for the great motivation and sincere support that I got from my Co-Supervisor, Dr. Burhan Aleessa Alam who played my best friend throughout this journey.

I am most grateful for the insightful recommendations of my committee members, Dr. Mustafa Şahmaran, Dr. Hande Işık Öztürk, Dr. Murat Güler and Dr. Can Baran Aktaş, who helped to improve the quality of this thesis.

I wish to thank Dr. Mustafa Tokyay and Dr. Sinan Turhan Erdoğan for their valuable comments and contributions throughout all my education at METU.

I also want to extend my appreciation to RCCP research team Dr. Emin Şengün, Dr. Reza Shabani, Mehmet Ali Aykutlu and Sadık Karakaç.

I am eternally indebted to all the members of the Materials of Construction Laboratory group, of which I am honored to be a part. Special thanks to Sahra, for her friendship and supports; Thanks to Cuma Yıldırım, Gülşah Bilici for their help working in Lab; Ozan, Kemal, Murat for being part of one of the best times of my life and Meltem for being a great friend and all the coffees she shared, thank you all from the first day of the program to the last.

And finally, I am very grateful to my wife, Nasim, for her patience, support, endurance, and her moral support encouraged me to adhere to this study, and my son, Adrian who scarified some of his playtime with his daddy.

TABLE OF CONTENTS

| | |
|---|------|
| ABSTRACT..... | v |
| ÖZ..... | vii |
| ACKNOWLEDGMENTS..... | x |
| TABLE OF CONTENTS..... | xi |
| LIST OF TABLES..... | xvi |
| LIST OF FIGURES..... | xvii |
| CHAPTERS: | |
| 1 INTRODUCTION | 1 |
| 1.1 History of road construction..... | 1 |
| 1.2 Wearing Course; Hot-Mix Asphalt vs Portland Cement Concrete | 3 |
| 1.3 PCC Pavements and Design Technologies..... | 4 |
| 1.4 RCC Pavement, The Best of the Two Worlds..... | 6 |
| 1.5 RCC Pavement Limitations | 6 |
| 1.6 Smoothness - Is It the Only Measure of Rideability?..... | 7 |
| 1.7 Objectives | 8 |
| 2 LITERATURE REVIEW | 11 |
| 2.1 Pavement Surface Characteristics | 11 |
| 2.2 Unevenness and Mega-texture | 12 |
| 2.2.1 Unevenness and Mega-Texture Measurements | 13 |
| 2.3 Macro-texture | 15 |
| 2.3.1 Macro-Texture Measurements | 15 |
| 2.3.1.1 Sand patch method..... | 16 |
| 2.3.1.2 Outflow meter | 16 |

| | | |
|---------|---|----|
| 2.3.1.3 | Circular texture meter (CT Meter) | 16 |
| 2.3.1.4 | Vehicle-mounted non-contact profiler | 17 |
| 2.4 | Micro-Texture | 17 |
| 2.4.1 | Micro-Texture Measurements | 18 |
| 2.5 | Friction..... | 18 |
| 2.6 | Factors Affecting Road-Tire Friction | 20 |
| 2.6.1 | Skid Resistance..... | 20 |
| 2.6.1.1 | British pendulum tester | 21 |
| 2.6.1.2 | Dynamic friction tester..... | 21 |
| 2.6.1.3 | Vehicle stopping distance tests | 21 |
| 2.6.1.4 | Locked-wheel skid trailer..... | 22 |
| 2.6.2 | Friction Indices..... | 22 |
| 2.6.2.1 | Relationship between indices..... | 23 |
| 2.7 | Laser Texture Scanner and Friction..... | 26 |
| 2.8 | Concrete Surface Treatment to Enhance Macro-Texture | 27 |
| 2.8.1 | Tining; Broom Finish, Burlap Drag | 27 |
| 2.8.2 | Diamond Grinding/Grooving | 29 |
| 2.8.3 | Abrading (Shot blasting) | 30 |
| 2.8.4 | Exposed Aggregate Texturing..... | 30 |
| 2.8.5 | Chip Sprinkling | 32 |
| 3 | EXPERIMENTAL PROGRAM | 33 |
| 3.1 | Development of the Non-Contact Laser Scanner | 33 |
| 3.2 | Materials and Test Specimens used in the Experiments..... | 36 |
| 3.2.1 | Material Selection and Mix Proportions | 37 |
| 3.2.2 | In-Lab Produced RCC Specimens..... | 39 |
| 3.2.3 | In-Lab Produced HMA Specimens | 42 |
| 3.3 | Experimental Test Procedures | 42 |
| 3.3.1 | Measurements of Texture Depth; Sand patch method | 43 |

| | | |
|---------|--|----|
| 3.3.2 | Skid Resistance Test; Portable Pendulum Tester..... | 43 |
| 3.3.3 | Roughness Parameters | 44 |
| 3.3.3.1 | Height parameters | 44 |
| 3.3.3.2 | Spatial parameters..... | 47 |
| 3.3.3.3 | Hybrid parameters..... | 50 |
| 3.3.3.4 | Functions and related parameters | 51 |
| 3.3.3.5 | Miscellaneous parameters..... | 56 |
| 3.3.3.6 | Feature parameters | 56 |
| 3.3.3.7 | Geometrical parameters; Fourier transform..... | 58 |
| 3.3.3.8 | Fractal Dimension..... | 59 |
| 3.3.4 | Demonstration of the results | 59 |
| 4 | PHASE I, CHARACTERIZATION OF RCC PAVEMENT SURFACE THROUGH SGC SAMPLES | 61 |
| 4.1 | Influence of the Mixture Parameters and Compaction Methods on Surface Texture | 61 |
| 4.1.1 | Maximum peak height (S_p) | 62 |
| 4.1.2 | Maximum valley depth (S_v) | 63 |
| 4.1.3 | Maximum height (S_z)..... | 65 |
| 4.1.4 | Arithmetical mean height (S_a)..... | 66 |
| 4.1.5 | Root mean square height (S_q)..... | 68 |
| 4.1.6 | Skewness (S_{sk}) | 69 |
| 4.1.7 | Kurtosis (S_{ku})..... | 71 |
| 4.1.8 | Conclusion..... | 72 |
| 5 | PHASE II, COMPARISON OF TEXTURE OF RCC AND HMA PAVEMENTS..... | 73 |
| 5.1 | Similarity Investigation of RCC And HMA Texture Through Roughness Parameters..... | 73 |
| 5.1.1 | Height Parameters | 73 |
| 5.1.2 | Spatial Parameters | 75 |

| | | |
|-------|--|-----|
| 5.1.3 | Hybrid Parameters | 76 |
| 5.1.4 | Functions and related Parameters | 77 |
| 5.1.5 | Miscellaneous Parameters | 79 |
| 5.1.6 | Feature Parameters | 80 |
| 5.2 | Investigation of Macro-Texture | 82 |
| 5.2.1 | Mean Texture Depth, Mean Profile Depth and Mean Surface Depth | 82 |
| 5.2.2 | Investigation of RCC Macro-texture based on MSD | 84 |
| 5.3 | Investigation of Micro-Texture..... | 86 |
| 5.3.1 | Skid resistance and affecting variables | 87 |
| 5.3.2 | Skid resistance and texture parameters | 90 |
| 6 | PHASE III, DURABILITY OF RCC PAVEMENT..... | 95 |
| 6.1 | Background..... | 95 |
| 6.2 | Materials and methods | 96 |
| 6.3 | Results and discussions..... | 96 |
| 7 | PHASE IV, MODIFICATION OF TEXTURE OF RCC Pavement | 109 |
| 7.1 | Methodology of the Experiments | 109 |
| 7.1.1 | Test Specimens for Exposed Aggregate Concrete Surface (EACS) | 109 |
| 7.1.2 | Test Specimens for Chip Sprinkled Concrete Surface (CSCS)..... | 111 |
| 7.1.3 | Experiments..... | 113 |
| 7.2 | Investigating Texture Properties..... | 114 |
| 7.3 | Conclusion | 117 |
| 8 | SUMMARY AND CONCLUSIONS | 119 |
| 8.1 | Findings and Conclusions..... | 119 |
| 8.2 | Suggestions for Future Studies | 122 |
| 9 | REFERENCES..... | 125 |
| 10 | APPENDICES | 135 |
| A. | Roughness Parameters of The Specimens..... | 135 |

| | |
|---|-----|
| B. Sand Patch Test Results and Estimated Mean Texture Depth Values..... | 163 |
| C. The Roughness Parameters in Correlation With BPN..... | 167 |
| CURRICULUM VITAE | 173 |

LIST OF TABLES

TABLES

| | |
|--|-----|
| Table 2-1, Commercially available road profilers..... | 17 |
| Table 2-2, factors affecting tire-road friction (the more critical factors are shown in bold)..... | 20 |
| Table 3-1, Physical properties of the aggregates..... | 37 |
| Table 3-2, In lab prepared mix proportions..... | 39 |
| Table 3-3, Measured properties of asphalt 50-70..... | 42 |
| Table 3-4, Height parameters of ISO 25178-2..... | 44 |
| Table 3-5, Spatial parameters of ISO 25178-2..... | 47 |
| Table 3-6, Hybrid parameters of ISO 25178-2..... | 50 |
| Table 3-7, Functions and related parameters of ISO 25178-2..... | 51 |
| Table 3-8, Miscellaneous parameters of ISO 25178-2..... | 56 |
| Table 3-9, Feature parameters of ISO 25178-2..... | 56 |
| Table 7-1, Mix proportions and properties of the specimens..... | 110 |
| Table 7-2, Chip sprinkling gradation, coating and spread rate..... | 112 |

LIST OF FIGURES

FIGURES

| | |
|---|----|
| Figure 2-1, Illustration of the different road surface domains and some general indicators as to which wavelengths affect which aspect of road transportation (Henry, 2000) (Andersen, 2015). | 12 |
| Figure 2-2, Reproduction of an individual present serviceability rating form..... | 14 |
| Figure 2-3, IRI roughness scale (replotted from Sayers, 1989). | 14 |
| Figure 2-4, Macro and Micro Texture (Flintsch, De León, McGhee, & Al-Qadi, 2003) | 15 |
| Figure 2-5, Friction force developed due to adhesion (on the right) and due to hysteresis (on the left) | 19 |
| Figure 2-6, Effect of Micro-texture/Macro-texture on Pavement Friction (Noyce et al., 2005)..... | 24 |
| Figure 2-7, Recommended correlations for mean texture depth by ASTM..... | 24 |
| Figure 3-1, The developed Non-contact 3D scanner | 34 |
| Figure 3-2, Close up of guide frame and samples under scan | 35 |
| Figure 3-3, Schematic demonstration of the scan logic | 35 |
| Figure 3-4, Top left; Picture of an exposed aggregate concrete surface. Top right: Virtual image of the surface generated by MATLAB. Bottom; 3D illustration of the surface. | 36 |
| Figure 3-5, Aggregates gradation (Şengün, 2019) | 38 |
| Figure 3-6 Left: The Superpave gyratory compactor, Right: schematic view of the gyratory compaction..... | 41 |
| Figure 3-7, Concrete and asphalt samples compacted with SGC | 41 |
| Figure 3-8 Two-steps compaction procedure. Left: initial step; plate compactor, Right: final step; hand roller compactor..... | 41 |
| Figure 3-9, left: BPN measurement on disk specimen, right: BPN measurement of asphalt block..... | 43 |
| Figure 3-10, Schematic illustration of Maximum peak height (S_p), Maximum pit depth (S_v), and Maximum height (S_z) | 45 |

| | |
|--|----|
| Figure 3-11, Physical definition of the parameters S_{sk} and S_{ku} which are expressed in 2d profiles as R_{sk} and R_{ku} (Bitelli, Simone, Girardi, & Lantieri, 2012). | 47 |
| Figure 3-12, a) actual Surface, b) Autocorrelation of the surface | 48 |
| Figure 3-13, Procedure to calculate S_{al} and S_{tr} , a) Autocorrelation function of the surface, b) Threshold autocorrelation at s (the black spots are above the threshold), c) Threshold boundary of the central threshold portion, d) Polar coordinates leading to the autocorrelation lengths in different directions | 49 |
| Figure 3-14, Demonstration of projected area and surface area in calculation of S_{dr} | 50 |
| Figure 3-15, Schematic view of cumulative probability function curve | 51 |
| Figure 3-16, Areal material ratio | 52 |
| Figure 3-17, Steps to draw ‘Equivalent line’ on areal material ratio curve. | 53 |
| Figure 3-18, The parameters S_{pk} and S_{vk} each are calculated as the height of the right-angle triangle which is constructed to have the same area as the “Peak cross-sectional area” or “Valley cross-sectional area”. This contributes to eliminating outlying peaks and valleys in the calculation of S_{pk} and S_{vk} . | 54 |
| Figure 3-19, Illustration of; a Peak extreme height (S_{xp}); b, Functional volume parameters | 55 |
| Figure 3-20, Illustration of “Density of peaks” | 57 |
| Figure 3-21, Components of a box-whisker plot | 59 |
| Figure 4-1, Effect of mixture parameters (binder content, water content and maximum aggregate size) on the Maximum peak height (S_p) | 62 |
| Figure 4-2, Effect of compaction (SGC and DDCHR) and binder types (cement and HMA) on the maximum peak-height parameter (S_p) | 63 |
| Figure 4-3, Effect of mixture parameters (binder content, water content and maximum aggregate size) on the Maximum valley depth (S_v) | 64 |
| Figure 4-4, Effect of compaction (SGC and DDCHR) and binder types (cement and HMA) on the Maximum valley depth (S_v) | 64 |
| Figure 4-5, Effect of mixture parameters (binder content, water content and maximum aggregate size) on the Maximum height (S_z) | 65 |
| Figure 4-6, Effect of compaction (SGC and DDCHR) and binder types (cement and HMA) on the Maximum height (S_z) | 66 |

| | |
|---|----|
| Figure 4-7, Effect of mixture parameters (binder content, water content and maximum aggregate size) on the Arithmetical mean height (S_a)..... | 67 |
| Figure 4-8, Effect of compaction (SGC and DDCHR) and binder types (cement and HMA) on the Arithmetical mean height (S_a) | 67 |
| Figure 4-9, Effect of mixture parameters (binder content, water content and maximum aggregate size) on the Root mean square height (S_q) | 68 |
| Figure 4-10, Effect of compaction (SGC and DDCHR) and binder types (cement and HMA) on the Root mean square height (S_q) | 69 |
| Figure 4-11, Schematic illustration of skewness variation (in 2D profiles skewness is denoted as R_{sk})..... | 69 |
| Figure 4-12, Effect of mixture parameters (binder content, water content and maximum aggregate size) on the Skewness (S_{sk})..... | 70 |
| Figure 4-13, Effect of compaction (SGC and DDCHR) and binder types (cement and HMA) on the Skewness (S_{sk}) | 70 |
| Figure 4-14, Schematic illustration of kurtosis variation (in 2D profiles skewness is denoted as R_{ku})..... | 71 |
| Figure 4-15, Effect of mixture parameters (binder content, water content and maximum aggregate size) on the Kurtosis (S_{ku}) | 71 |
| Figure 4-16, Effect of compaction (SGC and DDCHR) and binder types (cement and HMA) on the Kurtosis (S_{ku}) | 72 |
| Figure 5-1, Effect of binder type and content, and maximum aggregate size on the Arithmetical mean height (S_a) and the Root mean square height (S_q)..... | 74 |
| Figure 5-2, Effect of binder type and content, and maximum aggregate size on the Skewness (S_{sk}) and the kurtosis (S_{ku})..... | 75 |
| Figure 5-3, Effect of binder type and content, and maximum aggregate size on the Autocorrelation length (S_{al}) and the Texture aspect ratio (S_{tr})..... | 76 |
| Figure 5-4, A corrugated plate | 76 |
| Figure 5-5, Effect of binder type and content, and maximum aggregate size on the Root mean square gradient (S_{dq}) and the Developed interfacial area ratio (S_{dr}).... | 77 |
| Figure 5-6, Effect of binder type and content, and maximum aggregate size on the Core height (S_k), the Reduced peak height (S_{pk}) and the Reduced valley height (S_{vk}) | 78 |

| | |
|---|----|
| Figure 5-7, Effect of binder type and content, and maximum aggregate size on the Dale void volume (V_{vv}) and the Core void volume (V_{vc})..... | 79 |
| Figure 5-8, Effect of binder type and content, and maximum aggregate size on the Peak material volume (V_{mp}) and the Core material volume (V_{mc})..... | 79 |
| Figure 5-9, Effect of binder type and content, and maximum aggregate size on the Texture direction (S_{td}) | 80 |
| Figure 5-10, Effect of binder type and content, and maximum aggregate size on the Density of peaks (S_{pd}) and the Arithmetic mean peak curvature (S_{pc})..... | 81 |
| Figure 5-11, Effect of binder type and content, and maximum aggregate size on the Mean dale area (S_{da}) and the Mean heal area (S_{ha})..... | 81 |
| Figure 5-12, Effect of binder type and content, and maximum aggregate size on the Mean dale volume (S_{dv}) and the Mean hill volume (S_{hv})..... | 82 |
| Figure 5-13, Mean surface texture (uncorrected) correlation with sand patch test results, Dashed line is regression of the test, Solid line gives the estimate of PIARC model..... | 83 |
| Figure 5-14, Mean surface texture (measured at 10% of peaks' material ratio) correlation with sand patch test results, the Dashed line is regression of the test, Solid line gives the estimate of PIARC model..... | 84 |
| Figure 5-15, Comparison of estimated mean texture depth (eMTD) on various surfaces..... | 85 |
| Figure 5-16, Macro-texture difference between RCC texture and roller compacted asphalt texture..... | 86 |
| Figure 5-17, Skid resistance of gyratory compacted surfaces at wet and dry conditions | 88 |
| Figure 5-18, Skid resistance of roller compacted surfaces at wet and dry conditions | 88 |
| Figure 5-19, Average BPN of surfaces based on compaction method and binder type | 89 |
| Figure 5-20, The correlation found between BPN and fractal dimension..... | 90 |
| Figure 5-21, Evolution of Pearson's correlation factor with change in projected surface area of peaks at different depths | 91 |
| Figure 5-22, Linear regression of dry BPNs and autocorrelation length ($s=0.2$)... .. | 92 |
| Figure 5-23, Linear regression of wet BPNs and autocorrelation length ($s=0.2$) .. | 93 |

| | |
|---|-----|
| Figure 5-24, Linear regression of wet BPNs and magnitude of 2D Fourier transform | 93 |
| Figure 5-25, Linear regression of dry BPNs and magnitude of 2D Fourier transform | 93 |
| Figure 6-1, The initial and secondary rate of water absorption for 200 kg/m ³ binder content RCC | 97 |
| Figure 6-2, The initial and secondary rate of water absorption for 300 kg/m ³ binder content RCC | 98 |
| Figure 6-3, The initial and secondary rate of water absorption for 400 kg/m ³ binder content RCC | 98 |
| Figure 6-4, RCCP samples with 12 mm stone, before (two pictures on the left) and after 50 cycles of freeze-thaw (two pictures on the right) | 99 |
| Figure 6-5, RCCP samples with 19 mm stone, before (two pictures on the left) and after 50 cycles of freeze-thaw (two pictures on the right) | 100 |
| Figure 6-6, Change in Root mean square height for RCC with 12 mm max aggregate size..... | 101 |
| Figure 6-7, Change in Root mean square height for RCC with 19 mm max aggregate size..... | 102 |
| Figure 6-8, Change in texture skewness of RCCs with 12 mm max aggregate size | 103 |
| Figure 6-9, Change in texture skewness of RCCs with 19 mm max aggregate size | 103 |
| Figure 6-10, Change in texture kurtosis of RCCs with 12 mm max aggregate size | 104 |
| Figure 6-11, Change in texture kurtosis of RCCs with 19 mm max aggregate size | 104 |
| Figure 6-12, Macro-texture change under freeze-thaw cycling influence for 12 mm max aggregate size RCCs..... | 105 |
| Figure 6-13, Macro-texture change under freeze-thaw cycling influence for 19 mm max aggregate size RCCs..... | 106 |
| Figure 6-14, Change in volume of valleys after freeze-thaw cycling (Dmax = 12 mm) | 107 |

| | |
|---|-----|
| Figure 6-15, Change in volume of valleys after freeze-thaw cycling ($D_{max} = 19$ mm) | 107 |
| Figure 6-16, Overall volume loss of the RCC samples after 50 cycles of freeze-thaw | 107 |
| Figure 7-1, EACS and control specimens | 111 |
| Figure 7-2 a) Unchipped RCC surface. b) RCC surface sprinkled with 5.0-9.5 mm chips. c) RCC surface sprinkled with 9.5-12.7 mm chips. d) RCC surface sprinkled with 12.7-16 mm chips..... | 112 |
| Figure 7-3, Image simulation of surface data produced by MATLAB, a,b,c) CSCS 5~9, d,e,f) CSCS 9~12, g,h,i) CSCS 12~16 | 113 |
| Figure 7-4, Estimated mean texture depth of surface modified RCC pavement.. | 115 |
| Figure 7-5, Estimated mean texture depth of chip sprinkled RCC pavement..... | 115 |
| Figure 7-6, British pendulum numbers of exposed aggregate RCC pavement | 117 |
| Figure 7-7, British pendulum numbers of chip sprinkled RCC pavement..... | 117 |

CHAPTER 1

INTRODUCTION

1.1 History of road construction

Thousands of years before urban planning, motor vehicles, or even the wheel, the first roads appeared on the landscape. Very first roads were spontaneously formed by humans walking the same paths over and over to get water and find food. As small groups of people combined into villages, towns and cities, networks of walking paths became more formal roads. Following the introduction of the wheel about 7,000 years ago, the larger and heavier loads, that could be transported, showed the limitations of dirt paths that turned into muddy bogs when it rained. The earliest stone paved roads have been traced to about 4,000 B.C. in the Indian subcontinent and Mesopotamia.

The earliest long-distance road was a 1,500-mile route between the Persian Gulf and the Mediterranean Sea. It came into some use about 3500 B.C., but it was operated in an organized way only from about 1200 B.C. by the Assyrians, who used it to join Susa, near the Persian Gulf, to the Mediterranean ports of Smyrna (İzmir) and Ephesus. More a track than a constructed road, the route was duplicated between 550 and 486 B.C. by the great Persian kings Cyrus II and Darius I in their famous Royal Road (Briant, 2002). The Greek historian Herodotus, writing about 475 B.C., put the time for the journey from Susa to Ephesus at 93 days, although royal riders traversed the route in 20 days.

The Carthaginians are generally credited with being the first to construct and maintain a road system about 600 B.C. (Tillson, 1900). The Romans eventually decided that their neighbors across the Mediterranean were a bit of a threat to the empire destroying Carthage in 146 B.C. It is suggested that the Romans took up the

practice of a military road system from the Carthaginians. It is estimated that the Romans built about 87,000 km of roads within their empire.

Some of the earliest recorded information about the materials which were used in Roman pavements concern hydraulic cement; however, in fairness, the earliest known use of hydraulic lime was in Syria about 6,500 B.C. (over 6,000 years before the Romans) (Brown, 1975). The Romans “discovered” that grinding volcanic tuff with powdered hydraulic lime produced a hydraulic cement. The first known use of hydraulic cement by the Romans occurred at about 120 B.C. The “best” variety of volcanic tuff was found near the town of Pozzuoli (near Naples on the southwestern coast of Italy) and the material acquired the name of pozzolana. Further, the Romans learned a bit about the use of other additives such as blood, lard, and milk. Apparently, blood (hemoglobin actually) is an effective air-entraining agent and plasticizer (Jasiczak, 2006 and Akbulut, 2012).

The first recorded use of asphalt as a road building material was in Babylon around 615 BCE, in the reign of King Nabopolassa (Gillespie, 1992). Asphalt occurs naturally in both asphalt lakes and in rock asphalt (a mixture of sand, limestone, and asphalt). Many centuries later, Europeans exploring the New World discovered natural deposits of asphalt. Sir Walter Raleigh (1595) described a lake of asphalt on the Island of Trinidad, off the coast of Venezuela. Trinidad supplied about 90 percent of all asphalt worldwide from 1875 to 1900 (Baker, 1918).

Despite these early uses of asphalt, several hundred years passed before European or American builders tried it as a paving material. What they needed first was a good method of road building.

Thomas Telford (born 1757) introduced relatively flat grades pavement to roads in order to reduce the number of horses needed to haul cargos. Eventually, a Scottish engineer, John McAdam, in the early 19th century topped multi-layer roadbeds with a soil and crushed stone aggregate that was then packed down with heavy rollers to lock it all together. It proved successful enough that the term “macadamized” became a term for this type of pavement design and construction. The term “macadam” is also used to indicate “broken stone” pavement (Baker, 1918).

In 1900, Frederick J. Warren filed a patent for “Bitulithic” pavement, a mixture of bitumen and aggregate. Interestingly, portland cement concrete (PCC) was not much used as a pavement wearing course until the 1910’s (Radford, 1940). However, it was regularly used as a “stiff” base to support other wearing courses such as wooden blocks, bricks, cobble stones, etc. One likely reason for this was the lack of a consistent specification for the early cements.

According to Collins and Hart (1936), the first use of PCC as a wearing course was in Edinburgh, U.K., in 1872 and Grenoble, France, in 1876 (H. J. Collins & Hart, 1936); however, there are evidence that the first PCC pavement was placed in Inverness, Scotland. According to Blanchard's American Highway Engineers' Handbook of 1919, in 1879 in Scotland, a concrete road was made with Portland cement for binding. "The surface was very good, but when the road commenced to break, it went to pieces very fast." (Blanchard, 1919). However, many people believe that the history of portland cement concrete (PCC) pavements began in 1894 with the placement in Bellefontaine, Ohio which is still in use. A considerable amount of research and development has been done since that time in terms of concrete design, construction technology, and road test techniques as well, to make concrete an alternative material for road construction and pavement.

1.2 Wearing Course; Hot-Mix Asphalt vs Portland Cement Concrete

“Why still looking an alternative, while asphalt has been played a good role in road pavement during decades?”. Answering this question is not simple without bringing their advantages and disadvantages into a comparison.

Asphalt is more common than concrete in road pavement, it is less costly than conventional PCC pavement, and it takes less time to build a road made of asphalt (Horvath & Hendrickson, 1998). Nevertheless, PCC pavements have a longer working life (approximately 20-40 years), outlasting asphalt pavement by approximately 10 to 20 years. In addition, PCC pavements require less maintenance, while when repairs are necessary, they are typically smaller in scope than for asphalt pavements (Horvath & Hendrickson, 1998). Life cycle assessments reveal that PCC

pavements are clearly more cost-effective when results are normalized for traffic volumes (Embacher & Snyder, 2001).

Furthermore, asphalt pavements are prone to deformations in hot climate regions and under heavy traffic loads. PCC pavements, due to their stiffness, can withstand even the heaviest traffic loads without suffering the distress (e.g., rutting and shoving) common with asphalt pavements. PCC pavements continuously gain strength over time, and quite often exceed their design life expectancy as well as the design traffic loads (Tighe, Fung, & Smith, 2001). Moreover, restoration techniques can extend the life of PCC pavements up to nine times their original design life (Embacher & Snyder, 2001).

Asphalt pavement can provide a smooth and low noise driving experience as well as better traction and skid resistance (Hayden, 1982). Nonetheless, this does not mean it is ideal for every situation. Regions prone to heavy rains and cold, or icy winters, experience damaged asphalt roads from extreme weather conditions and wear and tear. Yet, PCC pavements are also not completely immune to the freeze-thaw cycles, yet they show better performance and more resistant. Furthermore, in the presence of heavy vehicles, asphalt pavements (so called flexible pavements) experience greater deflections compared to PCC pavements (which can be addressed as rigid pavements), causing 10-11% higher vehicle fuel consumption (Sumitsawan, Ardenkani, & Romanoschi, 2009). Fuel efficiency of PCC pavement reduces its carbon footprint and tends to make it greener than asphalt pavement, and at the same time because its brighter in color than asphalt pavement, it has low solar absorption during day time which contributes to its lower urban heat island effect (Kaloush, Carlson, Golden, & Phelan, 2008) and enhances its visibility at night times (Gibbons & Hankey, 2007). In all aspects, PCC pavement is accepted as a better sustainable choice (Tighe et al., 2001).

1.3 PCC Pavements and Design Technologies

Since the first strip of concrete pavement was constructed, concrete has been used extensively for paving highways and airports, as well as business and residential

streets. Different techniques have been developed to improve its application as roads wearing course. It was initially placed plain, and the use of dowels was introduced after to provide load transfer and prevent faulting. With the progress in pavement design, conventionally reinforced PCC pavements were introduced, which contained steel reinforcement in the road body and dowels in the contraction joints. Continuously reinforced PCC pavements that have no contraction joints with continuous longitudinal steel were another successful pavement construction technology. In addition to the conventional concrete pavement methods named above, several alternative paving technologies have emerged, which are challenging the traditional way of constructing concrete pavements, offering some unique design opportunities. Van Dam et al., (2011) listed those opportunities as below:

- Two-lift concrete pavement design – Two-lift pavements are constructed in two lifts, wet on wet, using two slip form pavers one immediately following the other. The concrete mixture in the bottom lift is often different from the mixture in the top lift.
- Precast concrete pavement systems – Fabricated off-site in precast plants, this type of pavement can offer many sustainability enhancements.
- Interlocking concrete pavers – Also fabricated off-site in a precast plant, pavers provide an aesthetically pleasing surface that can also be pervious, highly reflective, or even incorporating photocatalytic for use in streets and local roads.
- Thin concrete pavement (TCP) design – Based on a patented Chilean design, TCP is characterized by relatively thin slabs with short joint spacing.
- Pervious pavements – Pervious pavements allow rainwater to percolate and replenish groundwater rather than requiring rainwater to be handled by a stormwater or effluent system.
- Roller-Compacted Concrete (RCC) pavements – RCC pavement designs use stiff concrete mixtures placed and densified using equipment typical of hot-mix asphalt (HMA) construction. Traditionally used in hydraulic structures, pavement in industrial facilities, and cargo handling areas, RCC is starting to be used in streets and local roads.

1.4 RCC Pavement, The Best of the Two Worlds

Roller-compacted concrete (RCC) is a zero-slump mixture of aggregate, cementitious materials, water, and admixtures that is compacted in place by vibratory rollers or plate compaction equipment. The mixture is placed by a paver then compacted by a roller with the same commonly available equipment used for asphalt pavement construction. This construction method has the potential for savings of one-third or more of the cost of conventional (slip-form or fixed-form) concrete paving construction, therefore combines the more attractive features of concrete and asphalt paving (Pittman, 1986). Advantages of RCC pavement to the conventional portland cement pavement are its faster rate of construction, higher load bearing capacity, resistant to freeze/thaw cycles, higher durability, reduced initial costs, lower maintenance costs, and longer life cycle. In addition, RCC pavement can be constructed with minimum disruption of existing traffic.

1.5 RCC Pavement Limitations

RCC is normally placed with asphalt paving machines; most contractors who specialize in the construction of RCC pavements use high-density pavers with vibrating screeds and oscillating tamping bars. Placement of RCC with high performance paving machines contributes to highly uniform surfaces. However, the available evidence in literature limits the application of RCC pavement to low-speed traffic.

ACI 325.10R-95 reported the smoothness of RCC pavement surfaces (or lack thereof) has been one of the primary factors limiting the use of RCC to applications where relatively low-speed traffic is the primary user of the pavement, such as log sorting yards, port facilities, intermodal shipping yards, and tank parking areas (Tayabji et al., 1995). Another guide by Harrington et al., (2010) recommended low traffic speeds (less than 30 mph [48.3 km/hr]) for unsurfaced RCC pavement. Delatte, Amer, & Storey, (2003) stated that RCC has been a good replacement for asphalt under conditions where rideability and smoothness are not a necessity.

Halsted, (2009) reported that the resulting RCC pavement surface is not as smooth as conventional slip-form PCC paving, so a common use of RCC is to construct pavements in industrial areas where traffic speeds are slower and there is a requirement for a tough and durable pavement. However, the smoothness can be improved by using a maximum aggregate size no larger than 13 mm, limiting the pavement layer not exceeding 200 mm in thickness, using high-density pavers with string-line grade control and be able to achieve compaction without excessive rolling (Halsted, 2009). Canada who has the flag of RCC invention, states in its CSA A23.1 standard, that the new high-density pavers are now capable of performing the placing and compaction operations, thereby eliminating the need for rolling, as well as providing a surface suitable for high speed traffic.

1.6 Smoothness - Is It the Only Measure of Rideability?

The measurement of smoothness is usually expressed as the deviation in elevation of the pavement surface at any point along a 3 m straight-edge (Halsted, 2009). Halsted recommended surface smoothness to be checked using a straight-edge or profilometer. An early study by Pittman et al. (1986) stated that the finished surface of RCC pavement should not vary more than 3/8 in (9.5 mm) from the testing edge of a 10-ft (3 m) straight-edge, and also it should resemble that of an asphaltic-concrete pavement surface. Acceptable tolerances have generally ranged from 1/4 to 3/8 in (6.4 to 9.5 mm) deviation from a 10 or 12-ft (3 or 3.6 m) straight-edge. In another place, Harrington et al. (2010) confirmed the acceptable surface smoothness as 3/8 in (9.5 mm) maximum variance for a 10 ft (3 m) straight edge.

In 2009, Halsted reported that projects had been successfully constructed using a 5 to 6 mm straight-edge tolerance. However, operating speeds on RCC pavements typically do not exceed 55 to 65 km/h, and if high-speed operations are required, a thin (50 to 75 mm) layer of asphalt or bonded concrete can be placed over the RCC slab.

1.7 Objectives

From what has been discussed so far, it is interpreted that smoothness is not the only factor affecting rideability and safe operating speed of RCC roads. The existing gap in body of knowledge related to RCC finished surface characterization is an obstacle for understanding and improving the RCC pavement surfaces. ACI 325.10R-95 states: “Even though considerable progress has been made in RCC pavements, it is evident that more work is needed in the development of many areas. These include:

- Improved surface texture quality and smoothness of RCC pavements, particularly when high-speed traffic applications are considered.”

This study is aimed to take a closer look to the surface texture of RCC pavement and bring innovative measurement tools for categorization of RCC pavement surface texture and its quality improvement. For this purpose, a 3D profiler using a laser beam distance sensor was developed. The surfaces of RCC samples as well as HMA samples produced by different compaction types were scanned. Raw data were processed in MATLAB for generation of 3D surface and standard roughness parameters were determined. The computed parameters were analyzed to develop measurement tools for evaluating the generated textures.

The experimental program is divided into 4 phases:

- In the phase I, super-pave gyratory compactor, as an alternative compaction method for vibratory cylinder compactor in terms of representativeness of surface texture is discussed. It is aimed to evaluate a readily available compaction technique in laboratory for studying pavement texture properties.
- Phase II is divided into 2 parts. In the first part, vibratory roller compacted RCC and HMA samples are compared based on their texture parameters. This section aims to investigate application of a commonly used compaction technique on two different materials in other to characterize their generated textures. In the second part, it is tried to investigate potential correlations between roughness parameters of the textures and their macro-texture and micro-texture test results. The goal of this section is to estimate results of two

well-known pavement tests, namely Sand Patch test and British Pendulum test, based on 3d scanning of a surface.

- Phase III has a focus on the extent of surface scaling of RCC pavement under freeze-thaw cycling subjected to chemical deicers. It is intended to introduce a novel technique for determination of extent of damage.
- Phase IV discusses two surface treatment methods to be applied on RCC pavement to enhance its texture. The RCC samples are treated with exposed aggregate concrete surface and chip sprinkled concrete surface methods and the micro-texture and micro-textures values are determined.

This study contains seven chapters, including this one. In the second chapter, a literature review was briefly demonstrated, explaining road texture characterization, texture evaluation methods and how friction gains importance on road surface. In the third chapter, materials, testing tools and techniques are explained. The fourth chapter presents initial findings of the study, such as effect of compaction technique and pavement materials on the achieved surface texture, as well as investigation of correlation between computed parameters with texture physical properties. In chapter five, durability of RCC pavement to frost damage is discussed. Two pavement surface modification methods and their influence on texture properties are discussed in chapter six and eventually, chapter seven is dedicated to summarize findings of the study.

CHAPTER 2

LITERATURE REVIEW

This research is aimed to study RCC pavement surface from multiple perspectives and develop a methodology for characterizing the surface textures to address serviceability of the pavement. For this purpose, it is necessary to develop an understanding of the affecting factors initially by presenting the evidence available in literature. Therefore, this chapter provides background information about the related topics listed below:

- Friction basics
- Parameters of road/tire interaction
- Characterization of pavements texture
- Available texture measurement methods
- Concrete pavement texturing techniques
- Surface performance of RCC pavement

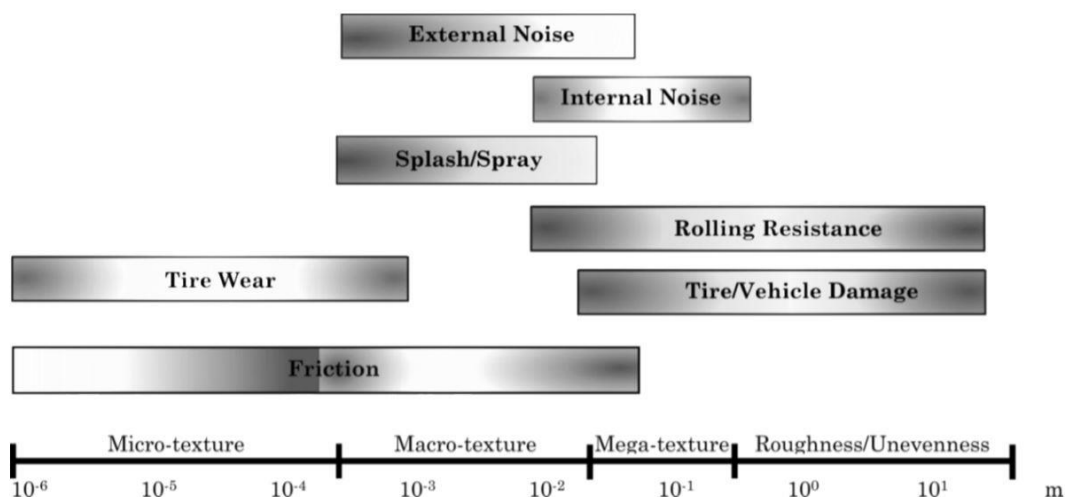
2.1 Pavement Surface Characteristics

According to the United States. Federal Highway Administration (UHWA), smoothness is a measure of the level of comfort experienced by the traveling public while riding over a pavement surface. As an important indicator of pavement performance, smoothness is used interchangeably with roughness as an expression of the deviation of a surface from a true planar surface (as defined by ASTM E867). Pavement roughness is generally defined as an expression of irregularities in the pavement surface that adversely not only affect the ride quality of a vehicle but also the safety of roads, the fuel consumption, the vehicle maintenance costs, and noise pollution.

The first reference categorizing surface irregularities relating to their wavelengths is a technical report by Permanent International Association of Road Congresses (PIARC) in 1978 (Juli, 1989). According to PIARC, the road surface roughness length scales are categorized as:

- Unevenness, with spatial wavelengths in the range of 0.5 m to 50 m
- Mega-texture, with spatial wavelengths in the range of 50 mm to 0.5 m
- Macro-texture, with spatial wavelengths in the range of 0.5 mm to 50 mm.
- Micro-texture' with spatial wavelengths in the range of 0 mm to 0.5 mm.

PIARC also suggested that the various discrete scales of texture influence various performance criteria such as noise, skid resistance, rolling resistance, etc., Figure 2-1.



Note: Darker shading is an indicator of a more favorable effect of texture

Figure 2-1, Illustration of the different road surface domains and some general indicators as to which wavelengths affect which aspect of road transportation (Henry, 2000) (Andersen, 2015).

2.2 Unevenness and Mega-texture

The unevenness of the road surface, with wavelengths from 0.5 m to 50 m, is associated with longitudinal profiles larger than the tire footprint. It affects vehicle

dynamics, ride quality, dynamic loads, and drainage. In extreme cases, unevenness can lead to loss of contact with the surface, and it is normally caused either by poor initial construction or deformation caused by loading.

The road's mega-texture refers to deviations with wavelengths from 50 mm to 500 mm. Examples of mega-texture include ruts, potholes, and major joints and cracks. It affects vibration in the tire walls but not the vehicle suspension, and it is therefore strongly associated with noise and rolling resistance. Although mega-texture generally has larger dimensions than those which affect skid resistance, it is possible that this scale of texture could influence tire/road contact.

2.2.1 Unevenness and Mega-Texture Measurements

Unevenness and mega-texture are mainly responsible for the ride quality. Ride quality of pavement is generally the primary parameter in the “serviceability-performance” concept developed at the AASHO Road Test in 1957. The serviceability of a pavement is expressed in terms of the present serviceability rating, or PSR. The PSR is a reflection of the feeling the average citizen gets as he or she travels down the roadway and rates their ride using the quantitative scale shown in Figure 2-2. PSR can be defined as a qualitative measure.

The second measure of ride quality is international roughness index, or IRI which was developed by the World Bank in the 1980s. IRI is used to define a characteristic of the longitudinal profile of a traveled wheel-track, and it constitutes a standardized roughness measurement. As a result, the IRI is always greater than zero. The higher the IRI, the rougher the roadway is, Figure 2-3. IRI and PSR can be derived from each other by means of imperial correlations (Eq. 2-1;2-2) (Janisch, 2006).

$$\text{Bituminous Pavements: PSR} = 5.697 - (2.104 \text{ IRI}^{1/2}) \quad \text{Eq. 2-1}$$

$$\text{Concrete Pavements: PSR} = 6.634 - (2.813 \text{ IRI}^{1/2}) \quad \text{Eq. 2-2}$$

| | | | |
|------------------------------|--------------------------|--------------|---------------|
| Acceptable? | | 5 | Very Good |
| Yes | <input type="checkbox"/> | 4 | Good |
| No | <input type="checkbox"/> | 3 | Fair |
| Undecided | <input type="checkbox"/> | 2 | Poor |
| | | 1 | Very Poor |
| | | 0 | |
| Section Identification _____ | | Rating _____ | |
| Rater _____ | Date _____ | Time _____ | Vehicle _____ |

Figure 2-2, Reproduction of an individual present serviceability rating form.

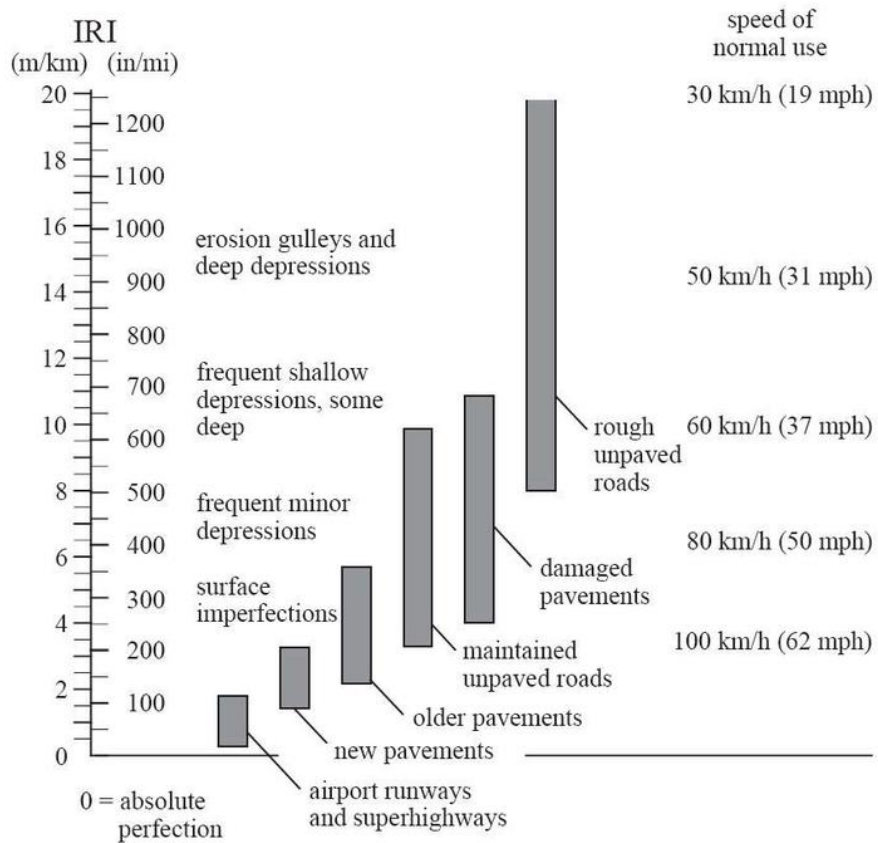


Figure 2-3, IRI roughness scale (replotted from Sayers, 1989).

2.3 Macro-texture

Macro-texture is the amplitude of deviations with wavelengths from 0.5 mm to 50 mm, and it is affected by the size, shape, spacing, and arrangement of coarse aggregate particles, Figure 2-4. Macro-texture affects mainly tire noise and water drainage from the tire footprint. This scale of texture is thought to be important for hysteretic friction, especially at high speed.

Pavement macro-texture provides the hysteresis component of the friction and allows for the rapid drainage of water from the pavement. Enhanced drainage improves the contact between the tire and the pavement surface and helps reduce the probability of hydroplaning.

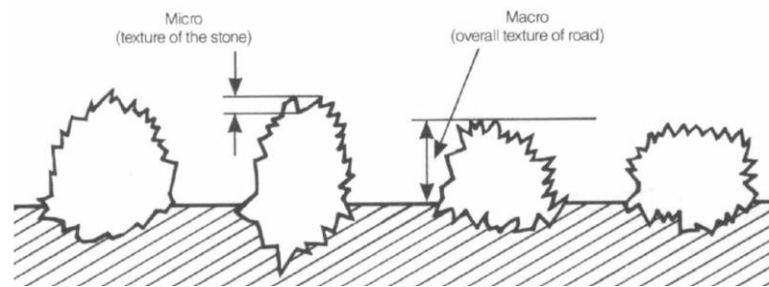


Figure 2-4, Macro and Micro Texture (Flintsch, De León, McGhee, & Al-Qadi, 2003)

2.3.1 Macro-Texture Measurements

The macro-texture of a pavement surface of HMA results from the large aggregate particles in the mixture. For concrete pavement, since the produced surface is highly smooth, macro-texture is obtained by tining which will be discussed later in this chapter. Macro-texture can be measured in two different classes:

- Static measurements:
 - Sand patch method
 - Circular texture meter (CT Meter)
 - Outflow meter
- Dynamic measurements:
 - Vehicle-mounted non-contact profiler

2.3.1.1 Sand patch method

The sand patch method (ASTM E965 or ISO 10844) is the most common volumetric method for macro-texture measurements. It is conducted by spreading a known volume of spherical sand particles on a pavement surface to form a circle and measuring the diameter of the spread to calculate the volumetric mean texture depth (MTD) of the pavement macro-texture.

2.3.1.2 Outflow meter

The outflow meter (ASTM E2380) is an indirect method for estimating volumetric MTD of macro-texture from the connectivity of texture. This method measures the escape time of certain volume of water flowing from bottom of a cylinder sticking to pavement surface. The technique is intended to provide a measure of the ability of the pavement to relieve pressure from the face of vehicular tires and thus an indication of hydroplaning potential under wet conditions.

2.3.1.3 Circular texture meter (CT Meter)

The Circular texture meter (ASTM E2157) rotates a displacement laser sensor on circumference of a circle with 142 mm radius and measures the vertical macro-texture depth of a surface in 8 segments. The collected data are processed as mean profile depth (MPD) and/or the root mean square (RMS) for each segment. ASTM E2157 referencing to PIARC, reports an extremely high correlation between MPD (CT Meter) and MTD (volumetric methods). The recommended relationship for the estimation of the MTD from the MPD is:

$$\text{MTD} = 0.947 \text{ MPD} + 0.069 \quad \text{Eq. 2-3}$$

Where MTD and MPD are expressed in millimeters.

2.3.1.4 Vehicle-mounted non-contact profiler

These methods typically use displacement laser measurement devices to measure macro-textures or even mega-textures without disrupting traffic flow. An example of a non-contact profiler for use in characterizing pavement surface texture is the Road Surface Analyzer (ROSAN_v), developed by the FHWA (Hall et al., 2009). A standard method for determining the mean profile depth (MPD) of a pavement profiler is provided in ASTM E-1845. Table 2-1 gives some of the commercially available profilers.

Table 2-1, Commercially available road profilers

| Profiler | Country of origin |
|-------------------------------------|--------------------------|
| ROSAN _v | U.S. |
| Dynatest Road Surface Profiler | Denmark |
| Greenwood Engineering | Denmark |
| ARAN Automatic Road Analyzer | Canada |
| WDM Multifunction Road Monitor | U.K. |
| Mandli Road Surface Profiler | U.S. |
| ARRB Australian Road Research Board | Australia |
| SSI High Speed Profiling Systems | U.S. |

2.4 Micro-Texture

Micro-texture is the amplitude of deviations with wavelengths less than or equal to 0.5 mm. This scale of texture is measured on the micron scale, and it is typically found on the surfaces of coarse aggregate particles (Figure 2-4) or the texture of the binder mortar and fine material. Micro-texture is frequently seen on aggregate surface; therefore, it is a function of aggregate particle mineralogy and petrology, and it is affected by climate/weather effects and traffic action. The micro-texture of the road surface is thought to affect skid resistance at all speeds for dry and wet

conditions. Micro-texture provides direct tire-pavement contact and contributes to the adhesion component of friction.

2.4.1 Micro-Texture Measurements

Micro-texture represents a surface-roughness quality on the microscopic scale, which is the result of the roughness of individual aggregate items used in road surface material, and therefore, it is tightly connected to the mineralogical composition of an aggregate (Dondi, Simone, Lantieri, & Vignali, 2010). Currently, there is no direct way to measure micro-texture in the field. Even in the laboratory, it has only been done with very special equipment (Hall et al., 2009). There are available researches recommending 3D scans, digital image processing, and mathematical models to define micro-texture measurements, but no standard method has been established yet (Scharnigg & Schwalbe, 2010).

Micro-texture generally explained to have the greatest share on providing frictional force between pavement surface and tire, therefore, micro-texture is often measured indirectly based on friction or so called “skid resistance”.

2.5 Friction

Friction is basically defined as the resisting force develops from the relative motion of material elements sliding against each other. In the context of pavement surface, friction represents the grip developed by a tire and road surface at a particular time, so called tire-pavement friction. It is the initial requirement to make driving possible. For that, a sufficient tire-pavement friction must develop to permit complete control while accelerating, cornering and decelerating. It is mainly based on two components: adhesion and hysteresis. The adhesion coefficient (F_A) is a function of the shear forces developed at the tire-pavement interface, whereas the hysteresis coefficient (F_H) is a function of the energy losses within the rubber as it is deformed by the textured pavement surface, Figure 2-4. The friction coefficient is the summation of the former two coefficients (Bazlamit & Reza, 2005) (Hall et al., 2009)

(Mataei, Zakeri, Zahedi, & Nejad, 2016). A high adhesion coefficient exists when shear strength and the actual contact area are high, but when the pavement is wet, a trapped water film weakens the interface shear strength and lowers the amount of adhesion. Hysteresis works by compressing the tire against the pavement surface, which creates a deformation energy to be stored within the rubber, and as the tire relaxes, part of the energy is lost in the form of heat.

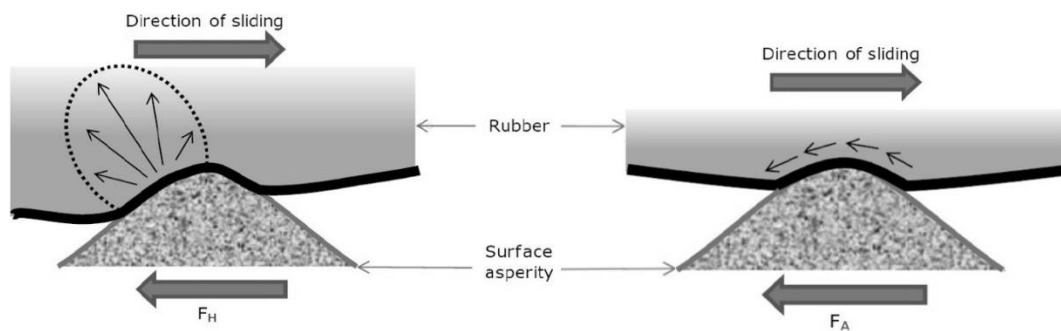


Figure 2-5, Friction force developed due to adhesion (on the right) and due to hysteresis (on the left)

Due to the development of adhesion force at the pavement–tire interface, adhesion is most responsive to the micro-level asperities (micro-texture) of the aggregate particles contained in the pavement surface. In contrast, the hysteresis force developed within the tire is most responsive to the macro-level asperities (macro-texture) formed in the surface via mix design and/or construction techniques. As a result of this phenomenon, adhesion governs the overall friction on smooth-textured and dry pavements at lower speeds, while hysteresis is the dominant component on wet and rough-textured pavements at higher speeds (Roberts, 1988; Hall et al., 2009).

Investigating rubber friction theory, in addition to adhesion and hysteresis components, a third component exists which is defined as cohesion losses due to the wearing of rubber as it slides over the pavement surface. However, it is not insignificant when compared to the adhesion and hysteresis force components. (Kummer, 1966).

2.6 Factors Affecting Road-Tire Friction

Kummer (1966) and Sandberg (1998) reported that the factors influencing road surface friction are divided into three main categories;

- Pavement surface texture and physical properties
- Contaminants exist on pavement surface
- Tire properties (tread pattern, rubber type, inflation pressure, sliding velocity)

Åström & Wallman, (2001) modified these affecting factors into four categories, which are shown in Table 2-2. Among these factors, the ones considered to be within a highway agency's control are micro-texture, macro-texture, pavement materials properties, and slip speed.

Table 2-2, factors affecting tire-road friction (the more critical factors are shown in bold)

| Pavement Surface Characteristics | Vehicle Operating Parameters | Tire Properties | Environment |
|--|---|---|--|
| Micro-texture Macro-texture Mega-texture/ unevenness Material properties Temperature | Slipping speed: Vehicle speed Braking action Driving maneuver: Turning Overtaking | Footprint Tread design and condition Rubber composition and hardness Inflation pressure Load Temperature | Climate: Wind Temperature Water (rainfall, condensation) Snow and Ice Contaminants: Anti-skid material (salt, sand) Dirt, mud, debris |

2.6.1 Skid Resistance

Skid resistance is the force developed when a tire, that is prevented from rotating, slides on a pavement surface (Highway Research Board, 1972). Skid resistance can be measured by different methods; some common test methods are:

- Energy loss of a pendulum; British pendulum tester (BPT)

- Deceleration of a rotating wheel; dynamic friction tester (DF tester)
- Stopping distance measurement
- Drag of a locked wheel trailer; locked-wheel skid trailer test

2.6.1.1 British pendulum tester

The British pendulum tester (ASTM E303 or AASHTO T278) is a dynamic pendulum impact-type tester used to measure the energy loss when a rubber slider edge is propelled over a test surface. The device measures low speed friction (about 10 km/h). value produced from this device is known as British pendulum number (BPN). UK department for international development suggested 55 as the minimum skid resistance value for motorways, trunk and class1 roads with heavily trafficked roads in urban areas (carrying more than 2000 vehicles per day), and 45 for all other sites (Jones, C.R.; Rolt, J.; Smith, H.R.; Parkman, 1999).

2.6.1.2 Dynamic friction tester

The dynamic friction tester (ASTM E1911) uses a spinning disk with a plane parallel to the test surface. Three rubber sliders are mounted on the lower surface of the disk. The disk is brought to the desired rotational velocity, then Water is introduced in front of the sliders and the disk is lowered to contact the test surface. The torque is monitored continuously as the disk rotational velocity reduces due to the friction between the sliders and the test surface. The reduction on torque is then converted to a measurement of friction. The friction at 20, 40, 60, and 80 km/h is recorded, and the friction-speed relationship can be then plotted.

2.6.1.3 Vehicle stopping distance tests

Stopping distance is a measure of the distance required to bring a vehicle to a stop from a specified speed. In the test (ASTM E445), a driver attains the desired speed, locks the brakes, and slides to a stop. The friction coefficient or skid number is the

square of the vehicle speed divided by the sliding distance multiplied by a constant. Alternatively, different speeds and a fully engaged antilock braking system (ABS) have been used. ASTM E2101 uses a similar procedure to measure deceleration rates at lower speeds (32 to 48 km/h) in winter contaminated conditions.

2.6.1.4 Locked-wheel skid trailer

This test (ASTM E274) consists of a trailer, with wheels equipped with standard pavement test tires, that is towed by a vehicle. The trailer is brought to the desired test speed, then water is delivered ahead of the test tires and the braking system is actuated to lock the tires. The skid resistance of the paved surface is determined from the force required to slide the locked test tires at a stated speed, and the results are reported as “Friction number or Skid number”. Testing can be done using a smooth (ASTM E 524) or ribbed tire (ASTM E 501). The ribbed tire is insensitive to the pavement surface water film thickness; thus, it is insensitive to the pavement macro-texture. The smooth tire, on the other hand, is sensitive to macro-texture (Hall et al., 2009).

2.6.2 Friction Indices

Friction indices have been changed over time. Skid number (SN) was first used by ASTM for the coefficient of friction in 1965 (ASTM E 274). It measured friction in a range of 0 to 100, where 100 represents complete friction, and 0 no friction. Friction number (FN), on the other hand, was adopted by AASHTO in later years (AASHTO E 274). FN values were designated by test speed and tire type. For instance, FN50R = 41 is an indication of friction number of 41 at 50 mph with ribbed tire (R). Eventually, in 1992, International Friction Index (IFI) was developed by PIARC in order to have the terminology of friction harmonized (ASTM E1960). IFI is composed of two components, $F(60)$ and S_P . S_P (IFI speed number) is derived from macro-texture measurement (MPD or MTD), and $F(60)$ is the friction value at a known speed adjusted to the friction measured at 60 km/h. IFI is reported in the

format of IFI ($F(60)$, S_p). Two years later, Rado (1994) modified IFI for ABS and developed Rado IFI model.

As an indirect measurement for the micro-texture scale of pavement, the primary index was introduced by British Pendulum Tester (BPT) which measures low-speed friction number (ASTM E303). Dynamic friction tester (DFT) is a newer method that evaluates friction as a function of slip speed (ASTM E1911). Despite the fact that DFT results have shown better reproducibility in comparison with BPT (Henry, 2000), due to portability and ease of use, BPT is still used worldwide as a measure of friction (Hall et al., 2009).

2.6.2.1 Relationship between indices

Numerous studies have been conducted to develop relations between data obtained from texture measurements and their frictional properties. An early study by Hogervorst, (1974) showed variation of skid resistance on different travel speeds, depends on both micro-texture and macro-texture. The magnitude of skid resistance is a factor of micro-texture, whilst macro-texture influences the slope of skid resistance as travel speed changes. In addition, macro-texture is the dominant affecting factor on skid resistance change at high speeds by its influence on surface water drainage. It is reported that at low speeds, micro-texture dominates and defines the level of friction, and macro-texture has only a little effect on friction levels. (Hall et al., 2009; Roe, Parry, & Viner, 1998; Rose, Gallaway, & Hankins, 1970). Figure 2-6 demonstrates a schematic plot of friction coefficient change by sliding velocity for a different combination of macro and micro textures.

For macro-texture measurement, it is widely accepted that the obtained results from volumetric measured methods (MTD) are in good correlation with non-contact profiler-derived measurements (MPD). ASTM E1845 describes MPD as a useful measure in predicting the speed gradient of wet pavement friction. Figure 2-7 illustrates the correlations for the calculation of Estimated Mean Texture Depth (EMTD).

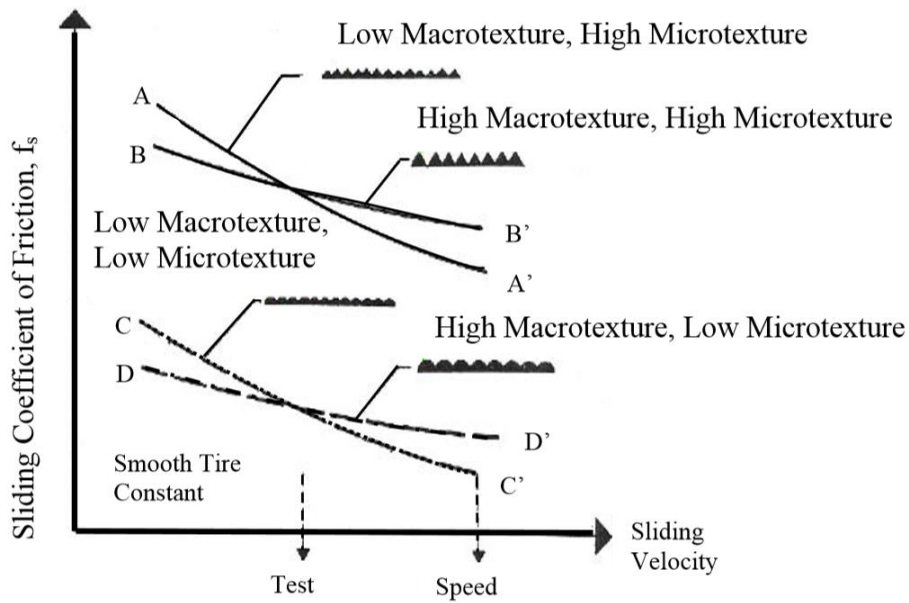


Figure 2-6, Effect of Micro-texture/Macro-texture on Pavement Friction (Noyce et al., 2005)

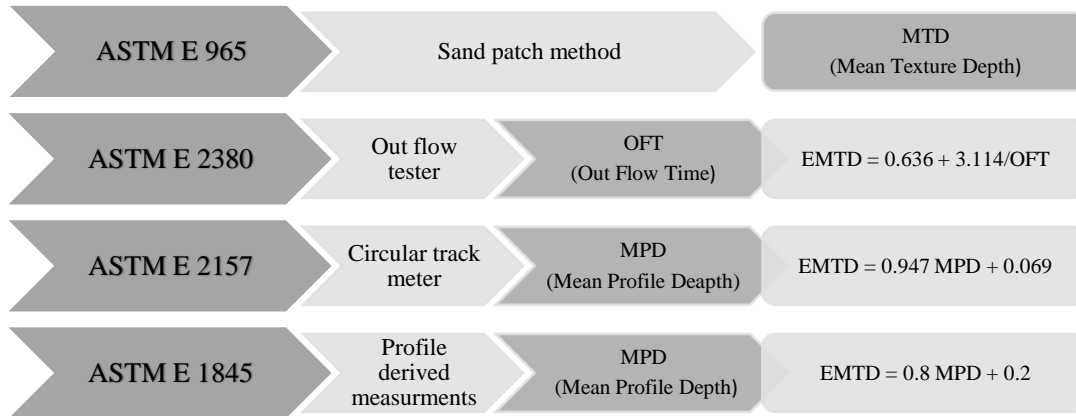


Figure 2-7, Recommended correlations for mean texture depth by ASTM

However, McGhee & Flintsch (2003) studied the correlation between EMTD measured from sand patch method and MPD by non-contact laser and reported a relationship (Eq. 2-4) different than the one given in ASTM E1845.

$$\text{EMTD} = 0.7796 \text{ MPD} - 0.379, \quad (R^2 = 0.884) \quad \text{Eq. 2-4}$$

Digging out the literature to find out studies correlating friction to texture reveals a fluctuation in this subject. In 1982, a study conducted by Yager & Bühlmann showed no correlation exists between macro-texture and BPN. One year after, in 1983, Henry & Saito presented a large number of regression models, with a good coefficient of correlation (r) values, for the prediction of SN, MTD, and BPN. A method provided by the international friction index (IFI) gave a set of correlations (Eq. 2-5; 2-6) for the estimation of friction number at 40 mph using BNP and MTD (Wambold, Henry, & Blackburn, 1984).

$$\text{BPN} = 20 + 0.405 \text{ FN40R} + 0.039 \text{ FN40S} \quad \text{Eq. 2-5}$$

$$\text{MTD} = 0.039 - 0.0029 \text{ FN40R} + 0.0035 \text{ FN40S} \quad \text{Eq. 2-6}$$

A few years later, Forster (1989) attempted to re-correlate the BPN or SN40 with texture shape factor but ended with the detection of problems in both texture and skid data. Years passed until Corley-Lay found in 1998 that the variation in BPN from section to section resembles the variation in SN. Eventually, in 2004, Olek et al. found a linear relationship between the BPN and macro-texture on PCC surfaces. Furthermore, in the same year, Wambold et al. presented a good correlation (Eq. 2-7) of BPN and IFI in the international PIARC experiment.

$$F(60) = 0.0079 \text{ BPN} + 0.0775 \quad \text{Eq. 2-7}$$

ASTM E 1960 defines the requirements to obtain MPD from a surface profile and gives a correlation (Eq. 2-8) for estimating the speed constant (S_p) in km/h from MPD, in order to calculate the IFI of pavement surface.

$$S_p = 14.2 + 89.7 \text{ MPD} \quad \text{Eq. 2-8}$$

Boscaino et al., (2004) compared mixes with different aggregate sizes and showed that mixes with a nominal aggregate size of 10 mm have greater BPN's compared to the mixes with 15 mm nominal aggregate size. The BPN values were between 60 to 72 and 58 to 68, respectively. The authors reported that after a specific level a higher

texture does not necessarily mean a greater friction. In another complex model developed by Ergun et al. in 2005, however, the authors themselves doubted its reliability.

In 2001, Davis established relationship between laser measured MPD and mixture parameters. She found linear correlation between MPD, maximum nominal aggregate size (NMS), and voids in mineral aggregates (VMA) with an r-squared of 0.965 (Eq. 2-9).

$$\text{MPD} = -2896 + 0.2993 (\text{NMS}) + 0.0698 (\text{VMA}) \quad \text{Eq. 2-9}$$

2.7 Laser Texture Scanner and Friction

Over the past few years, by the introduction of displacement laser sensors, high accuracy non-contact measurements of texture have become possible. Thanks to the high-speed reading rate of the sensors, measurements of pavement texture can be done without disturbing traffic or conducting road closures. Saving costs, time, and effort, obtaining frictional characteristics of pavements applying non-contact methods have always been a subject of interest. A study by Do et al. (2007) reported the feasibility of relating laser measured texture to BPN with a correlation factor of 0.84. It also recommended the use of a very small dot size laser for micro-texture measurements. Moreover, Virginia Tech conducted a study on the mix design of pavements and found that MPD and mixture parameters are in relation with frictional parameters. A laser texture device and a locked wheel friction device were used in this study (Meegoda, 2009). In contrast, a study by Viner et al. (2006) reported that a correlation between skidding and texture measurements could not be developed. In 2010, Li et al. correlated laser scanned measures to the friction numbers acquired from locked wheel trailers in both wet and dry conditions. The authors reported a high coefficient of determination of 1 for the model. However, doubted its reliability due to the limited number of test specimens. In 2001, a mathematical model was developed by Persson based on his own “theory of friction” to predict skid resistance. A study conducted by Ueckermann et al. (2015) confirmed that a close relation

between predicted friction coefficient and measured data can be found applying Persson model. They put emphasis on using high resolution texture measurements and reported that the reason behind unsuccessful approaches is either the lack of enough resolution or excluding rubber properties. Another approach was signal processing on generated 3D profiles from texture. Using Fourier analysis, 3D profiles can be mathematically represented as a series of sinusoidal components of various spatial frequencies or texture wavelengths (Zuniga-Garcia & Prozzi, 2016). Serigos et al., (2014) extracted several spatial and spectral parameters from laser scanned profiles in order to correlate with BPN. The authors reported that the intercept of the linearized surface roughness power spectrum (PSD) is in good correlation with BPN, while the slope does not. A strong correlation ($R^2=0.8$) between friction coefficient and top 20% portion of 3D profile is reported by Kanafi & Tuononen (2017) using PSD.

2.8 Concrete Surface Treatment to Enhance Macro-Texture

Unlike HMA, non-texturized conventional PCC pavement surface is fairly smooth and does not have the desired texture for providing adequate friction for safe driving. Although adequate micro-texture generally exists on dry pavements, due to the lack of macro-texture, the presence of water reduces the direct contact between the pavement surface and the tire. If this film of water becomes sufficiently thick or if vehicle speeds are sufficiently high, the tires can lose contact with the pavement surface, resulting in a dangerous phenomenon known as hydroplaning (Dahir & Gramling, 1990). To enhance macro-texture of PCC pavements and provide adequate drainage to overcome hydroplaning, artificial texturing of a finished surface is usually generated.

2.8.1 Tining; Broom Finish, Burlap Drag

Early methods for surface texturing of new PCC pavements primarily consisted of shallow texture techniques such as broom finishing or burlap dragging. In 1963, 60% of the United States highway departments used burlap drag, and 12% specified either

a burlap drag or a broom finish (Colley, Christensen, Nowlen, & Cement, 1969). By 1969, 46 states out of 50 states of the United States were using a burlap drag as their primary texturing technique on new PCC pavements (Wu & Nagi, 1995). However, research results from this time period indicated that although these shallow texture techniques resulted in a very quiet riding surface, they did not provide adequate skid resistance at high speeds. During the early 1970s, several studies demonstrated that improved surface friction characteristics could be provided by the practice of transverse tining (Ray & Norling, 1974; Thornton, 1974; Rugenstein, 1977; Mahone, 1977). Texturing guidelines published by the American Concrete Paving Association in 1975 and by AASHTO in 1976 reflected these research results as they recognized the friction characteristic improvements of transverse tining or grooving over the traditional practices of burlap dragging or brooming (ACPA, 1975)(AASHTO, 1976). By the end of the 1970s, more than 33 states of the United States changed their instructions to use transverse tining as their texturing technique on fresh PCC (Rugenstein, 1977). In 1999 the Minnesota Department of Transportation returned to the use of a longitudinal artificial turf drag texture as the sole texturing technique on all new PCC pavements, reporting that collected friction and noise data indicate that the artificial turf drag texture with an MTD of 1.0 mm provides surface friction and noise qualities equivalent to the one provided by asphalt pavements (ACPA, 2000). However, even though longitudinal grooving is quieter than transverse tining, transverse tining is currently the most commonly used surface texture method on new higher-speed PCC pavements. Transverse tining improves a pavement's friction characteristics since the transverse grooves are very effective at quickly removing surface water from the driving lanes onto the shoulders.

Although it is not as popular as transverse tining, longitudinal dragging has been used in a fair portion of pavement construction. A study in Spain has shown that longitudinal burlap drag followed by a plastic brush can be effective at providing high-friction characteristics while minimizing tire-pavement noise (Hibbs & Larson, 1996).

Federal Highway Administration (FHWA) of the United States Department of Transportations (1996) states that both transverse and longitudinal tining textures are acceptable for noise and safety requirements. This requires the mix to contain at least 25 percent siliceous sand and high-quality coarse aggregate. The texturing recommendations are uniform spacing of 20 mm for longitudinal tining. The transverse tines should be variably spaced between 10 and 40 mm (with no more than 50 percent of the spacing exceeding 25 mm), 3 mm wide, and 3 to 6 mm deep (resulting in an average texture depth of 0.8 mm with no individual test less than 0.5 mm as measured by the sand patch test). Both FHWA and AASHTO currently recommend that safety should not be compromised to obtain a slight, usually short-term, initial reduction in noise levels. Properly constructed PCC pavement, with a transversely tined or longitudinally tined surface, matches the performance of dense-graded asphalt considering both safety and noise factors.

2.8.2 Diamond Grinding/Grooving

A few years after the introduction of concrete paved roads, a diamond grinder was designed to shave high spots on the surface. For instance, in 1965, it was used on an existing highway in Los Angeles, California to restore its surface (Roemmele, 1986). Although diamond grinding was designed to remove surface irregularities, it was found to be effective at improving surface friction and decreasing tire-pavement noise. Mosher (1985) showed that diamond grinding positively affects a pavement's frictional characteristics by restoring surface micro-texture and providing some macro-texture. However, a ground surface suffers from inadequate macro-texture and respectively hydroplaning. Later, diamond grinding was replaced by diamond grooving in order to cut grooves in hardened PCC surface using diamond saw blades. The objective was to provide deep channels in the surface that could provide an escape route for surface water, thereby reducing hydroplaning and wet-weather crashes (ACPA, 2000).

2.8.3 Abrading (Shot blasting)

As a different texturizing technique, abrading or shot blasting is similar to sandblasting, which shoots small abrasive media at the pavement surface in order to remove a thin layer of mortar and aggregate. This process leaves exposed sand-sized particles that provide good micro-texture with beneficial friction characteristics (Hoerner, Smith, Larson, & Swanlund, 2003).

2.8.4 Exposed Aggregate Texturing

Exposed aggregate concrete surface (EACS) is the process of removing the surface mortar of concrete in order to expose hard and polish resistant aggregates (FHWA, 2001). EACS could be regarded as a European texturing technique since it has not been widely used in North America. A great deal of research and trials of EACS have been undertaken in Austria. EACS is commonly accomplished by two different techniques: (a) watering and brushing the fresh concrete surface with a rotary brush, and (b) spraying the surface with a set retarder immediately after placement, followed by a mechanical brushing 24 h later to remove the mortar that has not set. The average texture depth is targeted to be 0.9 mm (0.035 in.) as measured by the sand patch test (Descornet, Fuchs, & Buys, 1993). Though widely used in European countries, the exposed aggregate technique has not been widely used in the United States. Overall, the European experience has found that when exposed aggregate surfaces are properly designed and constructed, they have performed very well. The specific favorable characteristics include low noise (similar to porous asphalt), excellent high-speed skidding resistance (equivalent to transversely tined pavements), good surface durability, and low splash and spray. Disadvantages of this method include the requirement of high-quality aggregates throughout the thickness of the wearing course, and, although the construction of the surface is not difficult, the learning curve experienced by contractors as they gain familiarity with the practice (Hoerner et al., 2003).

In one of the conducted researches, Sommer suggests that the EACS technique is the cheapest method of building a rigid pavement with a surface that has noise reducing, skid resistance\ and durability features. The technique requires special adapted pavers, tolerant retarders, and very efficient curing (Sommer, 1998). He also emphasized that the contractor needs time to develop the correct technique for producing an EACS. The recommendations of his work are to use a maximum aggregate size of 8mm, a polished stone value (PSV) > 50, and that the stone count or contact points should be at least 55 points/25cm² of surfacing (Sommer, 1994).

Stinglhammer and Krenn also worked on the application of EACS in Austria using a two-layer system, the top layer being placed whilst the bottom layer was still fresh. Their experience has indicated that sand with a grading of 0-1 mm gives greater noise reduction than sand of 0-2 mm. The coarse aggregate used had a grading of 4-8 mm. The surface texture should be 0.9 ± 0.1 mm measured by the sand patch test, and there should be 55 profile peaks/25cm² of surfacing. The measurement of tire road noise at 100 km/h gave noise levels of 5 dB(A) less than conventional textured concrete. In addition, the skid resistance was improved and winter maintenance was unaffected (Stinglhammer, 1994).

Herrfeld (1998) indicated the requirements of surface retarders or more correctly surface-deactivators. They should be sprayable, free of any volatile solvents, free of any harmful chemicals, reliable during hot heather application, compatible with a rain-protection plastic, and capable of delaying the exposure for 24 hours to eliminate the need for night working. They should also not lead to a deeper texture depth (Herrfeld, n.d. 1998).

Chandler et al (2003) reported that to ensure good skid resistance a coarse aggregate with a relatively high PSV (Polished Stone Value) is required, and also that the noise generated at the tire/road interface is lessened by reducing the maximum aggregate size. They explained the application method as laying a concrete slab, either by slip-forming or between forms, in one or two layers, and spraying the finished surface with a retarder. After a suitable period of time the concrete surface is brushed or washed with a pressure hose to remove the mortar at the surface of the slab.

2.8.5 Chip Sprinkling

Originating in Belgium in the early 1970s, chip sprinkling is the practice of strewing polish-resistant stones of a specified size [e.g., 10 to 14 or 14 to 20 mm] evenly onto the surface of the already compacted and profiled fresh concrete. The stones are then set in such a way that they slightly protrude from the surface, thus creating macro-texture (Fuchs, 1981). Although this practice can result in an extremely noisy surface, the use of high-quality chippings (aggregates) can help to reduce the associated noise while providing satisfactory surface friction (Wu & Nagi, 1995).

This technique has been further developed in France and has been used on the A26 motorway between Reims and Calais. Since 1984, it has been used in France in combination with a chemically exposed aggregate finish (Chandler, Phillips, Roe, & Viner, 2003).

Descornet *et al.* (1993) indicated that the permitted surface treatments for concrete pavements in Belgium were transverse brushing, deep transverse grooving, chip sprinkling, and aggregate exposure. These have all proved adequate for providing wet skid resistance and rolling comfort (Descornet et al., 1993).

CHAPTER 3

EXPERIMENTAL PROGRAM

Before organizing the experimental program, a non-contact laser scanner and an analysis tool is developed. Later, the experimental program is conducted which can be divided into 4 phases. The first two phases tackle with the investigation of RCC and HMA surface texture parameters through the developed laser-scanner. Later, the effects of frost damage on the surface quality of RCC mixtures are investigated as the third phase. The last phase is devoted to two surface modification techniques utilized to improve the surface quality of RCC.

This chapter first explains the working principles of the developed non-contact laser scanner and the analysis tool. Later, the details of the experimental program, i.e. the materials and test methods are then described.

3.1 Development of the Non-Contact Laser Scanner

A three-dimensional non-contact scanner (Figure 3-1) was developed by the author to record high accuracy surface profiles from the specimens. A high-resolution computer numerical control (CNC) platform was equipped with a high accuracy optical distance sensor to build the physical body of the scanner. The custom-made CNC platform was capable of covering a scan area of 550 mm in X and Y directions. The Leuze Electronics manufactured optical distance sensor measuring principle was based on high speed (2 ms) triangulation on red laser light. For optimal performance, scan resolution was kept constant for all profiles at 100 micrometers for X and Y axes and 10 micrometers for Z. An algorithm for scanning pattern was developed in G-Code, and the motion of the scanner was controlled with “MACH3” software.



Figure 3-1, The developed Non-contact 3D scanner

The optical distance sensor is capable of continuously reading of distance values and storing the values as a single column of data into a text document. In order to recognize data for each row of the scan, a guide frame was designed to be placed over the test specimen in a known elevation range (Figure 3-2). This guide frame acts as a physical barrier between the sensor and specimen at the beginning and end of each row of the scan, thus, it causes a set of known distance values to be inserted into the column of data (Figure 3-3). The number of data for a 100 x 100 mm area with the mentioned resolution in the column exceeds one million. MATLAB was used for processing the raw data in multiple steps. In the first step, a script selects the values which were acquired inside the guide frame and generates rows of a scan. Several controls are done on the next step for validation of entries of each row. Then each row incorrect order is placed to generate a surface matrix. Then the generated matrix is detrended, leveled, and shifted to a defined base plane.



Figure 3-2, Close up of guide frame and samples under scan

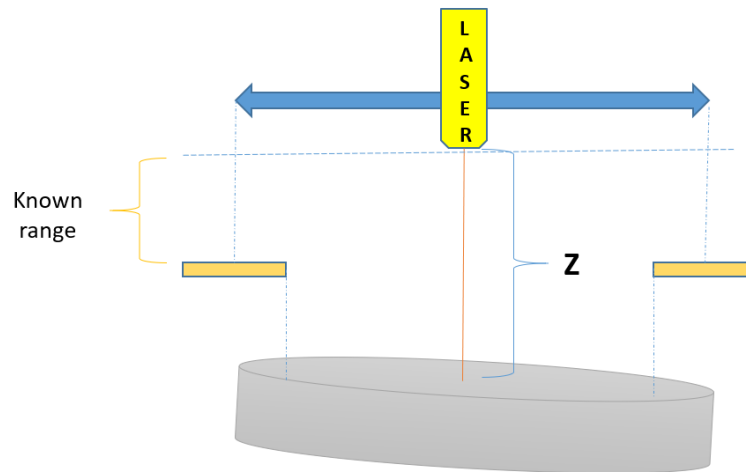


Figure 3-3, Schematic demonstration of the scan logic

Figure 3-4 demonstrates 3D visualization of a surface matrix produced by MATLAB and also the actual surface picture. Dimensions of the produced matrix depend on the scan area. For instance, from the 150 mm diameter disk specimen, a 100 mm by 100 mm area can be scanned and a 1000×1000 surface profile matrix can be obtained.

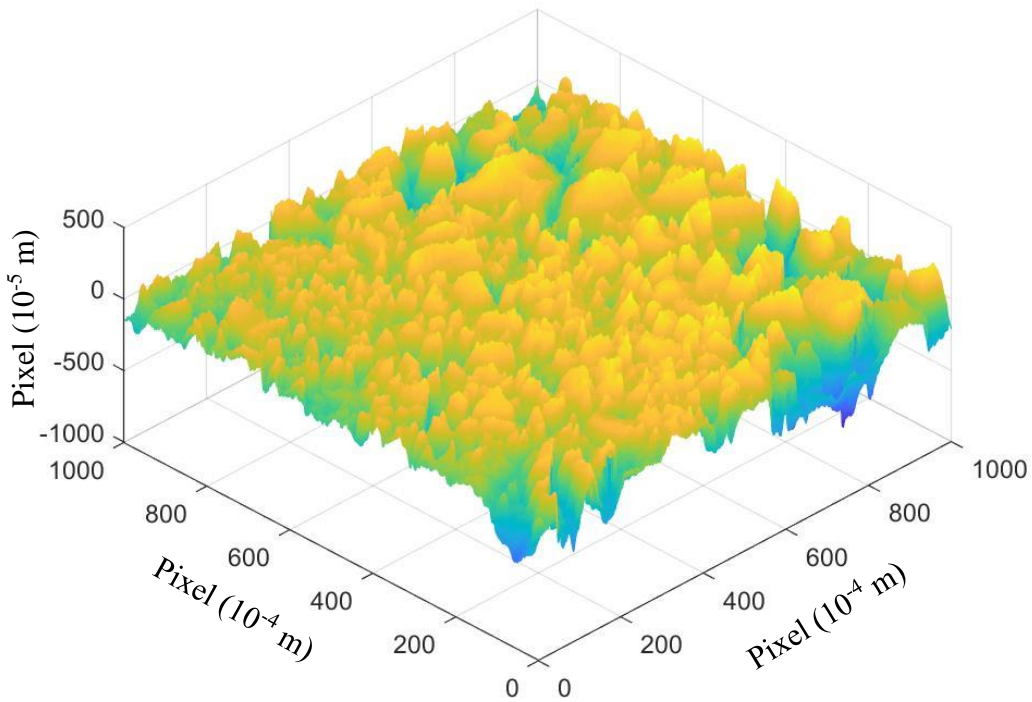
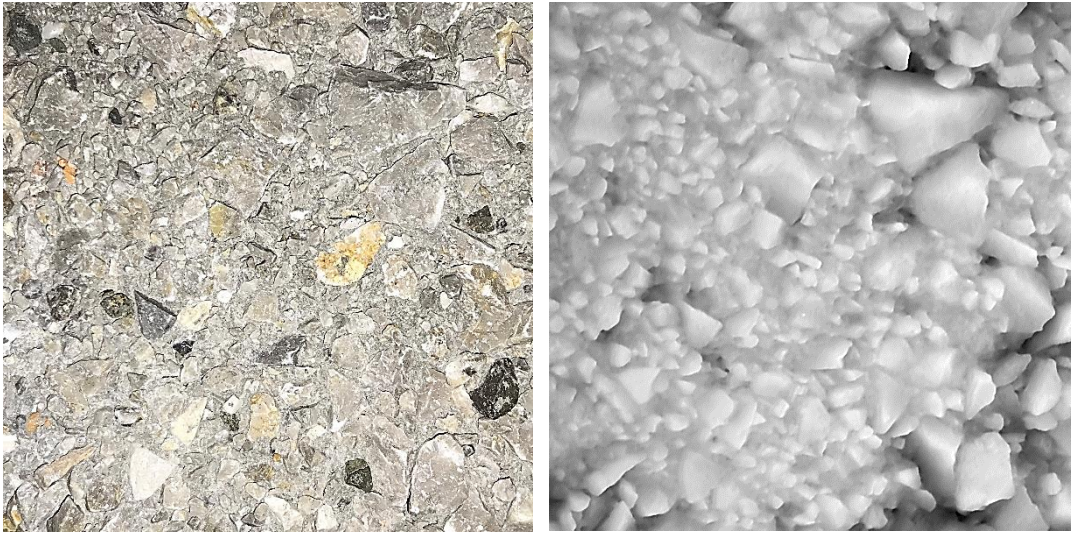


Figure 3-4, Top left; Picture of an exposed aggregate concrete surface. Top right: Virtual image of the surface generated by MATLAB. Bottom; 3D illustration of the surface.

3.2 Materials and Test Specimens used in the Experiments

RCC mix is a fairly dry mixture with a zero slump. This makes the RCC mix non-workable with conventional concrete equipment such as vibrating rods. Indeed, it is

designed in such a gradation that to be compactable utilizing roller compactors. Due to the size of roller compactors and the minimum required area for proper application, preparing RCC specimens in a lab environment for research purposes is quite challenging. Part of the RCC specimens that were used in this study was specifically prepared for this thesis, but the major part was prepared under an RCC pavement research project (Project no. 116M523) funded by The Scientific and Technological Research Council of Turkey (TÜBİTAK). For comparison purposes, in addition to the lab prepared RCC specimens, HMA pavement specimens were produced and tested.

3.2.1 Material Selection and Mix Proportions

CEM I 42.5 R type cement, with a specific gravity of 3.11 g/cm³ and a Blaine fineness of ~3500 cm²/g, was selected for the mixtures. Crushed limestone aggregate in three gradations, 0-5 mm, 5-12 mm, and 12-19 mm were chosen to produce gradation combinations. Test results of physical properties of the aggregate in accordance with ASTM C125, ASTM C127 and ASTM C128 are given in Table 3-1.

Table 3-1, Physical properties of the aggregates

| Physical Properties | Fine Aggregate | Coarse Aggregate | Coarse Aggregate |
|-------------------------------------|------------------------|------------------------|------------------------|
| | FA (0-5 mm) | CA (5-12 mm) | CA (12-19 mm) |
| Maximum aggregate size (mm) | 5 mm | 12 mm | 19 mm |
| Specific gravity (SSD) | 2.67 | 2.69 | 2.71 |
| Specific gravity (OD) | 2.64 | 2.68 | 2.70 |
| Bulk density in compacted condition | 1791 kg/m ³ | 1540 kg/m ³ | 1488 kg/m ³ |
| Bulk density in loose condition | 1668 kg/m ³ | 1466 kg/m ³ | 1395 kg/m ³ |
| Absorption % | 1.24 % | 0.29 % | 0.18 % |
| Fineness modulus | 3.2 | - | - |

Concrete proportions and mix design were engineered considering the American Concrete Pavement Association manual and HMA gradation limits from the Turkish General Directorate of Highways. The shared construction method of RCC and HMA pavements was the main reason behind speculating the HMA gradation. Şengün (2019) illustrated a comprehensive explanation and further details on the selection of optimal aggregate combination and gradation design. Two aggregate blends (A12 and B12) with maximum aggregate sizes of 12 mm and another two blends (A19 and B19) with maximum aggregate sizes of 19 mm were selected for the mixtures. The A12 blend designed to have 65% of fine aggregate (0-5 mm) and 35% coarse aggregate of size 5-12, while the A19 was consisted of 50% fine aggregate (0-5 mm) with a coarse aggregate blend of 40% of size 5-12 mm and 10% of size 12-19 mm. The B12 blend designed to have 54% of fine aggregate (0-5 mm) and 46% coarse aggregate of size 5-12, while the B19 was consisted of 44% fine aggregate (0-5 mm) with a coarse aggregate blend of 41% of size 5-12 mm and 15% of size 12-19 mm.. Table 3-2 illustrates mix IDs with ingredients proportions.

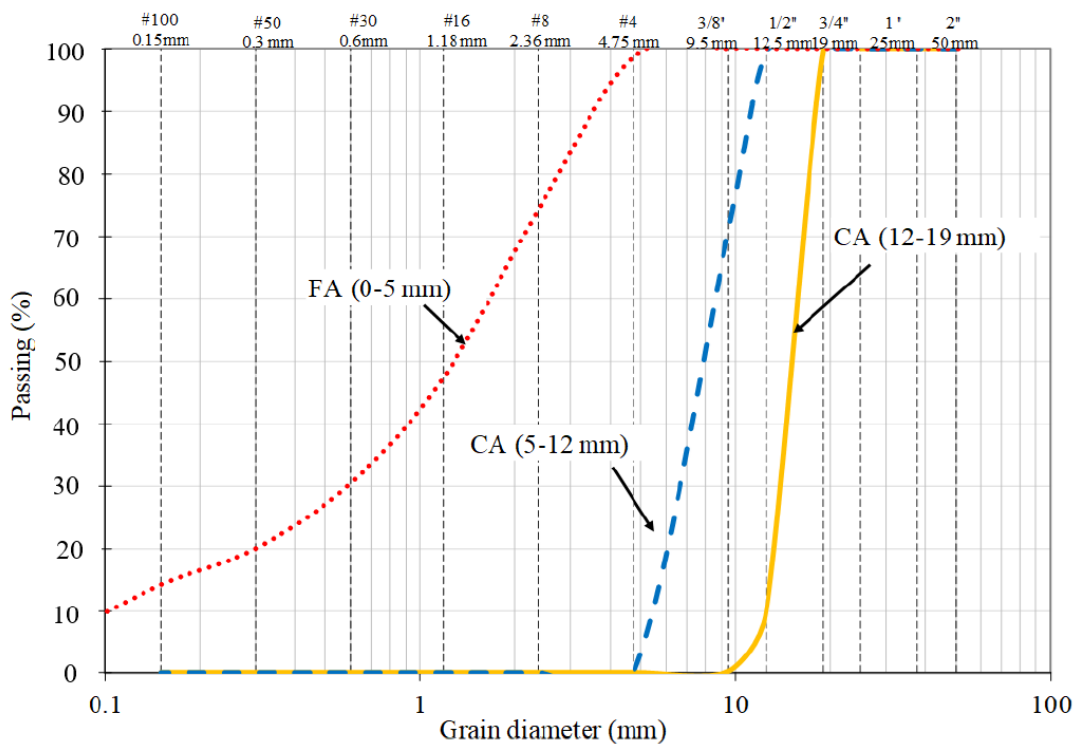


Figure 3-5, Aggregates gradation (Şengün, 2019)

Table 3-2, In lab prepared mix proportions

| Mix ID | Cement (kg) | D _{max} (mm) | Water (%) | Water (kg) | Aggregate (kg) | | | Agg. blend | W/C |
|---------------|----------------|--------------------------|--------------|---------------|----------------|--------|---------|---------------|------|
| | | | | | 0-5mm | 5-12mm | 12-19mm | | |
| SGCC-200-12-4 | 200 | 12 | 4 | 96 | 1424 | 770 | 0 | A12 | 0.48 |
| SGCC-200-12-5 | 200 | 12 | 5 | 117 | 1388 | 750 | 0 | A12 | 0.59 |
| SGCC-200-12-6 | 200 | 12 | 6 | 137 | 1353 | 731 | 0 | A12 | 0.69 |
| SGCC-200-19-4 | 200 | 19 | 4 | 96 | 1095 | 880 | 222 | A19 | 0.48 |
| SGCC-200-19-5 | 200 | 19 | 5 | 117 | 1067 | 857 | 216 | A19 | 0.59 |
| SGCC-200-19-6 | 200 | 19 | 6 | 137 | 1040 | 835 | 211 | A19 | 0.69 |
| SGCC-400-12-4 | 400 | 12 | 4 | 97 | 1312 | 709 | 0 | A12 | 0.24 |
| SGCC-400-12-5 | 400 | 12 | 5 | 118 | 1275 | 689 | 0 | A12 | 0.30 |
| SGCC-400-12-6 | 400 | 12 | 6 | 139 | 1240 | 670 | 0 | A12 | 0.35 |
| SGCC-400-19-4 | 400 | 19 | 4 | 97 | 1009 | 810 | 205 | A19 | 0.24 |
| SGCC-400-19-5 | 400 | 19 | 5 | 118 | 981 | 788 | 199 | A19 | 0.30 |
| SGCC-400-19-6 | 400 | 19 | 6 | 139 | 953 | 766 | 194 | A19 | 0.35 |
| SGCC-300-12-5 | 300 | 12 | 5.5 | 127 | 1095 | 922 | 0 | B12 | 0.42 |
| SGCC-300-19-5 | 300 | 19 | 5.5 | 128 | 896 | 820 | 308 | B19 | 0.42 |
| RCC-200-12 | 200 | 12 | 5 | 117 | 1157 | 974 | 0 | B12 | 0.59 |
| RCC-200-19 | 200 | 19 | 5 | 117 | 946 | 866 | 325 | B19 | 0.59 |
| RCC-300-12 | 300 | 12 | 5.5 | 127 | 1095 | 922 | 0 | B12 | 0.42 |
| RCC-300-19 | 300 | 19 | 5.5 | 127 | 896 | 820 | 308 | B19 | 0.42 |
| RCC-400-12 | 400 | 12 | 5.5 | 129 | 1048 | 883 | 0 | B12 | 0.32 |
| RCC-400-19 | 400 | 19 | 5.5 | 129 | 857 | 785 | 294 | B19 | 0.32 |

Note- SGCC and RCC denote for Superpave Gyratory Compacted Concrete and Roller Compacted Concrete, respectively.

3.2.2 In-Lab Produced RCC Specimens

The concrete was batched using a 0.35 m³ drum mixer. The mixing sequence was consisting of adding cement after aggregates to the drum and mixing for 2 minutes, followed by adding water and continue mixing for another 5 minutes. The mixture consistency was determined with Vebe test, in accordance with procedure A of ASTM C1170. The concrete was placed and compacted within 20 minutes after mixing.

Two different compaction practices were implemented for the production of the specimens:

- Superpave gyratory compactor (SGC)
- Double drum vibratory hand roller (DDVHR)

Superpave gyratory compactor (SGC) is a fairly new technique for HMA lab environment small sample compaction (Figure 3-6), which has been proved to be capable of simulating field compaction regime at laboratory (R. Collins et al., 1997; Masad et al., 1999; Peterson et al., 2003). The equipment applies a constant load to end plates of a 150 mm diameter cylindrical mold while rotating the mold with an angle of 1.25° against its longitudinal axis. The compaction is expressed as the number of the rotations, so called gyration number. The factors affecting compaction such as applied energy and desired density can get under control in SGC. However, in terms of surface texture, there is no available evidence in the literature illustrating the closeness of developed texture in SGC to the texture which is achieved on field. The specimens produced by SGC were cylinders with 150 mm diameter and 150 mm height. In this study, 30 mm of the top of the cylinders were cut using a water-cooled diamond blade for ease of transportation and testing (Figure 3-7).

In the second compaction practice, a two-step procedure was followed (Figure 3-8). The main purpose in this practice was simulating field compaction procedure, placing and initial compaction with paver and final compaction with rollers. To imitate the effect of initial compaction of a paver, a flat wooden plate was placed on the leveled concrete and a 100 kg vibratory compactor with a vibration force of 18 kN was traveled over the plate. Following removal of the plate, the final compaction was achieved employing a 700 kg walk-behind double drum vibratory compactor in 8 passes. The first 4 passes were applied with vibration and then followed by another 4 passes without vibration. The obtained block was then moist cured and cut into pieces for further testing.

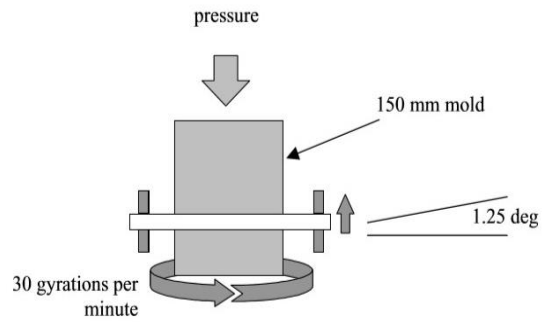


Figure 3-6 Left: The Superpave gyratory compactor, Right: schematic view of the gyratory compaction



Figure 3-7, Concrete and asphalt samples compacted with SGC



Figure 3-8 Two-steps compaction procedure. Left: initial step; plate compactor, Right: final step; hand roller compactor.

3.2.3 In-Lab Produced HMA Specimens

To gain a clear understanding of the compaction influence on the generated texture with different binder types, and for comparison purposes, two HMA mixes were designed with the super-pave method using the same aggregate types, gradations, and nominal aggregate size of the RCC mixes. (D_{max12} and D_{max19}). Mix formulae were designed with grade 50-70 asphalt, having 4.5% and 5.0% asphalt content for 19 mm and 12 mm maximum aggregate size, respectively. 4.0% of Air void was achieved for both mixes. Table 3-3 gives the properties of the asphalt. For the production of the HMA specimens, compaction regimes were kept identical as RCC. SGC and DDVHR methods were carried on for both HMA mixes.

Table 3-3, Measured properties of asphalt 50-70

| <i>Properties measured</i> | <i>Specification value</i> | <i>Standard</i> |
|--|----------------------------|------------------|
| Penetration | 51 | (ASTM D5 2008) |
| Specific gravity (kg/m ³) | 1.025 | (ASTM D36 2014) |
| Softening point (ring and ball method) | 47.5 | (ASTM D 70 2014) |
| Flash point (°C) | +300 | (ASTM D92 2005) |
| Ductility (5 cm/min, 25 °C) | +100 | (ASTM D113 2007) |
| Kinematic viscosity @135° (C.P) | 372 | (ASTM D445 2008) |

3.3 Experimental Test Procedures

This study is aimed to investigate the intrinsic surface texture of RCC pavement to find the main influencing factors on the texture properties in the interest of pavement safety and rideability. In order to evaluate the macro and micro-texture of the prepared surfaces, several measurement methods were selected from literature, covering most aspects of surface texture properties.

3.3.1 Measurements of Texture Depth; Sand patch method

The sand patch method in accordance with ASTM E965 was conducted for macro-texture measurements. This test method assesses the surface texture depth by measuring the spread area of a known volume of spherical glass beads. This is a suitable method for concrete and asphalt pavements with a texture depth of greater than 0.25 mm.

3.3.2 Skid Resistance Test; Portable Pendulum Tester

The portable skid resistance tester or portable pendulum tester is designed to determine the resistance of wet road surface to skidding. This test can provide a measure of friction by measuring energy loss between a rubber slider and the pavement surface and can be used in both lab and field. Portable pendulum test was carried out on all test surfaces in both dry and wet conditions. For wet condition, in this study water was spread on the surface using a hand spray. For consistency of readings, the water film tried to be kept 2 mm in depth for all tests. Gyratory compacted specimens were measured in four directions in 90° intervals. This was limited to two directions for roller compacted specimens to match the travel direction of the roller. Multiple readings for each direction were obtained and the mean of 5 successive readings was recorded for each surface.



Figure 3-9, left: BPN measurement on disk specimen, right: BPN measurement of asphalt block

3.3.3 Roughness Parameters

Roughness parameters are quantitative values derived mathematically from profiles. They have been defined in a handful of international standards for both 2D profiles and 3D surfaces acquired with various profilometers. ISO 25178-2 international standard for specification and measurement of 3D surface texture (non-contact profilometer) comprehensively illustrates 3D parameters in 6 different categories:

- Height parameters
- Spatial parameters
- Hybrid parameters
- Functional parameters
- Functional volume parameters
- Feature parameters

3.3.3.1 Height parameters

Height variants consist of 7 main parameters (Table 3-4). These parameters assess height deviation from mean plane of a surface.

Table 3-4, Height parameters of ISO 25178-2

| <i>Height Parameters</i> | <i>Symbol</i> | <i>Units</i> |
|--------------------------|-----------------|--------------|
| Maximum peak height | S _p | Length (m) |
| Maximum valley depth | S _v | Length (m) |
| Maximum height | S _z | Length (m) |
| Arithmetical mean height | S _a | Length (m) |
| Root mean square height | S _q | Length (m) |
| Skewness | S _{sk} | (Unitless) |
| Kurtosis | S _{ku} | (Unitless) |

- Maximum peak height (S_p)

It is the maximum value for peak's height. In other words, the height of the highest peak within the defined area from mean plane (Eq. 3-1). It should be noted that this parameter is significantly influenced by false irregularity, contamination, and measurement noise due to the utilization of single peak height value.

$$S_p = \max(Z(x, y)) \quad \text{Eq. 3-1}$$

- Maximum valley depth (S_v)

It is the maximum value for valley's depth. In other words, the depth of the deepest valley from mean plane within the defined area (Eq. 3-2). Similar to maximum height, this parameter is significantly influenced by false irregularity, contamination, and measurement noise due to the utilization of single pit depth value.

$$S_v = \min | (Z(x, y)) | \quad \text{Eq. 3-2}$$

- Maximum height (S_z)

The maximum height S_z is the vertical difference between the highest and the lowest points on the sample surface (Figure 3-10), equivalent to the sum of the maximum peak height S_p and maximum valley depth S_v (Eq. 3-3)

$$S_z = S_p + S_v \quad \text{Eq. 3-3}$$

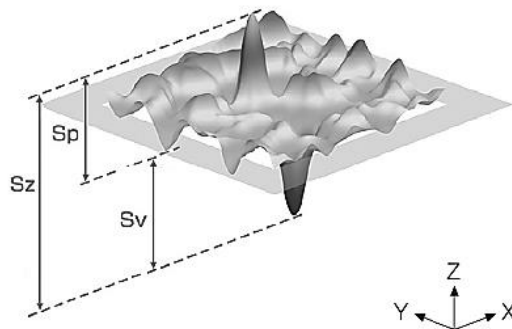


Figure 3-10, Schematic illustration of Maximum peak height (S_p), Maximum pit depth (S_v), and Maximum height (S_z)

- Arithmetical mean height (S_a)

It represents the arithmetic mean of the absolute ordinate $Z(x, y)$ within the evaluation area (Eq. 3-4). This is one of the most widely used parameters and is the mean of the average height difference for the average plane. It provides stable results since the parameter is not significantly influenced by the measurement noise. One of the main criticisms of S_a is that it cannot distinguish between profiles of different shapes. Profiles having the same S_a value may be entirely different in character. Despite this drawback, S_a is almost a universal use for quality control, being defined by standards.

$$S_a = \frac{1}{A} \iint_A |Z(x, y)| \, dx dy \quad \text{Eq. 3-4}$$

with A being the definition area

- Root mean square height (S_q)

S_q represents the root mean square value of ordinate values within the definition area (Eq. 3-5). It is equivalent to the standard deviation of heights. One advantage which the S_q parameter offers over S_a is that it appears to be more sensitive to changes in the shape of the profile than S_a .

$$S_q = \sqrt{\frac{1}{A} \iint_A Z^2(x, y) \, dx dy} \quad \text{Eq. 3-5}$$

- Skewness (S_{sk})

Surface skewness (S_{sk}) is a measure of the asymmetry of the surface deviation about the mean plane (Eq. 3-6). For a symmetric shape of surface height distribution, the skewness is zero (Figure 3-11). Negative values show higher height distribution above the mean plane and positive values represent higher height distribution beneath the mean plane.

$$S_{sk} = \frac{1}{S_q^3} \left[\frac{1}{A} \iint_A Z^3(x, y) \, dx dy \right] \quad \text{Eq. 3-6}$$

- Kurtosis (S_{ku})

Kurtosis (S_{ku}) is a measure of the sharpness of the surface height distribution. This parameter characterizes the spread of the height distribution (Eq. 3-7). A Gaussian surface has a kurtosis value of 3 (Figure 3-11). A centrally distributed surface has a kurtosis value larger than 3, whereas the kurtosis of a well-spread distribution is smaller than 3.

$$S_{ku} = \frac{1}{Sq^4} \left[\frac{1}{A} \iint_A Z^4(x, y) dx dy \right] \quad \text{Eq. 3-7}$$

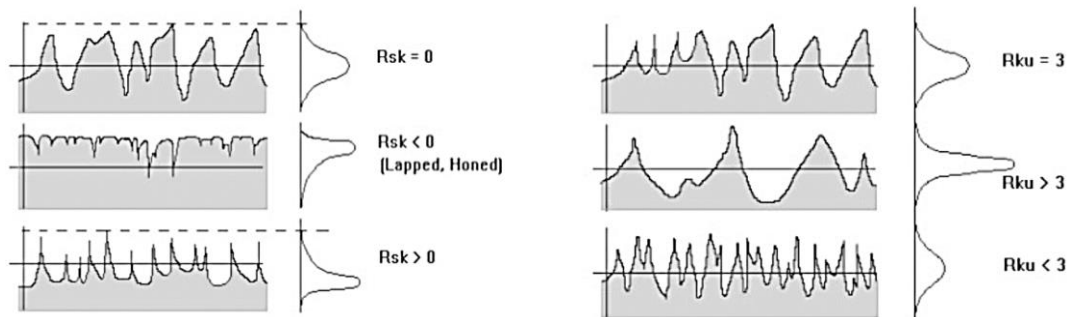


Figure 3-11, Physical definition of the parameters S_{sk} and S_{ku} which are expressed in 2d profiles as R_{sk} and R_{ku} (Bitelli, Simone, Girardi, & Lantieri, 2012).

3.3.3.2 Spatial parameters

The spatial properties are described by two parameters. These parameters are the autocorrelation length and texture aspect ratio (Table 3-5). They are used to evaluate the horizontal size and complexity of parallel grooves and grains instead of the height parameters.

Table 3-5, Spatial parameters of ISO 25178-2

| Spatial parameters | Symbol | Units (Default) |
|------------------------|----------|-----------------|
| Autocorrelation length | S_{al} | Length (m) |
| Texture aspect ratio | S_{tr} | (Unitless) |

These parameters are calculated based on the autocorrelation function (ACF). Autocorrelation function (Eq. 3-8) describes the correlation between a surface and the same surface translated by (t_x, t_y) . It can also evaluate the periodicity of each surface direction. The center of the image (Figure 3-12-b) is the highest point (ACF = 1), and ACF decays as the amount of shift away from the center increases. ACF falls rapidly to zero along a direction where the short wavelength component is dominant and falls slowly when shifting along a direction where a long wavelength component is dominant.

$$f_{ACF}(t_x, t_y) = \frac{\iint_A z(x,y)z(x-t_x, y-t_y) dx dy}{\iint_A z(x,y)z(x,y) dx dy} \quad \text{Eq. 3-8}$$

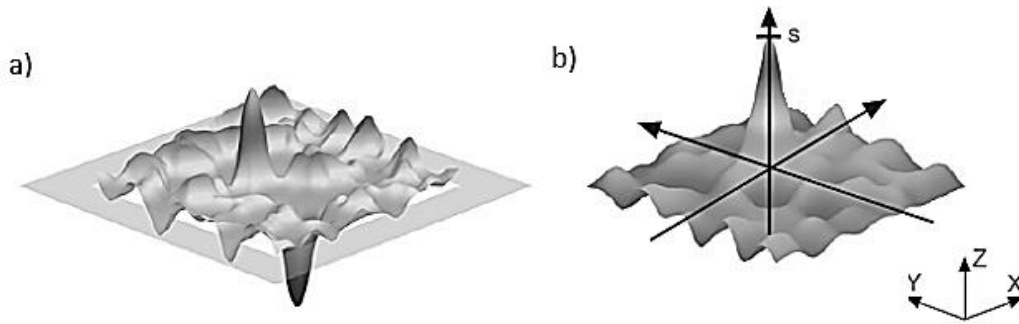


Figure 3-12, a) actual Surface, b) Autocorrelation of the surface

- Autocorrelation length (S_{al})

Autocorrelation length (S_{al}) is described as the horizontal distance of the autocorrelation function that has the fastest decay to a specified value s ($0 \leq s < 1$). S is assumed to be 0.2 in calculations.

$$S_{al} = \min_{t_x, t_y \in R} \sqrt{(t_x^2 + t_y^2)} \quad \text{Eq. 3-9}$$

where $R = \{(t_x, t_y): f_{ACF}(t_x, t_y) \leq s\}$

- Texture aspect ratio (S_{tr})

This parameter is defined as the ratio of the horizontal distance of the autocorrelation function that has the fastest decay to a specified value s to the horizontal distance of the autocorrelation function that has the slowest decay to s ($0 \leq s < 1$). It indicates the isotropic/anisotropic strength of the surface. S_{tr} value ranges from 0 to 1; normally $S_{tr} > 0.5$ indicates a strong isotropy while $S_{tr} < 0.3$ means strongly anisotropic.

$$S_{tr} = \frac{\min_{t_x, t_y \in R} \sqrt{(t_x^2 + t_y^2)}}{\max_{t_x, t_y \in Q} \sqrt{(t_x^2 + t_y^2)}} \quad \text{Eq. 3-9}$$

where $R = \{(t_x, t_y): f_{ACF}(t_x, t_y) \leq s\}$

and $Q = \{(t_x, t_y): f_{ACF}(t_x, t_y) \geq s\}$

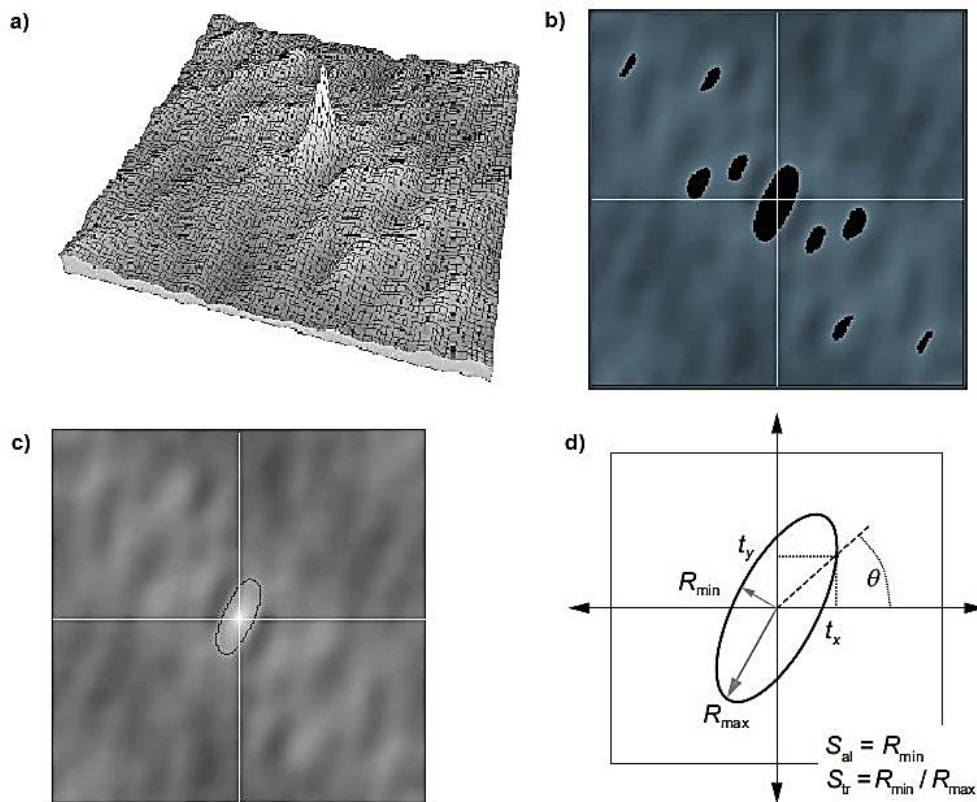


Figure 3-13, Procedure to calculate S_{al} and S_{tr} , a) Autocorrelation function of the surface, b) Threshold autocorrelation at s (the black spots are above the threshold), c) Threshold boundary of the central threshold portion, d) Polar coordinates leading to the autocorrelation lengths in different directions

3.3.3.3 Hybrid parameters

Hybrid parameters are consisting of two parameters that focus on both the height and the direction of the plane. These parameters are root mean square gradient (S_{dq}) and developed interfacial area ratio (S_{dr}) (Table 3-6).

Table 3-6, Hybrid parameters of ISO 25178-2

| Hybrid parameters | Symbol | Units (Default) |
|----------------------------------|----------|-----------------|
| Root mean square gradient | S_{dq} | (Unitless) |
| Developed interfacial area ratio | S_{dr} | % |

- Root mean square gradient (S_{dq})

This parameter indicates the mean magnitude of the local gradient (slope) of the surface (Eq. 3-10). The steepness of the surface can be numerically represented in this parameter. The surface is more steeply inclined for larger values of the parameter S_{dq} .

$$S_{dq} = \sqrt{\left(\frac{1}{A} \iint_A \left[\left(\frac{\partial z(x,y)}{\partial x}\right)^2 + \left(\frac{\partial z(x,y)}{\partial y}\right)^2 \right] dx dy\right)} \quad \text{Eq. 3-10}$$

- Developed interfacial area ratio (S_{dr})

This signifies the rate of an increase in the surface area (Figure 3-14). S_{dr} values increase as the surface texture becomes fine and rough.

$$S_{dr} = \frac{1}{A} \left[\iint_A \left(\sqrt{1 + \left(\frac{\partial z(x,y)}{\partial x}\right)^2 + \left(\frac{\partial z(x,y)}{\partial y}\right)^2} \right) - 1 \right] dx dy \quad \text{Eq. 3-10}$$

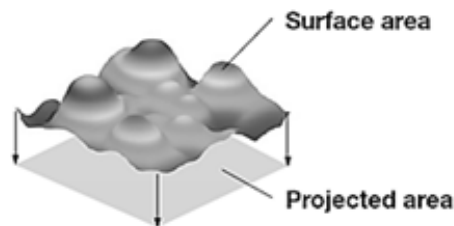


Figure 3-14, Demonstration of projected area and surface area in calculation of S_{dr}

3.3.3.4 Functions and related parameters

Functional parameters are calculated using the areal material ratio function (Table 3-7). This function can be interpreted as the sample cumulative probability function of the ordinates $Z(x,y)$ within the evaluation area (Figure 3-15). The application of these parameters is mostly on the evaluation of behavior of a surface that comes into strong mechanical contacts, such as friction and abrasion.

Table 3-7, Functions and related parameters of ISO 25178-2

| <i>Functions and related parameters</i> | <i>Symbol</i> | <i>Units (Default)</i> |
|---|---------------|------------------------|
| Core height | S_k | Length (m) |
| Reduced peak height | S_{pk} | Length (m) |
| Reduced valley height | S_{vk} | Length (m) |
| Material ratio | S_{mr1} | % |
| Material ratio | S_{mr2} | % |
| Peak extreme height | S_{xp} | Length (m) |
| Dale void volume | V_{vv} | ml/m ² |
| Core void volume | V_{vc} | ml/m ² |
| Peak material volume | V_{mp} | ml/m ² |
| Core material volume | V_{mc} | ml/m ² |

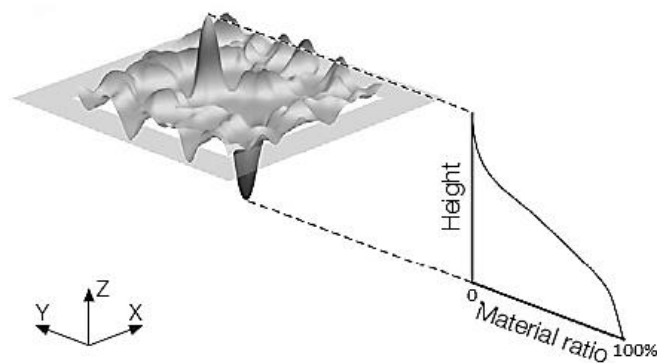


Figure 3-15, Schematic view of cumulative probability function curve

- Areal material ratio ($S_{mr(c)}$)

Areal material ratio is the ratio of the area of material at a specified height [c] from the reference plane to the evaluation area. An areal material ratio curve represents the heights at which the areal material ratio changes from 0% to 100%. An areal material ratio represents the area with a specific height [c].

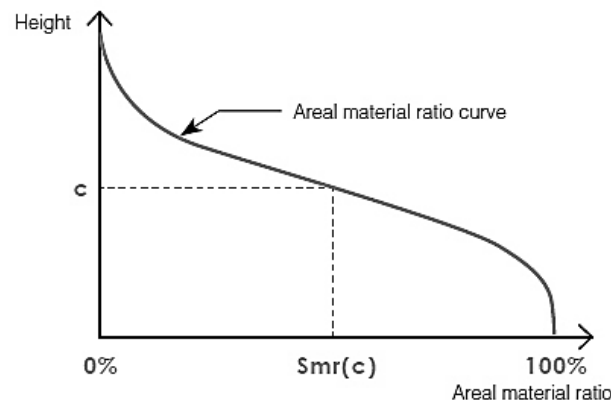


Figure 3-16, Areal material ratio

- Areal material ratio curve interpretation

In order to extract related parameters from the areal material ratio curve, 3 major steps are followed as bellow (Figure 3-17):

Step 1: A secant line, covering from 0% to 40% of the areal material ratio is drawn on the material ratio curve.

Step 2: The secant line is shifted from the areal material ratio of 0% to the position at which the secant line has the smallest gradient. The covered portion of the shifted secant line is called the center portion of the areal material ratio curve.

Step 3: The equivalent line is the line where the sum of the squared deviation in the vertical-axis direction is the smallest in the center portion.

The section of the equivalent line between the two height positions where the areal material ratio is 0% and 100% is called a core surface. The core surface represents

the height of the area that makes contact with other objects after initial abrasion. The peaks with a height above the core surface are called reduced peaks. The valleys below the core surface are called reduced valleys.

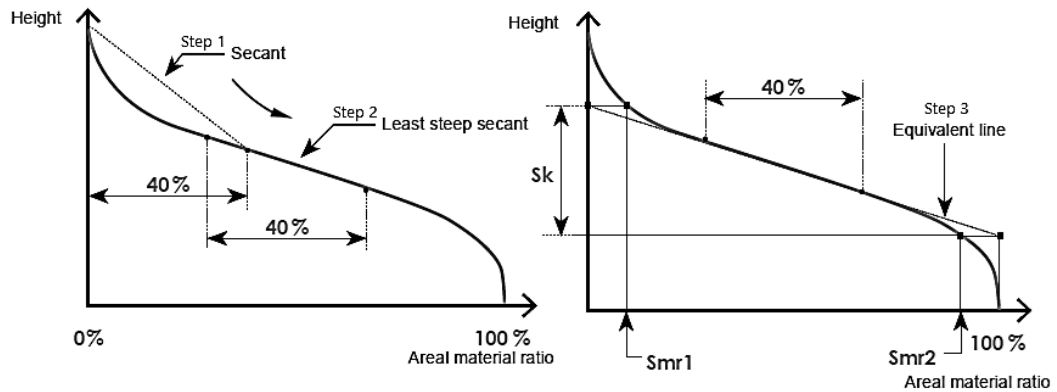


Figure 3-17, Steps to draw 'Equivalent line' on areal material ratio curve.

- Core height (S_k)

S_k represents the height of the core surface and can be calculated as the difference between the upper and lower levels of the core surface (Figure 3-18).

- Reduced peak height (S_{pk})

Reduced peak height is the average height of the peaks above the core surface (Figure 3-18).

- Reduced valley height (S_{vk})

Reduced valley height is the average depth of the valleys beneath the core surface (Figure 3-18).

- The areal material ratio S_{mr1}

The areal material ratio S_{mr1} is the ratio of area of the material at the intersection line which separates the peaks from the core surface (Figure 3-18).

- Areal material ratio S_{mr2}

Areal material ratio S_{mr2} is the ratio of area of the material at the intersection line which separates the valleys from the core surface (Figure 3-18).

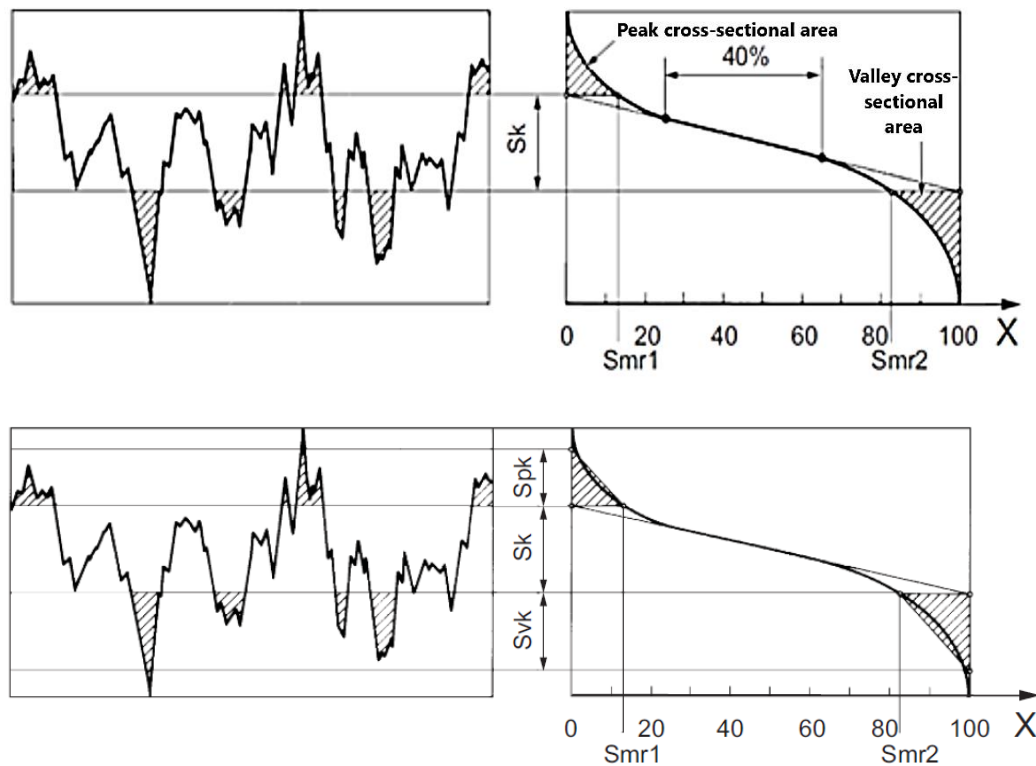


Figure 3-18, The parameters S_{pk} and S_{vk} each are calculated as the height of the right-angle triangle which is constructed to have the same area as the “Peak cross-sectional area” or “Valley cross-sectional area”. This contributes to eliminating outlying peaks and valleys in the calculation of S_{pk} and S_{vk} .

- Peak extreme height (S_{xp})

This parameter is the difference of heights at the areal material ratio values of 2.5% and 50%. S_{xp} represents the difference in the height between the average plane and peaks on the surface after especially high peaks on the surface are removed (Figure 3-19, a).

Additional set of functional volume parameters can be derived from areal material ratio curve if areal material ratios of “p” and “q” are considered. The default values for “p” and “q” are defined as 10% and 80% respectively in accordance with ISO 25178-3 (Figure 3-19, b).

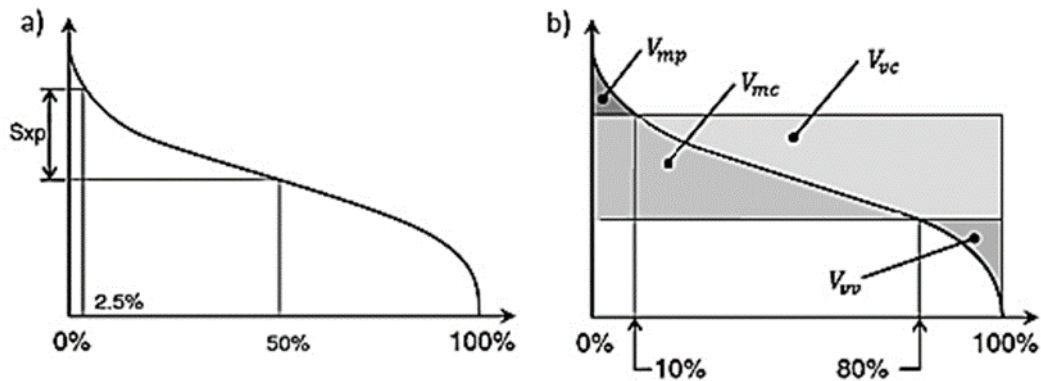


Figure 3-19, Illustration of: a) Peak extreme height (S_{xp}); b) Functional volume parameters

- Dale void volume (V_{vv})

Dale void volume represents the void volume of valley at areal material ratio 10%. It can be used to quantify the magnitude of the core surface, reduced peaks, and reduced valleys based on volume parameters (Figure 3-19-b).

- Core void volume (V_{vc})

This parameter represents the difference between the void volume at areal material ratio 10% and the void volume at areal material ratio 80%. It can also be used to quantify the magnitude of the core surface, reduced peaks, and reduced valleys based on volume parameters (Figure 3-19-b).

- Peak material volume (V_{mp})

This parameter represents the volume of material at areal material ratio 10%. It can also be used to quantify the magnitude of the core surface, reduced peaks, and reduced valleys based on volume parameters (Figure 3-19-b).

- Core material volume (V_{mc})

This parameter represents the difference between the material volume at areal material ratio 80% and the material volume at areal material ratio 10%. It can also be used to quantify the magnitude of the core surface, reduced peaks, and reduced valleys based on volume parameters (Figure 3-19-b).

3.3.3.5 Miscellaneous parameters

The only parameter in this category is “Texture direction” (S_{td}) (Table 3-8) which indicates the direction angle of the texture (parallel groove orientation, etc.). It is derived from the angle maximizing the spectrum angle of two-dimensional Fourier transformation images. S_{td} represents the angle for the strongest orientation, although the second and third strongest angles can also be defined on the directional chart.

Table 3-8, Miscellaneous parameters of ISO 25178-2

| <i>Miscellaneous parameter</i> | <i>Symbol</i> | <i>Units (Default)</i> |
|--------------------------------|---------------|------------------------|
| <i>Texture direction</i> | S_{td} | degrees |

3.3.3.6 Feature parameters

Feature parameters are defined by a multistep pattern recognition technique that is used to characterize the specified features (Table 3-9).

Table 3-9, Feature parameters of ISO 25178-2

| <i>Feature parameters</i> | <i>Symbol</i> | <i>Units (Default)</i> |
|---------------------------------------|---------------|------------------------|
| <i>Density of peaks</i> | S_{pd} | $1/m^2$ |
| <i>Arithmetic mean peak curvature</i> | S_{pc} | $1/m$ |
| <i>Ten-point height of surface</i> | S_{10z} | Length (m) |
| <i>Five-point peak height</i> | S_{5p} | Length (m) |
| <i>Five-point pit height</i> | S_{5v} | Length (m) |
| <i>Mean dale area</i> | S_{da} | m^2 |
| <i>Mean hill area</i> | S_{ha} | m^2 |
| <i>Mean dale volume</i> | S_{dv} | m^3 |
| <i>Mean hill volume</i> | S_{hv} | m^3 |

- Density of peaks (S_{pd})

The “Density of peaks”, S_{pd} is the number of peaks per unit area within a definition area (Figure 3-10). Only peaks that exceed a designated size are counted. The designated size is determined to be 5% of the maximum height “ S_z ”.

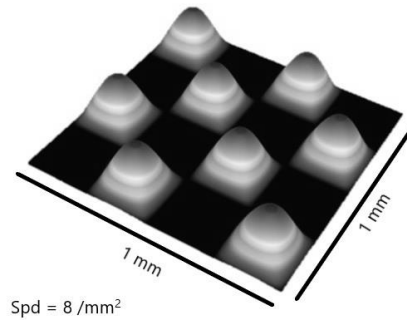


Figure 3-20, Illustration of “Density of peaks”

- Arithmetic mean peak curvature (S_{pc})

S_{pc} is the arithmetic mean of the principal curvatures of peaks within a definition area. Only peaks that exceed a designated curvature are taken into consideration, which is determined to be 5% of the maximum height “ S_z ”. A smaller value indicates that the points of contact with other objects have rounded shapes. A larger value indicates that the points of contact with other objects have pointed shapes.

$$S_{pc} = -\frac{1}{2} \frac{1}{n} \sum_{k=1}^n \left(\frac{\partial^2 z(x,y)}{\partial x^2} \right) + \left(\frac{\partial^2 z(x,y)}{\partial y^2} \right) \quad \text{Eq. 3-11}$$

- Ten-point height of surface (S_{10z})

The ten-point height of surface is defined as the average value of the heights of the five peaks with largest global peak height added to the average value of the heights of the five pits with largest global pit height, within the definition area (Eq. 3-12).

$$S_{10z} = S_{5p} + S_{5v} \quad \text{Eq. 3-12}$$

- Five-point peak height (S_{5p})

This parameter is defined as the average value of the heights of the five peaks with largest global peak height, within the definition area

- Five-point pit height (S_{5v})

This parameter is defined as the average value of the heights of the five pits with largest global pit height, within the definition area

- Mean dale area (S_{da})

The S_{da} parameter is the average area of dales connected to the edge at a designated height.

- Mean hill area (S_{ha})

The S_{ha} parameter is the average area of hills connected to the edge at a designated height.

- Mean dale volume (S_{dv})

The S_{dv} parameter is the average volume of dales connected to the edge at a designated height.

- Mean hill volume (S_{hv})

The S_{hv} parameter is the average volume of hills connected to the edge at a designated height.

3.3.3.7 Geometrical parameters; Fourier transform

Other than the above-mentioned parameters, ISO 25178-2 briefly points to Fourier transformation. The 2D Fourier transform is a powerful tool in image processing that can decompose a matrix or an image to frequency domain. Two main components can be extracted from each image: magnitude and phase. Briefly, the magnitude tells "how much" of a certain frequency component is present and the phase tells "where" the frequency component is in the image.

$$F(p, q) = \iint_A z(x, y) e^{-(ipx+iqy)} dx dy \quad \text{Eq. 3-13}$$

3.3.3.8 Fractal Dimension

A fractal is an object that looks approximately the same over some range of scales or magnification. The fractal dimension is a measure of the geometric complexity or intricacy components of a fractal or partially fractal surface. The fractal dimension increases with increasing complexity. It has a supportive application in correlations with friction, grinding condition, adhesion and gloss. Variation method applied to the test surfaces for calculation of fractal dimension based on international standard ISO 25178-2.

$$D_v = \lim_{s \rightarrow +0} \left(3 - \frac{d(\log_e[F(s)])}{d[\log_e(s)]} \right) \quad \text{Eq. 3-14}$$

3.3.4 Demonstration of the results

A script was generated in MATLAB to process the obtained surface matrices and calculate all the above-mentioned roughness parameters. The results are summarized in appendices A, B and C. Since this study investigates a pavement surface with a focus on the texture quality as well as any abnormalities which may compromise the quality and can be considered as pavement flaw, it is aimed to avoid outlier's removal. To simplify the demonstration of datasets, box-whisker plot system was selected. A box-whisker plot by summarizing variation in large dataset and showing outliers, can compare multiple distributions visually and can also indicate symmetry and skewness of obtained results to a degree.

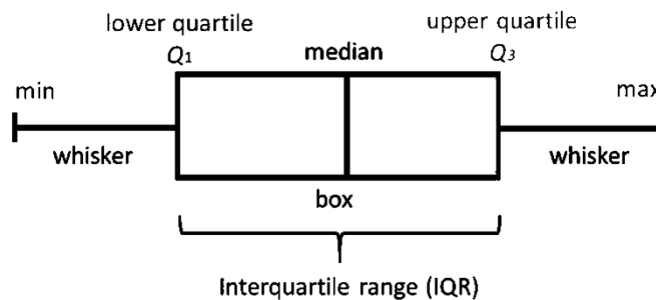


Figure 3-21, Components of a box-whisker plot

CHAPTER 4

PHASE I, CHARACTERIZATION OF RCC PAVEMENT SURFACE THROUGH SGC SAMPLES

In this chapter, height parameters of RCC and HMA pavement textures prepared by the roller compacter and the super-pave gyratory compacter are compared and discussed. The goal that this chapter is investigating the similarity of surface texture of pavements produced with different mixture parameters, materials and compaction techniques.

4.1 Influence of the Mixture Parameters and Compaction Methods on Surface Texture

The production of RCC pavement samples in lab, due to the requirement of roller compactors, excessive size and weight of samples, and the required manpower make it challenging to conduct studies in this field. Alternative compaction techniques, like gyratory compaction (Superpave compactor) that facilitate the production of samples in smaller size, are being used for studying the mechanical properties of RCC pavements. However, the representativeness of these samples (in terms of their surface texture) to the actual texture that is generated with roller compactors is the point of concern. This section compares the generated texture under different compaction methods for both RCC and HMA to verify the similarity of the surface finish. It is also tried to seek influence of mixture parameters such as binder and water content on surface texture investigating height parameters.

4.1.1 Maximum peak height (S_p)

A comparison on maximum peak height parameters is presented in Figure 4-1 and Figure 4-2. Considering Superpave gyratory compacted concrete samples which are denoted by SGCC, an apparent trend is seen with the change of water content inside the mixes of the same group, which by the increase in water content, S_p tends to decrease (Figure 4-1). Furthermore, with increase in the binder content from 200 to 400 kg/m³, a decrease in maximum peak height parameter is observed. Considering influence of the compaction method, it is seen that all HMA samples as well as the RCC samples, with an increase in maximum aggregate size from 12 mm to 19 mm, a significant increase in S_p can be seen. However, this change in maximum aggregate size does not lead to a noticeable change in S_p for the SGCC group (Figure 4-2). Other than RCC-300-19, concrete samples have slightly lower maximum peak height comparing to HMA samples.

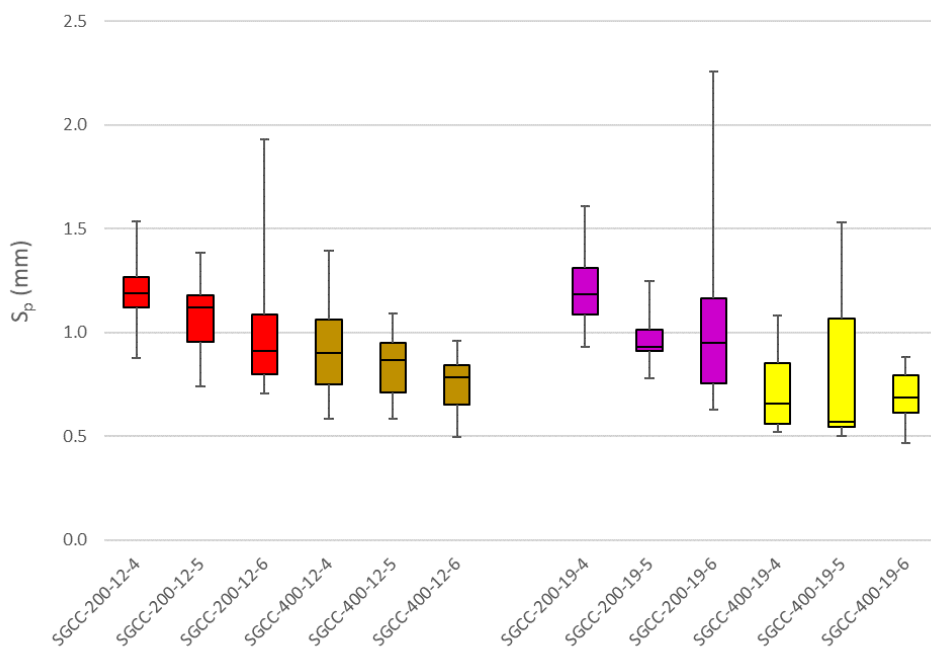


Figure 4-1, Effect of mixture parameters (binder content, water content and maximum aggregate size) on the Maximum peak height (S_p)

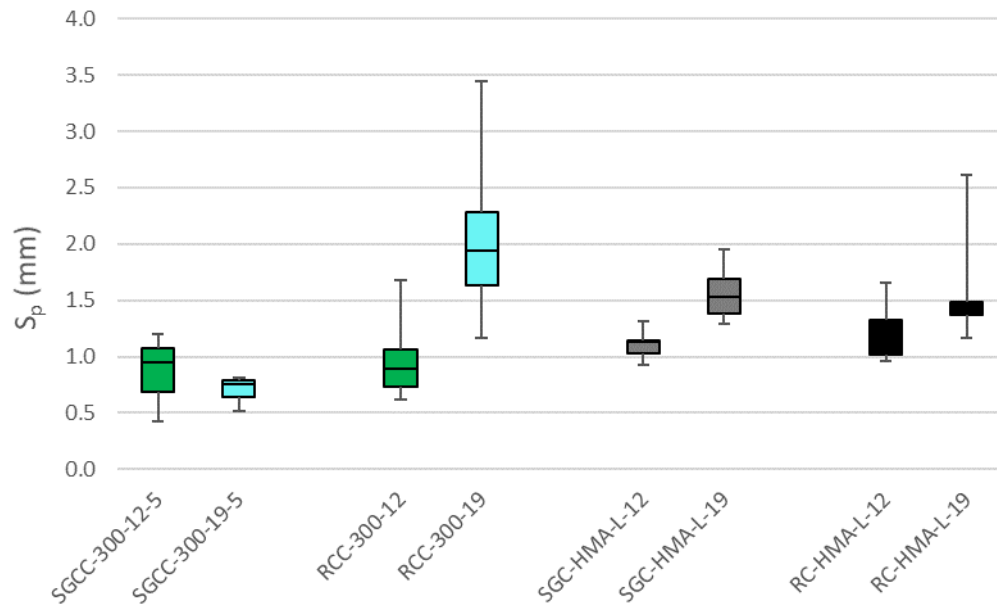


Figure 4-2, Effect of compaction (SGC and DDCHR) and binder types (cement and HMA) on the maximum peak-height parameter (S_p)

It can be concluded that the maximum aggregate size does not play an important role while concrete mix is being compacted with gyratory compactor. However, its effect on roller compaction is not negligible. Considering HMA, the change in maximum aggregate size in both compaction methods makes a difference in S_p value, and the larger D_{max} yields higher peaks.

4.1.2 Maximum valley depth (S_v)

Considering the maximum valley depth, both SGCC and RCC groups show a decrease in S_v as water content increases (Figure 4-3). Similar to S_p , Figure 4-4 shows a jump in S_v value for RCC samples and all HMA samples with increase in maximum aggregate size. However change in maximum aggregate size is not effective for super-pave gyratory compacted concrete.

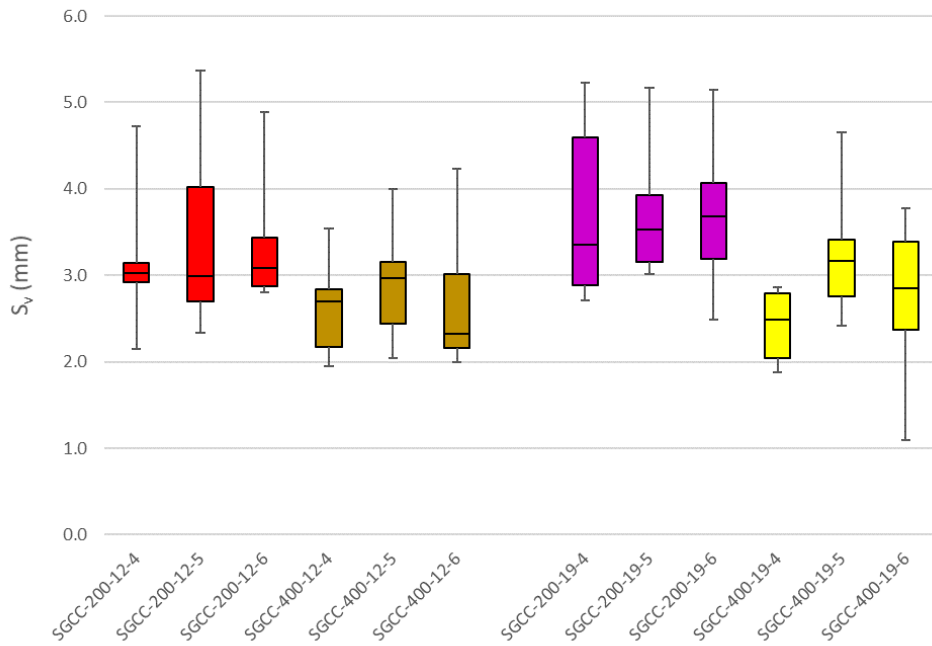


Figure 4-3, Effect of mixture parameters (binder content, water content and maximum aggregate size) on the Maximum valley depth (S_v)

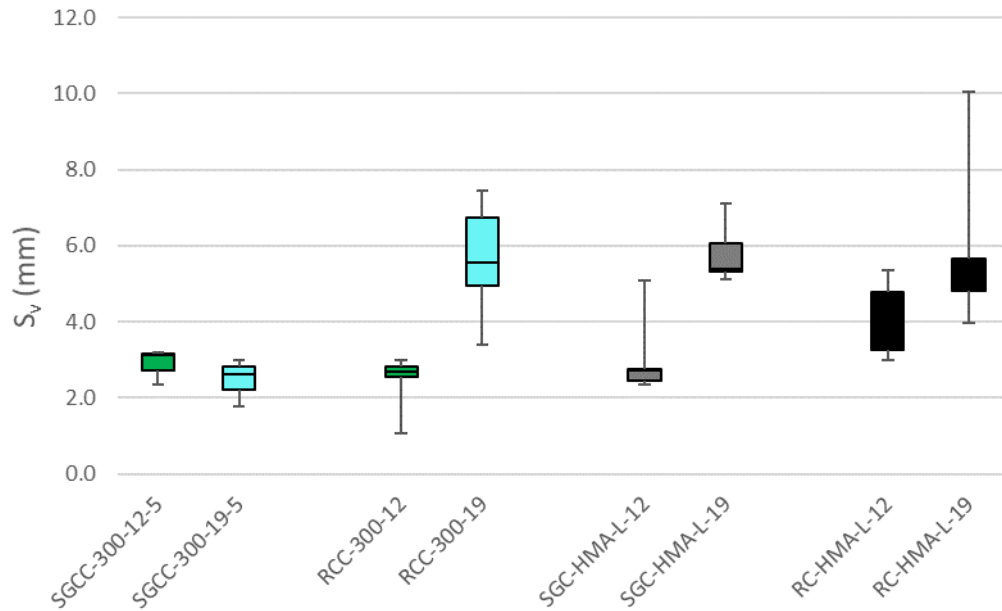


Figure 4-4, Effect of compaction (SGC and DDCHR) and binder types (cement and HMA) on the Maximum valley depth (S_v)

4.1.3 Maximum height (S_z)

Maximum height is the summation of peak heights and valley depths; hence it is not surprising to see results similar to the previous two parameters. It is seen that the change in water content of mixes compacted by SGC shows no considerable change in maximum height (Figure 4-5). However, the increase in cement content reduces the maximum height. Figure 4-6 makes a comparison between compaction methods of the RCC and HMA samples, the influence of D_{max} on the maximum height of the SGC concrete is not sensible. Nonetheless, it should be noted that S_a , S_v , and S_z are obtained based on a single profound point of each surface and susceptible to bear error. To achieve a definitive conclusion, further investigation is required.

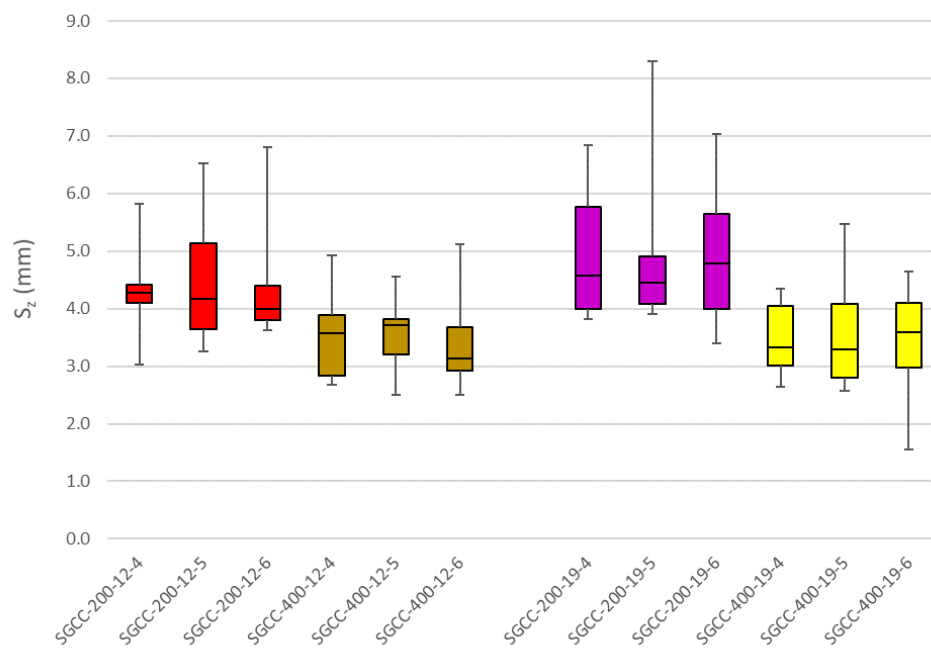


Figure 4-5, Effect of mixture parameters (binder content, water content and maximum aggregate size) on the Maximum height (S_z)

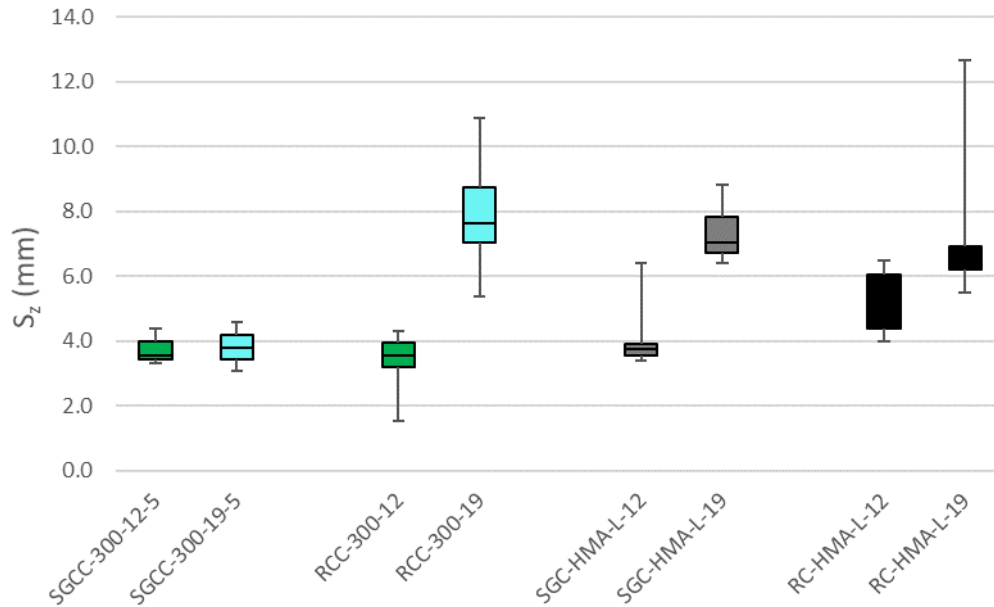


Figure 4-6, Effect of compaction (SGC and DDCHR) and binder types (cement and HMA) on the Maximum height (S_z)

4.1.4 Arithmetical mean height (S_a)

Figure 4-7 and Figure 4-8 illustrate a comparison of S_a throughout the samples. This parameter is prone to less error compared to S_p , S_v , and S_z , hence, provides higher reliability. The overall view is similar to the previous comparisons, just the uniformity in results has been increased. The water content effect is not deniable. By the increase in water content, S_a decreases (Figure 4-7). The same trend is traceable for the cement content increase which cause a decrease in arithmetical mean height. However, aggregate size effect is an exception. The aggregate size influence on the arithmetical mean height for gyratory compacted samples is negligible, while it causes a noticeable escalation for roller compacted concrete sample as well as all HMA samples (Figure 4-8).

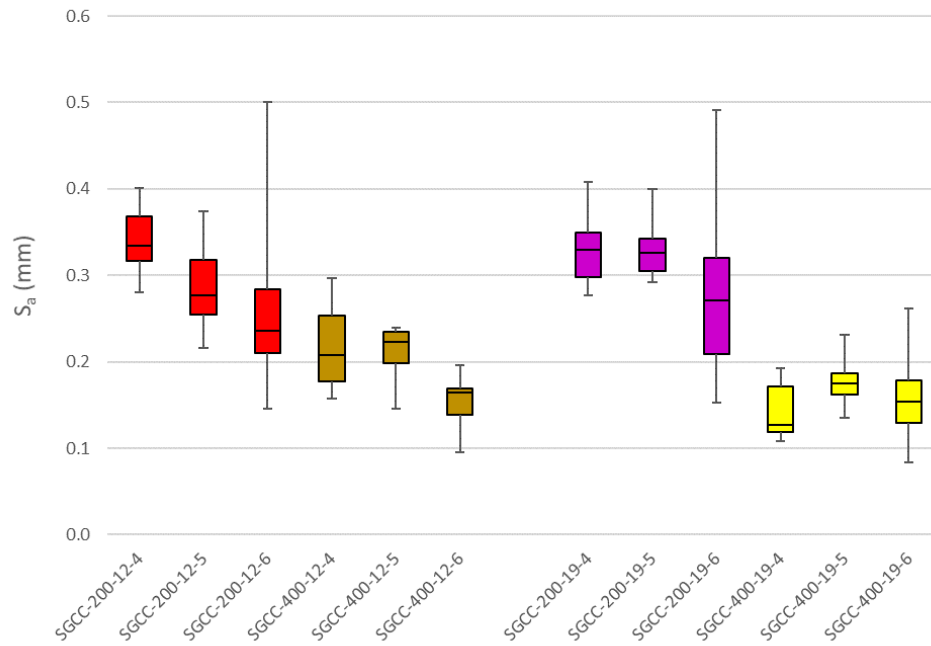


Figure 4-7, Effect of mixture parameters (binder content, water content and maximum aggregate size) on the Arithmetical mean height (S_a)

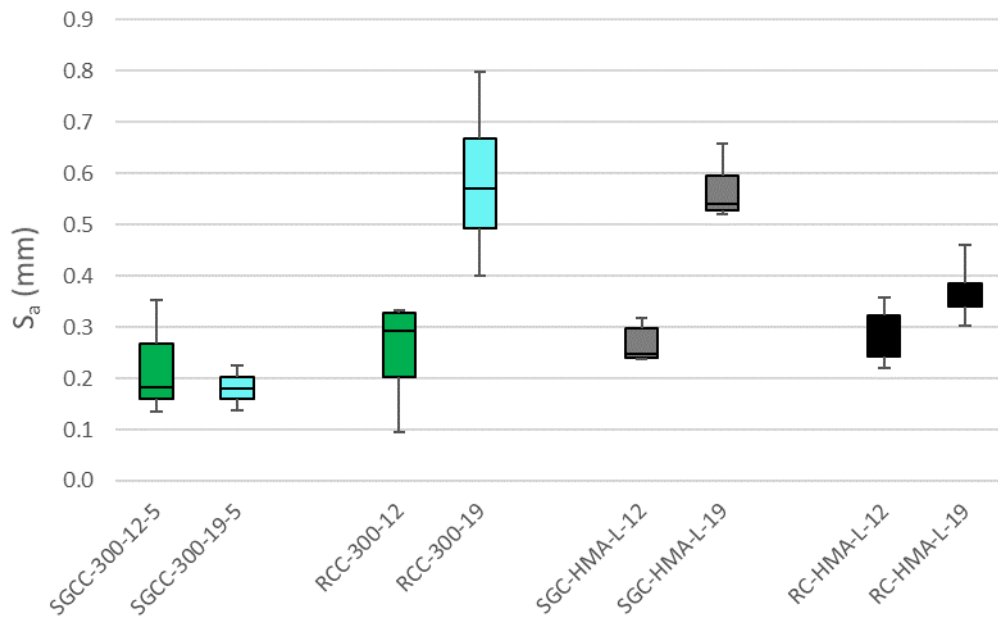


Figure 4-8, Effect of compaction (SGC and DDCHR) and binder types (cement and HMA) on the Arithmetical mean height (S_a)

4.1.5 Root mean square height (S_q)

Root mean square height is one of the best measures to assess the texture height of surfaces. It can be seen in Figure 4-10, the aggregate size does not have an influence on the height parameter of the SGC concrete. S_q changes by the change in water content (Figure 4-9) and cement content of the mixtures. Unlike the SGC concrete, RCC and HMA samples show a significant increase in root mean square height by using larger aggregate size. In addition, RCC samples with 19 mm aggregate size show less uniformity to other samples in terms of S_q .

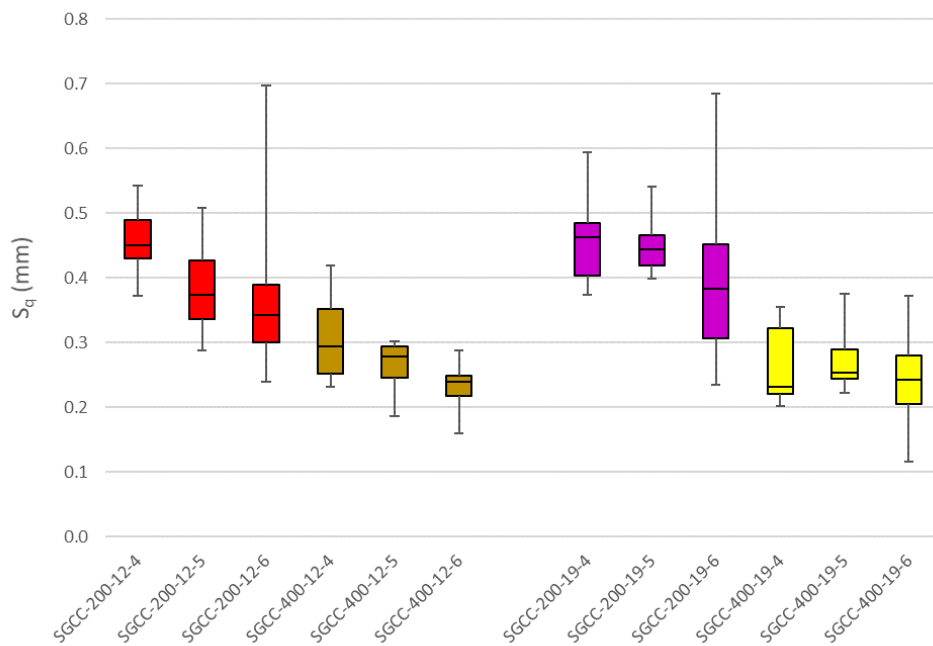


Figure 4-9, Effect of mixture parameters (binder content, water content and maximum aggregate size) on the Root mean square height (S_q)

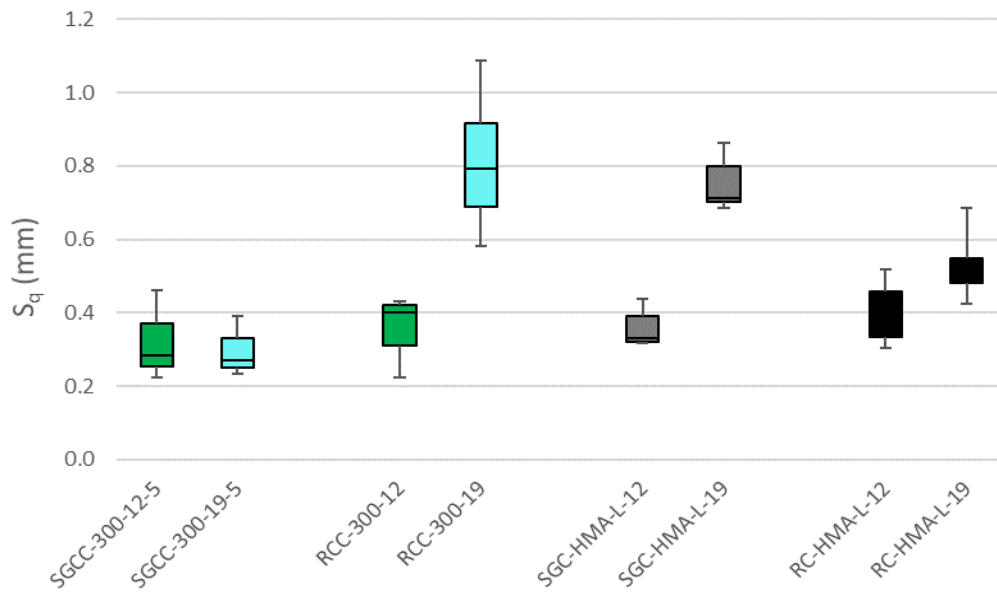


Figure 4-10, Effect of compaction (SGC and DDCHR) and binder types (cement and HMA) on the Root mean square height (S_q)

4.1.6 Skewness (S_{sk})

Figure 4-12 and Figure 4-13 illustrate a comparison in the skewness parameter of the samples. Skewness is a measure of the asymmetry of the probability distribution of peaks and pits about the mean plane. Negative values mean height distribution is skewed above the mean plane. In other words, the more negative the skewness value is, the beefier the peaks are (Figure 4-11). This parameter is suitable for evaluating surface abrasion. It is seen that HMA samples produce better uniformity in terms of skewness than concrete surfaces. Furthermore, the skewness decreases with an increase in paste content (water and binder).

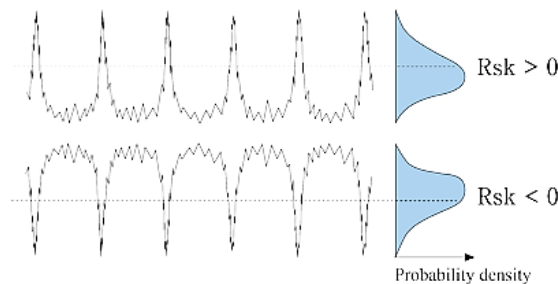


Figure 4-11, Schematic illustration of skewness variation (in 2D profiles skewness is denoted as R_{sk})

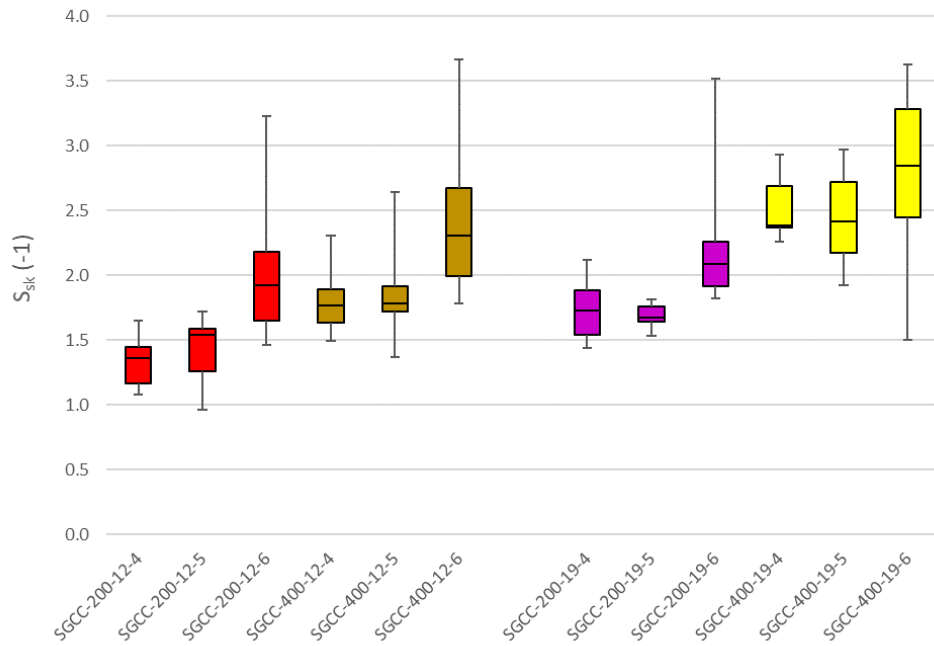


Figure 4-12, Effect of mixture parameters (binder content, water content and maximum aggregate size) on the Skewness (S_{sk})

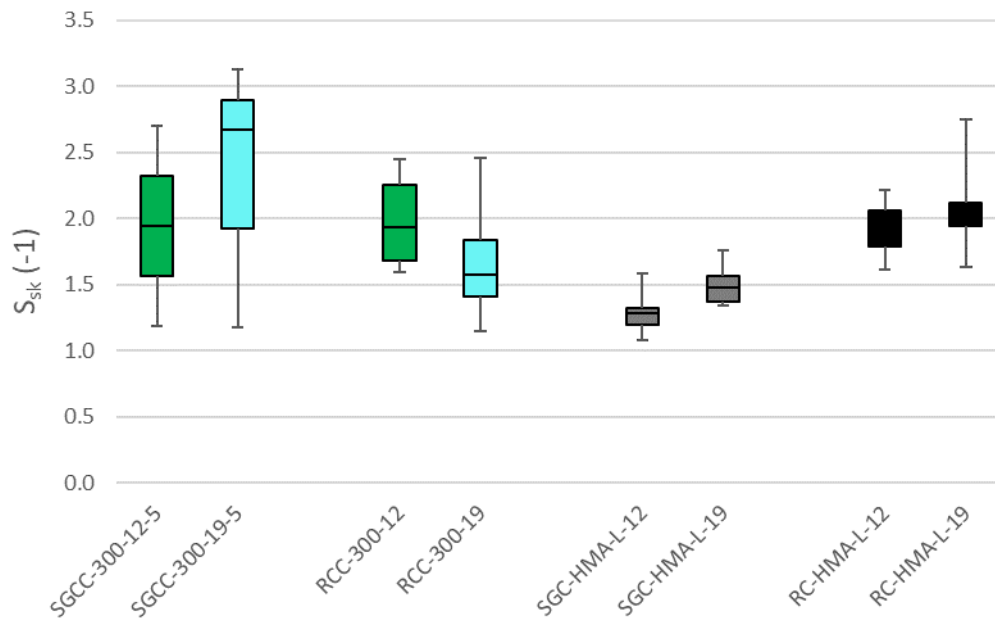


Figure 4-13, Effect of compaction (SGC and DDCHR) and binder types (cement and HMA) on the Skewness (S_{sk})

4.1.7 Kurtosis (S_{ku})

Figure 4-15 and Figure 4-16 give kurtosis values of compared samples. This parameter is a measure of the sharpness of peaks and pits. A texture with an S_{ku} value equals to 3 is defined normal for height distribution. It is seen in Figure 4-16 that the S_{ku} values for all samples are greater than 3, which means the height distribution is spiked. It is observe that HMA can produce more uniform texture in terms of kurtosis. In addition, increase in paste content of SGC concrete samples increased kurtosis value of the textures.

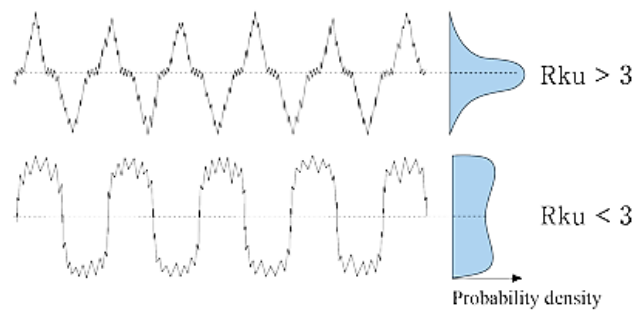


Figure 4-14, Schematic illustration of kurtosis variation (in 2D profiles skewness is denoted as R_{ku})

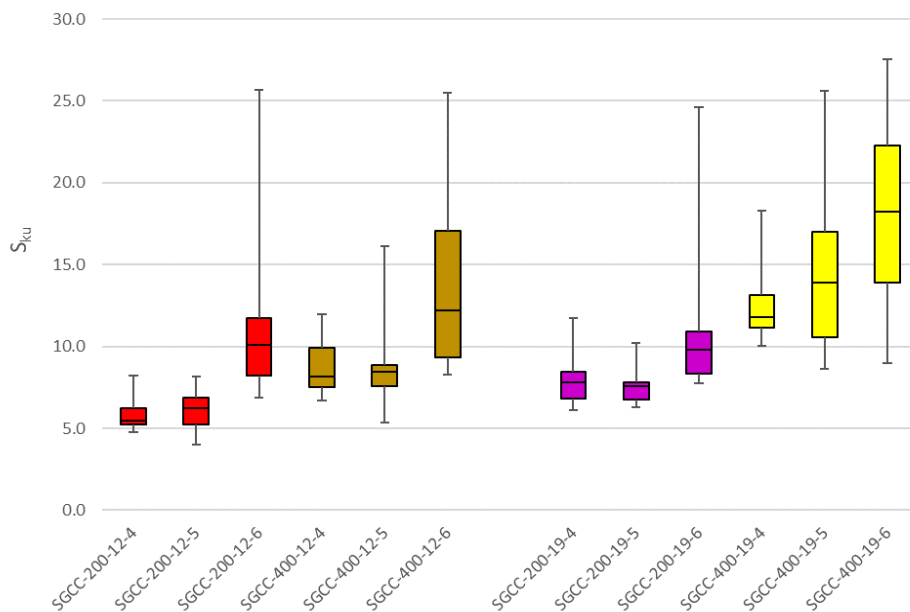


Figure 4-15, Effect of mixture parameters (binder content, water content and maximum aggregate size) on the Kurtosis (S_{ku})

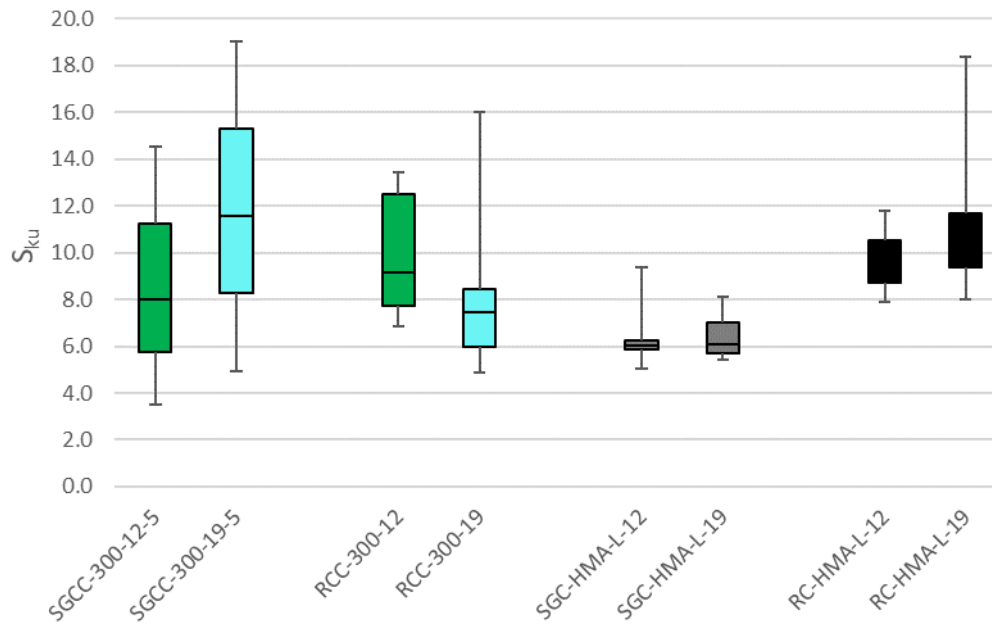


Figure 4-16, Effect of compaction (SGC and DDCHR) and binder types (cement and HMA) on the Kurtosis (S_{ku})

4.1.8 Conclusion

The texture of study mixes in terms of height parameters were investigated and effects of mixture parameters such as binder content, water content and maximum aggregate size were discussed. Furthermore, the influence of two compaction method (SGC and DDCHR) on concrete and HMA mixtures were studied. It was shown that increase in water content of a mix, tends to decrease peaks height. A similar influence was observed for increase in cement content. For both cases, it is contributed to change in total paste volume which provides extra materials to fill the valleys and decrease peak heights. As a result of having a comparison between the two different compaction methods, it is concluded that although both methods can provide maximum possible compaction, the generated textures are not identical and the surface texture of SGC is not representing the DDCHR. This imposes investigation of pavement texture to be limited on roller compaction techniques which cannot be readily available for laboratory environment sample production.

CHAPTER 5

PHASE II, COMPARISON OF TEXTURE OF RCC AND HMA PAVEMENTS

In this chapter, it is intended to compare RCC and HMA pavements' textures compacted by the DDVHR technique. Firstly, the comparison between texture parameters is studied. The main goal at this stage is the observation of similarities and differences of surface texture on RCC and HMA pavements. Secondly, this comparison is extended to macro-texture and micro-texture. Finally, regressions and data analyses are conducted to determine any possible correlation between texture parameters and conventional macro-texture and micro-texture testing results.

5.1 Similarity Investigation of RCC And HMA Texture Through Roughness Parameters

Conformity of RCC surfaces to HMA is the point of interest in this chapter. For this purpose, all of the surface parameters addressed in ISO 25178-2 were computed and brought to comparison in box-whisker graphs for better understanding of the similarities or differences.

5.1.1 Height Parameters

Calculation of all seven height parameters was completed on roller compacted samples. Three of these parameters, maximum peak height, maximum valley depth and maximum height are susceptible to be influenced with isolated high or low points, hence they were not included in the comparison. Figure 5-1 demonstrates comparisons of Arithmetical mean height and Root mean square height parameters. An increase in both parameters with change in maximum aggregate size is seen.

However, this increase is considerably significant for concrete samples. A slight decrease trend is also seen with an increase in cement content of concrete samples. This can be related to accumulation of excess paste in texture valleys. Another noticeable difference is the broad range of results on concrete samples to the asphalt samples. This can be interpreted as a lack of uniformity in terms of texture height for RCC pavement.

Skewness was previously described as a measure of asymmetry of texture irregularities about the mean plane and it is suitable for evaluating abrasion of texture. As it is seen in Figure 5-2, both concrete and asphalt samples produced in the lab show similar skewness values. It should be noted that all samples are new and have not yet been subjected to traffic and abrasion.

Comparison of Kurtosis of textures is shown in Figure 5-2 as well. This parameter which relates to the tip geometry of peaks and valleys is suitable for analyzing the degree of contact between two objects. It is interpreted from the comparison that asphalt texture shows a higher degree of contact to the concrete samples.

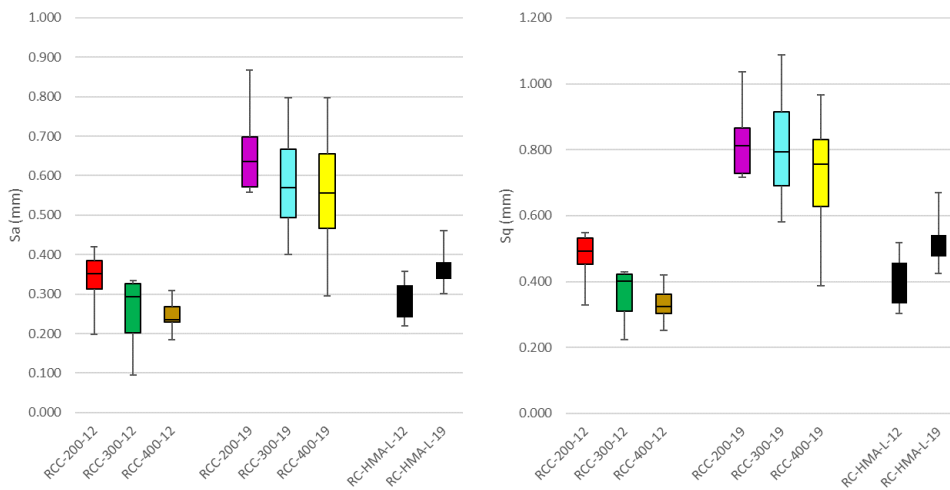


Figure 5-1, Effect of binder type and content, and maximum aggregate size on the Arithmetical mean height (S_a) and the Root mean square height (S_q)

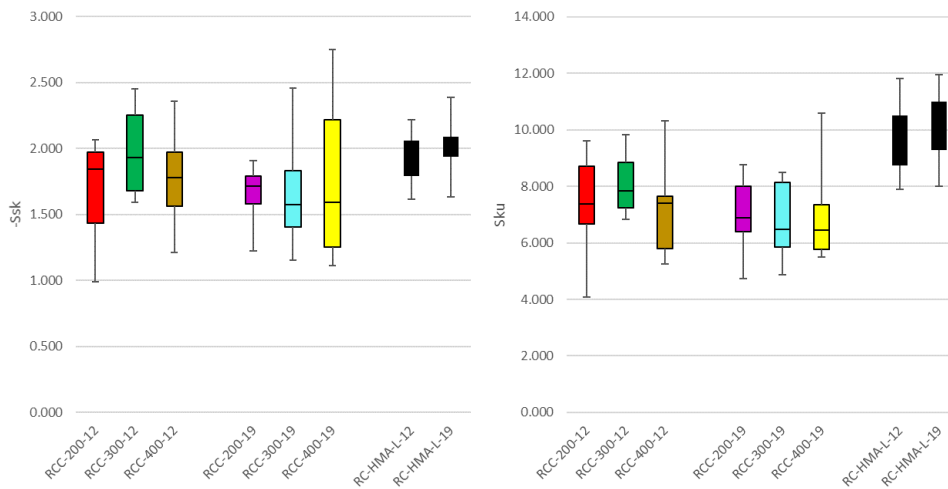


Figure 5-2, Effect of binder type and content, and maximum aggregate size on the Skewness (S_{sk}) and the kurtosis (S_{ku})

5.1.2 Spatial Parameters

S_{tr} or texture aspect ratio is a measure of uniformity of spread of texture direction, so it can be used to determine the presence of a surface pattern. Figure 5-3 shows both asphalt and concrete pavement are similar in terms of uniformity of spread of texture direction and both produce similar surface patterns. S_{al} or Autocorrelation length determines the distance at which the autocorrelation decreases the fastest so it can be used to determine whether there is a point at which surface height changes suddenly and unexpectedly. It is seen in the figure that concrete pavement has a higher tendency to show an unexpected change in height compared to asphalt pavement and this can be even greater with an increase in maximum aggregate size.

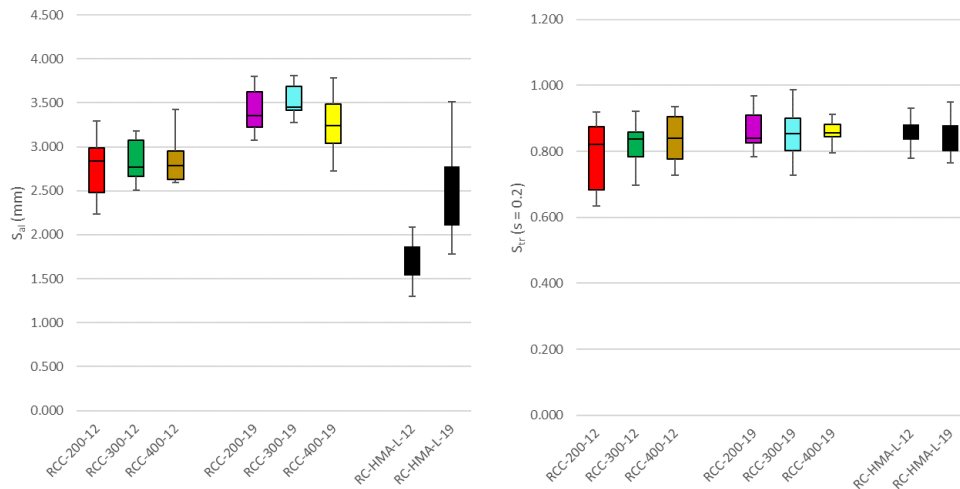


Figure 5-3, Effect of binder type and content, and maximum aggregate size on the Autocorrelation length (S_{at}) and the Texture aspect ratio (S_{tr})

5.1.3 Hybrid Parameters

Hybrid parameters account for both height and direction of texture, and they are measures for the determination of texture slope. Both Root mean square gradient, S_{dq} and Developed interfacial area ratio, S_{dr} of a completely leveled surface is zero. When a surface has any slope (texture), its S_{dq} and S_{dr} become larger. For instance, a plane surface with gradient components of 45 degrees (a corrugated plate similar to Figure 5-4) has an S_{dq} value of 1 and an S_{dr} value of 41.4 %.

Comparison of S_{dq} and S_{dr} values of concrete and asphalt pavement samples are shown in Figure 5-5. It can be concluded from S_{dq} comparison that asphalt pavement texture is more steeply inclined comparing to concrete. Furthermore, based on the S_{dr} comparison, the texture asphalt pavement generated is rougher and finer than the concrete texture.



Figure 5-4, A corrugated plate

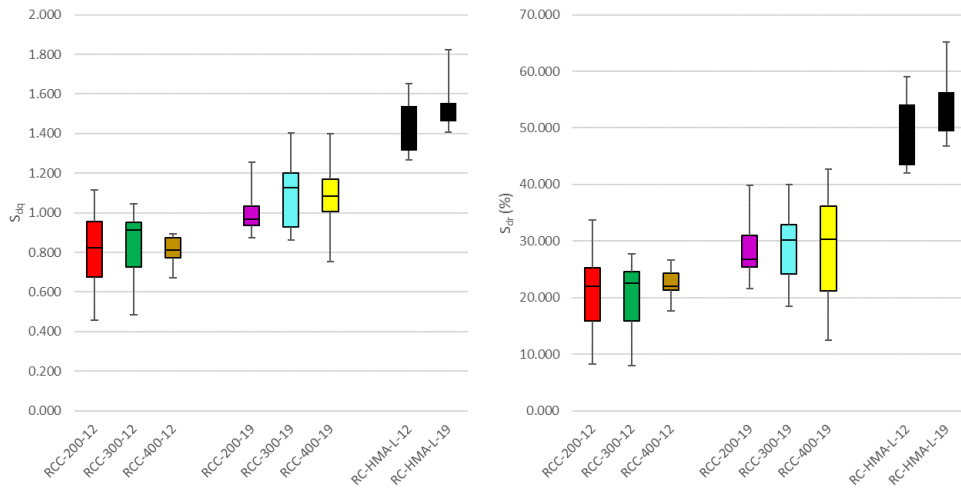


Figure 5-5, Effect of binder type and content, and maximum aggregate size on the Root mean square gradient (S_{dq}) and the Developed interfacial area ratio (S_{dr})

5.1.4 Functions and related Parameters

Function parameters divide the total height of texture into three portions, S_{pk} represents the average height of reduced peaks. The reduced peaks are the areas that are removed by initial abrasion. S_k represents the average height of core surface which is responsible for main contact of the surface and finally, S_{vk} represents the reduced valley height. The reduced valleys are the untouched areas of a surface that provides space to hold abrasion debris. It can be interpreted from Figure 5-6 concrete pavement with greater S_{pk} and S_{vk} to asphalt, leaves more room for abrasion and provides greater space to hold debris at the same time. Additionally, based on S_k comparison, greater average core height on concrete with 19 mm stone and greater macro-texture accordingly can be observed.

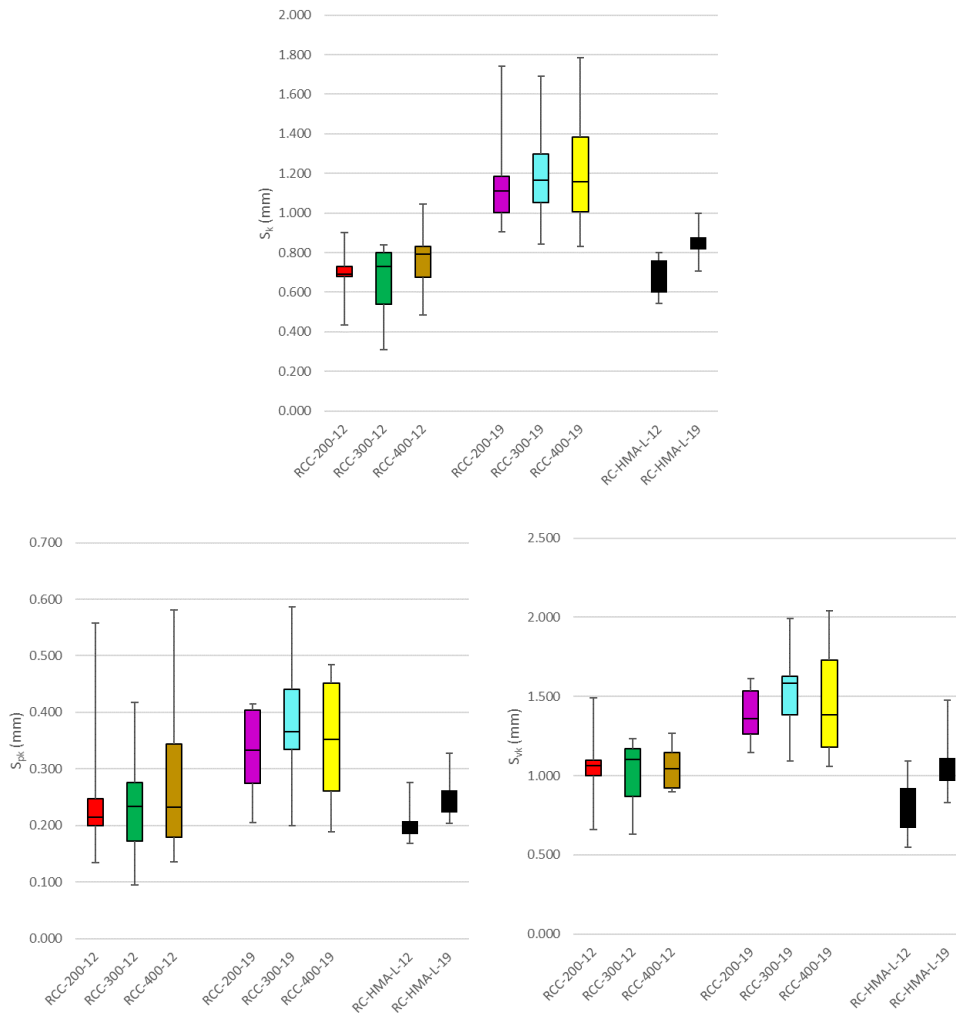


Figure 5-6, Effect of binder type and content, and maximum aggregate size on the Core height (S_k), the Reduced peak height (S_{pk}) and the Reduced valley height (S_{vk})

V_{mp} , V_{mc} , V_{vc} , and V_{vv} represent the volumes of the reduced peaks, core material, core void, and valley void, respectively. Figure 5-7 and Figure 5-8 show the normalized form of the parameters to their area. Importance of the mentioned parameters is because of their direct relationship to macro-texture. The comparisons clearly demonstrate that RCC can provide equal and greater macro-texture to asphalt. Influence of maximum aggregate size in the generated macro-texture is significant, especially for RCC pavement. It is seen that 12 mm stone for both pavement types can produce similar macro-texture, however, the generated macro-texture with 19 mm stone is considerably greater for RCC pavement.

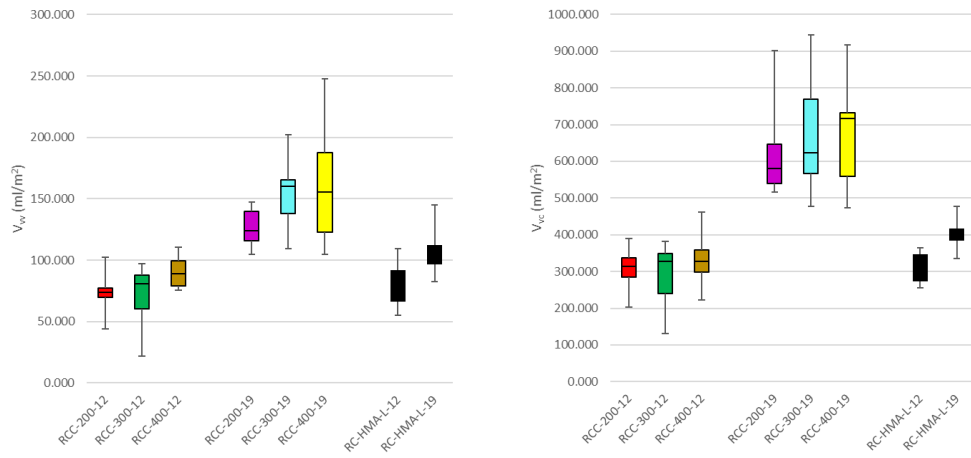


Figure 5-7, Effect of binder type and content, and maximum aggregate size on the Dale void volume (V_{vv}) and the Core void volume (V_{vc})

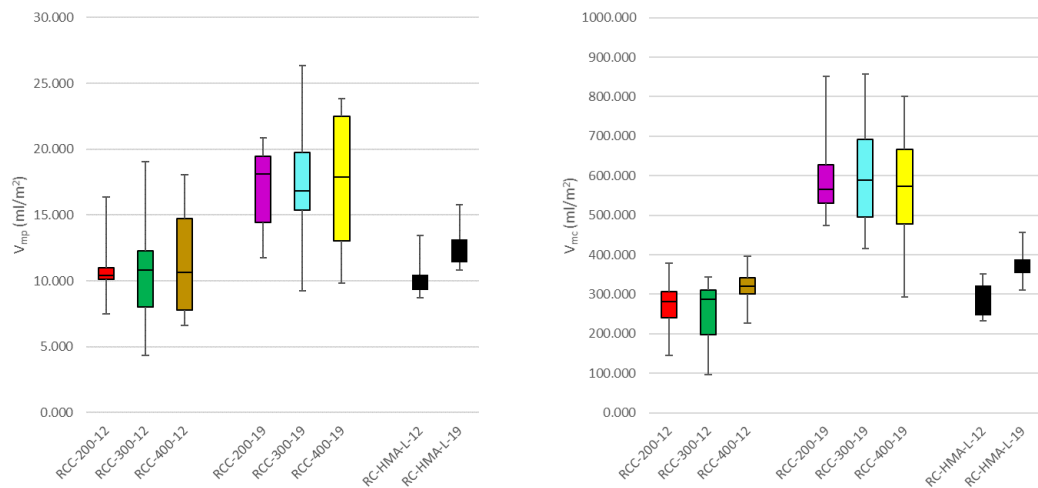


Figure 5-8, Effect of binder type and content, and maximum aggregate size on the Peak material volume (V_{mp}) and the Core material volume (V_{mc})

5.1.5 Miscellaneous Parameters

Std represents direction angle texture and orientation of grooves. Figure 5-9 shows the variation in texture direction of RCC samples is wider than asphalt samples. This shows the quality of texture is higher on asphalt compaction comparing to RCC compaction. Asphalt produces uniform texture under cylinder compactor while RCC is prone to get waviness from compaction.

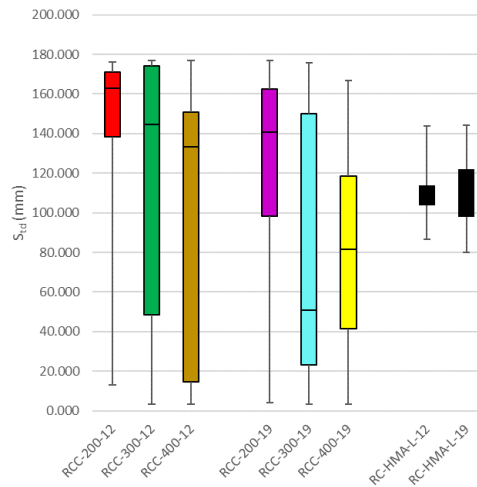


Figure 5-9, Effect of binder type and content, and maximum aggregate size on the Texture direction (S_d)

5.1.6 Feature Parameters

S_{pd} or density of peaks represents the number of peaks per unit area. A large number indicates more points of contact with other objects. The S_{pd} comparison shown in Figure 5-10 indicates a tremendous difference on the number of contact points between asphalt samples and RCC. Asphalt samples produced 4 to 7 times more contact points comparing to RCC samples. It is also observed with smaller maximum aggregate size, higher contact points can be achieved. Points of contact are one of the important factors on the friction of a surface.

S_{pc} or Arithmetic mean peak curvature represents shape of the points of contact. Larger values denote sharper shapes while smaller values indicate rounded contact points shape. The S_{pc} comparison given in Figure 5-10 indicates that shape of the contact points for asphalt samples is three times pointier than RCC samples. Shape of contact points is another effective factor on the friction of a surface.

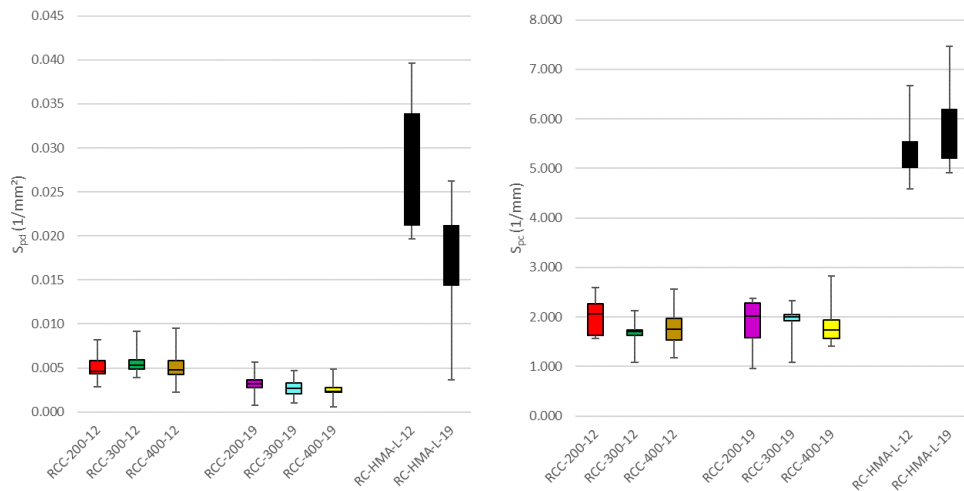


Figure 5-10, Effect of binder type and content, and maximum aggregate size on the Density of peaks (S_{pd}) and the Arithmetic mean peak curvature (S_{pc})

The other three feature parameters are S_{5p} , S_{pv} and S_{10z} . S_{5p} represents average value of the heights of five peaks with largest peak height. S_{5v} , similar to S_{5p} , represents average value of the heights of five pits with largest pit height and S_{10z} is the summation of the mentioned values. These parameters do not represent the whole surface and thus are not considered to be a reliable base of judgment in this study. Finally, segmentation analysis of the test surfaces is shown in Figure 5-11 and Figure 5-12 for area and volume, respectively. It is seen that RCC samples are generating coarser segments comparing to asphalt samples.

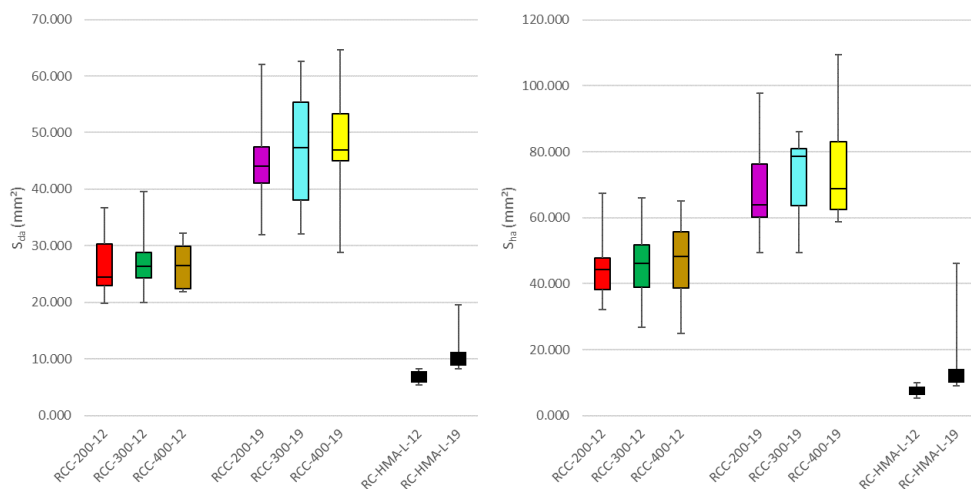


Figure 5-11, Effect of binder type and content, and maximum aggregate size on the Mean daled area (S_{da}) and the Mean heal area (S_{ha})

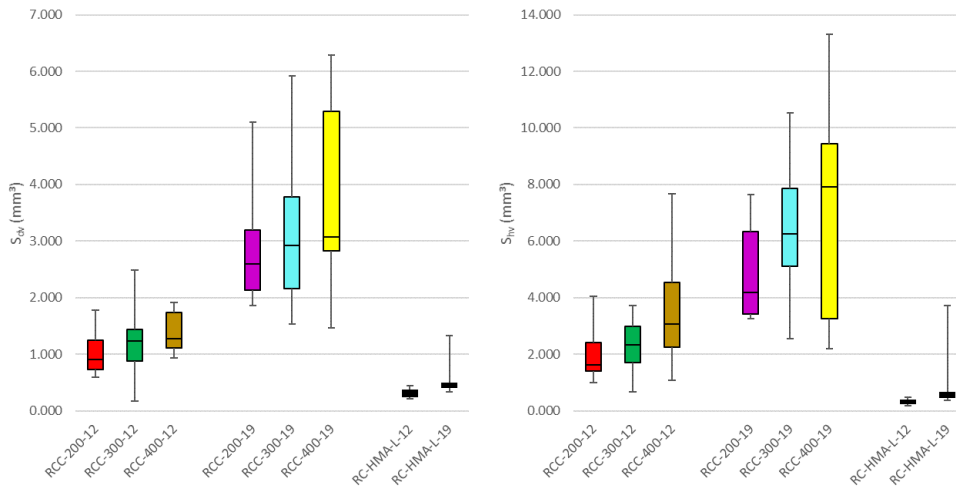


Figure 5-12, Effect of binder type and content, and maximum aggregate size on the Mean dale volume (S_{dv}) and the Mean hill volume (S_{hv})

5.2 Investigation of Macro-Texture

Macro-texture of pavement that refers to irregularities with a wavelength of 0.5 to 50 mm was mentioned previously as the main responsible factor for surface water drainage and tire noise. It contributes to the hysteresis component of friction as well. Macro-texture is expressed as mean texture depth (MTD) coming from sand patch test (ASTM E965) or mean profile depth (MPD) calculated from 2D profilers such as circular track meter (ASTM E2157). This section is allocated to investigation of Macro-texture on the study samples.

5.2.1 Mean Texture Depth, Mean Profile Depth and Mean Surface Depth

As discussed in paragraph 2.4.1.3, ASTM E2157 referencing PIARC reports an extremely high correlation between MPD and MTD. The test describes circular track meter as the apparatus for scanning texture and computing a 2D MPD afterward. It is expected that a 3D surface would give a more accurate result than a 2D profile. For this purpose, mean depth can be achieved by dividing volume of voids to the

area. The obtained depth value was called mean surface depth (MSD) in this study. For validation purpose, sand patch test was conducted on super-pave gyratory compacted samples and MTD's were measured. Figure 5-13 demonstrates MSD's to their corresponding MTD's. It appears that MSD's of the surfaces is greater than its actual MTD values. In addition, a significant error on some of the measured values is obvious. A close examination on surfaces with error revealed that any localized feature such as a loose particle or an abnormal peak (a significantly high peak compared to other peaks), could elevate the top plane of the measured area and generate illogical results. It is recommended in literature to avoid abnormal chips on surface for conducting sand patch test as well. To overcome this problem in calculating voids volume, the top plane was shifted down based on the peaks' material ratio, then the coefficients of determination (R^2) were compared. There was an impressive improvement in coefficient of determination while the top plane positioned at 10% of peaks' material ratio.

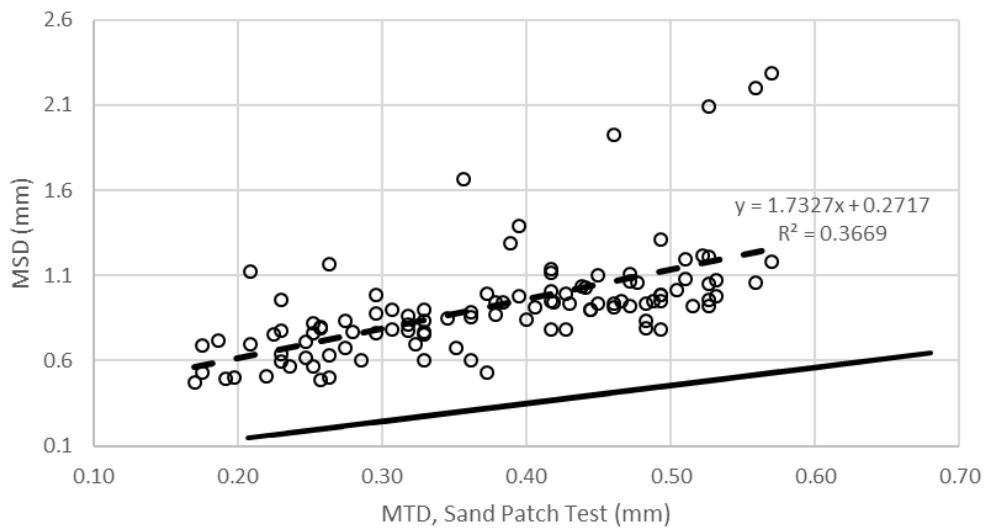


Figure 5-13, Mean surface texture (uncorrected) correlation with sand patch test results, Dashed line is regression of the test, Solid line gives the estimate of PIARC model.

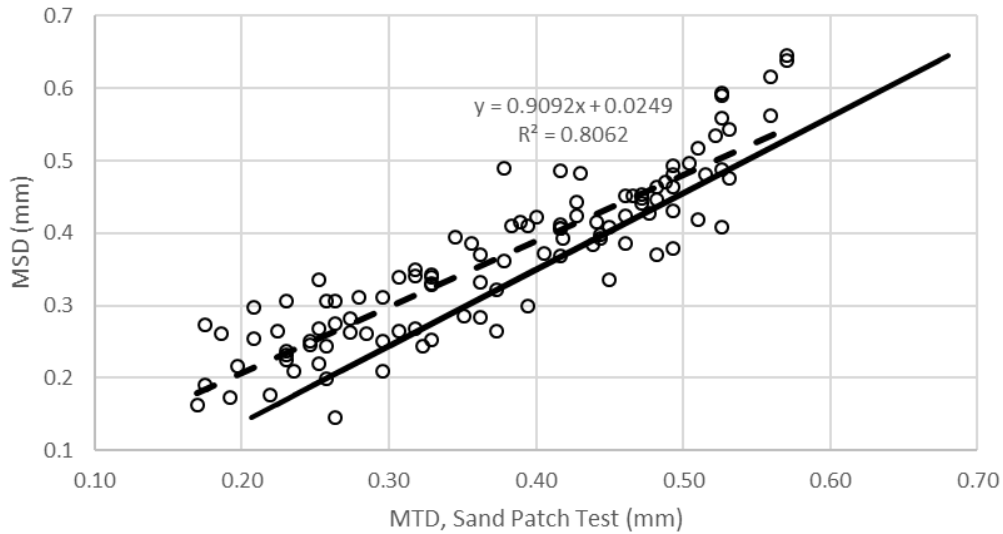


Figure 5-14, Mean surface texture (measured at 10% of peaks' material ratio) correlation with sand patch test results, the Dashed line is regression of the test, Solid line gives the estimate of PIARC model.

Measurement of MSD based on the volume of voids between 10% to 100% of peaks' material ratio exhibits a strong correlation with MTD data. Figure 5-14 demonstrates a strong similarity between the linear regression model (Eq. 4-1) and the one recommended by PIARC (Eq. 4-2). The average relative errors were 12.53% and 13.31%, respectively.

$$\text{Study model: } e\text{MTD} = 0.909 \text{ MSD} + 0.025 \quad \text{Eq. 4-1}$$

$$\text{PIARC model: } e\text{MTD} = 0.947 \text{ MPD} + 0.069 \quad \text{Eq. 4-2}$$

5.2.2 Investigation of RCC Macro-texture based on MSD

Understanding the fact that how mean texture depth can be estimated from 3D surfaces, facilitates the investigation of macro-texture of scanned surfaces and its affecting factors.

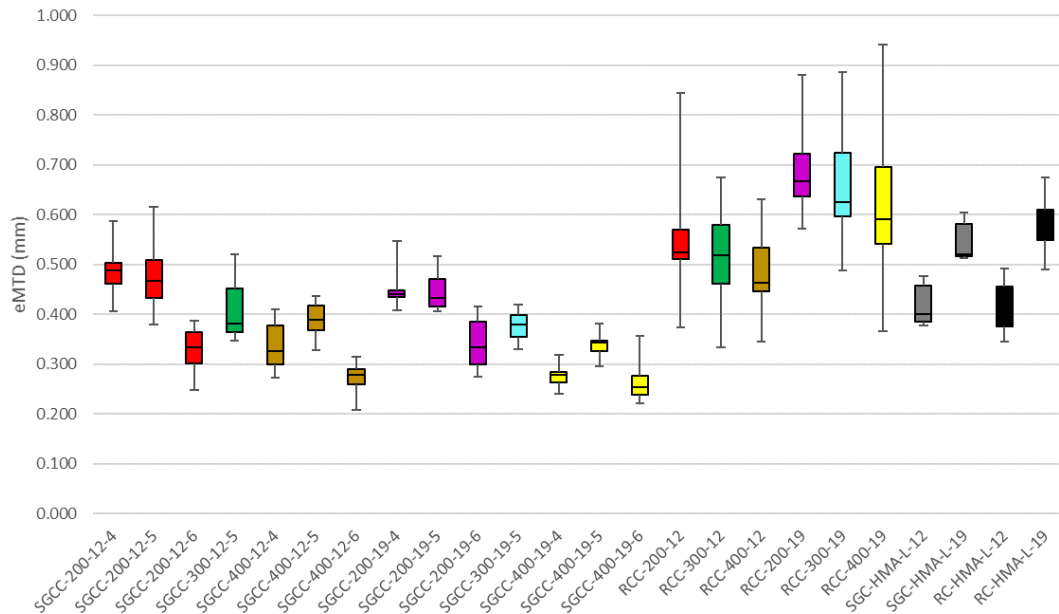


Figure 5-15, Comparison of estimated mean texture depth (eMTD) on various surfaces.

Figure 5-15 presents a comparison of macro-texture between concrete and asphalt, gyratory compaction and roller compaction, aggregate size, cement and water content. As discussed above, samples compacted with roller compactor obviously show macro-texture greater than the samples compacted with the gyratory compactor. Speaking of gyratory compacted samples, it is seen that the increase in water content of the mixes reduces the macro-texture. However, the change in the maximum aggregate size and cement content does not change the eMTDs. This can be associated with the high shear function of the compactor, which pushes the paste out of the matrix and fills the gaps between aggregate on the surface of the samples. On the flip side, roller compacted concrete samples have shown a better performance in terms of macro-texture. At a glance, the increase in the volume of macro-texture because of using a larger aggregate size is obvious. However, there is no intense change seen by the change in cement content. Yet, the broader range of results for each mix denotes weaker uniformity on RCC surface texture.

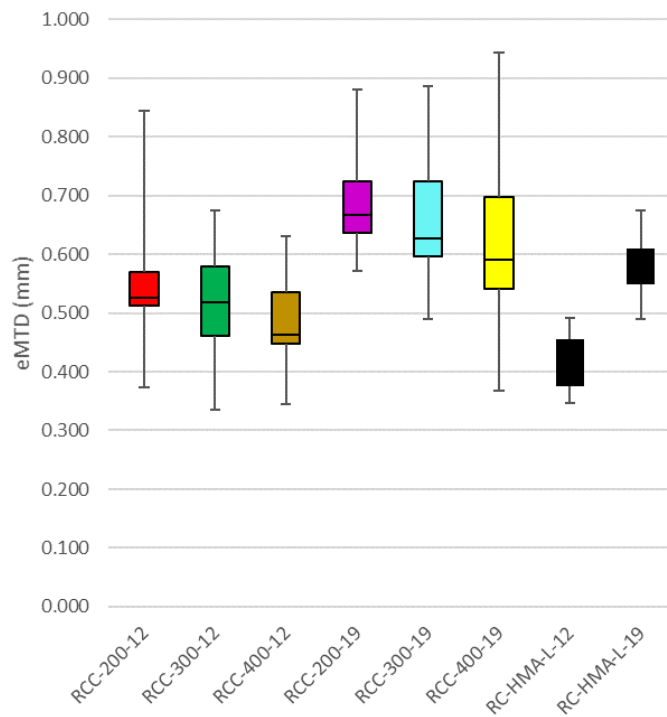


Figure 5-16, Macro-texture difference between RCC texture and roller compacted asphalt texture

The contrast in macro-texture of RCC and roller compacted asphalt (Figure 5-16), sounds promising for surface water drainage. The comparison exhibits that RCC produces a macro-texture slightly greater than the surface of asphalt pavement, which can enhance surface water drainage and reduce the risk of hydroplaning. However, the macro-texture of RCC shows and MTD slightly greater and less consistent compared to the macro-texture of paved asphalt, which can affect travel noise and tire wear.

5.3 Investigation of Micro-Texture

Previously, micro-texture that refers to the irregularities smaller than half millimeters (which are found on surface of coarse aggregate particles or surface of binder) was discussed. The lack of proper methods to measure and quantify micro-texture has

made researchers to introduce indirect methods for this purpose. Significant dependence of road surface texture and its skid resistance with vehicle tires has given micro-texture a friction-based definition. This section focuses on the skid resistance measurement of the surfaces to investigate the effect of mixture proportions, nominal aggregate size, compaction method, and binder types on the skid resistance. Moreover, it is aimed to seek a relationship between the surface roughness parameters and the skid resistance, in order to introduce an alternative method for quantifying micro-texture.

5.3.1 Skid resistance and affecting variables

Figure 5-17 gives the results of the British pendulum tester that was conducted on the surface of SGCC samples. It is obviously seen that dry skid resistance on all surfaces is high compared to the wet condition, which is expected because a film of water plays a lubricating role between the rubber head of the tester and the test surface. A decrease in BPN after introducing water to the surfaces is measured to be between 2 to 15%. The comparison of BPN within concrete samples shows a skid resistance decrease trend with the increase in cement content of the samples. This can be related to the paste to the aggregate ratio of the mixtures. The compaction of mixes with higher paste content moves more paste to the top surface, hence a less coarse aggregate surface becomes exposed. Furthermore, surprisingly, the maximum aggregate size does not show a significant change in BPN. Moreover, by comparing concrete and HMA results, the skid resistance of HMA stands higher by 11% on average for both maximum aggregate sizes. The greatest BPN was achieved by HMA samples designed with 19 mm aggregate size. It has to be noted that all the surfaces were unexposed to any kind of wear, and the aggregates on the surface were coated with binder, hence the type of binder contributes to the achieved skid resistance.

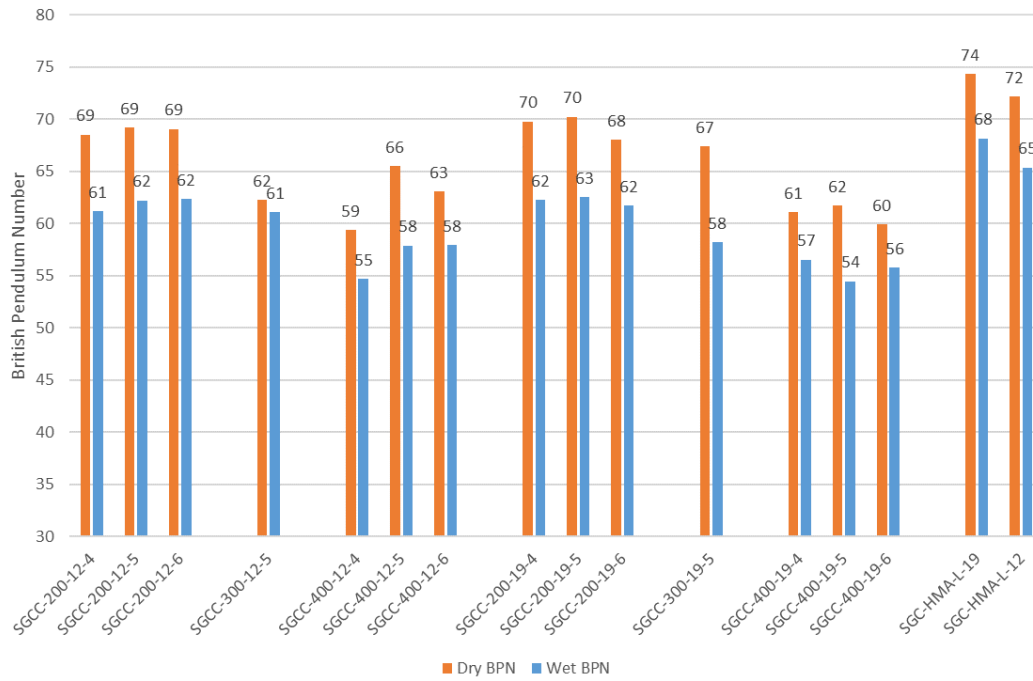


Figure 5-17, Skid resistance of gyratory compacted surfaces at wet and dry conditions

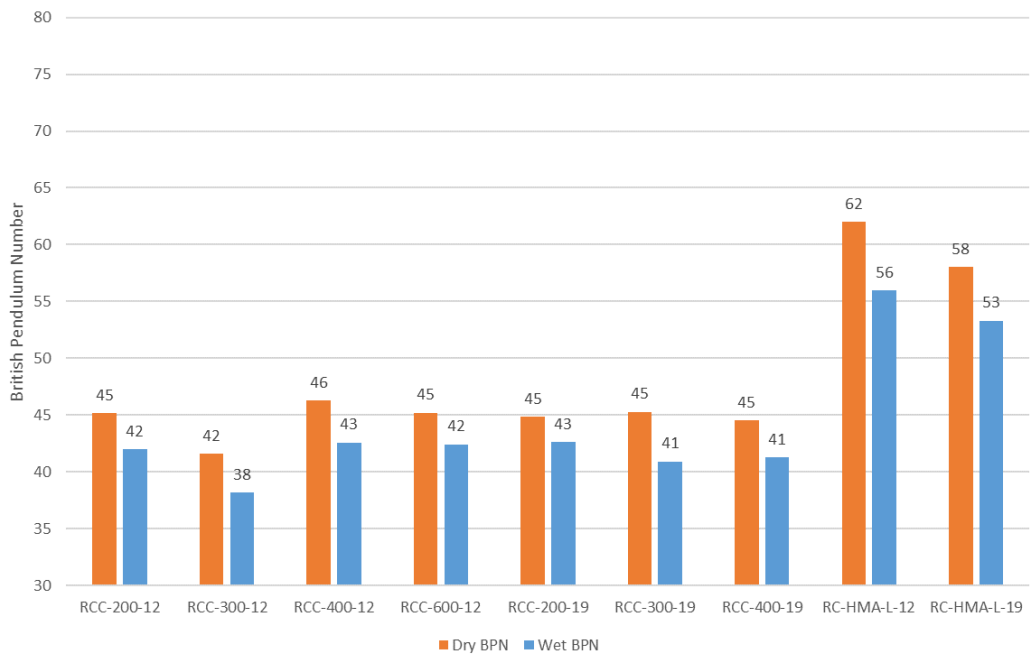


Figure 5-18, Skid resistance of roller compacted surfaces at wet and dry conditions

Figure 5-18 shows the result of roller compacted surfaces subjected to British pendulum tester. It is seen that the effect of maximum aggregate size of 12 and 19 mm on the skid resistance of RCC surfaces is negligible. However, roller compacted HMA with 12 mm aggregate size yields higher skid resistance compared to the 19 mm aggregate size. Moreover, RCC surfaces do not exhibit significant change in BPN with the change in cement content. Comparing the skid resistance of RCC surfaces to the roller compacted HMA surfaces shows 26% and 24% drop at dry and wet conditions, respectively.

Another significant point is the influence of compaction method on BPN. It was previously discussed that based on roughness parameters evaluation the surface texture of gyratory compacted samples does not represent roller compaction generated texture. Gyratory compactor tends to produce more uniform texture compared to roller compactor, and this difference in texture makes a significant variation in BPN. Figure 5-19 compares the average British pendulum numbers achieved by gyratory compacted and roller compacted on both concrete and asphalt. Although asphalt material gives higher BPNs for both compaction methods, roller compacted samples have lower BPN in contrast with gyratory compacted samples.

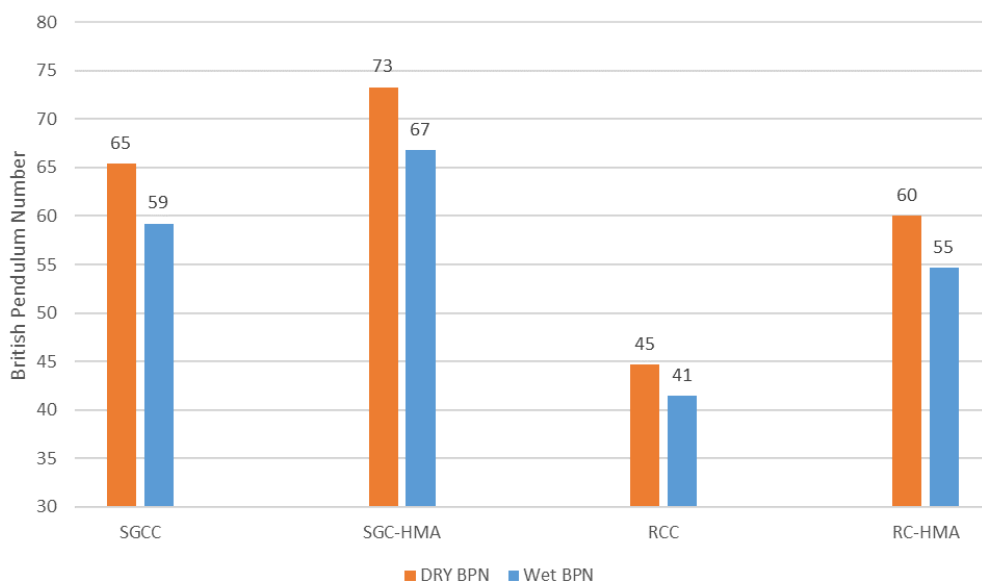


Figure 5-19, Average BPN of surfaces based on compaction method and binder type

5.3.2 Skid resistance and texture parameters

In the previous section, it was shown that the skid resistances achieved by various surfaces are different. The main reason behind this variation is the micro-texture of surface. Answering the question that how micro-texture can be quantified based on the geometry of texture has been investigated with different techniques. In this section, it is aimed to make a comparison between British pendulum numbers and roughness parameters to observe any possible correlation. In order to find out how statistically BPN and roughness parameters are correlated, 74 various roughness parameters were calculated. Then, for all the parameters and corresponding BPNs, Pearson's correlation coefficients (Eq. 4-1) were computed and compared.

$$r_{xy} = \frac{\sum_{i=1}^n (x_i - \bar{x})(y_i - \bar{y})}{\sqrt{\sum_{i=1}^n (x_i - \bar{x})^2} \sqrt{\sum_{i=1}^n (y_i - \bar{y})^2}} \quad \text{Eq. 4-1}$$

To narrow down the outputs for further analysis, only roughness parameters with a coefficient factor higher than 0.5 were selected. Linear and second order polynomial regressions were conducted for the selected 23 parameters. Four parameters (S_a , V_{mc} , S_{dq} and Fractal dimension) showed an R-squared value of greater than 0.5 and the greatest (with $R^2 = 0.54$) was observed for the Fractal dimension, which is not considered a strong correlation (Figure 5-20).

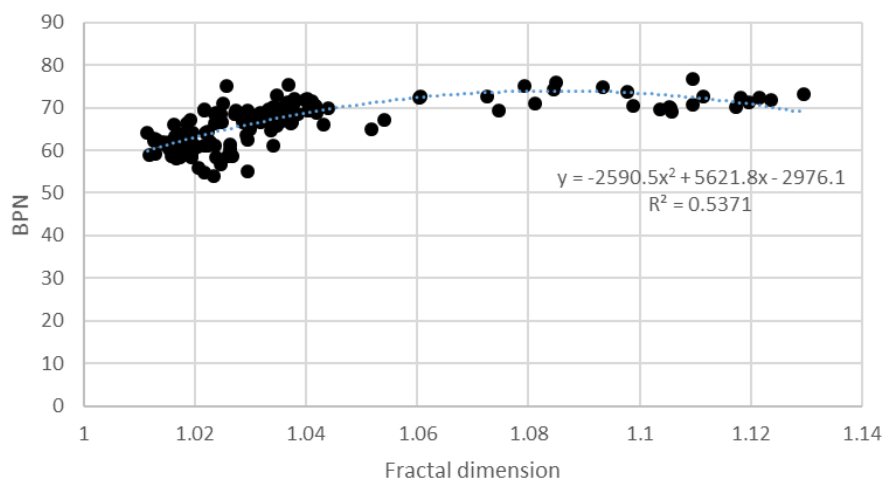


Figure 5-20, The correlation found between BPN and fractal dimension

Examining British pendulum test apparatus reveals that the rubber slider comes in contact with the test surface on a narrow path for a certain depth, and the surface characteristics beyond the effective depth cannot influence the test result significantly. In the second step, it was aimed to determine the effective depth of specimen surface that affects the test result. In this context, all test surfaces were sliced horizontally with 0.2 mm increments from the top. Hence, additional 15 sub-surfaces were generated for each surface starting with 0.2 mm height to 3 mm. The projected area of peaks for these sub-surfaces was calculated, and the evolution of Pearson's correlation coefficient was investigated.

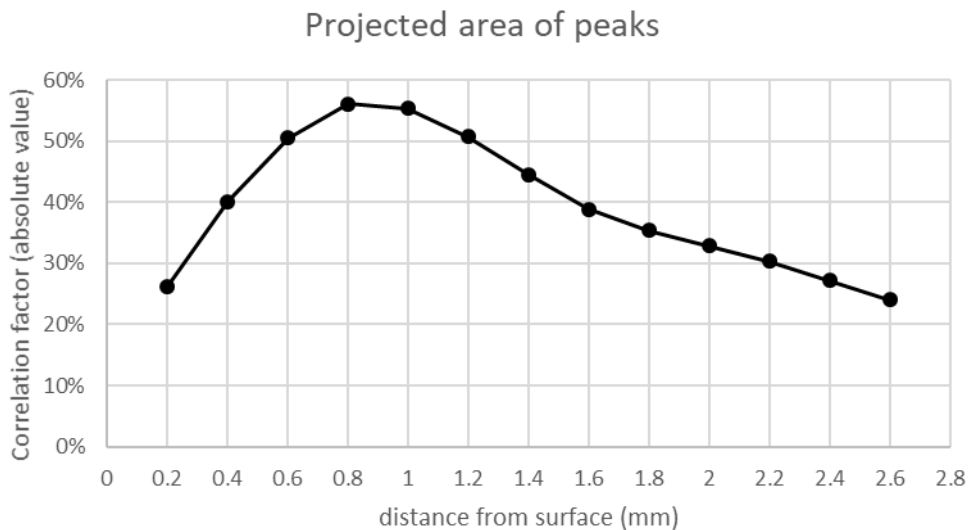


Figure 5-21, Evolution of Pearson's correlation factor with change in projected surface area of peaks at different depths

Figure 5-21 exhibits that Pearson's correlation factor is a function of the projected area of peaks, and it changes with depth change. Additionally, it can be concluded that the depths of 0.8 to 1.0 mm tend to give the greatest correlation factor. Hence, this depth can be accepted as the effective depth of a surface to be in correlation with BPNs.

Based on the evaluated effective depth, all the surfaces were sliced to limit the texture height to 1.0 mm from the top, then the roughness parameters were recalculated. The evaluation of Pearson's correlation factor of the new set of parameters resulted in an

increase for most of the parameters. However, two parameters showed significant increase:

- S_{al} (autocorrelation length)
- Magnitude of 2D Fourier transform

Figure 5-22 and Figure 5-23 demonstrate the linear regression of dry and wet BPNs with autocorrelation length calculated with “s” value of 0.2 as the default value found in ISO 25178-3. The coefficient of determination for dry and wet BPN’s are 0.34 and 0.40, respectively, which denotes a weak to moderate correlation between the BPNs and S_{al} .

Another correlation trend can be traceable in Figure 5-24 and Figure 5-25. Linear regression of dry and wet condition BPN’s are in correlation with the magnitude of frequency extracted from the surface by the Fourier transform function. The coefficients of determination of the regressions, 0.74 and 0.64 for wet and dry BPNs, stand for the probability of this parameter to predict the skid resistance, yet it is not adequate. Moreover, larger r-squares were obtained for BPNs in a wet condition for both parameters which demonstrates a better correlation. This can be interpreted as an indicator of BPN measurement error, which is lower for wet conducted surfaces.

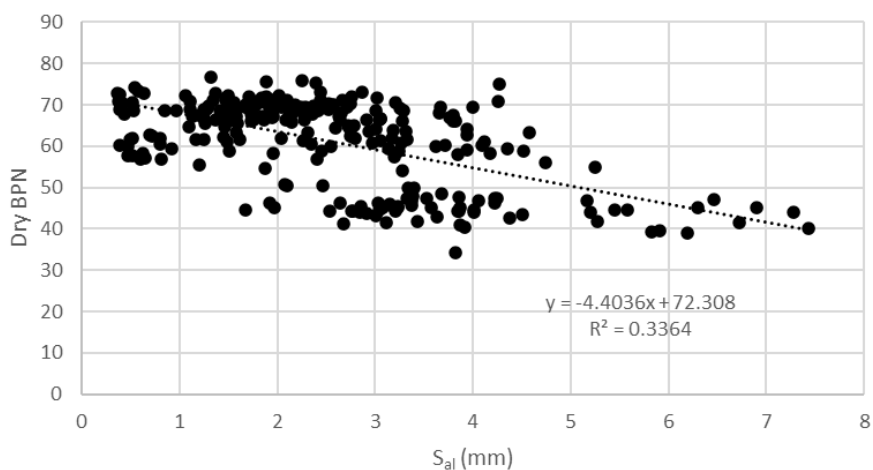


Figure 5-22, Linear regression of dry BPNs and autocorrelation length ($s=0.2$)

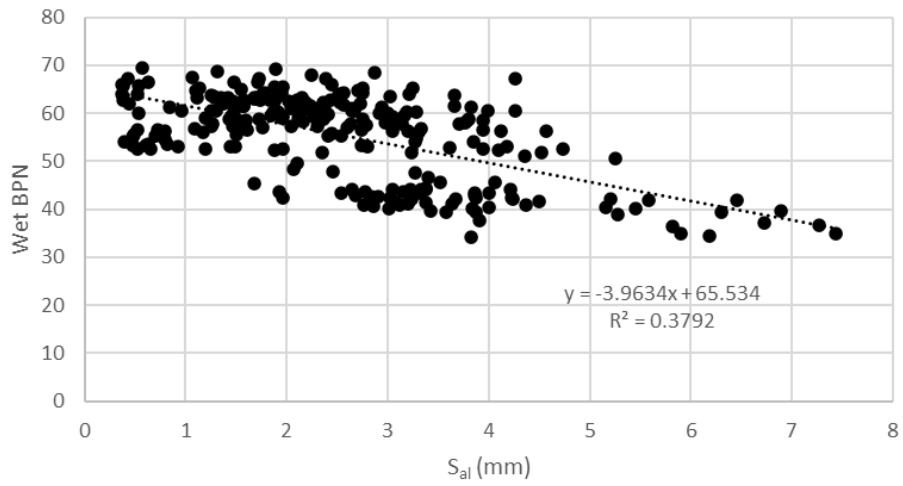


Figure 5-23, Linear regression of wet BPNs and autocorrelation length ($s=0.2$)

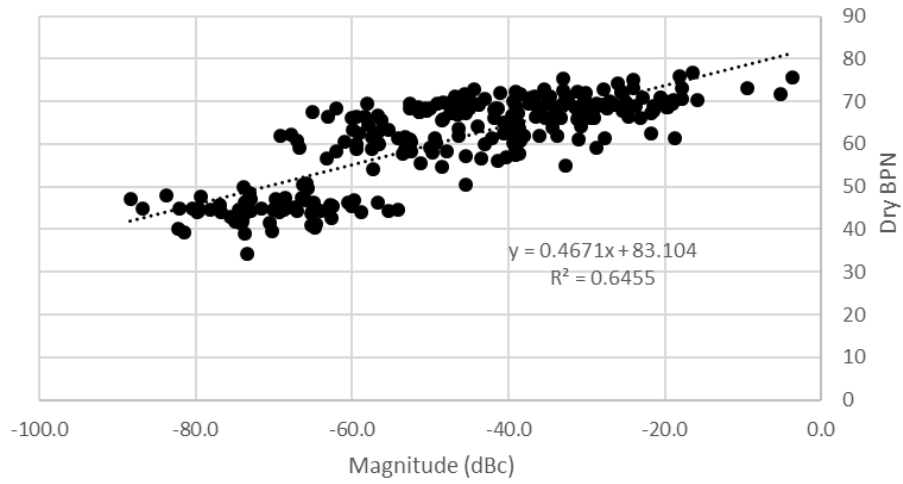


Figure 5-24, Linear regression of wet BPNs and magnitude of 2D Fourier transform

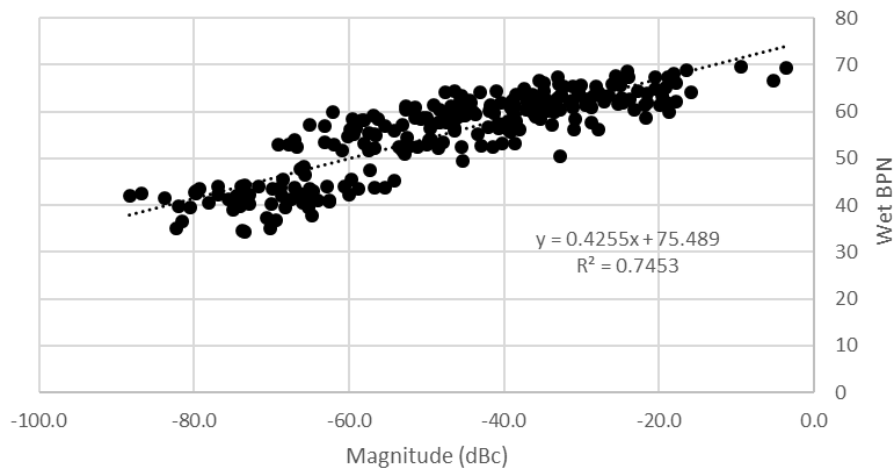


Figure 5-25, Linear regression of dry BPNs and magnitude of 2D Fourier transform

CHAPTER 6

PHASE III, DURABILITY OF RCC PAVEMENT

The longevity of RCC pavement, as a sustainable alternative to conventional pavement systems, is a matter of concern for decision-makers. A key deterioration factor for concrete pavement is frost and intensified contribution of deicers to the factor. In this phase of the study, it is intended to investigate the durability of RCC pavement subjected to frost and establish a novel measurement method for determination of extent of chloride-induced deterioration of pavement surface under freeze-thaw cycling. Moreover, the effect of salt-scaling on surface of the RCC pavement samples is also investigated.

6.1 Background

It is well known that deicing salts have a negative impact on concrete pavement, and it can significantly increase the freeze-thaw damage. The typical mitigation for freeze thaw cycling damage in conventional concrete is air entrainment, however, due to the dry nature of RCC mixture and low binder content, air entrainment of RCC mixtures is challenging (Delagrave et al., 1997; Pigeon & Malhotra, 1995; Piggott, 1999). It is worth mentioning although there are published data indicating the high performance of RCC pavement to freeze thaw cycling, some reports indicate unsatisfactory resistance of RCC pavement to deicers salt scaling (Nili & Zaheri, 2011; Ragan, 1986; Vahedifard et al., 2010). Apart from the variation in results, the mutual fact between most of these studies is the test method. ASTM C672 prescribes a test method for scaling resistance of concrete surfaces exposed to deicing chemicals. According to the test method, after 50 freeze-thaw cycles, a visual rating of frost damage of pavement surface is obtained. Some countries such as Canada

modified this test method and added quantitative measures by determining specimen mass loss based on mass measurement of loose materials at intervals of 5 cycles.

6.2 Materials and methods

To select test specimens, 6 RCC mixtures were considered. Three binders' content of 200, 300 and 400 kg/m³, nominal aggregate size of 12 mm and 19 mm. The mix designs are given in table Table 3-2. Two cylinders with a diameter and height of 150 mm and two prisms with dimensions of 300x100x75 mm were obtained from lab prepared roller compacted slabs.

The transport of liquids in capillary pore system of concrete is known as sorptivity. The surface tension of capillary pores is the reason for this action. It is well-known that the water transportability of concrete has a significant impact on its long-term performance and durability. Additionally, the moisture state of concrete is an effecting factor on its frost resistance. To gain a better understanding of the water absorption rate of the produced RCCP, ASTM C1585, standard test method for measuring the rate of water absorption by hydraulic-cement concrete was selected for sorptivity measurement of RCCP samples. Two cylinders from each RCCP were conditioned, sealed, and tested according to the standard. Furthermore, two RCCP prisms from each RCCP were selected for ASTM C672, test method for scaling resistance of concrete surfaces exposed to deicing chemicals. Cured specimens were diked with epoxy and subjected to 50 cycles of freeze-thaw. Apart from the requirements of ASTM C672, surfaces of all specimens were scanned at 3 stages with the study 3D laser scanner. The first scan was conducted before start of the test and two other scans on the 25th and 50th cycles. The scan direction and location of each specimen were kept constant for all three rounds of scanning.

6.3 Results and discussions

Figure 6-1 gives a comparison of the rate of water absorption of RCC specimens. The rate of water absorption or sorptivity represents the pore system and pores

connectivity of concrete. It is seen that sorptivity is in direct relationship with RCC cement content, hence less cement, provides less paste and more open pores generate for higher sorptivity. Another influencing factor is aggregate gradation and maximum aggregate size. The test reveals, with similar cement content, RCC with greater maximum aggregate size has lower sorptivity. Pictures of the RCC pavement samples, before and after 50 cycles of freeze-thaw cycling are provided in Figure 6-4 and Figure 6-5. Other than discoloration of the surfaces, damage on the surface texture of all samples can be observed. Comparing samples with 12 mm stone size shows scaling on the surface of all samples. Furthermore, the intensity of the scaling is greater on RCC samples with less cement content. This damage was expected based on sorptivity results. 200-12 samples with greater sorptivity value exhibit the greatest damage and 400-12 samples with lower sorptivity display better frost performance. Extending the comparison to RCC samples with 19 mm stone size gives exactly the same results, and the best performance belongs to the samples with 400 kg/m³ cement content with the lowest sorptivity value. However, the overall performance of the RCC samples does not follow the sorptivity comparison. The RCC samples with 12 mm maximum aggregate size performed better than their competitors with 19 mm maximum aggregate size whilst for all samples, 12 mm maximum aggregate size resulted in greater sorptivity value comparing to 19 mm.

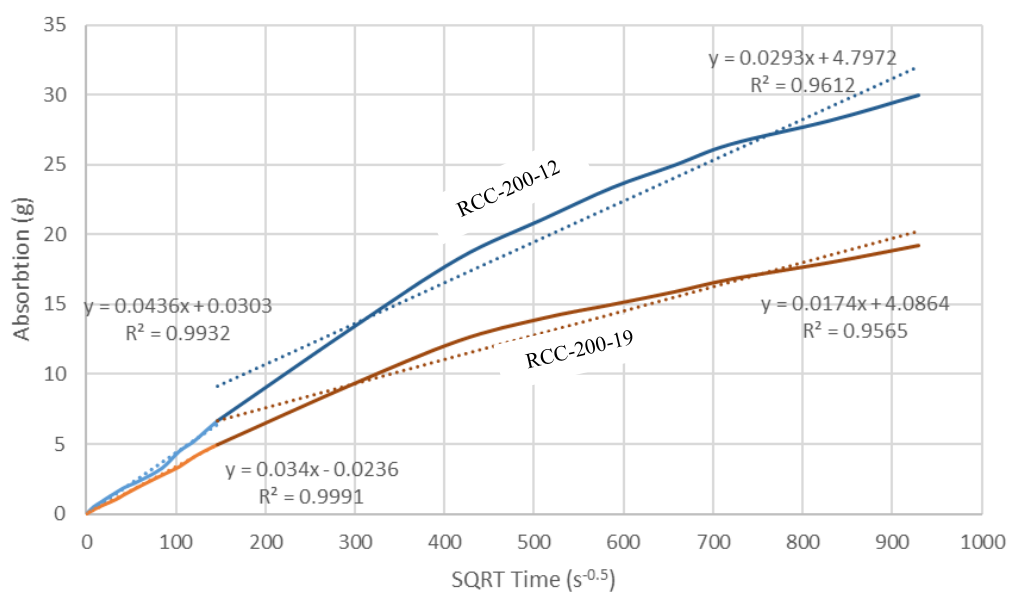


Figure 6-1, The initial and secondary rate of water absorption for 200 kg/m³ binder content RCC

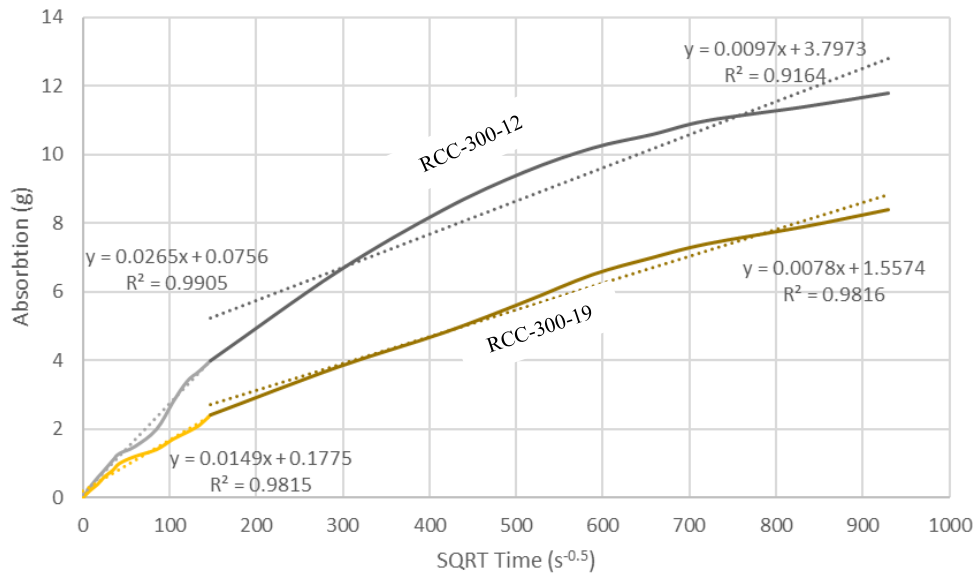


Figure 6-2, The initial and secondary rate of water absorption for 300 kg/m³ binder content RCC

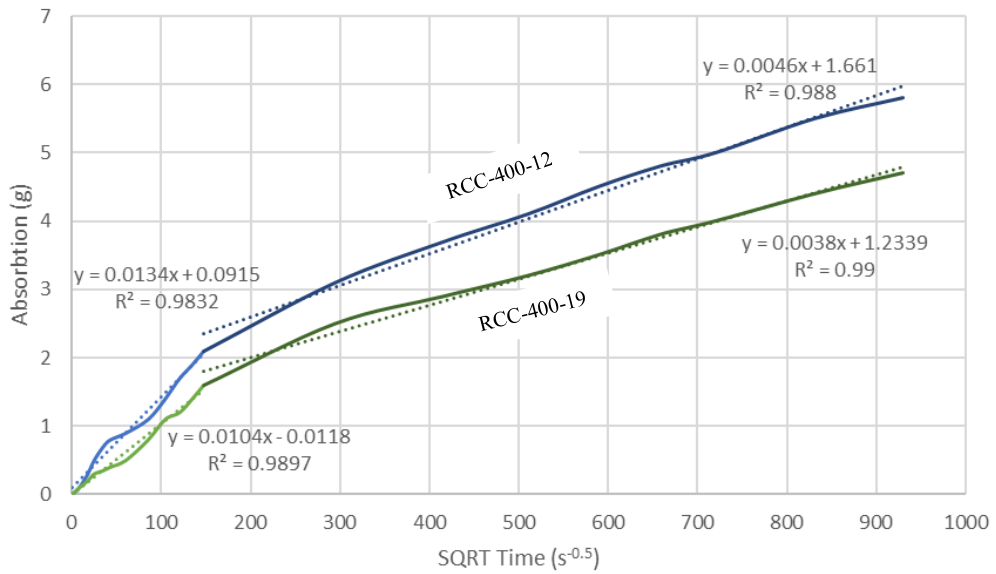


Figure 6-3, The initial and secondary rate of water absorption for 400 kg/m³ binder content RCC



Figure 6-4, RCCP samples with 12 mm stone, before (two pictures on the left) and after 50 cycles of freeze-thaw (two pictures on the right)

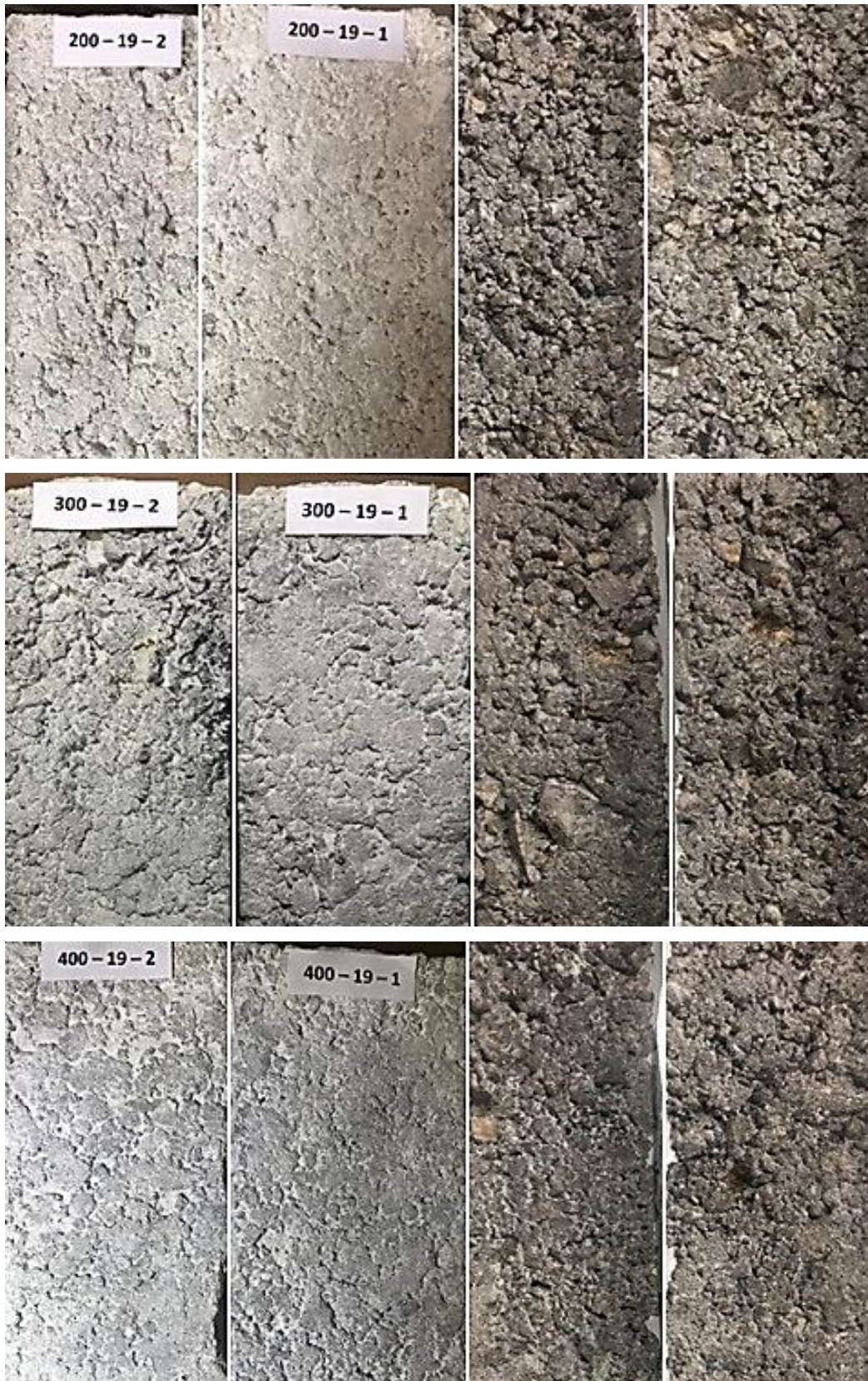


Figure 6-5, RCCP samples with 19 mm stone, before (two pictures on the left) and after 50 cycles of freeze-thaw (two pictures on the right)

Inspection of the samples surface visually shows 2 different types of surface damage. Surficial disintegration of paste, resulting in texture with deeper valleys and pop-outs on coarse aggregates. Pop-outs are more seen on the surface of RCC samples with 19 mm aggregate size, which represents low frost resistance of the utilized coarse aggregates.

To gain a better understanding of the extent of surficial frost damage and change in texture, all RCC samples were scanned and analyzed for texture parameters at cycles zero, 25 and 50. Figure 6-6 Figure 6-7 compare Root mean square height (S_q) of the textures as a height parameters representative. The comparison satisfies the expecting increase in average height of texture with increase in frost cycles, however, the point of interest is the extent of this increase. Undeniably increase in cement content promoted the performance of RCC samples to resist frost cycles. The comparisons reveal an increase in cement content, decreased both extent and rate of frost damage. Furthermore, RCC with smaller maximum aggregate size samples performed better in freeze-thaw cycling.

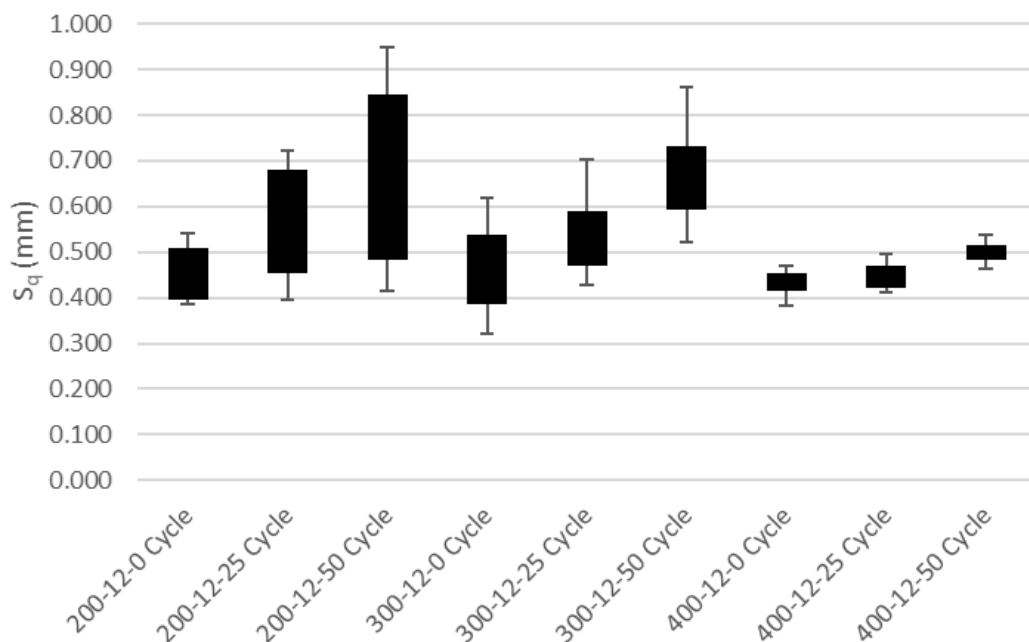


Figure 6-6, Change in Root mean square height for RCC with 12 mm max aggregate size

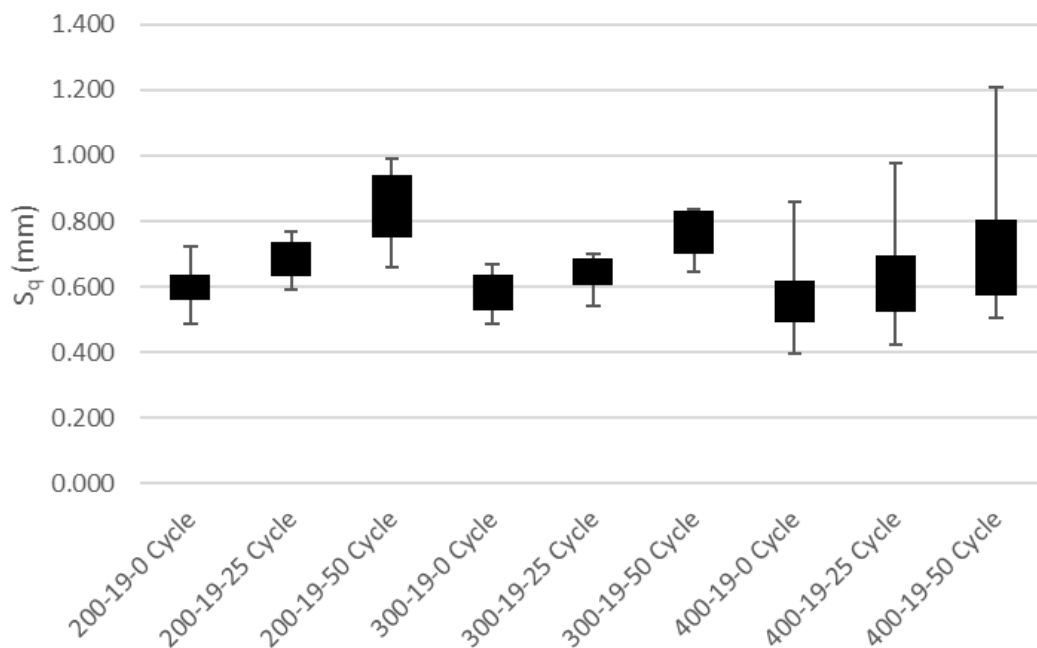


Figure 6-7, Change in Root mean square height for RCC with 19 mm max aggregate size

Previously it was discussed that shape texture irregularities can be assessed with Skewness and Kurtosis parameters. Skewness which is suitable for evaluating abrasion of texture is demonstrated in Figure 6-9 and Figure 6-8. For all RCC samples, a decrease in skewness is seen by the increase in frost cycles. This state abrasive influence of frost cycles on the texture of the RCC samples. In addition, tracing the rate of the decrease in skewness shows the greater abrasive influence of freeze-thaw cycling on RCC samples with smaller stone size.

Figure 6-10 and Figure 6-11 exhibit comparison of Kurtosis of the textures. This parameter which relates to the tip geometry of peaks and valleys is suitable for analyzing the degree of contact between two objects. It is seen the freeze-thaw cycling caused a slight decrease in Kurtosis values which can be interpreted as a decrease in the contact surface. This decrease appears to be similar for all specimens.

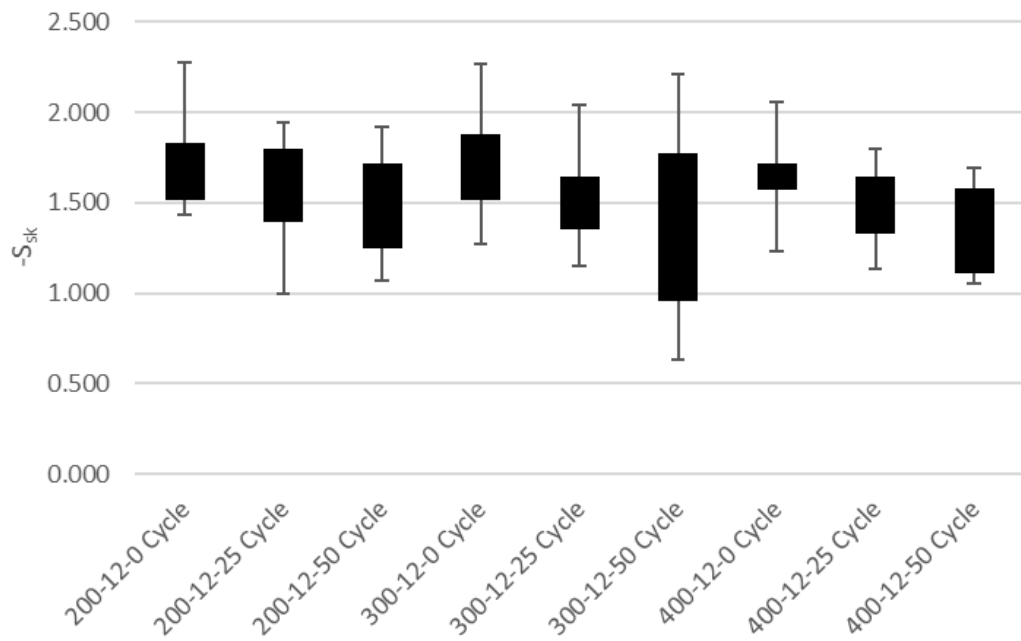


Figure 6-8, Change in texture skewness of RCCs with 12 mm max aggregate size

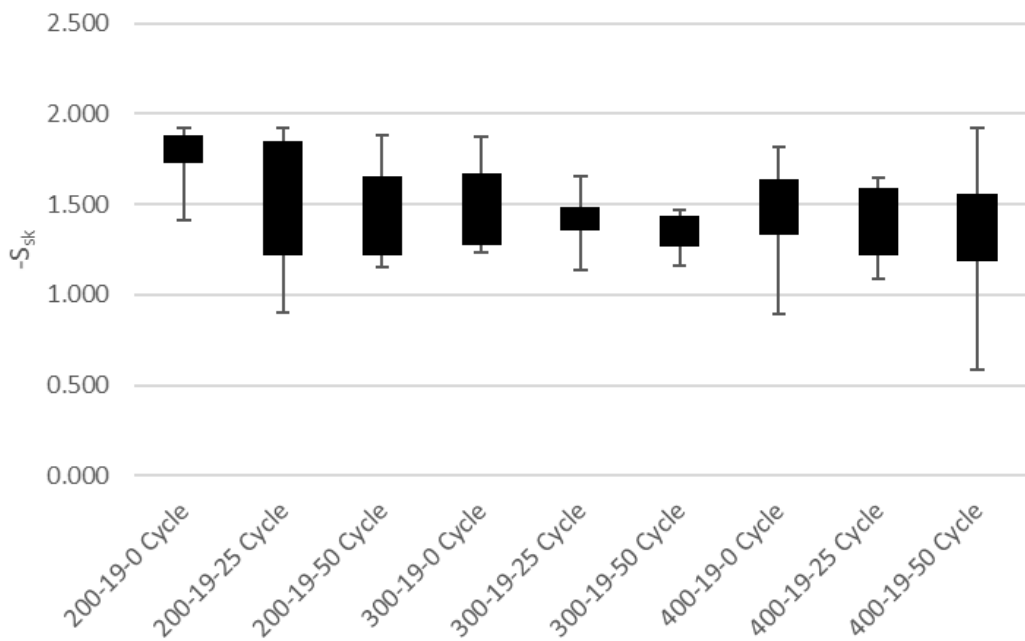


Figure 6-9, Change in texture skewness of RCCs with 19 mm max aggregate size

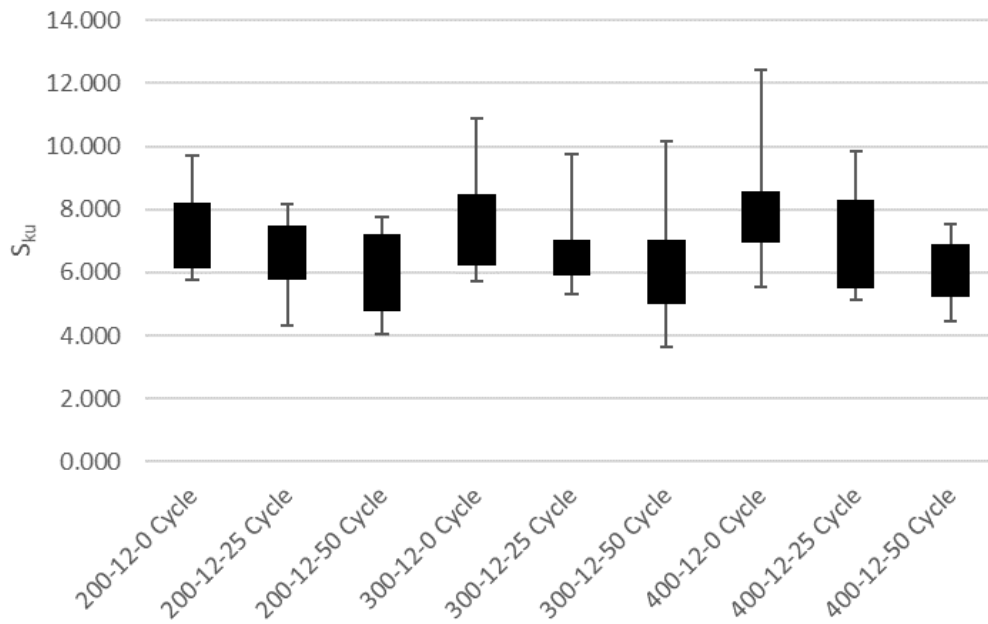


Figure 6-10, Change in texture kurtosis of RCCs with 12 mm max aggregate size

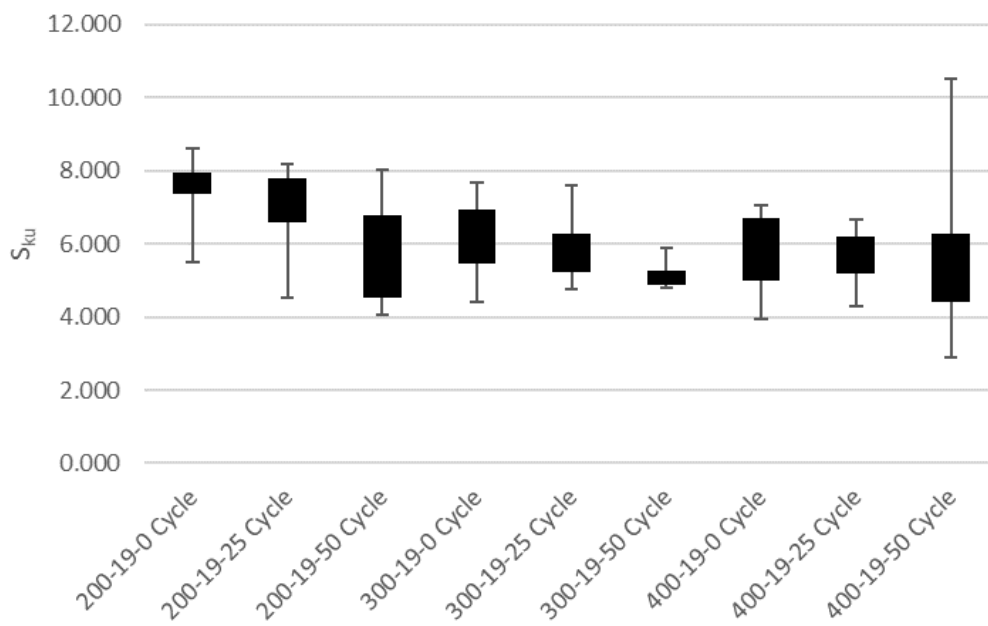


Figure 6-11, Change in texture kurtosis of RCCs with 19 mm max aggregate size

Evaluation of estimated Mean Texture Depth (eMTD) as a standard macro-texture representative, under freeze-thaw cycling influence, is presented in Figure 6-12 and Figure 6-13. The extent of change in macro-texture of the RCC samples shows a variation in both magnitude and rate. Speaking of RCC samples with 19 mm maximum aggregate, change in macro-texture magnitude remains close, however the rate of this change slows with an increase in cement content. It worth mentioning that pop-outs were seen on coarse aggregate of the samples. Hence, similar change in the magnitude of eMTD can be associated with the pop-outs and a decrease in rate of the change is due to the increase in cement content. Better performance in terms of macro-texture change belongs to RCC samples with 12 mm maximum aggregate size. It can be summarized that the cement content has a dramatic effect on promoting RCC texture resistance to freeze-thaw cycling, whereas poor resistance of aggregates to frost damage is not negligible.

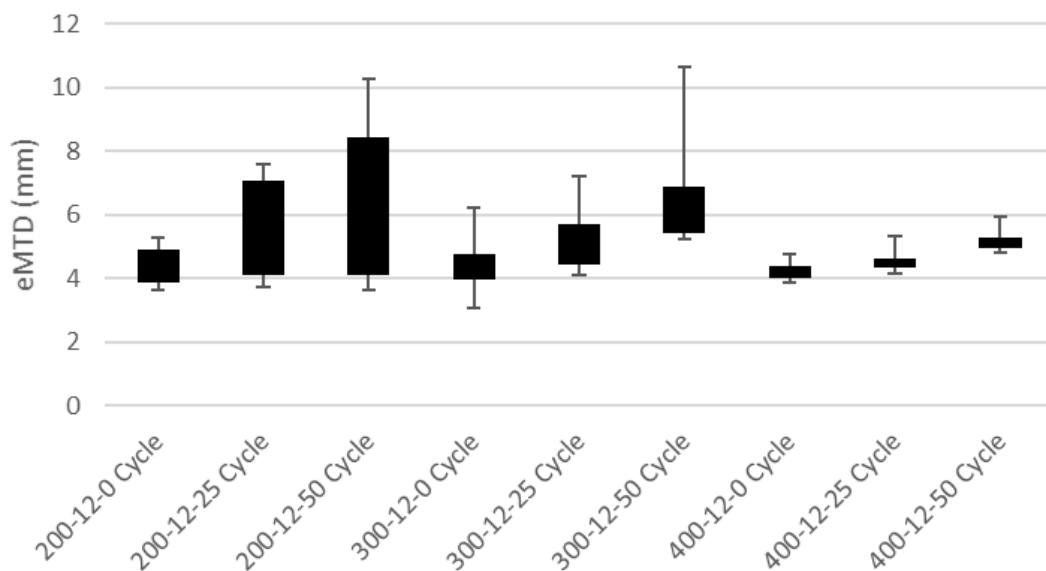


Figure 6-12, Macro-texture change under freeze-thaw cycling influence for 12 mm max aggregate size RCCs

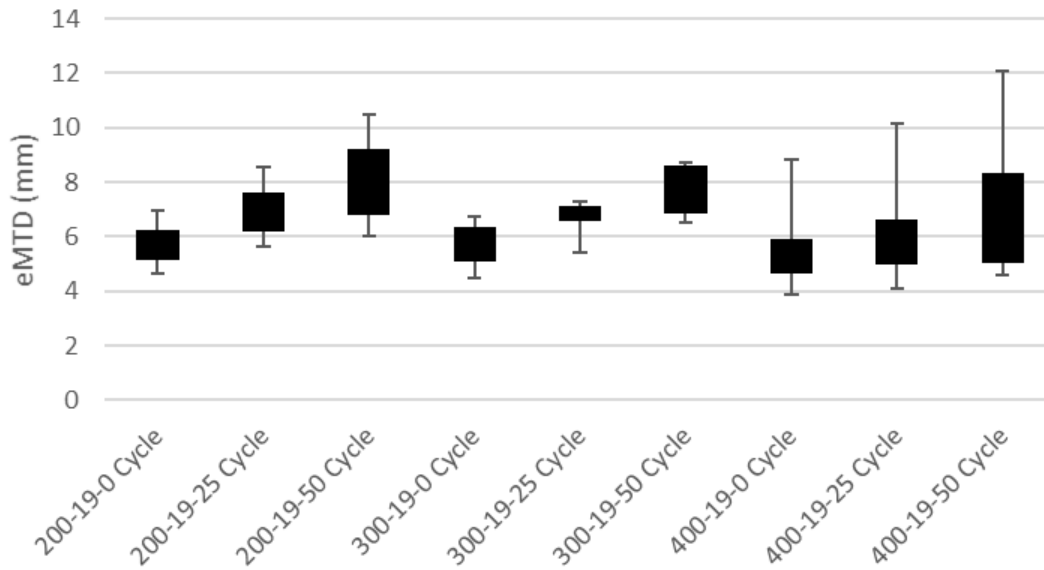


Figure 6-13, Macro-texture change under freeze-thaw cycling influence for 19 mm max aggregate size RCCs

Thanks to the high precision of laser scanner, volumetric parameters of scanned texture are readily computable. Figure 6-14 and Figure 6-15 demonstrate quantitative analysis of change in volume of valleys due to frost damage. Figure 6-16 gives a precise comparison of overall volume loss, based on the computed volume values. The comparison can clearly show, samples with smaller aggregate size performed better in terms of volume loss under cycles of freeze-thaw. An increase in cement content, increases resistance of the RCC samples to chemical deicers induced freeze-thaw damage, and the highest performance belongs to the 400-12 RCC sample.

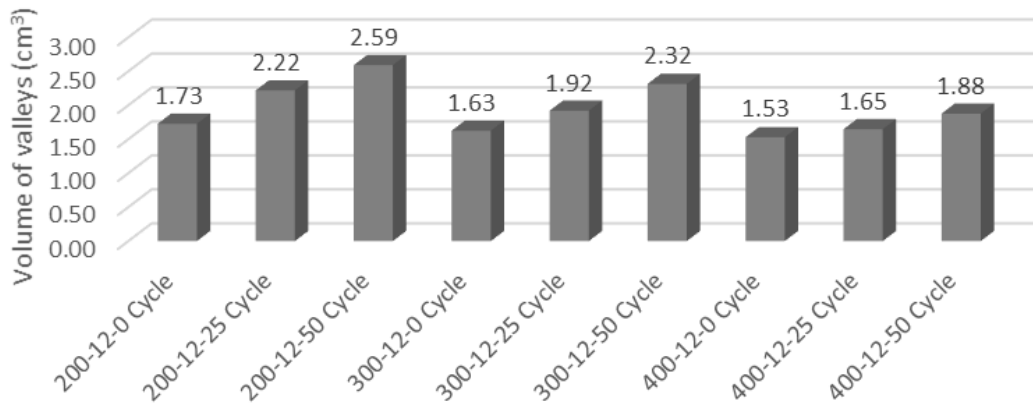


Figure 6-14, Change in volume of valleys after freeze-thaw cycling ($D_{max} = 12$ mm)

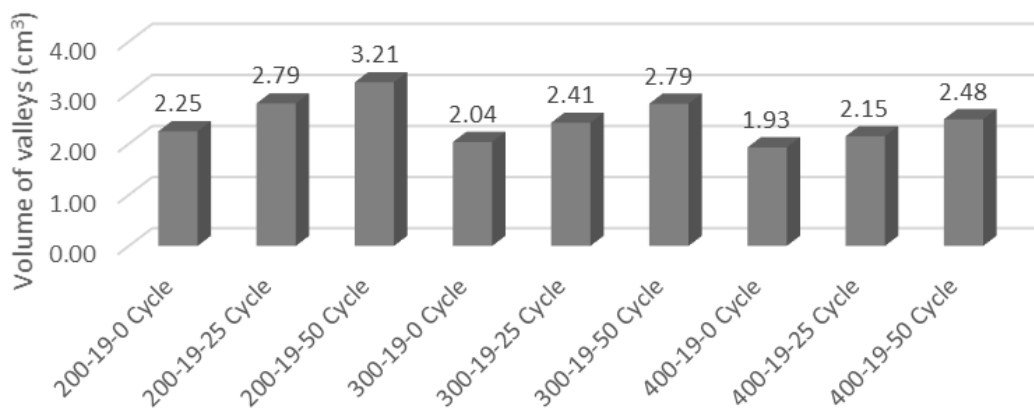


Figure 6-15, Change in volume of valleys after freeze-thaw cycling ($D_{max} = 19$ mm)

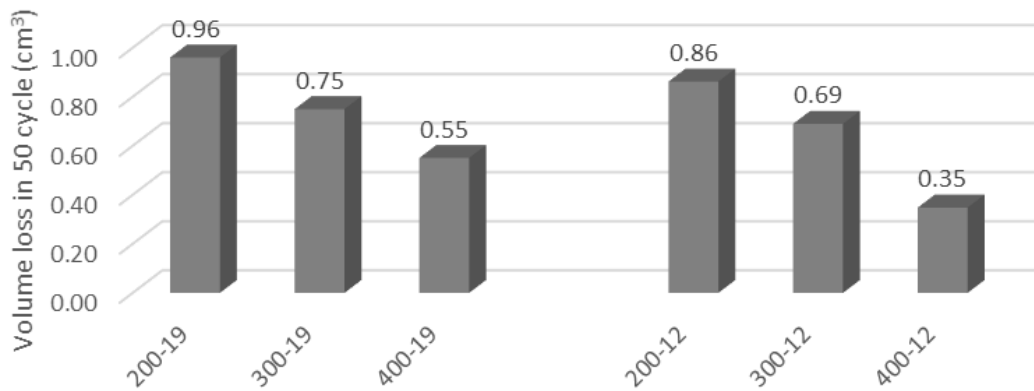


Figure 6-16, Overall volume loss of the RCC samples after 50 cycles of freeze-thaw

CHAPTER 7

PHASE IV, MODIFICATION OF TEXTURE OF RCC Pavement

7.1 Methodology of the Experiments

Investigating the texture characteristics of RCC pavement in the previous chapter demonstrated similarities to the texture of HMA pavement. Unlike conventional Portland cement concrete pavement, which happens to have a smooth surface after finishing and the necessity of additional texturizing, RCC surface is already generated with a texture. However, it was shown that this texture is not identical to HMA texture and it suffers from the lack of uniformity. Inspired by HMA texturizing, two methods were considered for improving the surface texture of RCC:

- Exposed aggregate concrete surface (EACS)
- Chip sprinkled concrete surface (CSCS)

This chapter will discuss macro-texture, micro-texture, and skid resistance of RCC pavement surface modified with the above-mentioned techniques.

7.1.1 Test Specimens for Exposed Aggregate Concrete Surface (EACS)

For better understanding of the influence of different variables such as compaction, aggregate size, and the depth of exposure on EACS, two different series of EACS specimens were prepared:

- Lab prepared gyratory compacted specimens
- Field obtained RCC specimens

Six mixes with three different cement contents, and two different maximum aggregate sizes of 12 mm and 19 mm were selected (Table 7-1). Two set retarders with various grades (elutriation depth) were also selected to stop the hydration of surface paste. The set retarders were provided by the RECKLI company. The products are commercially known as RECKLI-CR-Type PV (concrete surface retarder – positive process). The grades of 25 (L) and 100 (H) were selected with nominal elutriation depths of 2.5 mm and 4.0 mm respectively. According to the manufacturer, the real elutriation depth of each grade may vary depending on the cement class, water to cement ratio, shape of aggregate, and grain size distribution. The concrete mixtures were prepared in a pan mixer. Nine specimens from each mix were compacted with the gyratory compactor. The gyration cycles were kept at 75 cycles for all specimens. Immediately after compaction, the set retarder was brushed on the surface of each cylindrical specimens (the dosage used is 250 g/m²). After 24 hours, the surface of the specimens was power washed to an extent that no more paste could be cleaned off from the surface. Three replicates for each retarder grade as well as three control specimens were prepared.

Table 7-1, Mix proportions and properties of the specimens

| Mix ID | Cement (kg) | D _{max} (mm) | Water (%) | Water (kg) | Aggregate (kg) | | | W/C | Vebe Compaction | |
|------------|----------------|--------------------------|--------------|---------------|----------------|--------|---------|------|-----------------|--------------|
| | | | | | 0-5mm | 5-12mm | 12-19mm | | Time (s) | Ratio (%) |
| SGC-200-12 | 200 | 12 | 5 | 117 | 1388 | 750 | 0 | 0.59 | 32 | 98.8 |
| SGC-200-19 | 200 | 19 | 5 | 117 | 1067 | 857 | 216 | 0.59 | 32 | 99.5 |
| SGC-300-12 | 300 | 12 | 5.5 | 128 | 1332 | 720 | 0 | 0.42 | 22 | 98.9 |
| SGC-300-19 | 300 | 19 | 5.5 | 128 | 1024 | 823 | 208 | 0.42 | 20 | 98.4 |
| SGC-400-12 | 400 | 12 | 6 | 139 | 1240 | 670 | 0 | 0.35 | 35 | 98.0 |
| SGC-400-19 | 400 | 19 | 6 | 139 | 953 | 766 | 194 | 0.35 | 32 | 98.9 |

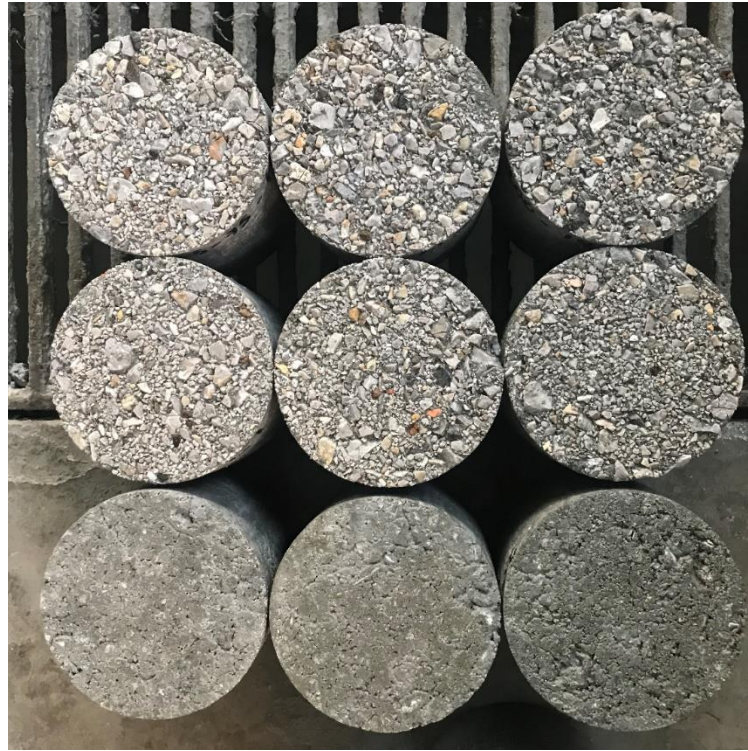


Figure 7-1, EACS and control specimens

7.1.2 Test Specimens for Chip Sprinkled Concrete Surface (CSCS)

Three different gradations were selected as test chips (aggregate). A substrate was prepared from 300 kg/m³ cement RCC mixture with a D_{max} of 12 mm using the same mix design of RCC-300-12 utilized in phase II. A cement slurry with water to cement ratio of 1 was prepared and the chips were mixed with the slurry, so the aggregate surfaces were coated in order to enhance the penetration and adhesion of the chips. Immediately after the initial compaction of the substrate, the fresh slurry coated chips were placed on the surface of the substrate, and compaction with DDVHR was carried out to reach maximum compaction. Table 7-2 gives the used gradation, ratio of spread, and coating dosage.

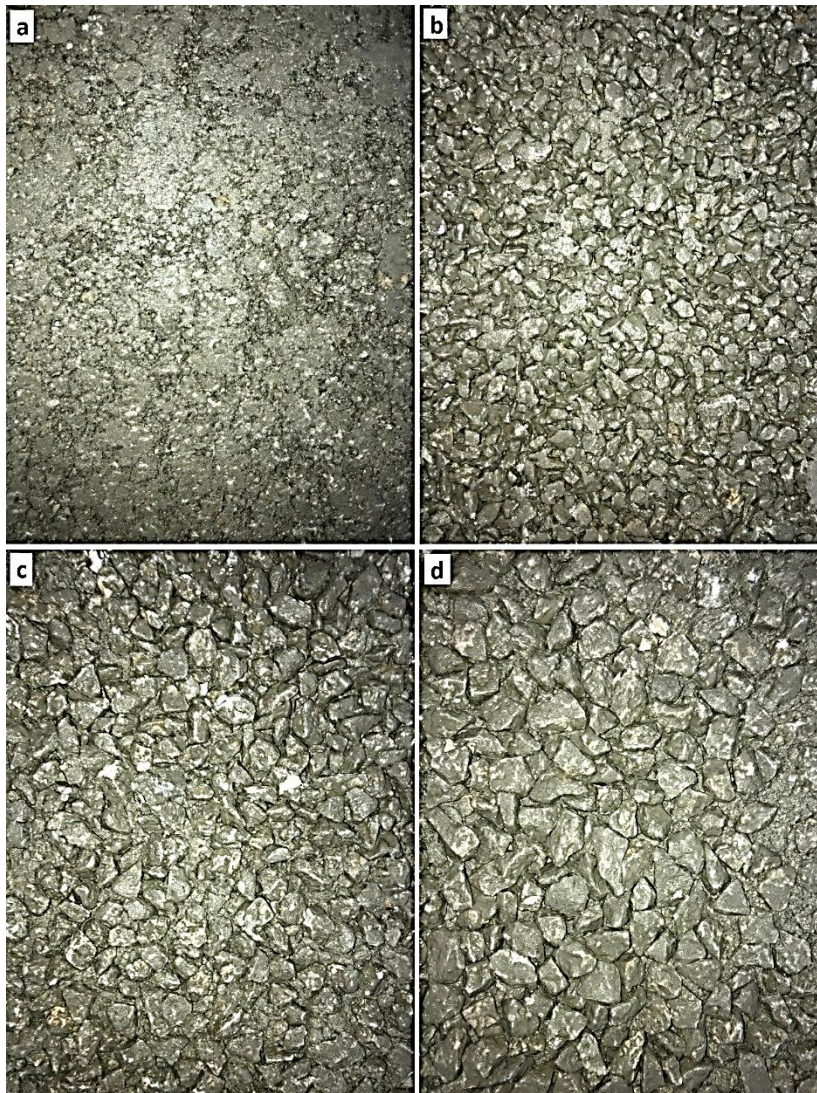


Figure 7-2 a) Unchipped RCC surface. b) RCC surface sprinkled with 5.0-9.5 mm chips. c) RCC surface sprinkled with 9.5-12.7 mm chips. d) RCC surface sprinkled with 12.7-16 mm chips.

Table 7-2, Chip sprinkling gradation, coating and spread rate

| Sample ID | Gradation (mm) | Spread ratio (kg/m ²) | Coating ratio (kg per agg. kg) |
|------------|----------------|-----------------------------------|--------------------------------|
| Unchipped | - | - | - |
| CSCS 5~9 | 5.0-9.5 | 9.6 | 0.25 |
| CSCS 9~12 | 9.5-12.7 | 13.1 | 0.16 |
| CSCS 12~16 | 12.7-16 | 16.9 | 0.12 |

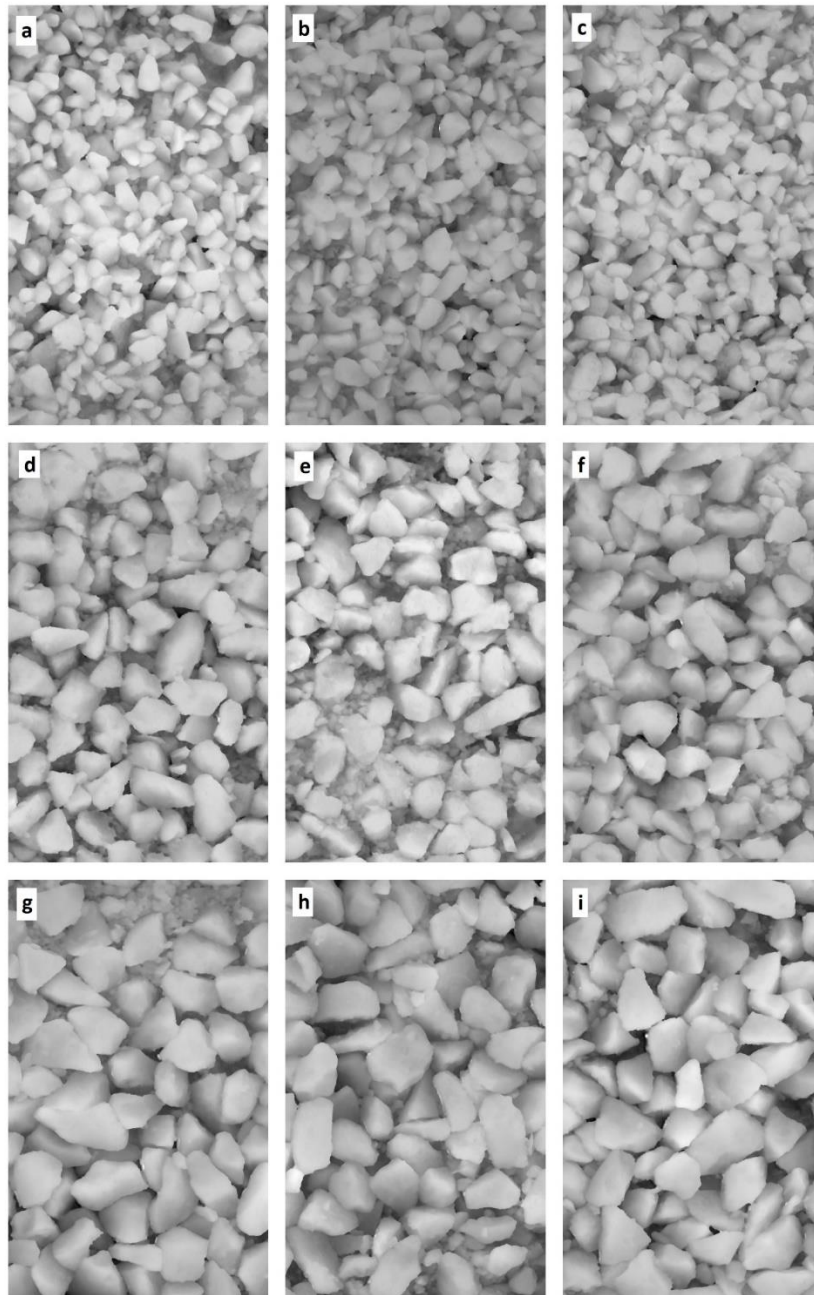


Figure 7-3, Image simulation of surface data produced by MATLAB, a,b,c) CSCS 5~9, d,e,f) CSCS 9~12, g,h,i) CSCS 12~16

7.1.3 Experiments

The core and cylinder samples obtained from exposed aggregate surfaces were cut with a water-cooled saw to make 30 mm thick disks of the top surfaces. Chip

sprinkled surface samples were cut in a similar way with strips of 25 cm width. The skid resistance of the specimens were measured under wet and dry conditions with British Pendulum tester in 4 directions with 90-degree intervals. Then, the surfaces of the specimens were scanned with the laser scanner developed in this work, and 3D surfaces were generated. Finally, roughness parameters were computed.

7.2 Investigating Texture Properties

To gain a clear view of how surface modification of RCC pavement affects its performance, the obtained results were analyzed in macro-texture and micro-texture contexts.

- **Macro-texture**

It was previously shown that mean texture depth as an indicator of macro-texture can be computed from 3D surface data with high precision. Figure 7-4 demonstrates the estimated mean texture depth (eMTD) computed from the following sample sets:

- Super-pave gyratory compacted, exposed aggregate concrete surface
 - Control sample
 - Low grade exposed
 - High grade exposed

- Roller compacted, chip sprinkled concrete surface
 - Unchipped RCC
 - Chip size 5 to 9.5mm
 - Chip size 9.5 to 12.7mm
 - Chip size 12.7 to 16.0mm

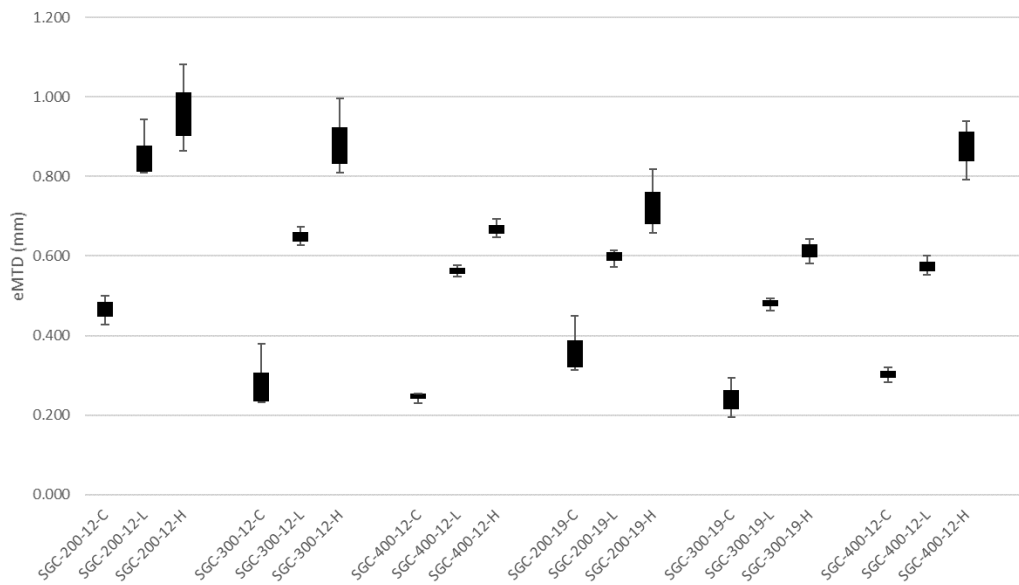


Figure 7-4, Estimated mean texture depth of surface modified RCC pavement

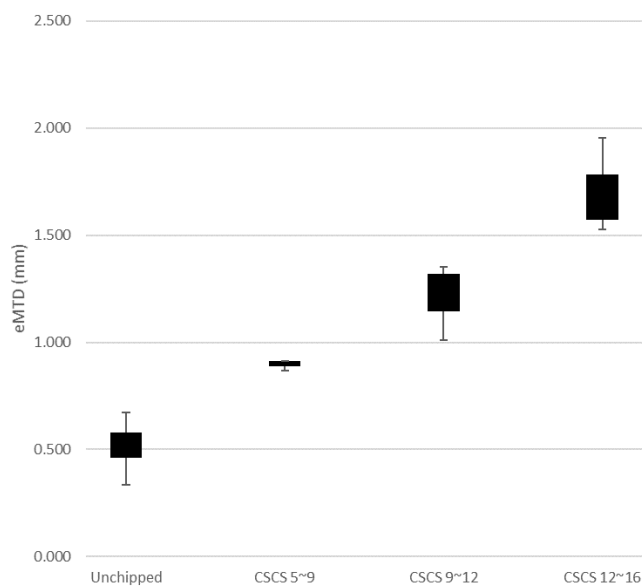


Figure 7-5, Estimated mean texture depth of chip sprinkled RCC pavement

As expected, Figure 7-4 shows that surface modification has a tremendous influence on macro-texture enhancement. While low-grade EACS can produce twice macro texture compared to control samples, high-grade EACS can increase MTD up to

three times. What is obvious here is that the effect of set retarder varies based on cement content. The gradation of aggregate can be considered as another affecting factor as well. Figure 7-5 demonstrates MTD results of chip sprinkled RCC samples. It is clearly seen that MTD increases with an increase in chip size. Spike in MTD is tremendous and chip sprinkled surface can enhance macro-texture almost two times of exposed aggregate concrete surface.

- **Micro-texture**

In a previous section, it was demonstrated that micro-texture indirectly can be explained with skid resistance. Similar to phase one, British pendulum tester was carried out on all of the test surfaces for the determination of skid resistance. Both wet and dry conditions of the surfaces were assessed for skid resistance measurements. Figure 7-6 exhibits the obtained skid numbers of test surfaces. Surprisingly at first glance, no significant change in skid numbers was observed. As experienced in the first phase of the study, gyratory compacted surfaces yielded noticeably higher skid numbers in contrast to roller compacted surfaces. Speaking of SGCC specimens, lower cement content tends to show a slightly higher skid number compared to the high cement content mixes. In addition, skid numbers on control surfaces show a greater fluctuation compared to the numbers obtained from exposed aggregate surfaces. However, no significant improvement is seen for exposed aggregate surface concrete in terms of skid numbers. Unlike exposed aggregate surface, chip sprinkled concrete surface shows a slight improvement in skid numbers using chip size 5 to 9.5 mm. However, an increase in chip size has a negative impact on skid resistance. Another observation is the difference between dry and wet skid numbers. Whilst the control RCC sample and EACS show a skid number drop of 8~14% on wet condition, CSCS samples give only 6% decrease. This shows the chip sprinkled surfaces perform better in wet condition in terms of skid resistance.

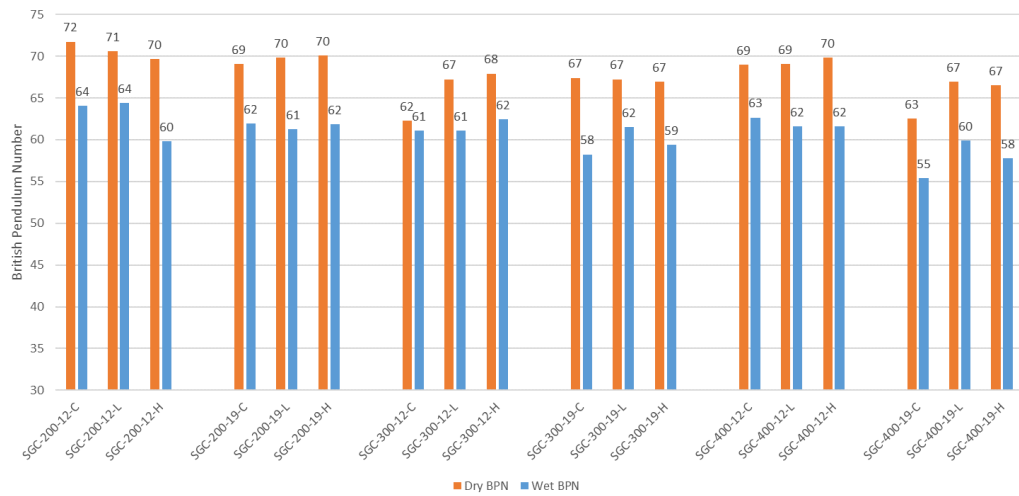


Figure 7-6, British pendulum numbers of exposed aggregate RCC pavement

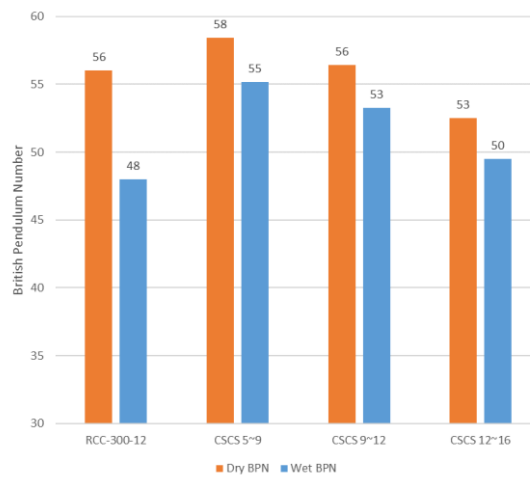


Figure 7-7, British pendulum numbers of chip sprinkled RCC pavement

7.3 Conclusion

In summary, two surface modification techniques were successfully implemented on RCC pavement. To produce EACS, the pavement was power washed 24 hours after the placement and compaction of RCC. Hydration retarders with two different effective penetration depths were applied to stop the hardening of superficial paste. The investigation of roughness parameters showed a significant improvement in the

macro-texture of the surfaces. However, no noticeable change was recorded for micro-texture.

In CSCS, three different aggregate gradations were forced to be implanted on the RCC pavement surface. The application was reached success after coating the aggregate with a layer of portland cement slurry. A tremendous increase in macro-texture was achieved. Furthermore, it was observed that the chip size is effective in skid resistance. The surface chip sprinkled with aggregate size 5 to 9.5 mm, showed higher BPN comparing to its substrate, RCC-300-12. However, by an increase in the grain size of chips, a decrease in BPN was observed.

Further investigations on chips stability under loading as well as noise and tire wear are required. To gain a better understanding of micro-texture, additional testing such as dynamic friction tester and locked-wheel skid trailer is recommended.

CHAPTER 8

SUMMARY AND CONCLUSIONS

Drivability of road surface is affected by its texture properties in different scales. Although available reports and studies have investigated asphalt and conventional concrete pavement texture, however, there is not much evidence in literature regarding RCC pavement texture. This Study utilized high precision laser measurement technique and standard roughness parameters to provide quantitative information of RCC pavement texture.

8.1 Findings and Conclusions

In the first phase of this study, a comparison between RCC and HMA with two different compaction methods was made and the influencing factors were investigated. In general, RCC and asphalt pavements are compacted with paver and rollers on field. However, in Laboratory environment, superpave gyratory compactor is utilized for sample preparation. This type of compaction is accepted to represent the mechanical properties of field compaction. To extend this representativeness to texture properties, a gyratory compactor and a walk-behind vibratory roller compactor were used to produce the study samples.

For evaluation of the obtained surfaces, a high precision 3D laser scanner was developed by the author. The texture of the study samples were scanned and processed in MATLAB. ISO 25178-2, International Standard for Specification and Measurement of 3D Surface Texture defines over 60 roughness parameters. These parameters were computed for all the study surfaces.

It has shown that roughness parameters of RCC and HMA specimens made with gyratory compactor are different than the parameters achieved from vibratory roller compactor. Speaking of concrete samples, it was observed that:

- On both compaction methods, two main mean height parameters, S_a and S_q tend to decrease by an increase in cement content.
- While the influence of aggregate gradation on gyratory compacted samples is negligible, a dramatic difference available between the nominal aggregate size of 12 mm and 19 mm on roller compacted samples.
- The skewness of all roller compacted samples are in close range to each other varying between -1 and -2.5, however, gyratory compacted samples exhibit great variation in results exceeding -3.5. In other words, peaks of gyratory compacted samples are beefier.
- The kurtosis of all roller compacted samples are in the same range to each other varying between 5 and 10, however, gyratory compacted samples show tremendous variation in results exceeding 25, which indicates peaks on gyratory compaction are sharper than roller compaction.

By investigating the height parameters of samples produced with these two compacting methods, it is concluded that generated textures are not identical and gyratory compaction is not able to represent the texture roller compaction generates.

In the lights of scanned surfaces and computed roughness parameters, the question that to what extent roller compacted concrete and asphalt are similar in terms of texture has been answered. Comparing both pavements:

- The RCC pavement samples showed less uniformity in terms of peaks' height and valleys' depth.
- The shape and geometry of generated peaks and valleys are different in these two different pavements.
- RCC pavement has a higher tendency to show an unexpected change in height compared to asphalt pavement.
- Asphalt pavement generates finer texture to RCC pavement.

- For RCC pavement, effect of change in maximum aggregate size on macro-texture is considerably greater to asphalt pavement.
- Asphalt produces uniform texture under cylinder compactor while RCC is prone to get waviness from compaction.
- Shape of the contact points for asphalt pavement samples are three times pointier than RCC pavement samples.
- RCC pavement samples are generating coarser segments comparing to asphalt samples.

From the above-mentioned observations, it has been concluded that using the same compaction techniques and similar effort, RCC and asphalt generate distinct textures.

Furthermore, this study has shown a good relationship between roughness parameters and MTD resulting from the sand patch test. Although this relationship was expected, to gain a deeper understanding of roughness parameters, all computed parameters were checked. The study showed a strong correlation exists between MTD and most of height and height-related parameters, however, the greatest correlation with R^2 of 0.80 was observed on Volume of Voids measured at 10% of peaks material ratio. Considering the high precision of volume calculation from a 3D profile, measurement error in the sand patch test can be the reason for slightly low R^2 value. Nevertheless, a model with a very small deviation from The World Road Association model was achieved.

Additionally, investigating a relationship between computed information and measured skid resistance has shown a weak to moderate relationship with Autocorrelation length of texture ($R^2 = 0.38$) and Magnitude of 2D Fourier Transform ($R^2 = 0.74$). The relationship was computed to be happening at only 1 millimeter depth of texture, hence, slices of only 1 mm height from top of texture were prepared virtually for calculation of Autocorrelation length and Magnitude of 2D Fourier Transform.

The study has shown that in general, asphalt pavement can give higher skid resistance to concrete pavement. It should be noted these results were obtained on

new pavement surface where aggregate had not been exposed to traffic or other abrasive factors, and aggregates were in binder coated condition.

In another step, the resistance of RCC pavement to chemical deicers induced freeze and thaw cycling damage were examined. ASTM C672 defines a procedure to test concrete for scaling resistance of concrete surfaces exposed to deicing chemicals. This is a qualitative test method that evaluates surface scaling based on visual observations. A novel procedure was followed to combine 3D scanning with the test and add quantitative analysis for better evaluation of results. The surfaces were scanned in three stages, on cycles zero, 25 and 50. And roughness parameters were compared. Changes in macro-texture of the surfaces as well as the volume of material loss were measured. It was observed that:

- An increase in cement content of mixtures can increase resistance to the damage.
- Freeze-thaw has an influence on valleys depth and can increase macro-texture depth.
- The resistance of aggregates to frost damage plays an important role in the scaling of RCC pavement.

Moreover, two surface modification techniques were conducted on the RCC surface. Lab prepared and field compacted RCC were subjected to set retarder immediately after compaction and power-washed after 24 hours to achieve Exposed Aggregate Concrete Surface. In another approach, certain gradation of aggregates was sprinkled onto improperly compacted RCC and compaction was carried out over the layer to achieve Chip Sprinkled Concrete Surface. Gathered information and testing demonstrated improvement on macro-texture of surfaces, however, no noticeable change in skid resistance was observed.

8.2 Suggestions for Future Studies

- The findings of this thesis all depend on extensive laboratory studies. The surface properties of RCC mixtures to include roughness or unevenness of actual field performance can be determined.

- This study is focused on plain RCC without additives or admixtures. Effect of using supplementary cementitious materials and concrete admixtures such as air entrainment agents can be investigated.
- Skid resistance is a function of speed. British pendulum measures low-speed friction (about 10 km/h). Investigation of micro-texture can be extended to Dynamic Friction Tester for determination of friction index at higher speeds.

REFERENCES

- AASHTO. (1976). *Guidelines for Skid Resistant Pavement Design*. American Association of State Highway and Transportation Officials .
- ACPA. (2000). *Concrete Pavement Surface Texture," a special report in Concrete Pavement Technology and Research*. SR902P.
- Akbulut, D. E., & Akoz, F. (2012). Effects of pozzolanas and fibers on mechanical properties of mortars in historical buildings. *Struct. Anal. Hist. Constr*, 1-3.
- Andersen, L. G. (2015). *Rolling resistance modelling: from functional data analysis to asset management system*. (Doctoral dissertation, Roskilde Universitet).
- Åström, H., & Wallman, C.-G. (2001). Friction Measurement Methods And The Correlation Between Road Friction And Traffic Safety. A Literature Review.
- Baker, I. O. (1918). *A treatise on roads and pavements*. John Wiley & Sons.
- Bazlamit, S. M., & Reza, F. (2005). Changes in asphalt pavement friction components and adjustment of skid number for temperature. *Journal of Transportation Engineering*, 131(6), 470–476.
- Bitelli, G., Simone, A., Girardi, F., & Lantieri, C. (2012). Laser scanning on road pavements: A new approach for characterizing surface texture. *Sensors (Switzerland)*, 12(7), 9110–9128. <https://doi.org/10.3390/s120709110>
- Blanchard, A. H. (1919). *American Highway Engineers' Handbook*. John Wiley & Sons, Incorporated.
- Board, H. R. (1972). *National Cooperative Highway Research Program Synthesis of highway practice 14: skid resistance*.
- Boscaino, G., Pratico, F. G., & Vaiana, R. (2004). Texture indicators and surface performance in flexible pavements. *Symposium on Pavement Surface Characteristics [of Roads and Airports], 5th, 2004, Toronto, Ontario, Canada*.

- Briant, P. (2002). *From Cyrus to Alexander: a history of the Persian Empire*. Eisenbrauns.
- Brown, G. E. (1975). Mineralogical Description of Two Samples of Giza Limestone'. *Electromagnetic Sounder Experiments at The Pyramids of Giza, Stanford Research International SRI*, 119–122.
- Chandler, J. W. E., Phillips, S. M., Roe, P. G., & Viner, H. E. (2003). Quieter concrete roads: construction, texture, skid resistance and noise. *TRL Report*, 576.
- Colley, B. E., Christensen, A. P., Nowlen, W. J., & Cement, P. (1969). Factors Affecting Skid Resistance and Safety of Concrete Pavements. *Special Report-Highway Research Board*, (101), 80.
- Collins, H. J., & Hart, C. A. (1936). *Principles of road engineering* (Vol. 6). E. Arnold.
- Collins, R., Watson, D., Johnson, A., & Wu, Y. (1997). Effect of aggregate degradation on specimens compacted by superpave gyratory compactor. *Transportation Research Record*, 1590(1), 1–9.
- Corley-Lay, J. B. (1998). Friction and surface texture characterization of 14 pavement test sections in Greenville, North Carolina. *Transportation Research Record*, 1639(1), 155–161.
- Dahir, S. H. M., & Gramling, W. L. (1990). NCHRP Synthesis of Highway Practice 158: Wet Pavement Safety Programs. *TRB, National Research Council, Washington, DC*.
- Davis, R. M. (2001). *Comparison of surface characteristics of hot-mix asphalt pavement surfaces at the Virginia Smart Road*. (Doctoral dissertation, Virginia Tech).
- Delatte, N., Amer, N., & Storey, C. (2003). Improved management of RCC pavement technology. *UTCA Report*, 1231, 54.
- Descornet, G., Fuchs, F., & Buys, R. (1993). Noise-reducing concrete pavements. *Fifth International Conference on Concrete Pavement Design and Rehabilitation* Purdue University, School of Civil Engineering; Federal

Highway Administration; Portland Cement Association; Transportation Research Board; Indiana Department of Transportation; Federal Aviation Administration; and American Concrete Pavement Association. (Vol. 2).

Do, M.-T., Tang, Z., Kane, M., & de Larrard, F. (2009). Evolution of road-surface skid-resistance and texture due to polishing. *Wear, 266*(5–6), 574–577.

Dondi, G., Simone, A., Lantieri, C., & Vignali, V. (2010). Characterization of pavement surface texture using 3D Laser scanner technique. *Proceedings of the 11th International Conference on Asphalt Pavement. August, 1–6.*

Embacher, R. A., & Snyder, M. B. (2001). Life-cycle cost comparison of asphalt and concrete pavements on low-volume roads; case study comparisons. *Transportation Research Record, 1749*(1), 28–37.

Ergun, M., Iyınam, S., & Iyınam, A. F. (2005). Prediction of road surface friction coefficient using only macro-and microtexture measurements. *Journal of Transportation Engineering, 131*(4), 311–319.

Flintsch, G. W., De León, E., McGhee, K. K., & Al-Qadi, I. L. (2003). Pavement surface macrotexture measurement and applications. *Transportation Research Record, 1860*(1), 168–177.

Forster, S. W. (1989). Pavement microtexture and its relation to skid resistance. *Transportation Research Record, 1215*, 151–164.

Fuchs, F. (1981). Texturing of cement concrete pavements by chip sprinkling the fresh concrete. *Transportation Research Record, 821*, 56–60.

Gibbons, R. B., & Hankey, J. (2007). Wet night visibility of pavement markings: dynamic experiment. *Transportation Research Record, 2015*(1), 73–80.

Gillespie, H. (1992). *A Century of Progress: The History of Hot Mix Asphalt* (1st Ed.). Lanham, MD: National Asphalt Pavement Association.

Hall, J. W., Smith, K. L., Titus-Glover, L., Wambold, J. C., Yager, T. J., & Rado, Z. (2009). Guide for pavement friction. *Final Report for NCHRP Project, 1*, 43.

Halsted, G. E. (2009). Roller-compacted concrete pavements for highways and

streets. *2009 Annual Conference And Exhibition Of The Transportation Association Of Canada-Transportation In A Climate Of Change.*

Harrington, D., Abdo, F., Adaska, W., Hazaree, C. V., Ceylan, H., & Bektas, F. (2010). *Guide for roller-compacted concrete pavements.*

Hayden, C. M. (1982). *Pavement Surface Characteristics and Materials* (Vol. 763). ASTM International.

Henry, J. J. (2000). NCHRP synthesis of highway practice 291: Evaluation of pavement friction characteristics. *TRB, National Research Council, Washington, DC.*

Henry, J. J., & Saito, K. (1983). *Skid-Resistance Measurements with Blank and Ribbed Test Tires and Their Relationship to Pavement Texture.*

Herrfeld, M. (n.d.). Requirements for the application of surface retarders in whisper concrete road projects. *Proc. 8 Th International Symposium on Concrete Roads, 5, 7–8.*

Hibbs, B. O., & Larson, R. M. (1996). *Tire Pavement Noise and Safety Performance, PCC Surface Texture Technical Working Group.* United States. Federal Highway Administration. Office of Engineering.

Hoerner, T. E., Smith, K. D., Larson, R. M., & Swanlund, M. E. (2003). Current practice of portland cement concrete pavement texturing. *Transportation Research Record, 1860(1), 178–186.*

Hogervorst, D. (1974). Some properties of crushed stone for road surfaces. *Bulletin of the International Association of Engineering Geology-Bulletin de l'Association Internationale de Géologie de l'Ingénieur, 10(1), 59–64.*

Horvath, A., & Hendrickson, C. (1998). Comparison of environmental implications of asphalt and steel-reinforced concrete pavements. *Transportation Research Record, 1626(1), 105–113.*

Janisch, D. (2006). An overview of Mn/DOT's pavement condition rating procedures and indices. *Minnesota Department of Transportation, Saint Paul, MN.*

- Jasiczak, J., & Zielinski, K. (2006). Effect of protein additive on properties of mortar. *Cement and Concrete Composites*, 28(5), 451-457.
- Jones, C.R.; Rolt, J.; Smith, H.R.; Parkman, C. (1999). *A guide to the pavement evaluation and maintenance of bitumen-surfaced roads in tropical and sub-tropical countries*.
- Juli, D. (1989). Technical Committee Report on Surface Characteristics. *RRU Newsletter*, 99, 9–11.
- Kaloush, K. E., Carlson, J. D., Golden, J. S., & Phelan, P. E. (2008). *The thermal and radiative characteristics of concrete pavements in mitigating urban heat island effects* (No. PCA R&D SN2969).
- Kanafi, M. M., & Tuononen, A. J. (2017). Top topography surface roughness power spectrum for pavement friction evaluation. *Tribology International*, 107, 240–249.
- Kummer, H. W. (1966). *Unified theory of rubber and tire friction*.
- Li, S., Noureldin, A. S., & Zhu, K. Q. (2011). *Characterization of microtexture on typical pavement surfaces: a pilot study* (No. 11-1457).
- Mahone, D. C. (1977). *Texturing new concrete pavements*. Virginia Transportation Research Council.
- Masad, E., Muhunthan, B., Shashidhar, N., & Harman, T. (1999). Quantifying laboratory compaction effects on the internal structure of asphalt concrete. *Transportation Research Record*, 1681(1), 179–185.
- Mataei, B., Zakeri, H., Zahedi, M., & Nejad, F. M. (2016). Pavement Friction and Skid Resistance Measurement Methods: A Literature Review. *Open Journal of Civil Engineering*, 06(04), 537–565. <https://doi.org/10.4236/ojce.2016.64046>
- McGhee, K. K., & Flintsch, G. W. (2003). *High-speed texture measurement of pavements*. Virginia Center for Transportation Innovation and Research.
- Meegoda, J. N. (2009). *Non-contact skid resistance measurement: final report, December 2009*. New Jersey. Dept. of Transportation.

- Mosher, L. G. (1985). Restoration of Final Surface to Concrete Pavement by Diamond Saw Grinding. *Third International Conference on Concrete Pavement Design and Rehabilitation* Purdue University, School of Civil Engineering; Federal Highway Administration; Portland Cement Association; Transportation Research Board; Federal Aviation Administration; and I, (1 Volume).
- Noyce, D. A., Bahia, H. U., Yambo, J., Chapman, J., & Bill, A. (2005). Incorporating Road Safety into Pavement Management: Maximizing Surface Friction for Road Safety Improvements. *University of Wisconsin*. Retrieved from <http://www.mrutc.org/research/0404/>
- Olek, J., Weiss, W. J., & Garcia-Villarreal, R. (2004). *Relating surface texture of rigid pavement with noise and skid resistance*.
- Persson, B. N. J. (2001). Theory of rubber friction and contact mechanics. *The Journal of Chemical Physics*, 115(8), 3840–3861.
- Peterson, R. L., Mahboub, K. C., Michael Anderson, R., Masad, E., & Tashman, L. (2003). Superpave® laboratory compaction versus field compaction. *Transportation Research Record*, 1832(1), 201–208.
- Pittman, D. W. (1986). Construction of roller-compacted concrete pavements. *Transportation Research Record*, 1062, 13–19.
- Properties, A. C. P. A. T. S. on S. (1975). *Guideline for Texturing of Portland Cement Concrete Highway Pavements*. American Concrete Paving Association.
- Radford, T. A. (1940). *The Construction of Roads and Pavements*. McGraw Hill.
- Rado, Z. (1994). Analysis of texture models. *Pennsylvania Transportation Institute, Pennsylvania State University, State College*.
- Ray, G. K., & Norling, L. T. (1974). *More Macrotecture in Concrete Pavement for Greater, Longer-lasting Skid Resistance*. Portland Cement Association.
- Roberts, A. D. (1988). *Rubber adhesion at high rolling speeds*.
- Roe, P. G., Parry, A. R., & Viner, H. E. (1998). *High and low speed skidding*

resistance: the influence of texture depth.

Roemmele, C. F. (1986). A History of Sawing, Grinding & Grooving with Diamond. *Solutions for Pavement Rehabilitation Problems*, 255–270. ASCE.

Rose, J. G., Gallaway, B. M., & Hankins, K. D. (1970). Macrotexture Measurement and Related Skid Resistance at Speeds from 20 to 60 Miles per Hour. *Highway Research Record*, (341).

Rugenstein, E. E. (1977). Summary and evaluation of concrete pavement texturing practices. *International Conference on Concrete Pavement Design* Purdue University, School of Civil Engineering; Federal Highway Administration; Portland Cement Association; Transportation Research Board; Federal Aviation Administration; and Indiana Department of High.

Sandberg, U. (1998). *Influence of road surface texture on traffic characteristics related to environment, economy and safety: A state-of-the-art study regarding measures and measuring methods*. Statens väg-och transportforskningsinstitut., VTI notat 53A-1997.

Sayers, M. W. (1989). Two quarter-car models for defining road roughness: IRI and HRI. *Transportation Research Record*, (1215).

Scharnigg, K., & Schwalbe, G. (2010). Report on knowledge gaps and proposals for further research concerning optimisation for road surfaces and tyres for skid resistance, rolling resistance and noise emissions TYROSAFE project <http://Tyrosafe.Fehrl.Org>.

Serigos, P. A., De Fortier Smit, A., & Prozzi, J. A. (2014). Incorporating surface microtexture in the prediction of skid resistance of flexible pavements. *Transportation Research Record*, 2457(1), 105–113.

Sommer, H. (1994). Developments for the exposed aggregate technique in Austria. *7th International Symposium on Concrete Roads*, 3(5).

Sommer, H. (1998). Longtime experience with exposed aggregate surfaces in Austria. Theme 3-Pavement Performance and Evaluation. *8 Th International Symposium on Concrete Roads, Lizbona, Portugalia*, 117–121.

Stinglhammer, H. (1994). Noise reducing exposed aggregate surfaces experience and

- recommendations. *1994/7th International Symposium on Concrete Roads*, 137–140.
- Sumitsawan, P., Ardenkani, S. A., & Romanoschi, S. (2009). Effect of pavement type on fuel consumption and emissions. *Proceedings of the 2009 Mid-Continent Transportation Research Symposium*.
- Tayabji, S. D., Sherman, T. W., Arent, W. L., Kohn, S., Piggott, R. W., Berry, J. R., ...& Zollinger, D. G. (1995). *Report on Roller-Compacted Concrete Pavements*.
- Thornton, J. B. (1974). *Determination of Desirable Finish for Concrete Pavement* (Publication)
- Tighe, S., Fung, R., & Smith, T. (2001). Concrete pavements in Canada: State-of-the-art practice. *Seventh International Conference on Concrete Pavements. The Use of Concrete in Developing Long-Lasting Pavement Solutions for the 21st Century International Society for Concrete Pavements, 1*.
- Tillson, G. W. (1900). *Street Pavements and Paving Materials: A Manual of City Pavements: the Methods and Materials of Their Construction*. J. Wiley.
- Ueckermann, A., Wang, D., Oeser, M., & Steinauer, B. (2015). Calculation of skid resistance from texture measurements. *Journal of Traffic and Transportation Engineering (English Edition)*, 2(1), 3–16.
- Van Dam, T., Taylor, P., Fick, G., Gress, D., VanGeem, M., & Lorenz, E. (2011). *Sustainable concrete pavements: a manual of practice*.
- Viner, H., Abbott, P., Dunford, A., Dhillon, N., Parsley, L., & Read, C. (2006). Surface texture measurement on local roads. *Report PPR148. TRL Ltd, UK*.
- Wambold, J. C., Henry, J. J., & Blackburn, R. R. (1984). *Evaluation Of Pavement Surface Texture: Significance And Measurement Techniques. Volume Ii: Comprehensive Report. Final Report*.
- Wambold, J. C., Henry, J. J., & Yager, T. (2004). NASA Wallops Tire/Runway Friction Workshops 1994-2003. *Proceedings of the Fifth International Symposium on Pavement Surface Characteristics-SURF*.

Wu, C.-L., & Nagi, M. A. (1995). *Optimizing surface texture of concrete pavement* (No. RD111T).

Yager, T. J., & Bühlmann, F. (1982). Macrotexture and drainage measurements on a variety of concrete and asphalt surfaces. In *Pavement Surface Characteristics and Materials*. ASTM International.

Zuniga-Garcia, N., & Prozzi, J. A. (2016). *Contribution of Micro-and Macro-Texture for Predicting Friction on Pavement Surfaces* (No. CHPP Report-UTA# 3-2016).

APPENDICES

A. Roughness Parameters of The Specimens

| Sample ID | Height Parameter | | | | | | |
|------------------|----------------------|----------------------|----------------------|----------------------|----------------------|-----------------|-----------------|
| | S _p mm | S _v mm | S _z mm | S _a mm | S _q mm | S _{sk} | S _{ku} |
| SGCC-200-12-4-1 | 1.110 | 2.357 | 3.468 | 0.324 | 0.425 | -1.227 | 4.781 |
| SGCC-200-12-4-2 | 1.251 | 3.066 | 4.318 | 0.346 | 0.458 | -1.373 | 5.781 |
| SGCC-200-12-4-3 | 1.538 | 3.489 | 5.027 | 0.401 | 0.540 | -1.077 | 5.555 |
| SGCC-200-12-4-4 | 1.147 | 2.916 | 4.063 | 0.325 | 0.444 | -1.149 | 5.166 |
| SGCC-200-12-4-5 | 1.223 | 3.172 | 4.395 | 0.376 | 0.496 | -1.379 | 5.439 |
| SGCC-200-12-4-6 | 1.437 | 2.994 | 4.432 | 0.398 | 0.543 | -1.124 | 5.262 |
| SGCC-200-12-4-7 | 1.275 | 2.930 | 4.205 | 0.314 | 0.424 | -1.470 | 6.364 |
| SGCC-200-12-4-8 | 1.101 | 4.723 | 5.824 | 0.344 | 0.470 | -1.635 | 7.675 |
| SGCC-200-12-4-9 | 0.879 | 2.145 | 3.024 | 0.281 | 0.372 | -1.346 | 5.262 |
| SGCC-200-12-4-10 | 1.159 | 3.075 | 4.234 | 0.306 | 0.442 | -1.649 | 8.211 |
| SGCC-200-12-5-1 | 0.972 | 4.199 | 5.171 | 0.262 | 0.353 | -1.580 | 6.962 |
| SGCC-200-12-5-2 | 1.119 | 3.895 | 5.015 | 0.291 | 0.394 | -1.591 | 6.413 |
| SGCC-200-12-5-3 | 0.923 | 2.335 | 3.258 | 0.254 | 0.332 | -1.396 | 5.273 |
| SGCC-200-12-5-4 | 0.947 | 2.698 | 3.645 | 0.222 | 0.298 | -1.519 | 6.048 |
| SGCC-200-12-5-5 | 1.383 | 4.068 | 5.452 | 0.374 | 0.508 | -1.563 | 7.066 |
| SGCC-200-12-5-6 | 0.738 | 2.705 | 3.444 | 0.216 | 0.289 | -1.642 | 6.527 |
| SGCC-200-12-5-7 | 1.167 | 5.364 | 6.532 | 0.310 | 0.433 | -1.721 | 8.145 |
| SGCC-200-12-5-8 | 1.181 | 2.454 | 3.635 | 0.258 | 0.345 | -1.213 | 5.234 |
| SGCC-200-12-5-9 | 1.244 | 2.996 | 4.241 | 0.342 | 0.448 | -1.010 | 4.286 |
| SGCC-200-12-5-10 | 1.119 | 2.978 | 4.097 | 0.320 | 0.412 | -0.966 | 4.019 |
| SGCC-200-12-6-1 | 0.971 | 3.430 | 4.401 | 0.284 | 0.394 | -1.827 | 9.056 |
| SGCC-200-12-6-2 | 0.798 | 3.602 | 4.400 | 0.146 | 0.239 | -3.225 | 25.687 |
| SGCC-200-12-6-3 | 0.722 | 3.085 | 3.807 | 0.236 | 0.342 | -2.001 | 10.932 |
| SGCC-200-12-6-4 | 1.173 | 2.829 | 4.002 | 0.210 | 0.301 | -1.923 | 10.123 |
| SGCC-200-12-6-5 | 0.856 | 2.805 | 3.661 | 0.286 | 0.389 | -1.510 | 6.866 |
| SGCC-200-12-6-6 | 1.088 | 2.874 | 3.962 | 0.252 | 0.365 | -1.647 | 8.246 |
| SGCC-200-12-6-7 | 0.913 | 3.097 | 4.010 | 0.223 | 0.329 | -2.181 | 11.760 |
| SGCC-200-12-6-8 | 0.705 | 2.928 | 3.633 | 0.166 | 0.272 | -2.937 | 18.776 |
| SGCC-300-12-5-1 | 0.952 | 2.350 | 3.301 | 0.183 | 0.283 | -1.940 | 7.988 |
| SGCC-300-12-5-2 | 0.430 | 3.117 | 3.547 | 0.136 | 0.223 | -2.697 | 14.509 |
| SGCC-300-12-5-3 | 1.197 | 3.196 | 4.392 | 0.353 | 0.462 | -1.184 | 3.525 |
| SGCC-400-12-4-1 | 0.877 | 2.846 | 3.723 | 0.287 | 0.392 | -1.628 | 6.722 |
| SGCC-400-12-4-2 | 0.582 | 2.128 | 2.710 | 0.184 | 0.262 | -1.862 | 8.508 |
| SGCC-400-12-4-3 | 1.098 | 2.920 | 4.017 | 0.242 | 0.341 | -1.753 | 7.677 |

| Sample ID | Height Parameter | | | | | | |
|------------------|----------------------|----------------------|----------------------|----------------------|----------------------|-----------------|-----------------|
| | S _p mm | S _v mm | S _z mm | S _a mm | S _q mm | S _{sk} | S _{ku} |
| SGCC-400-12-4-4 | 0.922 | 2.685 | 3.608 | 0.160 | 0.232 | -1.906 | 10.613 |
| SGCC-400-12-4-5 | 0.615 | 2.075 | 2.690 | 0.157 | 0.233 | -2.308 | 11.953 |
| SGCC-400-12-4-6 | 0.954 | 2.278 | 3.232 | 0.204 | 0.304 | -1.495 | 8.314 |
| SGCC-400-12-4-7 | 1.396 | 3.538 | 4.933 | 0.297 | 0.420 | -1.983 | 10.369 |
| SGCC-400-12-4-8 | 0.727 | 1.944 | 2.671 | 0.176 | 0.249 | -1.786 | 8.034 |
| SGCC-400-12-4-9 | 0.822 | 2.711 | 3.533 | 0.211 | 0.284 | -1.555 | 6.841 |
| SGCC-400-12-4-10 | 1.136 | 2.817 | 3.953 | 0.257 | 0.355 | -1.649 | 7.441 |
| SGCC-400-12-5-1 | 1.069 | 2.369 | 3.335 | 0.239 | 0.277 | -1.368 | 5.342 |
| SGCC-400-12-5-2 | 0.860 | 3.996 | 4.564 | 0.225 | 0.295 | -2.638 | 16.127 |
| SGCC-400-12-5-3 | 0.737 | 3.194 | 3.704 | 0.220 | 0.267 | -1.717 | 7.465 |
| SGCC-400-12-5-4 | 0.951 | 3.725 | 4.422 | 0.235 | 0.296 | -1.966 | 11.107 |
| SGCC-400-12-5-5 | 0.583 | 2.043 | 2.494 | 0.146 | 0.187 | -1.754 | 8.562 |
| SGCC-400-12-5-6 | 0.948 | 3.049 | 3.810 | 0.235 | 0.294 | -1.827 | 7.861 |
| SGCC-400-12-5-7 | 0.676 | 2.654 | 3.149 | 0.191 | 0.239 | -1.948 | 8.462 |
| SGCC-400-12-5-8 | 0.703 | 2.108 | 2.688 | 0.183 | 0.223 | -1.614 | 7.065 |
| SGCC-400-12-5-9 | 1.091 | 2.893 | 3.831 | 0.219 | 0.279 | -1.730 | 8.491 |
| SGCC-400-12-5-10 | 0.871 | 3.045 | 3.721 | 0.235 | 0.302 | -1.813 | 8.964 |
| SGCC-400-12-6-1 | 0.496 | 1.998 | 2.494 | 0.096 | 0.160 | -3.666 | 25.462 |
| SGCC-400-12-6-2 | 0.882 | 4.229 | 5.110 | 0.196 | 0.288 | -2.358 | 12.980 |
| SGCC-400-12-6-3 | 0.605 | 3.139 | 3.745 | 0.170 | 0.259 | -2.610 | 12.979 |
| SGCC-400-12-6-4 | 0.801 | 2.148 | 2.949 | 0.164 | 0.237 | -2.033 | 9.180 |
| SGCC-400-12-6-5 | 0.768 | 2.142 | 2.910 | 0.173 | 0.251 | -1.854 | 8.272 |
| SGCC-400-12-6-6 | 0.799 | 2.651 | 3.449 | 0.166 | 0.242 | -1.978 | 9.831 |
| SGCC-400-12-6-7 | 0.624 | 2.262 | 2.886 | 0.161 | 0.241 | -2.259 | 11.413 |
| SGCC-400-12-6-8 | 0.960 | 2.184 | 3.144 | 0.166 | 0.239 | -1.783 | 8.581 |
| SGCC-400-12-6-9 | 0.736 | 2.379 | 3.114 | 0.131 | 0.211 | -2.950 | 18.430 |
| SGCC-400-12-6-10 | 0.855 | 3.234 | 4.089 | 0.131 | 0.201 | -2.697 | 20.733 |
| SGCC-200-19-4-1 | 1.208 | 2.709 | 3.917 | 0.297 | 0.410 | -1.498 | 6.400 |
| SGCC-200-19-4-2 | 1.607 | 5.225 | 6.832 | 0.408 | 0.594 | -1.978 | 10.904 |
| SGCC-200-19-4-3 | 0.932 | 3.739 | 4.671 | 0.343 | 0.473 | -1.810 | 8.233 |
| SGCC-200-19-4-4 | 1.162 | 3.028 | 4.190 | 0.299 | 0.402 | -1.441 | 6.105 |
| SGCC-200-19-4-5 | 1.081 | 2.751 | 3.832 | 0.286 | 0.395 | -1.652 | 7.282 |
| SGCC-200-19-4-6 | 1.259 | 4.883 | 6.142 | 0.334 | 0.475 | -2.121 | 11.758 |
| SGCC-200-19-4-7 | 0.966 | 2.844 | 3.810 | 0.276 | 0.374 | -1.511 | 6.646 |
| SGCC-200-19-4-8 | 1.328 | 3.241 | 4.569 | 0.351 | 0.488 | -1.632 | 7.387 |
| SGCC-200-19-4-9 | 1.512 | 5.078 | 6.590 | 0.325 | 0.453 | -1.821 | 8.551 |
| SGCC-200-19-4-10 | 1.107 | 3.472 | 4.579 | 0.366 | 0.516 | -1.910 | 8.263 |
| SGCC-200-19-5-1 | 0.929 | 3.154 | 4.083 | 0.292 | 0.399 | -1.763 | 7.604 |
| SGCC-200-19-5-2 | 1.249 | 3.588 | 4.837 | 0.400 | 0.541 | -1.530 | 6.310 |
| SGCC-200-19-5-3 | 0.913 | 3.532 | 4.444 | 0.355 | 0.474 | -1.642 | 6.757 |
| SGCC-200-19-5-4 | 0.970 | 3.932 | 4.903 | 0.326 | 0.445 | -1.815 | 7.851 |
| SGCC-200-19-5-5 | 1.070 | 3.008 | 4.078 | 0.322 | 0.432 | -1.545 | 6.313 |

| Sample ID | Height Parameter | | | | | | |
|------------------|----------------------|----------------------|----------------------|----------------------|----------------------|-----------------|-----------------|
| | S _p mm | S _v mm | S _z mm | S _a mm | S _q mm | S _{sk} | S _{ku} |
| SGCC-200-19-5-6 | 0.930 | 5.167 | 6.097 | 0.342 | 0.460 | -1.662 | 7.603 |
| SGCC-200-19-5-7 | 1.011 | 3.335 | 4.347 | 0.305 | 0.419 | -1.812 | 7.782 |
| SGCC-200-19-5-8 | 0.783 | 3.119 | 3.901 | 0.304 | 0.409 | -1.710 | 7.086 |
| SGCC-200-19-5-9 | 0.780 | 5.038 | 8.294 | 0.332 | 0.465 | -1.670 | 10.187 |
| SGCC-200-19-6-1 | 1.044 | 3.764 | 4.808 | 0.321 | 0.441 | -1.821 | 7.767 |
| SGCC-200-19-6-2 | 1.879 | 5.148 | 7.027 | 0.491 | 0.402 | -1.847 | 8.111 |
| SGCC-200-19-6-3 | 1.205 | 4.733 | 5.938 | 0.452 | 0.456 | -1.887 | 8.273 |
| SGCC-200-19-6-4 | 0.863 | 3.092 | 3.955 | 0.290 | 0.364 | -2.024 | 9.120 |
| SGCC-200-19-6-5 | 2.255 | 3.609 | 5.864 | 0.320 | 0.303 | -2.016 | 8.634 |
| SGCC-200-19-6-6 | 0.985 | 3.995 | 4.980 | 0.251 | 0.306 | -2.147 | 10.452 |
| SGCC-200-19-6-7 | 0.625 | 3.491 | 4.116 | 0.212 | 0.311 | -2.243 | 11.002 |
| SGCC-200-19-6-8 | 0.717 | 2.812 | 3.530 | 0.208 | 0.234 | -2.260 | 10.756 |
| SGCC-200-19-6-9 | 0.686 | 4.085 | 4.771 | 0.194 | 0.685 | -3.518 | 24.640 |
| SGCC-200-19-6-10 | 0.912 | 2.492 | 3.404 | 0.152 | 0.631 | -2.572 | 14.067 |
| SGCC-300-19-5-1 | 0.814 | 2.986 | 4.560 | 0.225 | 0.390 | -2.671 | 11.587 |
| SGCC-300-19-5-2 | 0.514 | 2.632 | 3.776 | 0.138 | 0.233 | -3.126 | 19.002 |
| SGCC-300-19-5-3 | 0.760 | 1.786 | 3.055 | 0.181 | 0.269 | -1.173 | 4.919 |
| SGCC-400-19-4-1 | 0.886 | 2.788 | 4.042 | 0.189 | 0.350 | -2.528 | 10.804 |
| SGCC-400-19-4-2 | 0.659 | 2.107 | 3.042 | 0.127 | 0.231 | -2.388 | 11.924 |
| SGCC-400-19-4-3 | 1.082 | 2.865 | 4.342 | 0.172 | 0.323 | -2.366 | 11.796 |
| SGCC-400-19-4-4 | 0.655 | 2.733 | 3.727 | 0.119 | 0.221 | -2.689 | 16.492 |
| SGCC-400-19-4-5 | 0.523 | 1.874 | 2.636 | 0.117 | 0.228 | -2.724 | 13.136 |
| SGCC-400-19-4-6 | 0.694 | 2.038 | 3.005 | 0.130 | 0.233 | -2.258 | 11.163 |
| SGCC-400-19-4-7 | 0.561 | 2.043 | 2.864 | 0.120 | 0.220 | -2.361 | 11.195 |
| SGCC-400-19-4-8 | 0.853 | 2.860 | 4.084 | 0.192 | 0.355 | -2.378 | 10.045 |
| SGCC-400-19-4-9 | 0.535 | 2.489 | 3.326 | 0.108 | 0.202 | -2.928 | 18.266 |
| SGCC-400-19-5-1 | 0.566 | 2.772 | 2.864 | 0.183 | 0.259 | -1.921 | 8.601 |
| SGCC-400-19-5-2 | 1.344 | 3.429 | 4.280 | 0.135 | 0.222 | -2.866 | 25.612 |
| SGCC-400-19-5-3 | 0.541 | 2.438 | 2.568 | 0.167 | 0.244 | -2.176 | 10.299 |
| SGCC-400-19-5-4 | 0.536 | 3.291 | 3.245 | 0.152 | 0.229 | -2.751 | 17.671 |
| SGCC-400-19-5-5 | 0.549 | 3.370 | 3.324 | 0.188 | 0.295 | -2.972 | 16.360 |
| SGCC-400-19-5-6 | 1.118 | 4.297 | 4.716 | 0.226 | 0.345 | -2.179 | 12.556 |
| SGCC-400-19-5-7 | 0.914 | 3.047 | 3.482 | 0.160 | 0.249 | -2.634 | 15.290 |
| SGCC-400-19-5-8 | 1.530 | 4.653 | 5.471 | 0.231 | 0.375 | -2.525 | 17.185 |
| SGCC-400-19-5-9 | 0.570 | 2.417 | 2.586 | 0.184 | 0.274 | -2.145 | 9.825 |
| SGCC-400-19-5-10 | 0.501 | 2.747 | 2.770 | 0.168 | 0.247 | -2.311 | 11.373 |
| SGCC-400-19-6-1 | 0.809 | 3.551 | 4.360 | 0.262 | 0.372 | -2.298 | 11.075 |
| SGCC-400-19-6-2 | 0.627 | 2.499 | 3.127 | 0.158 | 0.233 | -2.377 | 12.675 |
| SGCC-400-19-6-3 | 0.636 | 3.089 | 3.726 | 0.157 | 0.253 | -3.320 | 23.181 |
| SGCC-400-19-6-4 | 0.863 | 3.773 | 4.637 | 0.185 | 0.296 | -3.168 | 19.657 |
| SGCC-400-19-6-5 | 0.732 | 3.486 | 4.217 | 0.188 | 0.289 | -2.859 | 17.604 |

| Sample ID | Height Parameter | | | | | | |
|------------------|----------------------|----------------------|----------------------|----------------------|----------------------|-----------------|-----------------|
| | S _p mm | S _v mm | S _z mm | S _a mm | S _q mm | S _{sk} | S _{ku} |
| SGCC-400-19-6-6 | 0.606 | 2.878 | 3.485 | 0.151 | 0.226 | -2.837 | 18.534 |
| SGCC-400-19-6-7 | 0.529 | 2.322 | 2.851 | 0.124 | 0.199 | -3.427 | 23.545 |
| SGCC-400-19-6-8 | 0.882 | 2.818 | 3.700 | 0.146 | 0.251 | -3.627 | 27.534 |
| SGCC-400-19-6-9 | 0.754 | 2.173 | 2.927 | 0.105 | 0.160 | -2.664 | 17.971 |
| SGCC-400-19-6-10 | 0.467 | 1.091 | 1.558 | 0.083 | 0.116 | -1.502 | 8.986 |
| SGC-HMA-L-19-1 | 1.295 | 5.105 | 6.400 | 0.538 | 0.718 | -1.538 | 6.332 |
| SGC-HMA-L-19-2 | 1.686 | 7.113 | 8.799 | 0.611 | 0.829 | -1.755 | 8.139 |
| SGC-HMA-L-19-3 | 1.951 | 5.393 | 7.344 | 0.659 | 0.862 | -1.351 | 5.612 |
| SGC-HMA-L-19-4 | 1.689 | 6.290 | 7.978 | 0.523 | 0.703 | -1.580 | 7.275 |
| SGC-HMA-L-19-5 | 1.375 | 5.378 | 6.753 | 0.543 | 0.704 | -1.340 | 5.408 |
| SGC-HMA-L-19-6 | 1.385 | 5.299 | 6.684 | 0.519 | 0.685 | -1.419 | 5.876 |
| SGC-HMA-L-12-1 | 1.145 | 2.360 | 3.505 | 0.237 | 0.317 | -1.307 | 6.165 |
| SGC-HMA-L-12-2 | 1.128 | 2.726 | 3.854 | 0.251 | 0.334 | -1.177 | 5.931 |
| SGC-HMA-L-12-3 | 0.992 | 2.379 | 3.371 | 0.237 | 0.318 | -1.331 | 6.269 |
| SGC-HMA-L-12-4 | 1.128 | 2.781 | 3.909 | 0.313 | 0.412 | -1.076 | 5.052 |
| SGC-HMA-L-12-5 | 0.931 | 2.708 | 3.639 | 0.246 | 0.327 | -1.266 | 5.813 |
| SGC-HMA-L-12-6 | 1.309 | 5.088 | 6.397 | 0.317 | 0.437 | -1.580 | 9.357 |
| RCC-200-12-1 | 1.236 | 3.915 | 5.150 | 0.386 | 0.548 | -1.961 | 8.703 |
| RCC-200-12-2 | 1.242 | 2.668 | 3.910 | 0.421 | 0.547 | -1.287 | 4.626 |
| RCC-200-12-3 | 0.956 | 3.242 | 4.198 | 0.312 | 0.454 | -2.067 | 9.051 |
| RCC-200-12-4 | 1.110 | 3.233 | 4.343 | 0.353 | 0.493 | -1.844 | 7.391 |
| RCC-200-12-5 | 1.323 | 3.959 | 5.282 | 0.342 | 0.482 | -1.996 | 9.614 |
| RCC-200-12-6 | 1.994 | 4.216 | 6.210 | 0.397 | 0.532 | -0.992 | 4.070 |
| RCC-200-12-7 | 1.225 | 3.612 | 4.837 | 0.198 | 0.329 | -1.720 | 6.674 |
| RCC-200-12-8 | 0.707 | 3.013 | 3.720 | 0.267 | 0.366 | -1.435 | 6.746 |
| RCC-200-12-9 | 1.361 | 2.733 | 4.093 | 0.359 | 0.514 | -1.970 | 8.624 |
| RCC-200-12-10 | 0.988 | 4.084 | 5.072 | 0.645 | 0.835 | -3.621 | 25.481 |
| RCC-300-12-1 | 1.378 | 2.826 | 4.204 | 0.334 | 0.423 | -1.592 | 7.079 |
| RCC-300-12-2 | 1.673 | 2.638 | 4.312 | 0.327 | 0.430 | -1.680 | 7.753 |
| RCC-300-12-3 | 0.957 | 1.073 | 1.544 | 0.095 | 0.429 | -1.735 | 9.821 |
| RCC-300-12-4 | 0.889 | 2.994 | 3.950 | 0.331 | 0.309 | -1.932 | 7.917 |
| RCC-300-12-5 | 0.732 | 2.782 | 3.671 | 0.228 | 0.402 | -2.390 | 9.169 |
| RCC-300-12-6 | 0.638 | 2.825 | 3.557 | 0.305 | 0.224 | -2.110 | 6.834 |
| RCC-300-12-7 | 0.884 | 2.101 | 2.739 | 0.165 | 0.368 | -2.450 | 13.460 |
| RCC-300-12-8 | 0.621 | 2.670 | 3.555 | 0.293 | 0.270 | -1.658 | 12.487 |
| RCC-300-12-9 | 1.061 | 2.557 | 3.178 | 0.202 | 0.409 | -2.254 | 12.558 |
| RCC-300-12-10 | 0.471 | 3.414 | 4.476 | 0.298 | 0.121 | -2.500 | 11.615 |
| RCC-400-12-1 | 0.989 | 2.017 | 3.006 | 0.263 | 0.354 | -1.927 | 7.538 |
| RCC-400-12-2 | 0.528 | 1.389 | 1.916 | 0.233 | 0.302 | -1.575 | 5.683 |
| RCC-400-12-3 | 1.333 | 1.923 | 3.256 | 0.239 | 0.330 | -1.823 | 7.456 |
| RCC-400-12-4 | 1.232 | 1.945 | 3.177 | 0.278 | 0.363 | -1.210 | 5.256 |

| Sample ID | Height Parameter | | | | | | |
|---------------|----------------------|----------------------|----------------------|----------------------|----------------------|-----------------|-----------------|
| | S _p mm | S _v mm | S _z mm | S _a mm | S _q mm | S _{sk} | S _{ku} |
| RCC-400-12-5 | 1.090 | 2.403 | 3.493 | 0.308 | 0.419 | -1.320 | 6.123 |
| RCC-400-12-6 | 0.775 | 2.325 | 3.100 | 0.269 | 0.372 | -1.988 | 8.491 |
| RCC-400-12-7 | 0.978 | 2.445 | 3.423 | 0.230 | 0.319 | -2.356 | 10.334 |
| RCC-400-12-8 | 0.743 | 1.821 | 2.564 | 0.227 | 0.303 | -1.731 | 7.373 |
| RCC-400-12-9 | 0.579 | 1.819 | 2.397 | 0.228 | 0.292 | -1.562 | 5.391 |
| RCC-400-12-10 | 0.647 | 1.398 | 2.045 | 0.184 | 0.253 | -2.114 | 7.705 |
| RCC-200-19-1 | 2.627 | 6.833 | 9.461 | 0.684 | 0.868 | -1.684 | 6.847 |
| RCC-200-19-2 | 3.192 | 7.591 | 10.783 | 0.867 | 1.037 | -1.223 | 4.726 |
| RCC-200-19-3 | 1.735 | 7.136 | 8.871 | 0.571 | 0.725 | -1.890 | 8.775 |
| RCC-200-19-4 | 1.999 | 5.330 | 7.330 | 0.605 | 0.773 | -1.721 | 6.752 |
| RCC-200-19-5 | 3.171 | 7.051 | 10.222 | 0.558 | 0.725 | -1.711 | 8.411 |
| RCC-200-19-6 | 1.770 | 5.162 | 6.932 | 0.574 | 0.716 | -1.547 | 6.263 |
| RCC-200-19-7 | 1.686 | 5.695 | 7.381 | 0.667 | 0.851 | -1.804 | 6.938 |
| RCC-200-19-8 | 1.807 | 5.980 | 7.787 | 0.558 | 0.739 | -1.905 | 8.271 |
| RCC-200-19-9 | 2.036 | 5.052 | 7.089 | 0.703 | 0.855 | -1.310 | 4.964 |
| RCC-200-19-10 | 2.204 | 6.863 | 9.066 | 0.704 | 0.908 | -1.751 | 7.160 |
| RCC-300-19-1 | 1.945 | 3.408 | 5.352 | 0.476 | 0.661 | -1.432 | 6.110 |
| RCC-300-19-2 | 2.245 | 5.096 | 7.342 | 0.548 | 0.778 | -1.829 | 8.493 |
| RCC-300-19-3 | 1.168 | 6.761 | 7.928 | 0.401 | 0.581 | -2.458 | 6.837 |
| RCC-300-19-4 | 3.440 | 7.447 | 10.887 | 0.797 | 1.087 | -1.445 | 8.114 |
| RCC-300-19-5 | 1.944 | 6.643 | 8.586 | 0.687 | 0.967 | -1.701 | 8.241 |
| RCC-300-19-6 | 1.560 | 4.428 | 5.988 | 0.442 | 0.614 | -1.834 | 4.880 |
| RCC-300-19-7 | 3.024 | 5.846 | 8.870 | 0.726 | 0.949 | -1.151 | 5.960 |
| RCC-300-19-8 | 2.297 | 4.889 | 7.186 | 0.594 | 0.807 | -1.399 | 5.482 |
| RCC-300-19-9 | 1.739 | 5.232 | 6.971 | 0.607 | 0.814 | -1.331 | 10.136 |
| RCC-300-19-10 | 1.602 | 7.163 | 8.765 | 0.546 | 0.782 | -2.071 | 16.028 |
| RCC-400-19-1 | 3.091 | 7.003 | 10.709 | 0.520 | 0.760 | -1.278 | 6.206 |
| RCC-400-19-2 | 2.089 | 5.428 | 6.364 | 0.648 | 0.756 | -1.113 | 5.618 |
| RCC-400-19-3 | 3.076 | 3.128 | 5.953 | 0.797 | 0.966 | -2.057 | 10.583 |
| RCC-400-19-4 | 1.109 | 6.532 | 2.966 | 0.295 | 0.387 | -2.751 | 7.563 |
| RCC-400-19-5 | 2.247 | 5.431 | 6.145 | 0.415 | 0.582 | -1.666 | 5.503 |
| RCC-400-19-6 | 1.950 | 3.511 | 10.241 | 0.663 | 0.903 | -1.167 | 6.707 |
| RCC-400-19-7 | 1.721 | 3.135 | 5.167 | 0.557 | 0.673 | -1.514 | 20.231 |
| RCC-400-19-8 | 1.341 | 6.356 | 3.663 | 0.503 | 0.583 | -2.691 | 32.951 |
| RCC-400-19-9 | 1.191 | 10.274 | 3.133 | 0.402 | 0.477 | -3.725 | 26.648 |
| RCC-400-19-10 | 4.356 | 12.208 | 5.283 | 0.322 | 0.426 | -3.289 | 18.345 |
| RC-HMA-L-12-1 | 0.989 | 3.434 | 4.424 | 0.220 | 0.304 | -1.728 | 9.824 |
| RC-HMA-L-12-2 | 1.200 | 4.709 | 5.909 | 0.242 | 0.332 | -1.618 | 8.737 |
| RC-HMA-L-12-3 | 1.019 | 2.976 | 3.995 | 0.241 | 0.332 | -1.653 | 7.891 |
| RC-HMA-L-12-4 | 1.020 | 3.313 | 4.333 | 0.238 | 0.336 | -1.827 | 8.600 |
| RC-HMA-L-12-5 | 0.963 | 4.375 | 5.337 | 0.250 | 0.363 | -2.216 | 11.810 |
| RC-HMA-L-12-6 | 1.015 | 3.154 | 4.169 | 0.242 | 0.342 | -1.810 | 8.745 |

| Sample ID | Height Parameter | | | | | | |
|----------------|------------------|-------|-------|-------|-------|----------|----------|
| | S_p | S_v | S_z | S_a | S_q | S_{sk} | S_{ku} |
| | mm | mm | mm | mm | mm | | |
| RC-HMA-L-12-7 | 1.310 | 5.017 | 6.327 | 0.322 | 0.460 | -2.078 | 10.778 |
| RC-HMA-L-12-8 | 1.652 | 4.277 | 5.929 | 0.291 | 0.409 | -1.824 | 8.820 |
| RC-HMA-L-12-9 | 1.102 | 5.367 | 6.469 | 0.322 | 0.457 | -2.040 | 10.431 |
| RC-HMA-L-12-10 | 1.437 | 5.000 | 6.437 | 0.322 | 0.462 | -2.052 | 11.060 |
| RC-HMA-L-12-11 | 1.273 | 3.139 | 4.412 | 0.296 | 0.419 | -1.957 | 9.289 |
| RC-HMA-L-12-12 | 1.386 | 4.278 | 5.663 | 0.359 | 0.517 | -2.144 | 10.400 |
| RC-HMA-L-19-1 | 1.690 | 3.959 | 5.648 | 0.359 | 0.508 | -1.827 | 8.056 |
| RC-HMA-L-19-2 | 1.396 | 4.769 | 6.165 | 0.375 | 0.525 | -1.952 | 9.548 |
| RC-HMA-L-19-3 | 1.397 | 4.828 | 6.225 | 0.387 | 0.551 | -1.970 | 9.616 |
| RC-HMA-L-19-4 | 1.427 | 4.056 | 5.483 | 0.325 | 0.462 | -1.979 | 9.065 |
| RC-HMA-L-19-5 | 1.280 | 5.182 | 6.462 | 0.380 | 0.539 | -2.066 | 9.612 |
| RC-HMA-L-19-6 | 1.165 | 5.519 | 6.684 | 0.302 | 0.425 | -1.926 | 10.315 |
| RC-HMA-L-19-7 | 1.261 | 5.136 | 6.398 | 0.340 | 0.486 | -2.142 | 11.685 |
| RC-HMA-L-19-8 | 1.419 | 4.852 | 6.270 | 0.339 | 0.464 | -1.633 | 8.013 |
| RC-HMA-L-19-9 | 1.401 | 5.105 | 6.507 | 0.371 | 0.528 | -1.982 | 9.514 |
| RC-HMA-L-19-10 | 1.471 | 6.123 | 7.594 | 0.383 | 0.546 | -2.113 | 11.701 |
| RC-HMA-L-19-11 | 1.533 | 6.596 | 8.130 | 0.461 | 0.669 | -2.386 | 11.966 |

| Sample ID | Spatial Parameters | | Hybrid Parameters | | Miscellaneous Parameters |
|------------------|--------------------|-----------|-------------------|----------|--------------------------|
| | S_{al} | S_{tr} | S_{dq} | S_{dr} | S_{td} |
| | mm | (s = 0.2) | | % | mm |
| SGCC-200-12-4-1 | 2.587 | 0.820 | 0.808 | 22.251 | 171.746 |
| SGCC-200-12-4-2 | 2.877 | 0.903 | 0.837 | 23.853 | 137.509 |
| SGCC-200-12-4-3 | 3.261 | 0.791 | 0.885 | 25.946 | 176.743 |
| SGCC-200-12-4-4 | 2.863 | 0.795 | 0.740 | 19.227 | 176.994 |
| SGCC-200-12-4-5 | 2.726 | 0.904 | 0.875 | 25.351 | 173.496 |
| SGCC-200-12-4-6 | 4.007 | 0.810 | 0.845 | 24.271 | 8.485 |
| SGCC-200-12-4-7 | 2.405 | 0.883 | 0.823 | 22.789 | 3.489 |
| SGCC-200-12-4-8 | 2.625 | 0.862 | 0.854 | 23.937 | 50.259 |
| SGCC-200-12-4-9 | 2.076 | 0.841 | 0.775 | 21.170 | 121.500 |
| SGCC-200-12-4-10 | 3.854 | 0.652 | 0.708 | 17.945 | 12.249 |
| SGCC-200-12-5-1 | 2.507 | 0.872 | 0.912 | 25.713 | 177.239 |
| SGCC-200-12-5-2 | 3.036 | 0.758 | 0.917 | 25.362 | 17.004 |
| SGCC-200-12-5-3 | 2.261 | 0.908 | 0.877 | 24.738 | 22.757 |
| SGCC-200-12-5-4 | 2.095 | 0.880 | 0.834 | 22.838 | 22.243 |
| SGCC-200-12-5-5 | 4.203 | 0.765 | 0.908 | 26.172 | 73.252 |
| SGCC-200-12-5-6 | 1.969 | 0.820 | 0.816 | 21.843 | 173.994 |
| SGCC-200-12-5-7 | 3.322 | 0.872 | 0.912 | 25.199 | 163.510 |
| SGCC-200-12-5-8 | 3.401 | 0.861 | 0.715 | 17.925 | 3.492 |
| SGCC-200-12-5-9 | 3.250 | 0.900 | 0.849 | 24.146 | 176.008 |
| SGCC-200-12-5-10 | 3.340 | 0.876 | 0.795 | 21.803 | 176.253 |

| Sample ID | Spatial Parameters | | Hybrid Parameters | | Miscellaneous Parameters |
|------------------|--------------------|---------------|-------------------|----------|--------------------------|
| | S_{al} | S_{tr} | S_{dq} | S_{dr} | S_{td} |
| | mm | ($s = 0.2$) | | % | mm |
| SGCC-200-12-6-1 | 1.901 | 0.792 | 0.877 | 21.920 | 132.500 |
| SGCC-200-12-6-2 | 1.809 | 0.774 | 0.601 | 12.198 | 128.749 |
| SGCC-200-12-6-3 | 2.337 | 0.807 | 0.709 | 15.948 | 121.497 |
| SGCC-200-12-6-4 | 1.931 | 0.803 | 0.679 | 15.267 | 163.253 |
| SGCC-200-12-6-5 | 3.186 | 0.883 | 0.720 | 16.481 | 2.510 |
| SGCC-200-12-6-6 | 2.642 | 0.768 | 0.719 | 16.080 | 137.015 |
| SGCC-200-12-6-7 | 2.709 | 0.849 | 0.685 | 14.374 | 151.746 |
| SGCC-200-12-6-8 | 1.820 | 0.808 | 0.611 | 12.476 | 42.501 |
| SGCC-300-12-5-1 | 2.470 | 0.545 | 0.450 | 8.004 | 118.264 |
| SGCC-300-12-5-2 | 2.406 | 0.809 | 0.432 | 7.220 | 97.509 |
| SGCC-300-12-5-3 | 2.150 | 0.929 | 0.773 | 20.178 | 160.747 |
| SGCC-400-12-4-1 | 3.090 | 0.917 | 0.718 | 18.993 | 3.494 |
| SGCC-400-12-4-2 | 3.011 | 0.776 | 0.490 | 9.984 | 39.003 |
| SGCC-400-12-4-3 | 2.539 | 0.796 | 0.653 | 15.999 | 176.503 |
| SGCC-400-12-4-4 | 3.596 | 0.826 | 0.435 | 7.866 | 3.745 |
| SGCC-400-12-4-5 | 3.607 | 0.902 | 0.438 | 7.996 | 11.258 |
| SGCC-400-12-4-6 | 3.163 | 0.822 | 0.583 | 13.441 | 3.740 |
| SGCC-400-12-4-7 | 3.196 | 0.777 | 0.705 | 18.154 | 8.491 |
| SGCC-400-12-4-8 | 3.041 | 0.714 | 0.518 | 11.122 | 86.251 |
| SGCC-400-12-4-9 | 2.593 | 0.847 | 0.599 | 14.174 | 140.748 |
| SGCC-400-12-4-10 | 2.685 | 0.891 | 0.660 | 16.312 | 8.753 |
| SGCC-400-12-5-1 | 2.436 | 0.847 | 0.753 | 20.566 | 16.250 |
| SGCC-400-12-5-2 | 4.044 | 0.762 | 0.723 | 19.173 | 129.004 |
| SGCC-400-12-5-3 | 2.426 | 0.870 | 0.757 | 20.626 | 28.258 |
| SGCC-400-12-5-4 | 3.303 | 0.798 | 0.767 | 21.482 | 4.256 |
| SGCC-400-12-5-5 | 2.546 | 0.842 | 0.538 | 11.335 | 12.747 |
| SGCC-400-12-5-6 | 3.404 | 0.754 | 0.727 | 18.835 | 129.005 |
| SGCC-400-12-5-7 | 2.749 | 0.856 | 0.684 | 17.687 | 176.255 |
| SGCC-400-12-5-8 | 2.277 | 0.830 | 0.688 | 17.833 | 159.753 |
| SGCC-400-12-5-9 | 2.798 | 0.842 | 0.742 | 19.589 | 129.249 |
| SGCC-400-12-5-10 | 3.746 | 0.786 | 0.684 | 17.011 | 12.749 |
| SGCC-400-12-6-1 | 1.822 | 0.854 | 0.439 | 7.601 | 92.998 |
| SGCC-400-12-6-2 | 2.157 | 0.850 | 0.638 | 13.039 | 93.254 |
| SGCC-400-12-6-3 | 2.428 | 0.803 | 0.553 | 10.768 | 112.747 |
| SGCC-400-12-6-4 | 2.433 | 0.863 | 0.514 | 9.887 | 93.255 |
| SGCC-400-12-6-5 | 2.585 | 0.833 | 0.514 | 10.025 | 163.259 |
| SGCC-400-12-6-6 | 2.727 | 0.869 | 0.498 | 9.564 | 3.256 |
| SGCC-400-12-6-7 | 2.806 | 0.776 | 0.501 | 9.173 | 163.999 |
| SGCC-400-12-6-8 | 3.103 | 0.813 | 0.444 | 7.739 | 87.000 |
| SGCC-400-12-6-9 | 2.972 | 0.819 | 0.451 | 7.669 | 106.993 |
| SGCC-400-12-6-10 | 2.794 | 0.791 | 0.426 | 6.748 | 137.005 |

| Sample ID | Spatial Parameters | | Hybrid Parameters | | Miscellaneous Parameters |
|------------------|--------------------|-----------------|-------------------|-----------------|--------------------------|
| | S _{al} | S _{tr} | S _{dq} | S _{dr} | S _{td} |
| | mm | (s = 0.2) | | % | mm |
| SGCC-200-19-4-1 | 2.406 | 0.893 | 0.825 | 22.469 | 3.998 |
| SGCC-200-19-4-2 | 2.777 | 0.790 | 1.104 | 30.316 | 176.994 |
| SGCC-200-19-4-3 | 2.760 | 0.902 | 0.856 | 23.509 | 16.752 |
| SGCC-200-19-4-4 | 2.262 | 0.840 | 0.820 | 22.448 | 8.010 |
| SGCC-200-19-4-5 | 2.360 | 0.749 | 0.804 | 22.276 | 176.255 |
| SGCC-200-19-4-6 | 3.190 | 0.932 | 0.866 | 24.379 | 2.747 |
| SGCC-200-19-4-7 | 2.221 | 0.932 | 0.839 | 23.512 | 148.752 |
| SGCC-200-19-4-8 | 3.080 | 0.742 | 0.828 | 23.088 | 32.499 |
| SGCC-200-19-4-9 | 2.580 | 0.874 | 0.909 | 25.820 | 86.495 |
| SGCC-200-19-4-10 | 3.989 | 0.827 | 0.747 | 19.544 | 16.997 |
| SGCC-200-19-5-1 | 2.094 | 0.881 | 0.866 | 23.929 | 171.505 |
| SGCC-200-19-5-2 | 2.922 | 0.830 | 0.966 | 28.442 | 3.002 |
| SGCC-200-19-5-3 | 2.688 | 0.872 | 0.907 | 25.737 | 176.754 |
| SGCC-200-19-5-4 | 2.283 | 0.861 | 0.891 | 25.318 | 16.498 |
| SGCC-200-19-5-5 | 2.245 | 0.883 | 0.891 | 25.397 | 163.008 |
| SGCC-200-19-5-6 | 2.425 | 0.848 | 0.927 | 26.176 | 169.746 |
| SGCC-200-19-5-7 | 2.368 | 0.847 | 0.844 | 22.939 | 3.502 |
| SGCC-200-19-5-8 | 2.237 | 0.774 | 0.813 | 22.021 | 175.998 |
| SGCC-200-19-5-9 | 2.869 | 0.839 | 0.785 | 20.516 | 19.752 |
| SGCC-200-19-6-1 | 1.786 | 0.827 | 0.979 | 27.684 | 3.007 |
| SGCC-200-19-6-2 | 3.403 | 0.780 | 1.131 | 34.152 | 140.744 |
| SGCC-200-19-6-3 | 3.992 | 0.935 | 1.001 | 28.514 | 3.246 |
| SGCC-200-19-6-4 | 1.884 | 0.813 | 0.891 | 23.659 | 3.243 |
| SGCC-200-19-6-5 | 2.860 | 0.779 | 0.838 | 22.266 | 25.747 |
| SGCC-200-19-6-6 | 1.813 | 0.905 | 0.831 | 20.969 | 2.742 |
| SGCC-200-19-6-7 | 1.647 | 0.762 | 0.690 | 16.106 | 163.245 |
| SGCC-200-19-6-8 | 1.708 | 0.802 | 0.716 | 16.855 | 16.750 |
| SGCC-200-19-6-9 | 2.280 | 0.702 | 0.659 | 13.997 | 3.490 |
| SGCC-200-19-6-10 | 1.800 | 0.787 | 0.565 | 11.584 | 176.502 |
| SGCC-300-19-5-1 | 2.744 | 0.791 | 0.541 | 9.972 | 69.252 |
| SGCC-300-19-5-2 | 2.549 | 0.597 | 0.366 | 5.622 | 50.996 |
| SGCC-300-19-5-3 | 2.742 | 0.876 | 0.440 | 8.098 | 148.003 |
| SGCC-400-19-4-1 | 3.732 | 0.792 | 0.518 | 10.499 | 3.011 |
| SGCC-400-19-4-2 | 3.010 | 0.691 | 0.442 | 8.334 | 93.504 |
| SGCC-400-19-4-3 | 2.743 | 0.702 | 0.509 | 10.477 | 154.998 |
| SGCC-400-19-4-4 | 2.165 | 0.901 | 0.467 | 8.948 | 118.255 |
| SGCC-400-19-4-5 | 3.148 | 0.753 | 0.405 | 7.026 | 98.498 |
| SGCC-400-19-4-6 | 2.659 | 0.702 | 0.451 | 8.548 | 81.503 |
| SGCC-400-19-4-7 | 2.639 | 0.736 | 0.461 | 8.841 | 113.001 |
| SGCC-400-19-4-8 | 2.986 | 0.816 | 0.535 | 11.558 | 86.501 |
| SGCC-400-19-4-9 | 3.250 | 0.771 | 0.410 | 7.294 | 78.251 |
| SGCC-400-19-5-1 | 2.896 | 0.800 | 0.649 | 15.743 | 6.001 |

| Sample ID | Spatial Parameters | | Hybrid Parameters | | Miscellaneous Parameters |
|------------------|--------------------|-----------------|-------------------|-----------------|--------------------------|
| | S _{al} | S _{tr} | S _{dq} | S _{dr} | S _{td} |
| | mm | (s = 0.2) | | % | mm |
| SGCC-400-19-5-2 | 2.492 | 0.765 | 0.556 | 11.047 | 86.753 |
| SGCC-400-19-5-3 | 3.206 | 0.875 | 0.579 | 12.794 | 173.749 |
| SGCC-400-19-5-4 | 2.804 | 0.623 | 0.594 | 13.481 | 3.762 |
| SGCC-400-19-5-5 | 3.837 | 0.872 | 0.622 | 14.390 | 176.506 |
| SGCC-400-19-5-6 | 3.195 | 0.653 | 0.689 | 15.981 | 176.740 |
| SGCC-400-19-5-7 | 2.624 | 0.725 | 0.578 | 12.773 | 3.008 |
| SGCC-400-19-5-8 | 3.103 | 0.645 | 0.708 | 16.610 | 163.006 |
| SGCC-400-19-5-9 | 3.586 | 0.755 | 0.589 | 13.219 | 39.500 |
| SGCC-400-19-5-10 | 3.479 | 0.884 | 0.560 | 12.292 | 137.491 |
| SGCC-400-19-6-1 | 2.087 | 0.841 | 0.803 | 20.735 | 176.754 |
| SGCC-400-19-6-2 | 1.734 | 0.853 | 0.603 | 13.353 | 137.501 |
| SGCC-400-19-6-3 | 2.158 | 0.787 | 0.573 | 12.218 | 108.747 |
| SGCC-400-19-6-4 | 1.901 | 0.739 | 0.666 | 14.486 | 99.996 |
| SGCC-400-19-6-5 | 1.837 | 0.877 | 0.687 | 15.741 | 137.740 |
| SGCC-400-19-6-6 | 1.875 | 0.842 | 0.588 | 12.909 | 177.002 |
| SGCC-400-19-6-7 | 2.059 | 0.795 | 0.488 | 9.203 | 87.255 |
| SGCC-400-19-6-8 | 3.071 | 0.737 | 0.533 | 10.070 | 97.999 |
| SGCC-400-19-6-9 | 1.573 | 0.629 | 0.458 | 8.345 | 141.001 |
| SGCC-400-19-6-10 | 1.397 | 0.747 | 0.416 | 7.574 | 106.997 |
| SGC-HMA-L-19-1 | 2.895 | 0.918 | 1.410 | 50.792 | 39.005 |
| SGC-HMA-L-19-2 | 2.310 | 0.747 | 1.941 | 72.587 | 3.755 |
| SGC-HMA-L-19-3 | 3.082 | 0.925 | 1.609 | 59.454 | 14.999 |
| SGC-HMA-L-19-4 | 2.096 | 0.859 | 1.909 | 74.966 | 69.753 |
| SGC-HMA-L-19-5 | 2.498 | 0.881 | 1.441 | 52.225 | 20.750 |
| SGC-HMA-L-19-6 | 2.345 | 0.879 | 1.804 | 63.170 | 81.750 |
| SGC-HMA-L-12-1 | 1.816 | 0.789 | 0.943 | 29.692 | 93.245 |
| SGC-HMA-L-12-2 | 1.571 | 0.884 | 1.139 | 40.129 | 122.498 |
| SGC-HMA-L-12-3 | 1.814 | 0.872 | 0.973 | 31.188 | 163.505 |
| SGC-HMA-L-12-4 | 1.952 | 0.849 | 1.279 | 47.805 | 128.995 |
| SGC-HMA-L-12-5 | 1.781 | 0.853 | 1.006 | 33.185 | 3.491 |
| SGC-HMA-L-12-6 | 2.098 | 0.823 | 1.475 | 56.985 | 93.753 |
| RCC-200-12-1 | 2.235 | 0.808 | 0.971 | 25.856 | 13.247 |
| RCC-200-12-2 | 2.989 | 0.740 | 0.828 | 22.874 | 176.263 |
| RCC-200-12-3 | 3.297 | 0.635 | 0.658 | 15.259 | 30.254 |
| RCC-200-12-4 | 2.477 | 0.643 | 0.821 | 21.265 | 166.503 |
| RCC-200-12-5 | 2.842 | 0.834 | 0.732 | 17.549 | 140.992 |
| RCC-200-12-6 | 3.202 | 0.663 | 1.117 | 33.745 | 176.000 |
| RCC-200-12-7 | 2.486 | 0.886 | 0.977 | 28.542 | 171.253 |
| RCC-200-12-8 | 2.858 | 0.920 | 0.456 | 8.291 | 159.002 |
| RCC-200-12-9 | 2.312 | 0.898 | 0.623 | 14.605 | 137.492 |
| RCC-200-12-10 | 4.442 | 0.845 | 0.918 | 23.549 | 170.744 |
| RCC-300-12-1 | 2.744 | 0.775 | 1.044 | 27.782 | 176.500 |

| Sample ID | Spatial Parameters | | Hybrid Parameters | | Miscellaneous Parameters |
|---------------|--------------------|-----------------|-------------------|-----------------|--------------------------|
| | S _{al} | S _{tr} | S _{dq} | S _{dr} | S _{td} |
| | mm | (s = 0.2) | | % | mm |
| RCC-300-12-2 | 3.183 | 0.852 | 0.924 | 23.502 | 176.752 |
| RCC-300-12-3 | 3.076 | 0.824 | 0.483 | 7.970 | 132.492 |
| RCC-300-12-4 | 2.722 | 0.915 | 1.039 | 27.666 | 169.999 |
| RCC-300-12-5 | 2.640 | 0.849 | 0.779 | 17.958 | 3.744 |
| RCC-300-12-6 | 3.065 | 0.921 | 0.944 | 23.775 | 32.001 |
| RCC-300-12-7 | 2.510 | 0.862 | 0.697 | 15.178 | 98.496 |
| RCC-300-12-8 | 2.545 | 0.771 | 0.956 | 24.963 | 156.501 |
| RCC-300-12-9 | 2.790 | 0.812 | 0.711 | 15.150 | 3.501 |
| RCC-300-12-10 | 3.074 | 0.698 | 0.899 | 21.596 | 175.745 |
| RCC-400-12-1 | 2.773 | 0.804 | 0.864 | 24.327 | 147.496 |
| RCC-400-12-2 | 2.691 | 0.867 | 0.785 | 22.056 | 176.505 |
| RCC-400-12-3 | 2.806 | 0.726 | 0.835 | 21.825 | 152.002 |
| RCC-400-12-4 | 2.907 | 0.917 | 0.891 | 26.678 | 3.747 |
| RCC-400-12-5 | 3.243 | 0.767 | 0.895 | 26.400 | 137.498 |
| RCC-400-12-6 | 2.969 | 0.845 | 0.877 | 24.173 | 176.750 |
| RCC-400-12-7 | 3.429 | 0.744 | 0.722 | 18.438 | 3.255 |
| RCC-400-12-8 | 2.594 | 0.833 | 0.776 | 21.094 | 20.503 |
| RCC-400-12-9 | 2.609 | 0.936 | 0.773 | 21.896 | 12.755 |
| RCC-400-12-10 | 2.611 | 0.919 | 0.673 | 17.611 | 128.995 |
| RCC-200-19-1 | 3.078 | 0.829 | 1.102 | 32.038 | 86.993 |
| RCC-200-19-2 | 3.804 | 0.825 | 1.255 | 39.845 | 4.244 |
| RCC-200-19-3 | 3.323 | 0.911 | 0.985 | 27.696 | 7.496 |
| RCC-200-19-4 | 3.665 | 0.907 | 0.947 | 25.899 | 163.250 |
| RCC-200-19-5 | 3.393 | 0.808 | 0.873 | 21.572 | 140.502 |
| RCC-200-19-6 | 3.224 | 0.967 | 0.883 | 24.847 | 159.500 |
| RCC-200-19-7 | 3.517 | 0.910 | 0.990 | 27.799 | 132.251 |
| RCC-200-19-8 | 3.223 | 0.785 | 0.931 | 25.414 | 176.757 |
| RCC-200-19-9 | 3.174 | 0.841 | 1.048 | 32.440 | 140.756 |
| RCC-200-19-10 | 3.805 | 0.839 | 0.953 | 25.607 | 176.494 |
| RCC-300-19-1 | 3.415 | 0.796 | 0.918 | 24.612 | 50.992 |
| RCC-300-19-2 | 3.449 | 0.822 | 0.966 | 24.022 | 8.498 |
| RCC-300-19-3 | 3.768 | 0.986 | 0.879 | 18.467 | 16.750 |
| RCC-300-19-4 | 3.364 | 0.767 | 1.404 | 39.968 | 171.246 |
| RCC-300-19-5 | 3.813 | 0.935 | 1.268 | 32.923 | 42.499 |
| RCC-300-19-6 | 3.281 | 0.859 | 0.864 | 21.252 | 175.746 |
| RCC-300-19-7 | 3.690 | 0.728 | 1.210 | 32.448 | 86.247 |
| RCC-300-19-8 | 3.416 | 0.907 | 1.155 | 32.761 | 3.502 |
| RCC-300-19-9 | 3.628 | 0.848 | 1.174 | 33.639 | 171.503 |
| RCC-300-19-10 | 4.290 | 0.881 | 1.097 | 27.946 | 51.006 |
| RCC-400-19-1 | 3.095 | 0.903 | 1.349 | 37.028 | 47.762 |
| RCC-400-19-2 | 2.940 | 0.812 | 1.399 | 39.651 | 77.007 |
| RCC-400-19-3 | 3.486 | 0.849 | 1.234 | 33.699 | 86.256 |
| RCC-400-19-4 | 3.245 | 0.795 | 0.865 | 12.429 | 120.504 |

| Sample ID | Spatial Parameters | | Hybrid Parameters | | Miscellaneous Parameters |
|----------------|--------------------|-----------------|-------------------|-----------------|--------------------------|
| | S _{al} | S _{tr} | S _{dq} | S _{dr} | S _{td} |
| | mm | (s = 0.2) | | % | mm |
| RCC-400-19-5 | 3.323 | 0.885 | 1.109 | 23.470 | 132.499 |
| RCC-400-19-6 | 3.787 | 0.858 | 1.482 | 42.775 | 39.245 |
| RCC-400-19-7 | 3.039 | 0.913 | 1.085 | 28.528 | 39.005 |
| RCC-400-19-8 | 3.685 | 0.855 | 1.074 | 32.022 | 3.499 |
| RCC-400-19-9 | 2.721 | 0.843 | 0.753 | 19.074 | 166.759 |
| RCC-400-19-10 | 4.369 | 0.873 | 0.943 | 20.506 | 112.501 |
| RC-HMA-L-12-1 | 1.297 | 0.865 | 1.267 | 42.984 | 99.246 |
| RC-HMA-L-12-2 | 1.542 | 0.903 | 1.316 | 45.176 | 119.748 |
| RC-HMA-L-12-3 | 1.431 | 0.826 | 1.313 | 44.865 | 92.498 |
| RC-HMA-L-12-4 | 1.523 | 0.839 | 1.313 | 43.465 | 109.257 |
| RC-HMA-L-12-5 | 1.792 | 0.877 | 1.327 | 42.036 | 138.000 |
| RC-HMA-L-12-6 | 1.540 | 0.898 | 1.313 | 42.595 | 109.746 |
| RC-HMA-L-12-7 | 1.847 | 0.778 | 1.585 | 56.580 | 112.000 |
| RC-HMA-L-12-8 | 1.546 | 0.866 | 1.497 | 52.615 | 107.499 |
| RC-HMA-L-12-9 | 2.017 | 0.807 | 1.533 | 54.415 | 106.254 |
| RC-HMA-L-12-10 | 1.919 | 0.860 | 1.551 | 53.996 | 144.001 |
| RC-HMA-L-12-11 | 1.623 | 0.931 | 1.476 | 51.569 | 105.497 |
| RC-HMA-L-12-12 | 2.090 | 0.856 | 1.652 | 58.991 | 86.753 |
| RC-HMA-L-19-1 | 2.556 | 0.890 | 1.474 | 50.346 | 112.504 |
| RC-HMA-L-19-2 | 2.811 | 0.841 | 1.460 | 49.605 | 79.998 |
| RC-HMA-L-19-3 | 2.718 | 0.790 | 1.539 | 52.556 | 121.997 |
| RC-HMA-L-19-4 | 2.050 | 0.766 | 1.440 | 48.694 | 100.746 |
| RC-HMA-L-19-5 | 2.793 | 0.876 | 1.464 | 48.296 | 144.244 |
| RC-HMA-L-19-6 | 1.782 | 0.802 | 1.407 | 46.813 | 99.252 |
| RC-HMA-L-19-7 | 2.106 | 0.805 | 1.513 | 54.637 | 122.249 |
| RC-HMA-L-19-8 | 2.104 | 0.856 | 1.470 | 54.421 | 94.496 |
| RC-HMA-L-19-9 | 2.576 | 0.948 | 1.562 | 57.302 | 143.494 |
| RC-HMA-L-19-10 | 2.399 | 0.843 | 1.553 | 56.135 | 113.745 |
| RC-HMA-L-19-11 | 3.514 | 0.784 | 1.586 | 56.930 | 83.753 |

| Sample ID | Functions and Related Parameters | | | | | | |
|-----------------|----------------------------------|-----------------|-----------------|-------------------|-------------------|-------------------|-----------------|
| | S _k | S _{pk} | S _{vk} | V _{vv} | V _{vc} | V _{mp} | V _{mc} |
| | mm | mm | mm | ml/m ² | ml/m ² | ml/m ² | mm |
| SGCC-200-12-4-1 | 0.72 | 0.20 | 0.78 | 77.85 | 372.15 | 10.62 | 364.53 |
| SGCC-200-12-4-2 | 0.78 | 0.22 | 0.83 | 83.22 | 390.85 | 11.46 | 385.32 |
| SGCC-200-12-4-3 | 0.98 | 0.42 | 0.91 | 92.84 | 514.75 | 20.25 | 437.99 |
| SGCC-200-12-4-4 | 0.75 | 0.32 | 0.84 | 84.54 | 423.17 | 13.89 | 343.17 |
| SGCC-200-12-4-5 | 0.89 | 0.16 | 0.92 | 92.06 | 427.54 | 9.14 | 420.64 |
| SGCC-200-12-4-6 | 0.93 | 0.40 | 0.99 | 99.99 | 506.85 | 19.34 | 420.22 |
| SGCC-200-12-4-7 | 0.70 | 0.23 | 0.81 | 81.10 | 347.93 | 11.64 | 338.31 |
| SGCC-200-12-4-8 | 0.81 | 0.20 | 0.91 | 91.67 | 389.63 | 10.82 | 366.19 |
| SGCC-200-12-4-9 | 0.65 | 0.17 | 0.70 | 70.40 | 307.86 | 9.08 | 309.96 |

| Sample ID | Functions and Related Parameters | | | | | | |
|------------------|----------------------------------|-----------------------|-----------------------|--------------------------------------|--------------------------------------|--------------------------------------|-----------------------|
| | S _k mm | S _{pk} mm | S _{vk} mm | V _{vv} ml/m ² | V _{vc} ml/m ² | V _{mp} ml/m ² | V _{mc} mm |
| SGCC-200-12-4-10 | 0.71 | 0.32 | 0.88 | 87.18 | 381.96 | 15.16 | 299.03 |
| SGCC-200-12-5-1 | 0.76 | 0.17 | 0.85 | 85.04 | 357.17 | 9.29 | 356.06 |
| SGCC-200-12-5-2 | 0.76 | 0.21 | 0.98 | 98.74 | 375.27 | 11.13 | 389.64 |
| SGCC-200-12-5-3 | 0.66 | 0.16 | 0.80 | 77.36 | 331.11 | 8.21 | 361.28 |
| SGCC-200-12-5-4 | 0.56 | 0.18 | 0.74 | 73.36 | 288.10 | 9.01 | 300.23 |
| SGCC-200-12-5-5 | 1.17 | 0.27 | 1.15 | 116.85 | 545.99 | 14.73 | 508.92 |
| SGCC-200-12-5-6 | 0.55 | 0.10 | 0.72 | 71.17 | 272.00 | 5.80 | 296.85 |
| SGCC-200-12-5-7 | 0.85 | 0.30 | 1.08 | 109.09 | 425.46 | 15.28 | 401.77 |
| SGCC-200-12-5-8 | 0.73 | 0.30 | 0.79 | 78.96 | 366.12 | 15.13 | 353.17 |
| SGCC-200-12-5-9 | 1.06 | 0.31 | 0.95 | 96.70 | 540.45 | 15.75 | 484.12 |
| SGCC-200-12-5-10 | 1.01 | 0.28 | 0.88 | 89.10 | 479.57 | 15.24 | 449.92 |
| SGCC-200-12-6-1 | 0.54 | 0.11 | 0.82 | 81.88 | 270.17 | 5.97 | 297.96 |
| SGCC-200-12-6-2 | 0.30 | 0.11 | 0.54 | 52.29 | 139.54 | 5.11 | 125.47 |
| SGCC-200-12-6-3 | 0.49 | 0.15 | 0.74 | 74.31 | 233.30 | 7.61 | 230.33 |
| SGCC-200-12-6-4 | 0.41 | 0.13 | 0.65 | 65.57 | 203.49 | 6.24 | 208.54 |
| SGCC-200-12-6-5 | 0.58 | 0.16 | 0.80 | 79.90 | 289.31 | 8.39 | 305.06 |
| SGCC-200-12-6-6 | 0.50 | 0.26 | 0.79 | 80.22 | 260.63 | 12.60 | 239.24 |
| SGCC-200-12-6-7 | 0.41 | 0.13 | 0.74 | 75.31 | 206.43 | 6.29 | 209.82 |
| SGCC-200-12-6-8 | 0.30 | 0.12 | 0.62 | 62.60 | 145.63 | 5.87 | 136.28 |
| SGCC-300-12-5-1 | 0.27 | 0.13 | 0.51 | 47.54 | 131.25 | 6.27 | 107.33 |
| SGCC-300-12-5-2 | 0.22 | 0.07 | 0.39 | 33.98 | 101.92 | 3.50 | 82.41 |
| SGCC-300-12-5-3 | 0.49 | 0.15 | 0.75 | 76.37 | 246.34 | 7.53 | 255.56 |
| SGCC-400-12-4-1 | 0.63 | 0.16 | 0.78 | 78.49 | 306.24 | 8.69 | 308.31 |
| SGCC-400-12-4-2 | 0.42 | 0.13 | 0.54 | 54.65 | 203.85 | 6.49 | 183.44 |
| SGCC-400-12-4-3 | 0.52 | 0.18 | 0.71 | 71.54 | 257.88 | 8.90 | 245.34 |
| SGCC-400-12-4-4 | 0.39 | 0.14 | 0.50 | 48.24 | 190.55 | 6.80 | 151.44 |
| SGCC-400-12-4-5 | 0.36 | 0.12 | 0.50 | 49.86 | 164.38 | 5.70 | 148.62 |
| SGCC-400-12-4-6 | 0.46 | 0.30 | 0.63 | 61.00 | 259.34 | 14.36 | 187.14 |
| SGCC-400-12-4-7 | 0.70 | 0.19 | 0.81 | 82.02 | 339.26 | 9.39 | 310.94 |
| SGCC-400-12-4-8 | 0.40 | 0.13 | 0.51 | 51.65 | 191.62 | 6.76 | 175.30 |
| SGCC-400-12-4-9 | 0.50 | 0.13 | 0.54 | 53.77 | 231.97 | 6.48 | 227.82 |
| SGCC-400-12-4-10 | 0.56 | 0.18 | 0.70 | 70.70 | 284.99 | 9.10 | 272.56 |
| SGCC-400-12-5-1 | 0.65 | 0.18 | 0.76 | 74.89 | 325.07 | 9.65 | 333.51 |
| SGCC-400-12-5-2 | 0.65 | 0.20 | 0.85 | 84.67 | 308.01 | 10.37 | 276.70 |
| SGCC-400-12-5-3 | 0.62 | 0.16 | 0.78 | 78.16 | 300.25 | 8.39 | 286.50 |
| SGCC-400-12-5-4 | 0.65 | 0.30 | 0.83 | 83.19 | 331.64 | 14.82 | 296.71 |
| SGCC-400-12-5-5 | 0.41 | 0.20 | 0.56 | 55.18 | 210.68 | 9.93 | 172.20 |
| SGCC-400-12-5-6 | 0.64 | 0.22 | 0.90 | 90.38 | 306.70 | 10.45 | 290.26 |
| SGCC-400-12-5-7 | 0.51 | 0.15 | 0.72 | 72.70 | 248.44 | 7.79 | 236.86 |
| SGCC-400-12-5-8 | 0.50 | 0.18 | 0.65 | 65.12 | 253.88 | 9.08 | 236.22 |
| SGCC-400-12-5-9 | 0.62 | 0.31 | 0.82 | 81.22 | 317.38 | 15.25 | 262.37 |
| SGCC-400-12-5-10 | 0.68 | 0.31 | 0.90 | 87.28 | 358.07 | 14.78 | 280.06 |

| Sample ID | Functions and Related Parameters | | | | | | |
|------------------|----------------------------------|-----------------------|-----------------------|--------------------------------------|--------------------------------------|--------------------------------------|-----------------------|
| | S _k mm | S _{pk} mm | S _{vk} mm | V _{vv} ml/m ² | V _{vc} ml/m ² | V _{mp} ml/m ² | V _{mc} mm |
| SGCC-400-12-6-1 | 0.22 | 0.08 | 0.36 | 32.34 | 101.44 | 3.99 | 83.72 |
| SGCC-400-12-6-2 | 0.34 | 0.16 | 0.64 | 64.86 | 176.52 | 7.49 | 186.92 |
| SGCC-400-12-6-3 | 0.31 | 0.09 | 0.62 | 61.96 | 150.72 | 4.74 | 148.72 |
| SGCC-400-12-6-4 | 0.33 | 0.13 | 0.53 | 53.00 | 159.77 | 6.04 | 156.54 |
| SGCC-400-12-6-5 | 0.34 | 0.17 | 0.57 | 57.36 | 169.35 | 7.98 | 159.76 |
| SGCC-400-12-6-6 | 0.37 | 0.15 | 0.53 | 51.95 | 178.37 | 7.13 | 158.11 |
| SGCC-400-12-6-7 | 0.31 | 0.16 | 0.54 | 53.91 | 157.20 | 7.87 | 146.19 |
| SGCC-400-12-6-8 | 0.36 | 0.16 | 0.51 | 50.83 | 173.53 | 7.83 | 158.93 |
| SGCC-400-12-6-9 | 0.29 | 0.14 | 0.47 | 44.22 | 137.85 | 6.68 | 115.16 |
| SGCC-400-12-6-10 | 0.29 | 0.14 | 0.42 | 40.76 | 141.64 | 6.71 | 121.64 |
| SGCC-200-19-4-1 | 0.68 | 0.23 | 0.81 | 81.65 | 332.53 | 11.83 | 308.55 |
| SGCC-200-19-4-2 | 0.83 | 0.48 | 1.17 | 117.65 | 448.85 | 23.58 | 404.70 |
| SGCC-200-19-4-3 | 0.78 | 0.17 | 0.92 | 93.25 | 369.84 | 9.21 | 365.21 |
| SGCC-200-19-4-4 | 0.71 | 0.19 | 0.77 | 77.26 | 338.91 | 9.56 | 319.26 |
| SGCC-200-19-4-5 | 0.63 | 0.21 | 0.78 | 78.38 | 311.17 | 10.60 | 299.41 |
| SGCC-200-19-4-6 | 0.73 | 0.29 | 0.93 | 94.37 | 345.18 | 13.72 | 338.95 |
| SGCC-200-19-4-7 | 0.65 | 0.18 | 0.71 | 71.91 | 308.43 | 9.60 | 296.90 |
| SGCC-200-19-4-8 | 0.83 | 0.26 | 0.95 | 95.56 | 402.73 | 13.47 | 363.63 |
| SGCC-200-19-4-9 | 0.75 | 0.22 | 0.90 | 90.65 | 344.86 | 10.70 | 336.30 |
| SGCC-200-19-4-10 | 0.77 | 0.22 | 1.07 | 108.10 | 377.92 | 11.87 | 372.86 |
| SGCC-200-19-5-1 | 0.59 | 0.17 | 0.80 | 80.07 | 295.73 | 8.61 | 310.90 |
| SGCC-200-19-5-2 | 0.85 | 0.27 | 1.06 | 106.34 | 424.64 | 13.95 | 430.28 |
| SGCC-200-19-5-3 | 0.74 | 0.13 | 0.93 | 92.38 | 365.96 | 7.98 | 390.78 |
| SGCC-200-19-5-4 | 0.66 | 0.16 | 0.89 | 90.14 | 323.42 | 7.95 | 347.72 |
| SGCC-200-19-5-5 | 0.69 | 0.20 | 0.84 | 84.23 | 337.18 | 10.19 | 346.59 |
| SGCC-200-19-5-6 | 0.79 | 0.14 | 0.90 | 89.51 | 365.30 | 8.29 | 369.11 |
| SGCC-200-19-5-7 | 0.61 | 0.19 | 0.83 | 83.94 | 302.65 | 9.04 | 323.48 |
| SGCC-200-19-5-8 | 0.62 | 0.12 | 0.81 | 80.37 | 305.85 | 6.92 | 332.48 |
| SGCC-200-19-5-9 | 0.69 | 0.38 | 0.91 | 91.28 | 334.30 | 14.31 | 345.30 |
| SGCC-200-19-6-1 | 0.66 | 0.17 | 0.89 | 88.93 | 320.72 | 8.54 | 340.44 |
| SGCC-200-19-6-2 | 1.07 | 0.29 | 1.38 | 139.97 | 514.34 | 14.83 | 506.46 |
| SGCC-200-19-6-3 | 0.93 | 0.26 | 1.31 | 131.97 | 464.66 | 13.63 | 462.77 |
| SGCC-200-19-6-4 | 0.57 | 0.13 | 0.81 | 82.29 | 280.75 | 6.76 | 303.47 |
| SGCC-200-19-6-5 | 0.60 | 0.23 | 0.98 | 100.13 | 303.60 | 10.72 | 314.71 |
| SGCC-200-19-6-6 | 0.51 | 0.19 | 0.77 | 77.69 | 257.35 | 9.29 | 245.74 |
| SGCC-200-19-6-7 | 0.42 | 0.10 | 0.65 | 65.28 | 203.60 | 5.32 | 212.67 |
| SGCC-200-19-6-8 | 0.44 | 0.14 | 0.66 | 66.62 | 210.06 | 6.93 | 199.51 |
| SGCC-200-19-6-9 | 0.39 | 0.14 | 0.66 | 66.36 | 184.40 | 6.88 | 174.65 |
| SGCC-200-19-6-10 | 0.31 | 0.14 | 0.52 | 51.24 | 151.40 | 6.44 | 137.61 |
| SGCC-300-19-5-1 | 0.36 | 0.15 | 0.63 | 55.50 | 174.80 | 7.19 | 136.87 |
| SGCC-300-19-5-2 | 0.25 | 0.09 | 0.34 | 29.45 | 118.12 | 4.45 | 91.61 |
| SGCC-300-19-5-3 | 0.33 | 0.19 | 0.38 | 34.55 | 165.62 | 9.24 | 121.71 |

| Sample ID | Functions and Related Parameters | | | | | | |
|------------------|----------------------------------|-----------------------|-----------------------|--------------------------------------|--------------------------------------|--------------------------------------|-----------------------|
| | S _k mm | S _{pk} mm | S _{vk} mm | V _{vv} ml/m ² | V _{vc} ml/m ² | V _{mp} ml/m ² | V _{mc} mm |
| SGCC-400-19-4-1 | 0.42 | 0.11 | 0.66 | 64.26 | 189.82 | 5.32 | 171.61 |
| SGCC-400-19-4-2 | 0.30 | 0.11 | 0.41 | 39.45 | 139.65 | 5.55 | 118.40 |
| SGCC-400-19-4-3 | 0.38 | 0.21 | 0.58 | 56.83 | 178.30 | 9.79 | 151.87 |
| SGCC-400-19-4-4 | 0.29 | 0.12 | 0.38 | 35.45 | 139.64 | 5.78 | 111.40 |
| SGCC-400-19-4-5 | 0.27 | 0.12 | 0.45 | 38.13 | 134.31 | 5.74 | 101.94 |
| SGCC-400-19-4-6 | 0.32 | 0.11 | 0.39 | 37.18 | 152.76 | 5.44 | 126.42 |
| SGCC-400-19-4-7 | 0.29 | 0.11 | 0.39 | 36.36 | 134.94 | 5.30 | 113.42 |
| SGCC-400-19-4-8 | 0.40 | 0.15 | 0.67 | 65.34 | 196.79 | 7.15 | 172.40 |
| SGCC-400-19-4-9 | 0.27 | 0.10 | 0.36 | 31.45 | 128.00 | 4.77 | 102.00 |
| SGCC-400-19-5-1 | 0.51 | 0.14 | 0.68 | 68.84 | 236.71 | 7.13 | 229.92 |
| SGCC-400-19-5-2 | 0.37 | 0.25 | 0.57 | 55.06 | 177.57 | 11.25 | 148.55 |
| SGCC-400-19-5-3 | 0.43 | 0.15 | 0.65 | 66.02 | 210.92 | 7.33 | 201.79 |
| SGCC-400-19-5-4 | 0.45 | 0.13 | 0.60 | 57.61 | 214.62 | 6.44 | 183.90 |
| SGCC-400-19-5-5 | 0.47 | 0.13 | 0.83 | 82.99 | 224.71 | 6.81 | 208.14 |
| SGCC-400-19-5-6 | 0.62 | 0.35 | 0.96 | 92.65 | 307.03 | 16.72 | 250.81 |
| SGCC-400-19-5-7 | 0.47 | 0.18 | 0.70 | 65.31 | 222.84 | 8.80 | 180.30 |
| SGCC-400-19-5-8 | 0.57 | 0.39 | 1.01 | 98.32 | 315.18 | 19.56 | 247.02 |
| SGCC-400-19-5-9 | 0.53 | 0.16 | 0.77 | 75.17 | 247.66 | 7.97 | 212.45 |
| SGCC-400-19-5-10 | 0.46 | 0.12 | 0.66 | 66.25 | 216.11 | 6.28 | 201.95 |
| SGCC-400-19-6-1 | 0.47 | 0.11 | 0.79 | 80.02 | 238.97 | 5.48 | 268.93 |
| SGCC-400-19-6-2 | 0.34 | 0.11 | 0.49 | 49.03 | 162.55 | 5.46 | 153.54 |
| SGCC-400-19-6-3 | 0.34 | 0.14 | 0.55 | 52.70 | 165.26 | 6.90 | 140.04 |
| SGCC-400-19-6-4 | 0.38 | 0.15 | 0.64 | 63.21 | 178.76 | 7.26 | 165.72 |
| SGCC-400-19-6-5 | 0.37 | 0.14 | 0.63 | 63.74 | 178.96 | 6.79 | 172.29 |
| SGCC-400-19-6-6 | 0.33 | 0.11 | 0.46 | 46.14 | 157.71 | 5.13 | 146.97 |
| SGCC-400-19-6-7 | 0.27 | 0.10 | 0.42 | 41.18 | 127.24 | 4.80 | 112.27 |
| SGCC-400-19-6-8 | 0.32 | 0.21 | 0.52 | 46.72 | 167.21 | 10.55 | 125.77 |
| SGCC-400-19-6-9 | 0.25 | 0.11 | 0.34 | 31.44 | 119.79 | 5.19 | 98.54 |
| SGCC-400-19-6-10 | 0.23 | 0.09 | 0.21 | 19.95 | 105.92 | 4.24 | 86.12 |
| SGC-HMA-L-19-1 | 1.29 | 0.19 | 1.34 | 134.70 | 597.27 | 12.29 | 592.65 |
| SGC-HMA-L-19-2 | 1.42 | 0.27 | 1.58 | 158.87 | 657.87 | 15.65 | 659.80 |
| SGC-HMA-L-19-3 | 1.68 | 0.28 | 1.52 | 153.83 | 750.72 | 16.29 | 732.30 |
| SGC-HMA-L-19-4 | 1.29 | 0.27 | 1.28 | 129.93 | 587.69 | 14.85 | 570.09 |
| SGC-HMA-L-19-5 | 1.31 | 0.18 | 1.26 | 126.25 | 602.55 | 11.06 | 612.00 |
| SGC-HMA-L-19-6 | 1.24 | 0.24 | 1.26 | 126.23 | 576.07 | 13.42 | 577.18 |
| SGC-HMA-L-12-1 | 0.61 | 0.19 | 0.55 | 55.76 | 282.08 | 9.37 | 260.20 |
| SGC-HMA-L-12-2 | 0.70 | 0.20 | 0.56 | 56.37 | 316.93 | 10.13 | 274.04 |
| SGC-HMA-L-12-3 | 0.61 | 0.19 | 0.56 | 56.75 | 282.99 | 9.30 | 257.05 |
| SGC-HMA-L-12-4 | 0.89 | 0.22 | 0.69 | 70.54 | 395.46 | 11.88 | 341.11 |
| SGC-HMA-L-12-5 | 0.65 | 0.17 | 0.57 | 57.91 | 297.28 | 8.87 | 268.77 |
| SGC-HMA-L-12-6 | 0.87 | 0.27 | 0.79 | 76.31 | 400.38 | 13.64 | 332.82 |

| Sample ID | Functions and Related Parameters | | | | | | |
|---------------|----------------------------------|-----------------------|-----------------------|--------------------------------------|--------------------------------------|--------------------------------------|-----------------------|
| | S _k mm | S _{pk} mm | S _{vk} mm | V _{vv} ml/m ² | V _{vc} ml/m ² | V _{mp} ml/m ² | V _{mc} mm |
| RCC-200-12-1 | 0.68 | 0.33 | 1.14 | 81.59 | 329.28 | 16.37 | 307.66 |
| RCC-200-12-2 | 0.90 | 0.23 | 1.06 | 72.78 | 389.59 | 10.81 | 378.81 |
| RCC-200-12-3 | 0.68 | 0.20 | 1.00 | 69.55 | 285.24 | 10.14 | 239.95 |
| RCC-200-12-4 | 0.73 | 0.18 | 1.07 | 76.03 | 305.28 | 9.39 | 278.24 |
| RCC-200-12-5 | 0.69 | 0.21 | 1.00 | 70.68 | 314.37 | 10.43 | 282.11 |
| RCC-200-12-7 | 0.73 | 0.13 | 1.09 | 75.03 | 342.49 | 7.49 | 348.90 |
| RCC-200-12-8 | 0.44 | 0.21 | 0.66 | 43.87 | 203.11 | 10.12 | 144.99 |
| RCC-200-12-9 | 0.60 | 0.25 | 0.68 | 48.28 | 268.92 | 12.41 | 228.45 |
| RCC-200-12-10 | 0.75 | 0.22 | 1.10 | 77.61 | 337.76 | 11.00 | 285.51 |
| RCC-300-12-1 | 0.82 | 0.36 | 1.10 | 85.99 | 377.73 | 15.85 | 343.06 |
| RCC-300-12-2 | 0.84 | 0.42 | 1.18 | 90.47 | 381.01 | 19.02 | 313.64 |
| RCC-300-12-3 | 0.31 | 0.09 | 0.54 | 21.51 | 130.14 | 4.36 | 97.49 |
| RCC-300-12-4 | 0.74 | 0.26 | 1.23 | 96.89 | 349.26 | 12.00 | 319.86 |
| RCC-300-12-5 | 0.57 | 0.21 | 0.87 | 66.76 | 255.74 | 9.62 | 214.81 |
| RCC-300-12-6 | 0.74 | 0.19 | 1.13 | 88.14 | 335.82 | 9.39 | 296.88 |
| RCC-300-12-7 | 0.40 | 0.12 | 0.63 | 48.61 | 180.23 | 5.62 | 157.52 |
| RCC-300-12-8 | 0.72 | 0.28 | 0.98 | 76.11 | 319.54 | 12.37 | 298.97 |
| RCC-300-12-9 | 0.53 | 0.17 | 0.76 | 57.85 | 234.63 | 7.57 | 193.18 |
| RCC-300-12-10 | 0.82 | 0.26 | 1.17 | 85.61 | 347.98 | 12.03 | 277.97 |
| RCC-400-12-1 | 0.79 | 0.24 | 1.16 | 100.24 | 341.17 | 11.55 | 342.40 |
| RCC-400-12-2 | 0.79 | 0.15 | 0.92 | 77.93 | 330.00 | 7.79 | 320.61 |
| RCC-400-12-3 | 0.72 | 0.33 | 1.11 | 96.90 | 313.08 | 14.70 | 297.66 |
| RCC-400-12-4 | 0.96 | 0.39 | 1.04 | 87.92 | 423.92 | 18.07 | 385.24 |
| RCC-400-12-5 | 1.04 | 0.58 | 1.27 | 110.53 | 462.36 | 18.43 | 395.62 |
| RCC-400-12-6 | 0.82 | 0.35 | 1.23 | 107.73 | 365.06 | 16.39 | 336.63 |
| RCC-400-12-7 | 0.65 | 0.23 | 1.05 | 90.36 | 281.93 | 10.12 | 299.80 |
| RCC-400-12-8 | 0.84 | 0.23 | 0.90 | 78.96 | 324.64 | 10.67 | 303.47 |
| RCC-400-12-9 | 0.66 | 0.16 | 0.94 | 75.46 | 292.70 | 7.74 | 320.22 |
| RCC-400-12-10 | 0.48 | 0.14 | 0.91 | 79.67 | 222.52 | 6.60 | 226.57 |
| RCC-200-19-1 | 1.16 | 0.40 | 1.50 | 135.39 | 630.69 | 17.77 | 630.04 |
| RCC-200-19-2 | 1.74 | 0.33 | 1.56 | 140.96 | 902.03 | 18.52 | 850.71 |
| RCC-200-19-3 | 0.97 | 0.28 | 1.21 | 109.82 | 530.45 | 14.17 | 529.84 |
| RCC-200-19-4 | 1.08 | 0.28 | 1.36 | 125.53 | 562.27 | 14.11 | 533.34 |
| RCC-200-19-5 | 0.98 | 0.41 | 1.25 | 114.02 | 531.35 | 19.79 | 496.75 |
| RCC-200-19-6 | 1.07 | 0.27 | 1.15 | 104.51 | 570.91 | 15.16 | 538.39 |
| RCC-200-19-7 | 1.14 | 0.20 | 1.55 | 141.87 | 588.10 | 11.73 | 593.39 |
| RCC-200-19-8 | 0.91 | 0.41 | 1.31 | 120.94 | 515.39 | 20.39 | 473.77 |
| RCC-200-19-9 | 1.31 | 0.34 | 1.36 | 122.30 | 705.32 | 18.40 | 672.83 |
| RCC-200-19-10 | 1.19 | 0.41 | 1.61 | 147.09 | 651.73 | 20.83 | 624.28 |
| RCC-300-19-1 | 1.08 | 0.35 | 1.33 | 131.45 | 562.46 | 15.91 | 480.06 |
| RCC-300-19-2 | 1.08 | 0.41 | 1.56 | 157.48 | 587.46 | 17.80 | 559.56 |
| RCC-300-19-3 | 0.84 | 0.25 | 1.09 | 109.43 | 476.65 | 10.85 | 414.87 |
| RCC-300-19-4 | 1.69 | 0.59 | 1.99 | 201.91 | 944.91 | 26.35 | 857.81 |

| Sample ID | Functions and Related Parameters | | | | | | |
|----------------|----------------------------------|-----------------------|-----------------------|--------------------------------------|--------------------------------------|--------------------------------------|-----------------------|
| | S _k mm | S _{pk} mm | S _{vk} mm | V _{vv} ml/m ² | V _{vc} ml/m ² | V _{mp} ml/m ² | V _{mc} mm |
| RCC-300-19-5 | 1.30 | 0.58 | 1.88 | 189.34 | 788.91 | 25.16 | 707.63 |
| RCC-300-19-6 | 0.93 | 0.20 | 1.19 | 119.44 | 487.57 | 9.22 | 470.53 |
| RCC-300-19-7 | 1.68 | 0.38 | 1.63 | 165.94 | 887.23 | 18.78 | 806.15 |
| RCC-300-19-8 | 1.25 | 0.45 | 1.57 | 158.74 | 660.79 | 20.06 | 618.22 |
| RCC-300-19-9 | 1.28 | 0.34 | 1.59 | 161.08 | 706.75 | 15.72 | 645.97 |
| RCC-300-19-10 | 1.05 | 0.33 | 1.63 | 164.02 | 577.46 | 15.28 | 542.87 |
| RCC-400-19-1 | 1.30 | 0.48 | 2.04 | 191.21 | 744.88 | 23.81 | 519.08 |
| RCC-400-19-2 | 1.64 | 0.45 | 1.71 | 171.57 | 720.11 | 22.60 | 800.07 |
| RCC-400-19-4 | 1.01 | 0.26 | 1.13 | 114.32 | 512.75 | 13.02 | 294.01 |
| RCC-400-19-5 | 1.02 | 0.45 | 1.41 | 139.62 | 569.83 | 20.86 | 443.38 |
| RCC-400-19-6 | 1.78 | 0.35 | 1.84 | 244.39 | 916.66 | 17.89 | 677.57 |
| RCC-400-19-7 | 1.15 | 0.34 | 1.77 | 175.41 | 716.65 | 17.44 | 662.51 |
| RCC-400-19-8 | 1.17 | 0.45 | 1.36 | 133.57 | 719.52 | 22.51 | 626.96 |
| RCC-400-19-9 | 0.98 | 0.19 | 1.19 | 118.97 | 548.34 | 9.82 | 490.33 |
| RCC-400-19-10 | 0.83 | 0.25 | 1.06 | 104.65 | 474.18 | 12.63 | 289.14 |
| RC-HMA-L-12-1 | 0.54 | 0.19 | 0.55 | 55.10 | 254.73 | 9.54 | 233.21 |
| RC-HMA-L-12-2 | 0.60 | 0.20 | 0.62 | 61.37 | 278.24 | 9.77 | 256.75 |
| RC-HMA-L-12-3 | 0.60 | 0.18 | 0.63 | 63.42 | 271.23 | 8.95 | 252.33 |
| RC-HMA-L-12-4 | 0.55 | 0.18 | 0.68 | 68.35 | 256.61 | 8.98 | 239.60 |
| RC-HMA-L-12-5 | 0.60 | 0.17 | 0.76 | 73.36 | 274.34 | 8.70 | 245.95 |
| RC-HMA-L-12-6 | 0.61 | 0.18 | 0.68 | 66.83 | 274.26 | 9.43 | 245.40 |
| RC-HMA-L-12-7 | 0.80 | 0.21 | 0.94 | 91.54 | 356.42 | 10.46 | 323.78 |
| RC-HMA-L-12-8 | 0.72 | 0.22 | 0.82 | 80.33 | 326.52 | 10.55 | 295.67 |
| RC-HMA-L-12-9 | 0.76 | 0.20 | 0.94 | 92.73 | 345.82 | 10.32 | 324.55 |
| RC-HMA-L-12-10 | 0.76 | 0.28 | 0.92 | 91.71 | 352.45 | 13.45 | 321.52 |
| RC-HMA-L-12-11 | 0.67 | 0.21 | 0.85 | 85.47 | 313.77 | 10.14 | 298.12 |
| RC-HMA-L-12-12 | 0.78 | 0.24 | 1.09 | 109.58 | 364.76 | 12.07 | 352.25 |
| RC-HMA-L-19-1 | 0.81 | 0.25 | 1.06 | 106.13 | 386.75 | 12.63 | 357.75 |
| RC-HMA-L-19-2 | 0.85 | 0.22 | 1.04 | 104.77 | 407.48 | 11.56 | 385.67 |
| RC-HMA-L-19-3 | 0.86 | 0.30 | 1.12 | 112.39 | 413.65 | 15.11 | 388.66 |
| RC-HMA-L-19-4 | 0.71 | 0.22 | 0.97 | 97.17 | 334.47 | 10.99 | 322.87 |
| RC-HMA-L-19-5 | 0.82 | 0.20 | 1.11 | 112.07 | 387.07 | 10.80 | 384.01 |
| RC-HMA-L-19-6 | 0.73 | 0.22 | 0.83 | 82.58 | 339.50 | 10.93 | 310.65 |
| RC-HMA-L-19-7 | 0.82 | 0.24 | 0.96 | 95.32 | 374.15 | 11.94 | 345.02 |
| RC-HMA-L-19-8 | 0.87 | 0.24 | 0.88 | 87.37 | 390.74 | 11.96 | 355.83 |
| RC-HMA-L-19-9 | 0.87 | 0.26 | 1.07 | 106.51 | 399.26 | 12.81 | 374.34 |
| RC-HMA-L-19-10 | 0.91 | 0.28 | 1.07 | 106.70 | 424.20 | 14.11 | 389.77 |
| RC-HMA-L-19-11 | 0.93 | 0.23 | 1.42 | 143.68 | 442.03 | 11.54 | 455.85 |

| Sample ID | Functions and Related Parameters | | | | Feature Parameters | | |
|------------------|----------------------------------|------------------|-----------------|-----------------|--------------------|-----------------|-----------------|
| | S _{mr1} | S _{mr2} | S _{a1} | S _{a2} | S _{10z} | S _{5p} | S _{5v} |
| | % | % | mm | mm | mm | mm | mm |
| SGCC-200-12-4-1 | 8.42 | 77.97 | 0.01 | 0.09 | 2.456 | 0.643 | 1.814 |
| SGCC-200-12-4-2 | 7.29 | 78.26 | 0.01 | 0.09 | 2.480 | 0.705 | 1.775 |
| SGCC-200-12-4-3 | 10.17 | 81.38 | 0.02 | 0.09 | 2.742 | 0.919 | 1.823 |
| SGCC-200-12-4-4 | 12.25 | 81.04 | 0.02 | 0.08 | 2.217 | 0.651 | 1.566 |
| SGCC-200-12-4-5 | 6.17 | 79.33 | 0.00 | 0.09 | 2.170 | 0.550 | 1.620 |
| SGCC-200-12-4-6 | 11.31 | 81.27 | 0.02 | 0.09 | 1.989 | 0.730 | 1.260 |
| SGCC-200-12-4-7 | 7.60 | 79.03 | 0.01 | 0.08 | 2.255 | 0.555 | 1.701 |
| SGCC-200-12-4-8 | 7.47 | 80.40 | 0.01 | 0.09 | 1.900 | 0.593 | 1.307 |
| SGCC-200-12-4-9 | 6.41 | 79.00 | 0.01 | 0.07 | 2.144 | 0.614 | 1.530 |
| SGCC-200-12-4-10 | 11.69 | 82.99 | 0.02 | 0.08 | 2.463 | 0.771 | 1.692 |
| SGCC-200-12-5-1 | 5.86 | 79.44 | 0.01 | 0.09 | 3.258 | 0.519 | 2.739 |
| SGCC-200-12-5-2 | 6.41 | 77.46 | 0.01 | 0.11 | 2.648 | 0.536 | 2.112 |
| SGCC-200-12-5-3 | 5.36 | 75.93 | 0.00 | 0.10 | 2.580 | 0.567 | 2.014 |
| SGCC-200-12-5-4 | 7.07 | 76.56 | 0.01 | 0.09 | 2.614 | 0.476 | 2.138 |
| SGCC-200-12-5-5 | 6.88 | 81.34 | 0.01 | 0.11 | 2.814 | 0.803 | 2.011 |
| SGCC-200-12-5-6 | 4.74 | 76.08 | 0.00 | 0.09 | 2.366 | 0.460 | 1.906 |
| SGCC-200-12-5-7 | 8.60 | 79.65 | 0.01 | 0.11 | 2.930 | 0.529 | 2.401 |
| SGCC-200-12-5-8 | 8.28 | 78.82 | 0.01 | 0.08 | 2.078 | 0.742 | 1.336 |
| SGCC-200-12-5-9 | 9.38 | 80.54 | 0.01 | 0.09 | 2.342 | 0.763 | 1.579 |
| SGCC-200-12-5-10 | 7.53 | 80.63 | 0.01 | 0.09 | 2.654 | 0.767 | 1.886 |
| SGCC-200-12-6-1 | 4.86 | 75.83 | 0.00 | 0.10 | 2.679 | 0.641 | 2.038 |
| SGCC-200-12-6-2 | 7.27 | 81.77 | 0.00 | 0.05 | 1.785 | 0.404 | 1.380 |
| SGCC-200-12-6-3 | 7.03 | 79.54 | 0.01 | 0.08 | 1.784 | 0.389 | 1.395 |
| SGCC-200-12-6-4 | 6.90 | 78.16 | 0.00 | 0.07 | 2.204 | 0.425 | 1.780 |
| SGCC-200-12-6-5 | 6.55 | 77.14 | 0.01 | 0.09 | 2.894 | 0.578 | 2.315 |
| SGCC-200-12-6-6 | 9.49 | 79.50 | 0.01 | 0.08 | 2.557 | 0.541 | 2.016 |
| SGCC-200-12-6-7 | 7.27 | 78.44 | 0.00 | 0.08 | 1.726 | 0.420 | 1.306 |
| SGCC-200-12-6-8 | 8.20 | 80.01 | 0.00 | 0.06 | 1.725 | 0.435 | 1.290 |
| SGCC-300-12-5-1 | 9.49 | 83.31 | 0.01 | 0.04 | 1.804 | 0.238 | 1.566 |
| SGCC-300-12-5-2 | 7.78 | 85.16 | 0.00 | 0.03 | 1.632 | 0.305 | 1.326 |
| SGCC-300-12-5-3 | 6.90 | 77.69 | 0.01 | 0.08 | 2.405 | 0.458 | 1.947 |
| SGCC-400-12-4-1 | 6.95 | 78.71 | 0.01 | 0.08 | 1.853 | 0.535 | 1.318 |
| SGCC-400-12-4-2 | 8.65 | 81.10 | 0.01 | 0.05 | 1.572 | 0.434 | 1.137 |
| SGCC-400-12-4-3 | 8.08 | 79.74 | 0.01 | 0.07 | 2.324 | 0.632 | 1.692 |
| SGCC-400-12-4-4 | 9.48 | 84.14 | 0.01 | 0.04 | 1.139 | 0.241 | 0.898 |
| SGCC-400-12-4-5 | 7.07 | 82.11 | 0.00 | 0.05 | 1.288 | 0.359 | 0.929 |
| SGCC-400-12-4-6 | 13.09 | 83.71 | 0.02 | 0.05 | 1.924 | 0.610 | 1.314 |
| SGCC-400-12-4-7 | 7.97 | 80.82 | 0.01 | 0.08 | 2.432 | 0.862 | 1.570 |
| SGCC-400-12-4-8 | 7.94 | 81.19 | 0.01 | 0.05 | 1.848 | 0.488 | 1.361 |
| SGCC-400-12-4-9 | 5.55 | 79.97 | 0.00 | 0.05 | 1.696 | 0.450 | 1.246 |
| SGCC-400-12-4-10 | 8.81 | 78.89 | 0.01 | 0.07 | 2.013 | 0.675 | 1.338 |

| Sample ID | Functions and Related Parameters | | | | Feature Parameters | | |
|------------------|----------------------------------|-----------|----------|----------|--------------------|----------|----------|
| | S_{mr1} | S_{mr2} | S_{a1} | S_{a2} | S_{10z} | S_{5p} | S_{5v} |
| | % | % | mm | mm | mm | mm | mm |
| SGCC-400-12-5-1 | 7.21 | 77.41 | 0.01 | 0.09 | 1.910 | 0.578 | 1.333 |
| SGCC-400-12-5-2 | 7.91 | 82.03 | 0.01 | 0.08 | 2.497 | 0.640 | 1.858 |
| SGCC-400-12-5-3 | 7.34 | 80.23 | 0.01 | 0.08 | 2.753 | 0.577 | 2.176 |
| SGCC-400-12-5-4 | 9.51 | 80.55 | 0.01 | 0.08 | 1.728 | 0.633 | 1.095 |
| SGCC-400-12-5-5 | 10.64 | 82.40 | 0.01 | 0.05 | 1.563 | 0.458 | 1.104 |
| SGCC-400-12-5-6 | 7.39 | 80.34 | 0.01 | 0.09 | 2.679 | 0.511 | 2.168 |
| SGCC-400-12-5-7 | 7.72 | 79.93 | 0.01 | 0.07 | 1.539 | 0.504 | 1.036 |
| SGCC-400-12-5-8 | 8.88 | 79.87 | 0.01 | 0.07 | 1.717 | 0.604 | 1.113 |
| SGCC-400-12-5-9 | 10.39 | 82.23 | 0.02 | 0.07 | 2.225 | 0.696 | 1.529 |
| SGCC-400-12-5-10 | 11.34 | 83.22 | 0.02 | 0.08 | 1.768 | 0.486 | 1.283 |
| SGCC-400-12-6-1 | 8.60 | 84.52 | 0.00 | 0.03 | 1.931 | 0.332 | 1.600 |
| SGCC-400-12-6-2 | 7.54 | 77.05 | 0.01 | 0.07 | 3.544 | 0.534 | 3.010 |
| SGCC-400-12-6-3 | 7.52 | 79.22 | 0.00 | 0.06 | 1.885 | 0.352 | 1.533 |
| SGCC-400-12-6-4 | 7.20 | 79.75 | 0.00 | 0.05 | 1.539 | 0.476 | 1.063 |
| SGCC-400-12-6-5 | 8.68 | 79.77 | 0.01 | 0.06 | 1.679 | 0.299 | 1.380 |
| SGCC-400-12-6-6 | 8.49 | 81.68 | 0.01 | 0.05 | 2.063 | 0.376 | 1.687 |
| SGCC-400-12-6-7 | 9.01 | 79.92 | 0.01 | 0.05 | 2.044 | 0.442 | 1.602 |
| SGCC-400-12-6-8 | 7.91 | 81.24 | 0.01 | 0.05 | 1.552 | 0.463 | 1.089 |
| SGCC-400-12-6-9 | 9.01 | 83.34 | 0.01 | 0.04 | 2.109 | 0.300 | 1.810 |
| SGCC-400-12-6-10 | 8.71 | 82.21 | 0.01 | 0.04 | 1.378 | 0.252 | 1.126 |
| SGCC-200-19-4-1 | 8.23 | 80.50 | 0.01 | 0.08 | 2.240 | 0.643 | 1.598 |
| SGCC-200-19-4-2 | 10.04 | 79.25 | 0.02 | 0.12 | 3.386 | 0.806 | 2.580 |
| SGCC-200-19-4-3 | 6.24 | 79.37 | 0.01 | 0.10 | 3.052 | 0.482 | 2.570 |
| SGCC-200-19-4-4 | 6.92 | 80.48 | 0.01 | 0.07 | 2.144 | 0.656 | 1.488 |
| SGCC-200-19-4-5 | 7.76 | 79.53 | 0.01 | 0.08 | 2.040 | 0.440 | 1.600 |
| SGCC-200-19-4-6 | 6.62 | 79.32 | 0.01 | 0.10 | 2.501 | 0.700 | 1.802 |
| SGCC-200-19-4-7 | 7.02 | 80.07 | 0.01 | 0.07 | 1.839 | 0.434 | 1.405 |
| SGCC-200-19-4-8 | 8.31 | 81.45 | 0.01 | 0.09 | 2.360 | 0.545 | 1.815 |
| SGCC-200-19-4-9 | 5.84 | 80.37 | 0.01 | 0.09 | 2.414 | 0.688 | 1.726 |
| SGCC-200-19-4-10 | 7.55 | 79.00 | 0.01 | 0.11 | 2.643 | 0.727 | 1.916 |
| SGCC-200-19-5-1 | 6.34 | 76.84 | 0.01 | 0.09 | 2.236 | 0.530 | 1.705 |
| SGCC-200-19-5-2 | 7.23 | 77.87 | 0.01 | 0.12 | 3.012 | 0.943 | 2.070 |
| SGCC-200-19-5-3 | 5.31 | 76.65 | 0.00 | 0.11 | 2.485 | 0.608 | 1.877 |
| SGCC-200-19-5-4 | 4.99 | 76.41 | 0.00 | 0.11 | 2.736 | 0.625 | 2.111 |
| SGCC-200-19-5-5 | 6.44 | 77.52 | 0.01 | 0.09 | 2.654 | 0.529 | 2.125 |
| SGCC-200-19-5-6 | 4.90 | 79.15 | 0.00 | 0.09 | 3.090 | 0.545 | 2.546 |
| SGCC-200-19-5-7 | 5.78 | 76.25 | 0.01 | 0.10 | 2.858 | 0.485 | 2.374 |
| SGCC-200-19-5-8 | 4.94 | 76.18 | 0.00 | 0.10 | 2.703 | 0.462 | 2.241 |
| SGCC-200-19-5-9 | 5.55 | 78.03 | 0.01 | 0.10 | 2.550 | 0.591 | 1.959 |
| SGCC-200-19-6-1 | 5.31 | 77.33 | 0.00 | 0.10 | 3.116 | 0.765 | 2.351 |
| SGCC-200-19-6-2 | 6.58 | 79.10 | 0.01 | 0.14 | 3.515 | 0.826 | 2.690 |
| SGCC-200-19-6-3 | 7.48 | 78.36 | 0.01 | 0.14 | 3.608 | 0.724 | 2.884 |

| Sample ID | Functions and Related Parameters | | | | Feature Parameters | | |
|------------------|----------------------------------|------------------|-----------------|-----------------|--------------------|-----------------|-----------------|
| | S _{mr1} | S _{mr2} | S _{a1} | S _{a2} | S _{10z} | S _{5p} | S _{5v} |
| | % | % | mm | mm | mm | mm | mm |
| SGCC-200-19-6-4 | 4.97 | 76.03 | 0.00 | 0.10 | 2.549 | 0.608 | 1.941 |
| SGCC-200-19-6-5 | 7.39 | 77.09 | 0.01 | 0.11 | 2.495 | 1.134 | 1.361 |
| SGCC-200-19-6-6 | 8.52 | 78.90 | 0.01 | 0.08 | 3.119 | 0.580 | 2.539 |
| SGCC-200-19-6-7 | 5.93 | 77.93 | 0.00 | 0.07 | 2.414 | 0.365 | 2.049 |
| SGCC-200-19-6-8 | 7.49 | 80.15 | 0.01 | 0.07 | 2.378 | 0.422 | 1.956 |
| SGCC-200-19-6-9 | 7.21 | 80.38 | 0.01 | 0.07 | 3.038 | 0.392 | 2.646 |
| SGCC-200-19-6-10 | 8.33 | 80.92 | 0.01 | 0.05 | 1.942 | 0.546 | 1.396 |
| SGCC-300-19-5-1 | 9.83 | 84.99 | 0.01 | 0.05 | 2.469 | 0.451 | 2.018 |
| SGCC-300-19-5-2 | 8.94 | 86.39 | 0.00 | 0.02 | 0.994 | 0.350 | 0.644 |
| SGCC-300-19-5-3 | 10.93 | 86.18 | 0.01 | 0.03 | 1.501 | 0.435 | 1.065 |
| SGCC-400-19-4-1 | 6.45 | 82.54 | 0.00 | 0.06 | 1.793 | 0.343 | 1.451 |
| SGCC-400-19-4-2 | 8.13 | 83.63 | 0.00 | 0.03 | 1.350 | 0.360 | 0.991 |
| SGCC-400-19-4-3 | 8.62 | 82.81 | 0.01 | 0.05 | 1.616 | 0.436 | 1.180 |
| SGCC-400-19-4-4 | 8.77 | 84.90 | 0.01 | 0.03 | 1.411 | 0.373 | 1.038 |
| SGCC-400-19-4-5 | 10.15 | 85.90 | 0.01 | 0.03 | 1.608 | 0.387 | 1.221 |
| SGCC-400-19-4-6 | 8.61 | 84.42 | 0.00 | 0.03 | 1.446 | 0.449 | 0.996 |
| SGCC-400-19-4-7 | 8.16 | 84.12 | 0.00 | 0.03 | 1.661 | 0.377 | 1.284 |
| SGCC-400-19-4-8 | 8.77 | 81.67 | 0.01 | 0.06 | 1.941 | 0.339 | 1.603 |
| SGCC-400-19-4-9 | 8.59 | 85.83 | 0.00 | 0.03 | 1.388 | 0.331 | 1.057 |
| SGCC-400-19-5-1 | 6.44 | 80.19 | 0.00 | 0.07 | 1.951 | 0.375 | 1.576 |
| SGCC-400-19-5-2 | 8.39 | 83.18 | 0.01 | 0.05 | 2.088 | 0.565 | 1.523 |
| SGCC-400-19-5-3 | 7.72 | 79.88 | 0.01 | 0.07 | 1.571 | 0.433 | 1.138 |
| SGCC-400-19-5-4 | 8.19 | 83.03 | 0.01 | 0.05 | 1.526 | 0.416 | 1.110 |
| SGCC-400-19-5-5 | 7.62 | 80.91 | 0.01 | 0.08 | 2.422 | 0.361 | 2.061 |
| SGCC-400-19-5-6 | 9.66 | 83.05 | 0.02 | 0.08 | 2.512 | 0.380 | 2.132 |
| SGCC-400-19-5-7 | 9.30 | 84.12 | 0.01 | 0.06 | 1.788 | 0.418 | 1.370 |
| SGCC-400-19-5-8 | 12.22 | 82.14 | 0.02 | 0.09 | 2.869 | 0.952 | 1.917 |
| SGCC-400-19-5-9 | 8.23 | 82.99 | 0.01 | 0.07 | 1.738 | 0.302 | 1.436 |
| SGCC-400-19-5-10 | 6.87 | 80.99 | 0.00 | 0.06 | 2.100 | 0.213 | 1.887 |
| SGCC-400-19-6-1 | 5.41 | 75.51 | 0.00 | 0.10 | 2.692 | 0.536 | 2.156 |
| SGCC-400-19-6-2 | 7.52 | 80.24 | 0.00 | 0.05 | 1.560 | 0.364 | 1.197 |
| SGCC-400-19-6-3 | 8.93 | 82.60 | 0.01 | 0.05 | 2.232 | 0.399 | 1.833 |
| SGCC-400-19-6-4 | 7.44 | 80.79 | 0.01 | 0.06 | 2.417 | 0.370 | 2.047 |
| SGCC-400-19-6-5 | 7.07 | 79.94 | 0.01 | 0.06 | 1.771 | 0.503 | 1.268 |
| SGCC-400-19-6-6 | 6.98 | 80.89 | 0.00 | 0.04 | 1.582 | 0.411 | 1.172 |
| SGCC-400-19-6-7 | 7.98 | 82.07 | 0.00 | 0.04 | 1.706 | 0.345 | 1.361 |
| SGCC-400-19-6-8 | 11.04 | 84.71 | 0.01 | 0.04 | 1.607 | 0.258 | 1.350 |
| SGCC-400-19-6-9 | 8.64 | 84.27 | 0.00 | 0.03 | 1.558 | 0.268 | 1.290 |
| SGCC-400-19-6-10 | 8.54 | 85.38 | 0.00 | 0.02 | 0.977 | 0.280 | 0.697 |
| SGC-HMA-L-19-1 | 5.22 | 79.75 | 0.00 | 0.14 | 4.021 | 0.863 | 3.158 |
| SGC-HMA-L-19-2 | 5.21 | 79.36 | 0.01 | 0.16 | 4.783 | 1.228 | 3.555 |
| SGC-HMA-L-19-3 | 4.29 | 80.85 | 0.01 | 0.15 | 4.524 | 0.848 | 3.676 |

| Sample ID | Functions and Related Parameters | | | | Feature Parameters | | |
|----------------|----------------------------------|-----------|----------|----------|--------------------|----------|----------|
| | S_{mr1} | S_{mr2} | S_{a1} | S_{a2} | S_{10z} | S_{5p} | S_{5v} |
| | % | % | mm | mm | mm | mm | mm |
| SGC-HMA-L-19-4 | 5.46 | 80.51 | 0.01 | 0.13 | 5.317 | 1.169 | 4.147 |
| SGC-HMA-L-19-5 | 3.43 | 78.90 | 0.00 | 0.13 | 4.224 | 0.986 | 3.239 |
| SGC-HMA-L-19-6 | 4.96 | 79.37 | 0.01 | 0.13 | 3.837 | 0.939 | 2.898 |
| SGC-HMA-L-12-1 | 6.94 | 81.84 | 0.01 | 0.05 | 2.151 | 0.787 | 1.364 |
| SGC-HMA-L-12-2 | 7.13 | 84.40 | 0.01 | 0.04 | 2.238 | 0.805 | 1.433 |
| SGC-HMA-L-12-3 | 6.89 | 82.42 | 0.01 | 0.05 | 2.103 | 0.723 | 1.379 |
| SGC-HMA-L-12-4 | 6.94 | 84.61 | 0.01 | 0.05 | 2.680 | 0.907 | 1.774 |
| SGC-HMA-L-12-5 | 6.59 | 82.76 | 0.01 | 0.05 | 2.108 | 0.645 | 1.463 |
| SGC-HMA-L-12-6 | 8.10 | 85.02 | 0.01 | 0.06 | 2.707 | 0.882 | 1.824 |
| RCC-200-12-1 | 8.28 | 75.61 | 0.01 | 0.08 | 3.360 | 0.683 | 2.601 |
| RCC-200-12-2 | 4.16 | 76.47 | 0.00 | 0.07 | 2.572 | 0.641 | 1.860 |
| RCC-200-12-3 | 6.92 | 81.15 | 0.01 | 0.06 | 1.719 | 0.491 | 1.173 |
| RCC-200-12-4 | 5.18 | 78.91 | 0.00 | 0.07 | 2.615 | 0.555 | 1.998 |
| RCC-200-12-5 | 7.43 | 78.15 | 0.01 | 0.07 | 2.200 | 0.405 | 1.749 |
| RCC-200-12-6 | 8.23 | 77.77 | 0.02 | 0.10 | 3.512 | 0.992 | 2.410 |
| RCC-200-12-7 | 4.65 | 73.84 | 0.00 | 0.09 | 3.023 | 0.402 | 2.577 |
| RCC-200-12-8 | 10.55 | 83.09 | 0.01 | 0.03 | 1.641 | 0.415 | 1.179 |
| RCC-200-12-9 | 8.31 | 79.20 | 0.01 | 0.04 | 1.889 | 0.451 | 1.387 |
| RCC-200-12-10 | 8.27 | 79.68 | 0.01 | 0.07 | 3.063 | 0.606 | 2.390 |
| RCC-300-12-1 | 7.73 | 76.74 | 0.01 | 0.09 | 3.075 | 0.327 | 2.500 |
| RCC-300-12-2 | 8.92 | 79.48 | 0.01 | 0.09 | 3.363 | 1.087 | 2.354 |
| RCC-300-12-3 | 8.06 | 83.93 | 0.00 | 0.02 | 1.578 | 0.383 | 1.500 |
| RCC-300-12-4 | 8.07 | 76.63 | 0.01 | 0.10 | 2.779 | 0.687 | 2.141 |
| RCC-300-12-5 | 8.15 | 79.28 | 0.01 | 0.06 | 2.284 | 0.402 | 1.911 |
| RCC-300-12-6 | 7.67 | 78.05 | 0.01 | 0.09 | 2.501 | 0.473 | 2.062 |
| RCC-300-12-7 | 7.45 | 78.52 | 0.00 | 0.05 | 2.208 | 0.660 | 1.595 |
| RCC-300-12-8 | 6.48 | 76.71 | 0.01 | 0.08 | 2.157 | 0.265 | 1.910 |
| RCC-300-12-9 | 8.17 | 79.94 | 0.01 | 0.05 | 1.873 | 0.501 | 1.408 |
| RCC-300-12-10 | 7.44 | 81.76 | 0.01 | 0.07 | 3.028 | 0.873 | 2.217 |
| RCC-400-12-1 | 7.16 | 76.81 | 0.01 | 0.11 | 3.516 | 0.751 | 2.671 |
| RCC-400-12-2 | 6.16 | 77.69 | 0.01 | 0.08 | 1.926 | 0.365 | 1.515 |
| RCC-400-12-3 | 8.65 | 78.45 | 0.02 | 0.10 | 2.279 | 0.222 | 2.029 |
| RCC-400-12-4 | 9.26 | 78.67 | 0.02 | 0.09 | 3.387 | 0.999 | 2.263 |
| RCC-400-12-5 | 10.27 | 80.27 | 0.03 | 0.10 | 3.240 | 1.090 | 2.014 |
| RCC-400-12-6 | 9.39 | 78.41 | 0.02 | 0.11 | 3.077 | 0.707 | 2.282 |
| RCC-400-12-7 | 6.70 | 75.85 | 0.01 | 0.10 | 2.951 | 0.569 | 2.311 |
| RCC-400-12-8 | 5.99 | 80.40 | 0.01 | 0.07 | 2.262 | 0.576 | 1.614 |
| RCC-400-12-9 | 4.99 | 73.63 | 0.00 | 0.10 | 2.094 | 0.525 | 1.503 |
| RCC-400-12-10 | 8.46 | 76.28 | 0.01 | 0.09 | 1.933 | 0.258 | 1.643 |
| RCC-200-19-1 | 6.93 | 78.23 | 0.01 | 0.16 | 4.119 | 1.085 | 3.239 |
| RCC-200-19-2 | 6.17 | 79.64 | 0.01 | 0.16 | 4.444 | 1.301 | 3.368 |
| RCC-200-19-3 | 7.41 | 77.32 | 0.01 | 0.13 | 3.614 | 0.914 | 2.879 |

| Sample ID | Functions and Related Parameters | | | | Feature Parameters | | |
|----------------|----------------------------------|-----------|----------|----------|--------------------|----------|----------|
| | S_{mr1} | S_{mr2} | S_{a1} | S_{a2} | S_{10z} | S_{5p} | S_{5v} |
| | % | % | mm | mm | mm | mm | mm |
| RCC-200-19-4 | 6.83 | 79.84 | 0.01 | 0.13 | 2.871 | 0.824 | 2.192 |
| RCC-200-19-5 | 9.24 | 79.77 | 0.02 | 0.12 | 2.776 | 0.908 | 2.011 |
| RCC-200-19-6 | 8.07 | 79.22 | 0.01 | 0.12 | 3.297 | 0.924 | 2.539 |
| RCC-200-19-7 | 5.41 | 78.90 | 0.01 | 0.16 | 3.700 | 0.897 | 2.986 |
| RCC-200-19-8 | 10.33 | 79.03 | 0.02 | 0.13 | 3.538 | 0.758 | 2.952 |
| RCC-200-19-9 | 7.71 | 78.63 | 0.01 | 0.14 | 3.696 | 1.053 | 2.829 |
| RCC-200-19-10 | 8.92 | 79.03 | 0.02 | 0.17 | 3.886 | 1.128 | 2.954 |
| RCC-300-19-1 | 8.25 | 83.40 | 0.01 | 0.11 | 3.187 | 0.979 | 2.429 |
| RCC-300-19-2 | 7.87 | 79.78 | 0.01 | 0.16 | 3.356 | 0.992 | 2.601 |
| RCC-300-19-3 | 9.53 | 81.25 | 0.01 | 0.10 | 2.495 | 0.827 | 1.983 |
| RCC-300-19-4 | 9.09 | 80.46 | 0.02 | 0.19 | 4.800 | 1.130 | 3.633 |
| RCC-300-19-5 | 10.43 | 79.22 | 0.03 | 0.20 | 2.700 | 0.708 | 2.732 |
| RCC-300-19-6 | 5.94 | 80.33 | 0.01 | 0.12 | 3.500 | 0.862 | 1.939 |
| RCC-300-19-7 | 7.50 | 81.49 | 0.01 | 0.15 | 4.215 | 1.305 | 3.201 |
| RCC-300-19-8 | 7.61 | 80.74 | 0.02 | 0.15 | 4.185 | 1.054 | 3.444 |
| RCC-300-19-9 | 8.62 | 80.60 | 0.01 | 0.15 | 4.025 | 1.304 | 2.993 |
| RCC-300-19-10 | 8.37 | 79.88 | 0.01 | 0.16 | 3.287 | 0.796 | 2.740 |
| RCC-400-19-1 | 8.84 | 83.45 | 0.02 | 0.17 | 5.671 | 1.169 | 3.449 |
| RCC-400-19-2 | 6.54 | 78.36 | 0.01 | 0.19 | 5.015 | 1.276 | 3.738 |
| RCC-400-19-3 | 10.67 | 81.91 | 0.04 | 0.22 | 4.705 | 1.154 | 3.551 |
| RCC-400-19-4 | 8.95 | 80.10 | 0.01 | 0.11 | 2.952 | 0.889 | 2.063 |
| RCC-400-19-5 | 7.05 | 81.24 | 0.02 | 0.13 | 4.385 | 1.089 | 3.296 |
| RCC-400-19-6 | 5.18 | 84.30 | 0.01 | 0.21 | 4.329 | 1.190 | 3.492 |
| RCC-400-19-7 | 6.81 | 75.47 | 0.01 | 0.22 | 3.837 | 0.958 | 2.879 |
| RCC-400-19-8 | 7.33 | 76.38 | 0.02 | 0.16 | 3.465 | 0.996 | 2.470 |
| RCC-400-19-9 | 3.89 | 77.96 | 0.00 | 0.13 | 2.824 | 0.734 | 2.090 |
| RCC-400-19-10 | 7.65 | 81.91 | 0.01 | 0.10 | 4.057 | 0.756 | 3.301 |
| RC-HMA-L-12-1 | 7.52 | 81.49 | 0.01 | 0.05 | 2.823 | 0.821 | 2.002 |
| RC-HMA-L-12-2 | 7.02 | 81.46 | 0.01 | 0.06 | 2.952 | 0.999 | 1.953 |
| RC-HMA-L-12-3 | 6.40 | 81.91 | 0.01 | 0.06 | 2.864 | 0.690 | 2.173 |
| RC-HMA-L-12-4 | 6.85 | 81.27 | 0.01 | 0.06 | 3.488 | 0.878 | 2.610 |
| RC-HMA-L-12-5 | 6.91 | 82.83 | 0.01 | 0.07 | 3.098 | 0.778 | 2.320 |
| RC-HMA-L-12-6 | 7.00 | 83.06 | 0.01 | 0.06 | 3.044 | 0.783 | 2.261 |
| RC-HMA-L-12-7 | 6.11 | 82.86 | 0.01 | 0.08 | 3.910 | 0.761 | 3.149 |
| RC-HMA-L-12-8 | 6.72 | 82.55 | 0.01 | 0.07 | 3.638 | 1.007 | 2.631 |
| RC-HMA-L-12-9 | 6.07 | 81.58 | 0.01 | 0.09 | 3.448 | 0.849 | 2.599 |
| RC-HMA-L-12-10 | 7.15 | 81.81 | 0.01 | 0.08 | 3.857 | 0.664 | 3.192 |
| RC-HMA-L-12-11 | 6.68 | 80.68 | 0.01 | 0.08 | 3.374 | 0.648 | 2.726 |
| RC-HMA-L-12-12 | 6.70 | 80.26 | 0.01 | 0.11 | 2.937 | 0.927 | 2.010 |
| RC-HMA-L-19-1 | 7.71 | 80.89 | 0.01 | 0.10 | 3.173 | 0.483 | 2.690 |
| RC-HMA-L-19-2 | 6.95 | 80.19 | 0.01 | 0.10 | 3.913 | 0.844 | 3.069 |
| RC-HMA-L-19-3 | 7.62 | 80.42 | 0.01 | 0.11 | 3.952 | 0.870 | 3.082 |
| RC-HMA-L-19-4 | 6.74 | 80.05 | 0.01 | 0.10 | 3.858 | 1.028 | 2.829 |

| Sample ID | Functions and Related Parameters | | | | Feature Parameters | | |
|----------------|----------------------------------|-----------|----------|----------|--------------------|----------|----------|
| | S_{mr1} | S_{mr2} | S_{a1} | S_{a2} | S_{10z} | S_{5p} | S_{5v} |
| | % | % | mm | mm | mm | mm | mm |
| RC-HMA-L-19-5 | 6.10 | 79.47 | 0.01 | 0.11 | 3.214 | 0.846 | 2.369 |
| RC-HMA-L-19-6 | 6.96 | 81.71 | 0.01 | 0.08 | 4.431 | 0.783 | 3.648 |
| RC-HMA-L-19-7 | 6.56 | 81.95 | 0.01 | 0.09 | 4.189 | 0.826 | 3.363 |
| RC-HMA-L-19-8 | 6.37 | 82.60 | 0.01 | 0.08 | 3.866 | 0.994 | 2.872 |
| RC-HMA-L-19-9 | 6.48 | 81.36 | 0.01 | 0.10 | 4.212 | 0.800 | 3.411 |
| RC-HMA-L-19-10 | 6.98 | 81.50 | 0.01 | 0.10 | 4.217 | 1.235 | 2.982 |
| RC-HMA-L-19-11 | 5.38 | 78.46 | 0.01 | 0.15 | 4.179 | 0.609 | 3.570 |

| Sample ID | Feature Parameters | | | | | |
|------------------|-------------------------------|------------------|-----------------------------|-----------------------------|-----------------------------|-----------------------------|
| | S_{pd} 1/mm ² | S_{pc} 1/mm | S_{da} mm ² | S_{ha} mm ² | S_{dv} mm ³ | S_{hv} mm ³ |
| SGCC-200-12-4-1 | 0.009 | 1.407 | 13.979 | 17.550 | 0.540 | 0.640 |
| SGCC-200-12-4-2 | 0.008 | 2.025 | 14.811 | 20.141 | 0.638 | 0.985 |
| SGCC-200-12-4-3 | 0.005 | 1.218 | 17.558 | 27.187 | 0.909 | 1.443 |
| SGCC-200-12-4-4 | 0.005 | 1.523 | 17.238 | 26.836 | 0.775 | 0.970 |
| SGCC-200-12-4-5 | 0.007 | 1.641 | 16.819 | 23.100 | 0.905 | 1.097 |
| SGCC-200-12-4-6 | 0.005 | 1.578 | 16.176 | 26.146 | 0.778 | 1.224 |
| SGCC-200-12-4-7 | 0.007 | 1.478 | 15.423 | 21.318 | 0.763 | 0.825 |
| SGCC-200-12-4-8 | 0.005 | 1.329 | 20.764 | 32.436 | 1.033 | 1.551 |
| SGCC-200-12-4-9 | 0.012 | 1.762 | 11.250 | 13.353 | 0.409 | 0.432 |
| SGCC-200-12-4-10 | 0.005 | 1.437 | 16.609 | 28.713 | 0.682 | 0.914 |
| SGCC-200-12-5-1 | 0.006 | 2.695 | 18.457 | 25.296 | 1.054 | 1.315 |
| SGCC-200-12-5-2 | 0.006 | 1.668 | 16.418 | 28.785 | 0.799 | 1.538 |
| SGCC-200-12-5-3 | 0.010 | 1.574 | 11.307 | 15.105 | 0.572 | 0.461 |
| SGCC-200-12-5-4 | 0.010 | 1.657 | 12.122 | 17.470 | 0.509 | 0.737 |
| SGCC-200-12-5-5 | 0.004 | 1.683 | 20.069 | 33.634 | 1.049 | 1.729 |
| SGCC-200-12-5-6 | 0.010 | 1.566 | 12.465 | 15.853 | 0.520 | 0.547 |
| SGCC-200-12-5-7 | 0.003 | 1.577 | 23.689 | 63.824 | 1.353 | 3.894 |
| SGCC-200-12-5-8 | 0.005 | 1.445 | 16.892 | 23.558 | 0.662 | 0.750 |
| SGCC-200-12-5-9 | 0.008 | 1.790 | 18.613 | 26.613 | 0.830 | 1.040 |
| SGCC-200-12-5-10 | 0.006 | 1.445 | 18.508 | 26.004 | 0.815 | 0.974 |
| SGCC-200-12-6-1 | 0.007 | 2.038 | 18.792 | 35.991 | 0.733 | 1.627 |
| SGCC-200-12-6-2 | 0.003 | 1.060 | 23.220 | 46.453 | 0.792 | 1.322 |
| SGCC-200-12-6-3 | 0.007 | 1.654 | 19.115 | 29.559 | 0.622 | 0.971 |
| SGCC-200-12-6-4 | 0.007 | 1.260 | 20.107 | 30.629 | 0.656 | 1.089 |
| SGCC-200-12-6-5 | 0.005 | 1.602 | 20.236 | 30.855 | 0.614 | 1.093 |
| SGCC-200-12-6-6 | 0.004 | 1.434 | 21.347 | 30.739 | 0.642 | 0.997 |
| SGCC-200-12-6-7 | 0.004 | 2.066 | 23.268 | 34.991 | 0.660 | 0.980 |
| SGCC-200-12-6-8 | 0.006 | 1.406 | 18.836 | 35.219 | 0.572 | 0.829 |

| Sample ID | Feature Parameters | | | | | |
|------------------|-------------------------------|------------------|-----------------------------|-----------------------------|-----------------------------|-----------------------------|
| | S_{pd} 1/mm ² | S_{pc} 1/mm | S_{da} mm ² | S_{ha} mm ² | S_{dv} mm ³ | S_{hv} mm ³ |
| SGCC-300-12-5-1 | 0.005 | 1.793 | 28.236 | 26.667 | 0.625 | 0.430 |
| SGCC-300-12-5-2 | 0.002 | 1.593 | 31.004 | 54.363 | 0.702 | 1.218 |
| SGCC-300-12-5-3 | 0.006 | 1.434 | 16.749 | 29.638 | 0.687 | 1.109 |
| SGCC-400-12-4-1 | 0.012 | 2.165 | 15.451 | 17.055 | 0.590 | 0.502 |
| SGCC-400-12-4-2 | 0.013 | 1.351 | 14.015 | 21.011 | 0.373 | 0.394 |
| SGCC-400-12-4-3 | 0.011 | 1.903 | 19.132 | 21.933 | 0.756 | 0.637 |
| SGCC-400-12-4-4 | 0.003 | 1.193 | 25.952 | 40.728 | 0.812 | 0.825 |
| SGCC-400-12-4-5 | 0.006 | 1.334 | 16.679 | 23.011 | 0.382 | 0.381 |
| SGCC-400-12-4-6 | 0.011 | 1.540 | 15.562 | 17.669 | 0.524 | 0.473 |
| SGCC-400-12-4-7 | 0.006 | 2.577 | 21.228 | 33.809 | 0.857 | 1.363 |
| SGCC-400-12-4-8 | 0.018 | 2.154 | 12.437 | 12.613 | 0.338 | 0.247 |
| SGCC-400-12-4-9 | 0.014 | 2.245 | 13.150 | 21.032 | 0.479 | 0.562 |
| SGCC-400-12-4-10 | 0.010 | 2.367 | 17.085 | 25.061 | 0.654 | 0.784 |
| SGCC-400-12-5-1 | 0.013 | 2.277 | 14.259 | 18.051 | 0.572 | 0.645 |
| SGCC-400-12-5-2 | 0.006 | 2.808 | 18.273 | 28.696 | 0.877 | 0.961 |
| SGCC-400-12-5-3 | 0.015 | 2.328 | 13.929 | 18.486 | 0.650 | 0.673 |
| SGCC-400-12-5-4 | 0.007 | 1.993 | 16.335 | 25.548 | 0.901 | 0.904 |
| SGCC-400-12-5-5 | 0.013 | 1.954 | 13.711 | 16.712 | 0.449 | 0.310 |
| SGCC-400-12-5-6 | 0.010 | 2.695 | 17.635 | 24.398 | 0.734 | 0.690 |
| SGCC-400-12-5-7 | 0.009 | 1.312 | 12.838 | 13.778 | 0.463 | 0.370 |
| SGCC-400-12-5-8 | 0.016 | 2.272 | 10.961 | 10.653 | 0.355 | 0.252 |
| SGCC-400-12-5-9 | 0.008 | 1.805 | 17.230 | 20.481 | 0.653 | 0.704 |
| SGCC-400-12-5-10 | 0.006 | 1.426 | 16.415 | 30.914 | 0.816 | 0.831 |
| SGCC-400-12-6-1 | 0.008 | 1.485 | 15.063 | 15.902 | 0.293 | 0.263 |
| SGCC-400-12-6-2 | 0.002 | 1.180 | 30.921 | 58.083 | 1.063 | 2.333 |
| SGCC-400-12-6-3 | 0.003 | 1.482 | 25.537 | 44.580 | 0.641 | 1.051 |
| SGCC-400-12-6-4 | 0.006 | 1.309 | 19.991 | 26.765 | 0.423 | 0.545 |
| SGCC-400-12-6-5 | 0.006 | 1.224 | 20.488 | 26.846 | 0.400 | 0.542 |
| SGCC-400-12-6-6 | 0.003 | 2.081 | 21.112 | 38.326 | 0.424 | 0.872 |
| SGCC-400-12-6-7 | 0.006 | 1.896 | 22.636 | 27.871 | 0.416 | 0.494 |
| SGCC-400-12-6-8 | 0.004 | 1.978 | 29.485 | 36.660 | 0.622 | 0.878 |
| SGCC-400-12-6-9 | 0.004 | 1.394 | 24.536 | 37.895 | 0.429 | 0.782 |
| SGCC-400-12-6-10 | 0.002 | 1.840 | 40.681 | 70.302 | 0.854 | 1.644 |
| SGCC-200-19-4-1 | 0.006 | 1.560 | 14.502 | 18.813 | 0.661 | 0.668 |
| SGCC-200-19-4-2 | 0.002 | 2.147 | 21.939 | 45.623 | 1.336 | 4.014 |
| SGCC-200-19-4-3 | 0.006 | 1.930 | 18.204 | 28.568 | 0.830 | 1.379 |
| SGCC-200-19-4-4 | 0.008 | 1.681 | 16.220 | 18.781 | 0.717 | 0.789 |
| SGCC-200-19-4-5 | 0.010 | 1.611 | 13.337 | 16.434 | 0.566 | 0.612 |
| SGCC-200-19-4-6 | 0.004 | 1.636 | 19.581 | 34.777 | 0.981 | 1.823 |
| SGCC-200-19-4-7 | 0.013 | 2.074 | 12.377 | 13.833 | 0.507 | 0.470 |
| SGCC-200-19-4-8 | 0.010 | 2.729 | 17.739 | 24.512 | 0.871 | 1.005 |
| SGCC-200-19-4-9 | 0.004 | 2.411 | 20.268 | 41.202 | 1.042 | 2.747 |
| SGCC-200-19-4-10 | 0.005 | 1.375 | 20.573 | 34.008 | 0.983 | 1.251 |

| Sample ID | Feature Parameters | | | | | |
|------------------|-------------------------------|------------------|-----------------------------|-----------------------------|-----------------------------|-----------------------------|
| | S_{pd} 1/mm ² | S_{pc} 1/mm | S_{da} mm ² | S_{ha} mm ² | S_{dv} mm ³ | S_{hv} mm ³ |
| SGCC-200-19-5-1 | 0.006 | 1.609 | 13.608 | 22.763 | 0.627 | 0.891 |
| SGCC-200-19-5-2 | 0.007 | 1.941 | 16.186 | 26.966 | 0.750 | 1.290 |
| SGCC-200-19-5-3 | 0.009 | 1.724 | 15.701 | 23.690 | 0.737 | 1.064 |
| SGCC-200-19-5-4 | 0.009 | 1.723 | 16.570 | 28.309 | 0.809 | 1.423 |
| SGCC-200-19-5-5 | 0.014 | 2.226 | 14.138 | 20.114 | 0.668 | 0.871 |
| SGCC-200-19-5-6 | 0.007 | 2.380 | 19.964 | 35.688 | 1.154 | 2.155 |
| SGCC-200-19-5-7 | 0.007 | 1.621 | 15.098 | 26.341 | 0.755 | 1.288 |
| SGCC-200-19-5-8 | 0.010 | 1.528 | 14.358 | 22.761 | 0.596 | 0.918 |
| SGCC-200-19-5-9 | 0.001 | 2.677 | 34.843 | 67.941 | 2.298 | 4.939 |
| SGCC-200-19-6-1 | 0.007 | 1.561 | 15.157 | 25.032 | 0.831 | 1.343 |
| SGCC-200-19-6-2 | 0.004 | 1.816 | 22.603 | 38.919 | 1.456 | 2.928 |
| SGCC-200-19-6-3 | 0.005 | 1.515 | 23.159 | 39.168 | 1.196 | 2.400 |
| SGCC-200-19-6-4 | 0.010 | 1.969 | 14.716 | 23.754 | 0.756 | 0.873 |
| SGCC-200-19-6-5 | 0.005 | 3.081 | 25.187 | 46.982 | 1.280 | 2.009 |
| SGCC-200-19-6-6 | 0.007 | 2.028 | 18.595 | 38.721 | 0.885 | 1.657 |
| SGCC-200-19-6-7 | 0.007 | 1.290 | 19.827 | 32.742 | 0.784 | 1.049 |
| SGCC-200-19-6-8 | 0.008 | 1.696 | 16.728 | 21.125 | 0.611 | 0.557 |
| SGCC-200-19-6-9 | 0.002 | 1.377 | 25.851 | 52.246 | 1.086 | 1.462 |
| SGCC-200-19-6-10 | 0.009 | 1.466 | 18.442 | 23.066 | 0.594 | 0.530 |
| SGCC-300-19-5-1 | 0.004 | 1.740 | 28.131 | 33.503 | 0.673 | 0.712 |
| SGCC-300-19-5-2 | 0.006 | 1.373 | 26.726 | 35.882 | 0.437 | 0.620 |
| SGCC-300-19-5-3 | 0.011 | 1.442 | 14.934 | 14.497 | 0.318 | 0.231 |
| SGCC-400-19-4-1 | 0.005 | 1.950 | 22.976 | 30.095 | 0.872 | 0.626 |
| SGCC-400-19-4-2 | 0.011 | 1.797 | 15.883 | 14.466 | 0.344 | 0.237 |
| SGCC-400-19-4-3 | 0.007 | 2.335 | 26.425 | 28.356 | 0.916 | 0.571 |
| SGCC-400-19-4-4 | 0.006 | 1.891 | 21.445 | 19.831 | 0.532 | 0.390 |
| SGCC-400-19-4-5 | 0.010 | 1.353 | 16.057 | 13.416 | 0.292 | 0.191 |
| SGCC-400-19-4-6 | 0.008 | 1.538 | 14.208 | 13.468 | 0.263 | 0.232 |
| SGCC-400-19-4-7 | 0.015 | 1.816 | 13.289 | 11.875 | 0.295 | 0.195 |
| SGCC-400-19-4-8 | 0.007 | 2.309 | 21.474 | 21.357 | 0.750 | 0.501 |
| SGCC-400-19-4-9 | 0.008 | 1.691 | 21.346 | 15.699 | 0.449 | 0.247 |
| SGCC-400-19-5-1 | 0.010 | 1.897 | 14.478 | 19.604 | 0.546 | 0.430 |
| SGCC-400-19-5-2 | 0.002 | 2.366 | 33.141 | 79.344 | 1.094 | 1.623 |
| SGCC-400-19-5-3 | 0.012 | 2.235 | 15.200 | 20.402 | 0.382 | 0.448 |
| SGCC-400-19-5-4 | 0.006 | 2.238 | 17.959 | 25.349 | 0.608 | 0.649 |
| SGCC-400-19-5-5 | 0.006 | 2.300 | 20.641 | 27.850 | 0.658 | 0.765 |
| SGCC-400-19-5-6 | 0.003 | 2.165 | 33.431 | 57.448 | 0.986 | 2.455 |
| SGCC-400-19-5-7 | 0.004 | 1.762 | 23.334 | 30.035 | 0.855 | 0.689 |
| SGCC-400-19-5-8 | 0.002 | 1.379 | 41.949 | 81.402 | 1.993 | 3.965 |
| SGCC-400-19-5-9 | 0.009 | 1.851 | 18.484 | 17.944 | 0.538 | 0.350 |
| SGCC-400-19-5-10 | 0.008 | 1.762 | 18.537 | 19.678 | 0.479 | 0.434 |

| Sample ID | Feature Parameters | | | | | |
|------------------|-------------------------------|------------------|-----------------------------|-----------------------------|-----------------------------|-----------------------------|
| | S_{pd} 1/mm ² | S_{pc} 1/mm | S_{da} mm ² | S_{ha} mm ² | S_{dv} mm ³ | S_{hv} mm ³ |
| SGCC-400-19-6-1 | 0.004 | 1.786 | 16.770 | 32.584 | 0.772 | 1.123 |
| SGCC-400-19-6-2 | 0.008 | 1.999 | 14.593 | 18.002 | 0.327 | 0.405 |
| SGCC-400-19-6-3 | 0.005 | 1.802 | 19.425 | 28.622 | 0.656 | 0.768 |
| SGCC-400-19-6-4 | 0.003 | 2.060 | 25.992 | 42.742 | 0.883 | 1.304 |
| SGCC-400-19-6-5 | 0.004 | 1.840 | 16.988 | 30.062 | 0.626 | 0.927 |
| SGCC-400-19-6-6 | 0.008 | 1.683 | 15.799 | 22.305 | 0.458 | 0.551 |
| SGCC-400-19-6-7 | 0.007 | 1.511 | 17.789 | 21.567 | 0.507 | 0.428 |
| SGCC-400-19-6-8 | 0.003 | 1.455 | 23.261 | 40.077 | 0.537 | 0.867 |
| SGCC-400-19-6-9 | 0.005 | 1.612 | 16.123 | 19.643 | 0.350 | 0.379 |
| SGCC-400-19-6-10 | 0.046 | 1.787 | 6.073 | 5.496 | 0.088 | 0.076 |
| SGC-HMA-L-19-1 | 0.011 | 4.041 | 15.438 | 20.644 | 0.997 | 1.209 |
| SGC-HMA-L-19-2 | 0.007 | 8.335 | 15.951 | 17.691 | 1.256 | 1.222 |
| SGC-HMA-L-19-3 | 0.011 | 4.255 | 18.509 | 21.021 | 1.240 | 1.370 |
| SGC-HMA-L-19-4 | 0.012 | 11.336 | 12.200 | 12.905 | 0.833 | 0.741 |
| SGC-HMA-L-19-5 | 0.007 | 2.924 | 15.956 | 20.290 | 1.158 | 1.495 |
| SGC-HMA-L-19-6 | 0.015 | 8.030 | 12.500 | 17.715 | 0.740 | 1.018 |
| SGC-HMA-L-12-1 | 0.020 | 2.493 | 7.169 | 6.544 | 0.269 | 0.180 |
| SGC-HMA-L-12-2 | 0.037 | 4.840 | 5.774 | 5.054 | 0.200 | 0.177 |
| SGC-HMA-L-12-3 | 0.024 | 2.918 | 6.493 | 6.005 | 0.222 | 0.166 |
| SGC-HMA-L-12-4 | 0.046 | 4.446 | 5.684 | 4.676 | 0.209 | 0.173 |
| SGC-HMA-L-12-5 | 0.032 | 3.593 | 7.128 | 6.091 | 0.268 | 0.172 |
| SGC-HMA-L-12-6 | 0.023 | 6.262 | 8.644 | 6.549 | 0.413 | 0.338 |
| RCC-200-12-1 | 0.005 | 1.485 | 22.704 | 48.477 | 1.076 | 2.653 |
| RCC-200-12-2 | 0.008 | 1.627 | 22.524 | 32.208 | 0.730 | 1.361 |
| RCC-200-12-3 | 0.004 | 2.587 | 23.762 | 47.263 | 0.726 | 1.698 |
| RCC-200-12-4 | 0.004 | 2.265 | 23.745 | 47.826 | 0.916 | 1.528 |
| RCC-200-12-5 | 0.003 | 2.375 | 36.756 | 67.375 | 1.776 | 2.913 |
| RCC-200-12-6 | 0.004 | 1.866 | 31.526 | 42.925 | 1.328 | 4.037 |
| RCC-200-12-7 | 0.004 | 1.561 | 19.877 | 37.965 | 0.895 | 1.637 |
| RCC-200-12-8 | 0.005 | 1.573 | 36.032 | 45.828 | 0.596 | 0.988 |
| RCC-200-12-9 | 0.006 | 2.060 | 25.176 | 34.945 | 0.747 | 1.013 |
| RCC-200-12-10 | 0.006 | 2.070 | 26.779 | 38.472 | 1.304 | 1.592 |
| RCC-300-12-1 | 0.006 | 1.712 | 26.266 | 66.000 | 1.193 | 2.987 |
| RCC-300-12-2 | 0.005 | 1.553 | 31.985 | 52.964 | 1.481 | 3.175 |
| RCC-300-12-3 | 0.005 | 1.701 | 20.000 | 31.000 | 0.168 | 2.945 |
| RCC-300-12-4 | 0.005 | 1.690 | 28.005 | 52.178 | 1.278 | 2.504 |
| RCC-300-12-5 | 0.005 | 1.703 | 29.037 | 50.380 | 1.319 | 2.133 |
| RCC-300-12-6 | 0.005 | 1.777 | 25.692 | 45.949 | 1.678 | 1.717 |
| RCC-300-12-7 | 0.009 | 2.119 | 20.897 | 26.875 | 0.628 | 0.662 |
| RCC-300-12-8 | 0.004 | 1.756 | 23.788 | 36.752 | 1.077 | 1.597 |
| RCC-300-12-9 | 0.006 | 1.611 | 26.587 | 46.535 | 0.812 | 2.335 |
| RCC-300-12-10 | 0.004 | 1.081 | 39.529 | 45.045 | 2.489 | 3.716 |

| Sample ID | Feature Parameters | | | | | |
|---------------|-------------------------------|------------------|-----------------------------|-----------------------------|-----------------------------|-----------------------------|
| | S_{pd} 1/mm ² | S_{pc} 1/mm | S_{da} mm ² | S_{ha} mm ² | S_{dv} mm ³ | S_{hv} mm ³ |
| RCC-400-12-1 | 0.005 | 1.998 | 29.853 | 55.981 | 1.538 | 7.670 |
| RCC-400-12-2 | 0.010 | 2.564 | 21.823 | 25.000 | 0.936 | 1.082 |
| RCC-400-12-3 | 0.004 | 2.210 | 29.742 | 58.469 | 1.873 | 3.894 |
| RCC-400-12-4 | 0.006 | 1.703 | 23.256 | 45.677 | 1.132 | 3.065 |
| RCC-400-12-5 | 0.005 | 1.799 | 31.795 | 54.575 | 1.811 | 4.743 |
| RCC-400-12-6 | 0.005 | 1.538 | 32.278 | 50.921 | 1.913 | 3.065 |
| RCC-400-12-7 | 0.002 | 1.177 | 29.835 | 65.000 | 1.076 | 4.825 |
| RCC-400-12-8 | 0.004 | 1.466 | 22.513 | 38.638 | 1.282 | 2.278 |
| RCC-400-12-9 | 0.007 | 1.552 | 22.396 | 31.877 | 1.273 | 2.245 |
| RCC-400-12-10 | 0.006 | 1.909 | 22.470 | 38.644 | 1.102 | 1.923 |
| RCC-200-19-1 | 0.003 | 2.349 | 47.569 | 85.369 | 3.375 | 6.378 |
| RCC-200-19-2 | 0.004 | 1.860 | 38.678 | 63.951 | 2.549 | 6.223 |
| RCC-200-19-3 | 0.004 | 2.288 | 32.000 | 62.153 | 2.032 | 3.791 |
| RCC-200-19-4 | 0.003 | 2.189 | 43.980 | 67.615 | 2.631 | 3.542 |
| RCC-200-19-5 | 0.001 | 0.954 | 61.000 | 97.635 | 5.106 | 6.373 |
| RCC-200-19-6 | 0.004 | 1.545 | 40.639 | 50.332 | 1.859 | 3.265 |
| RCC-200-19-7 | 0.003 | 2.276 | 44.073 | 60.102 | 2.642 | 3.380 |
| RCC-200-19-8 | 0.003 | 1.669 | 47.470 | 76.258 | 2.169 | 4.606 |
| RCC-200-19-9 | 0.006 | 2.376 | 42.619 | 49.302 | 2.125 | 3.306 |
| RCC-200-19-10 | 0.002 | 1.401 | 62.024 | 57.464 | 3.502 | 7.634 |
| RCC-300-19-1 | 0.005 | 1.776 | 34.166 | 49.374 | 1.531 | 2.549 |
| RCC-300-19-2 | 0.002 | 2.033 | 62.547 | 84.757 | 3.509 | 5.711 |
| RCC-300-19-3 | 0.001 | 1.089 | 54.977 | 61.390 | 2.337 | 6.625 |
| RCC-300-19-4 | 0.002 | 1.983 | 62.302 | 58.952 | 5.921 | 9.134 |
| RCC-300-19-5 | 0.002 | 2.005 | 45.983 | 79.087 | 3.339 | 7.193 |
| RCC-300-19-6 | 0.003 | 1.984 | 47.815 | 80.976 | 2.502 | 4.491 |
| RCC-300-19-7 | 0.003 | 1.435 | 46.776 | 86.177 | 4.245 | 10.519 |
| RCC-300-19-8 | 0.004 | 2.010 | 32.074 | 64.754 | 1.661 | 5.103 |
| RCC-300-19-9 | 0.003 | 2.108 | 35.507 | 63.634 | 2.106 | 6.258 |
| RCC-300-19-10 | 0.002 | 2.321 | 55.456 | 78.707 | 3.867 | 7.872 |
| RCC-400-19-1 | 0.001 | 1.456 | 56.991 | 87.766 | 5.912 | 9.087 |
| RCC-400-19-2 | 0.002 | 1.528 | 40.495 | 60.908 | 2.818 | 13.297 |
| RCC-400-19-3 | 0.002 | 1.791 | 53.254 | 81.325 | 2.875 | 8.279 |
| RCC-400-19-4 | 0.003 | 1.694 | 53.313 | 58.785 | 4.752 | 2.767 |
| RCC-400-19-5 | 0.002 | 1.309 | 45.975 | 65.185 | 2.508 | 9.660 |
| RCC-400-19-6 | 0.001 | 1.416 | 64.646 | 109.503 | 6.281 | 8.673 |
| RCC-400-19-7 | 0.002 | 1.492 | 46.278 | 72.198 | 3.185 | 9.386 |
| RCC-400-19-8 | 0.005 | 2.820 | 28.838 | 79.375 | 1.469 | 3.432 |
| RCC-400-19-9 | 0.004 | 1.989 | 47.517 | 78.034 | 5.481 | 2.205 |
| RCC-400-19-10 | 0.003 | 1.198 | 44.664 | 62.861 | 2.956 | 7.566 |
| RC-HMA-L-12-1 | 0.038 | 5.025 | 5.590 | 5.617 | 0.215 | 0.217 |
| RC-HMA-L-12-2 | 0.021 | 5.162 | 7.705 | 8.787 | 0.343 | 0.395 |
| RC-HMA-L-12-3 | 0.040 | 5.315 | 5.394 | 5.363 | 0.213 | 0.190 |
| RC-HMA-L-12-4 | 0.033 | 4.835 | 5.849 | 6.404 | 0.244 | 0.228 |

| Sample ID | Feature Parameters | | | | | |
|----------------|-------------------------------|------------------|-----------------------------|-----------------------------|-----------------------------|-----------------------------|
| | S_{pd} 1/mm ² | S_{pc} 1/mm | S_{da} mm ² | S_{ha} mm ² | S_{dv} mm ³ | S_{hv} mm ³ |
| RC-HMA-L-12-5 | 0.025 | 4.922 | 8.302 | 8.671 | 0.352 | 0.337 |
| RC-HMA-L-12-6 | 0.036 | 4.585 | 6.025 | 5.904 | 0.238 | 0.202 |
| RC-HMA-L-12-7 | 0.021 | 6.666 | 7.803 | 9.261 | 0.403 | 0.439 |
| RC-HMA-L-12-8 | 0.023 | 6.323 | 7.494 | 8.715 | 0.372 | 0.401 |
| RC-HMA-L-12-9 | 0.020 | 5.587 | 8.322 | 10.013 | 0.449 | 0.473 |
| RC-HMA-L-12-10 | 0.020 | 5.234 | 7.985 | 10.059 | 0.426 | 0.493 |
| RC-HMA-L-12-11 | 0.033 | 5.536 | 5.568 | 6.263 | 0.267 | 0.224 |
| RC-HMA-L-12-12 | 0.029 | 5.164 | 6.951 | 8.368 | 0.370 | 0.359 |
| RC-HMA-L-19-1 | 0.021 | 6.177 | 8.277 | 9.986 | 0.411 | 0.408 |
| RC-HMA-L-19-2 | 0.020 | 5.140 | 9.472 | 12.263 | 0.432 | 0.583 |
| RC-HMA-L-19-3 | 0.018 | 5.435 | 9.593 | 11.773 | 0.481 | 0.503 |
| RC-HMA-L-19-4 | 0.026 | 5.202 | 8.305 | 9.186 | 0.335 | 0.372 |
| RC-HMA-L-19-5 | 0.014 | 4.915 | 11.423 | 13.968 | 0.483 | 0.647 |
| RC-HMA-L-19-6 | 0.017 | 4.984 | 10.046 | 12.695 | 0.472 | 0.570 |
| RC-HMA-L-19-7 | 0.019 | 5.721 | 8.868 | 9.423 | 0.391 | 0.424 |
| RC-HMA-L-19-8 | 0.024 | 5.523 | 8.592 | 9.068 | 0.373 | 0.450 |
| RC-HMA-L-19-9 | 0.021 | 6.268 | 8.904 | 10.043 | 0.406 | 0.460 |
| RC-HMA-L-19-10 | 0.015 | 7.352 | 11.134 | 14.867 | 0.552 | 0.762 |
| RC-HMA-L-19-11 | 0.010 | 5.858 | 13.049 | 20.611 | 0.669 | 1.186 |

B. Sand Patch Test Results and Estimated Mean Texture Depth Values

| Sample ID | MTD | Volume of Voids / Area | | eMTD | Relative error |
|-----------------|-------------------------|------------------------|--------------------------------------|------|----------------|
| | Sand Patch Test Results | at Max Height Plane | at 10% of Peaks Material Ratio Plane | | |
| | (mm) | (mm) | (mm) | (mm) | (%) |
| SGCC-200-12-4-1 | 0.47 | 1.11 | 0.45 | 0.43 | 9.27 |
| SGCC-200-12-4-2 | 0.49 | 0.95 | 0.46 | 0.45 | 10.47 |
| SGCC-200-12-4-3 | 0.53 | 1.05 | 0.56 | 0.53 | 1.35 |
| SGCC-200-12-4-4 | 0.43 | 0.79 | 0.44 | 0.43 | 0.07 |
| SGCC-200-12-4-5 | 0.51 | 1.19 | 0.52 | 0.50 | 2.87 |
| SGCC-200-12-4-6 | 0.53 | 1.07 | 0.54 | 0.52 | 2.45 |
| SGCC-200-12-4-7 | 0.49 | 0.99 | 0.43 | 0.42 | 18.25 |
| SGCC-200-12-4-8 | 0.48 | 0.93 | 0.46 | 0.45 | 8.16 |
| SGCC-200-12-4-9 | 0.44 | 0.90 | 0.39 | 0.38 | 16.37 |
| SGCC-200-12-5-1 | 0.47 | 0.92 | 0.45 | 0.44 | 7.94 |
| SGCC-200-12-5-2 | 0.53 | 0.98 | 0.47 | 0.46 | 16.43 |
| SGCC-200-12-5-3 | 0.53 | 0.95 | 0.41 | 0.40 | 32.80 |
| SGCC-200-12-5-4 | 0.48 | 0.79 | 0.37 | 0.36 | 33.76 |
| SGCC-200-12-5-5 | 0.57 | 1.18 | 0.64 | 0.61 | 5.86 |
| SGCC-200-12-5-6 | 0.49 | 0.79 | 0.38 | 0.37 | 33.44 |
| SGCC-200-12-5-7 | 0.52 | 0.92 | 0.48 | 0.46 | 11.65 |
| SGCC-200-12-5-8 | 0.49 | 1.31 | 0.48 | 0.46 | 6.89 |
| SGCC-200-12-5-9 | 0.53 | 1.21 | 0.59 | 0.56 | 6.29 |
| SGCC-200-12-6-1 | 0.57 | 2.29 | 0.65 | 0.61 | 6.76 |
| SGCC-200-12-6-2 | 0.44 | 0.90 | 0.40 | 0.39 | 15.08 |
| SGCC-200-12-6-3 | 0.26 | 0.80 | 0.20 | 0.20 | 25.69 |
| SGCC-200-12-6-4 | 0.36 | 0.89 | 0.37 | 0.36 | 0.08 |
| SGCC-200-12-6-5 | 0.39 | 0.98 | 0.30 | 0.30 | 32.89 |
| SGCC-200-12-6-6 | 0.42 | 0.79 | 0.41 | 0.40 | 4.35 |
| SGCC-200-12-6-7 | 0.44 | 1.04 | 0.38 | 0.37 | 17.49 |
| SGCC-200-12-6-8 | 0.37 | 0.99 | 0.32 | 0.32 | 17.38 |
| SGCC-200-12-6-9 | 0.30 | 0.76 | 0.21 | 0.22 | 37.55 |
| SGCC-400-12-4-1 | 0.35 | 0.85 | 0.39 | 0.38 | 9.78 |
| SGCC-400-12-4-2 | 0.26 | 0.49 | 0.24 | 0.25 | 4.25 |

| Sample ID | MTD | Volume of Voids / Area | | eMTD | Relative error |
|-----------------|----------------------------------|---------------------------|--|------|-------------------|
| | Sand Patch Test Results | at Max Height Plane | at 10% of Peaks Material Ratio Plane | | |
| | (mm) | (mm) | (mm) | | |
| SGCC-400-12-4-3 | 0.32 | 0.77 | 0.35 | 0.34 | 6.98 |
| SGCC-400-12-4-4 | 0.23 | 0.96 | 0.24 | 0.24 | 3.97 |
| SGCC-400-12-4-5 | 0.23 | 0.64 | 0.23 | 0.24 | 2.12 |
| SGCC-400-12-4-6 | 0.30 | 0.98 | 0.31 | 0.31 | 3.81 |
| SGCC-400-12-4-7 | 0.39 | 1.29 | 0.41 | 0.40 | 3.23 |
| SGCC-400-12-4-8 | 0.25 | 0.82 | 0.27 | 0.27 | 6.21 |
| SGCC-400-12-4-9 | 0.33 | 0.76 | 0.34 | 0.33 | 1.07 |
| SGCC-400-12-5-1 | 0.39 | 1.39 | 0.41 | 0.40 | 0.90 |
| SGCC-400-12-5-2 | 0.42 | 1.12 | 0.37 | 0.36 | 15.60 |
| SGCC-400-12-5-3 | 0.41 | 0.91 | 0.37 | 0.36 | 11.99 |
| SGCC-400-12-5-4 | 0.42 | 1.01 | 0.41 | 0.39 | 5.58 |
| SGCC-400-12-5-5 | 0.30 | 0.88 | 0.25 | 0.25 | 17.07 |
| SGCC-400-12-5-6 | 0.38 | 0.94 | 0.41 | 0.40 | 3.44 |
| SGCC-400-12-5-7 | 0.36 | 0.86 | 0.33 | 0.33 | 10.70 |
| SGCC-400-12-5-8 | 0.33 | 0.84 | 0.33 | 0.32 | 1.76 |
| SGCC-400-12-5-9 | 0.36 | 1.67 | 0.39 | 0.38 | 5.30 |
| SGCC-400-12-6-1 | 0.26 | 0.50 | 0.15 | 0.16 | 67.24 |
| SGCC-400-12-6-2 | 0.33 | 0.90 | 0.33 | 0.32 | 1.28 |
| SGCC-400-12-6-3 | 0.26 | 0.63 | 0.28 | 0.28 | 4.51 |
| SGCC-400-12-6-4 | 0.32 | 0.70 | 0.24 | 0.25 | 30.97 |
| SGCC-400-12-6-5 | 0.31 | 0.90 | 0.27 | 0.27 | 15.35 |
| SGCC-400-12-6-6 | 0.27 | 0.68 | 0.26 | 0.26 | 3.73 |
| SGCC-400-12-6-7 | 0.37 | 0.53 | 0.27 | 0.27 | 40.05 |
| SGCC-400-12-6-8 | 0.32 | 0.81 | 0.27 | 0.27 | 18.48 |
| SGCC-400-12-6-9 | 0.25 | 0.62 | 0.25 | 0.25 | 2.44 |
| SGCC-200-19-4-1 | 0.44 | 1.03 | 0.42 | 0.40 | 9.42 |
| SGCC-200-19-4-2 | 0.53 | 2.09 | 0.59 | 0.56 | 6.81 |
| SGCC-200-19-4-3 | 0.49 | 0.95 | 0.47 | 0.45 | 7.72 |
| SGCC-200-19-4-4 | 0.43 | 0.99 | 0.42 | 0.41 | 4.10 |
| SGCC-200-19-4-5 | 0.42 | 1.14 | 0.41 | 0.39 | 5.50 |
| SGCC-200-19-4-6 | 0.43 | 0.94 | 0.48 | 0.46 | 7.28 |
| SGCC-200-19-4-7 | 0.42 | 0.94 | 0.39 | 0.38 | 9.42 |
| SGCC-200-19-4-8 | 0.42 | 0.95 | 0.49 | 0.47 | 10.76 |
| SGCC-200-19-4-9 | 0.46 | 0.92 | 0.45 | 0.44 | 5.79 |

| Sample ID | MTD | Volume of Voids / Area | | eMTD | Relative error |
|-----------------|-------------------------|------------------------|--------------------------------------|------|----------------|
| | Sand Patch Test Results | at Max Height Plane | at 10% of Peaks Material Ratio Plane | | |
| | (mm) | (mm) | (mm) | | |
| SGCC-200-19-5-1 | 0.45 | 0.93 | 0.41 | 0.40 | 13.31 |
| SGCC-200-19-5-2 | 0.52 | 1.22 | 0.53 | 0.51 | 2.16 |
| SGCC-200-19-5-3 | 0.53 | 0.92 | 0.49 | 0.47 | 12.49 |
| SGCC-200-19-5-4 | 0.47 | 0.95 | 0.45 | 0.43 | 7.12 |
| SGCC-200-19-5-5 | 0.48 | 1.06 | 0.43 | 0.41 | 15.46 |
| SGCC-200-19-5-6 | 0.49 | 0.98 | 0.49 | 0.47 | 4.20 |
| SGCC-200-19-5-7 | 0.47 | 1.07 | 0.44 | 0.43 | 10.63 |
| SGCC-200-19-5-8 | 0.48 | 0.83 | 0.45 | 0.43 | 11.90 |
| SGCC-200-19-5-9 | 0.50 | 1.02 | 0.50 | 0.48 | 5.72 |
| SGCC-200-19-6-1 | 0.51 | 1.08 | 0.42 | 0.41 | 25.77 |
| SGCC-200-19-6-2 | 0.56 | 2.20 | 0.62 | 0.59 | 4.50 |
| SGCC-200-19-6-3 | 0.56 | 1.06 | 0.56 | 0.54 | 4.24 |
| SGCC-200-19-6-4 | 0.46 | 0.93 | 0.39 | 0.38 | 22.40 |
| SGCC-200-19-6-5 | 0.46 | 1.93 | 0.42 | 0.41 | 12.29 |
| SGCC-200-19-6-6 | 0.45 | 1.10 | 0.34 | 0.33 | 36.25 |
| SGCC-200-19-6-7 | 0.36 | 0.60 | 0.28 | 0.28 | 28.18 |
| SGCC-200-19-6-8 | 0.35 | 0.67 | 0.29 | 0.28 | 23.43 |
| SGCC-200-19-6-9 | 0.33 | 0.61 | 0.25 | 0.25 | 29.01 |
| SGCC-400-19-4-1 | 0.21 | 1.12 | 0.30 | 0.30 | 29.46 |
| SGCC-400-19-4-2 | 0.22 | 0.75 | 0.26 | 0.27 | 15.38 |
| SGCC-400-19-4-3 | 0.27 | 0.83 | 0.28 | 0.28 | 2.41 |
| SGCC-400-19-4-4 | 0.21 | 0.70 | 0.25 | 0.26 | 18.80 |
| SGCC-400-19-4-5 | 0.19 | 0.49 | 0.17 | 0.18 | 5.22 |
| SGCC-400-19-4-6 | 0.19 | 0.72 | 0.26 | 0.26 | 28.91 |
| SGCC-400-19-4-7 | 0.18 | 0.69 | 0.27 | 0.27 | 35.99 |
| SGCC-400-19-4-8 | 0.26 | 0.79 | 0.31 | 0.30 | 15.18 |
| SGCC-400-19-4-9 | 0.18 | 0.53 | 0.19 | 0.20 | 11.01 |
| SGCC-400-19-5-1 | 0.31 | 0.78 | 0.34 | 0.33 | 7.71 |
| SGCC-400-19-5-2 | 0.26 | 1.17 | 0.31 | 0.30 | 13.23 |
| SGCC-400-19-5-3 | 0.25 | 0.76 | 0.34 | 0.33 | 23.49 |
| SGCC-400-19-5-4 | 0.23 | 0.78 | 0.31 | 0.30 | 24.03 |
| SGCC-400-19-5-5 | 0.33 | 0.77 | 0.34 | 0.34 | 2.36 |
| SGCC-400-19-5-6 | 0.40 | 0.84 | 0.42 | 0.41 | 2.25 |

| Sample ID | MTD | Volume of Voids / Area | | eMTD | Relative error |
|-----------------|-------------------------|------------------------|--------------------------------------|------|----------------|
| | Sand Patch Test Results | at Max Height Plane | at 10% of Peaks Material Ratio Plane | | |
| | (mm) | (mm) | (mm) | | |
| SGCC-400-19-5-7 | 0.28 | 0.77 | 0.31 | 0.31 | 9.29 |
| SGCC-400-19-5-8 | 0.38 | 0.94 | 0.49 | 0.47 | 19.57 |
| SGCC-400-19-5-9 | 0.32 | 0.86 | 0.34 | 0.33 | 4.88 |
| SGCC-400-19-6-1 | 0.38 | 0.87 | 0.36 | 0.35 | 7.08 |
| SGCC-400-19-6-2 | 0.25 | 0.56 | 0.22 | 0.22 | 12.25 |
| SGCC-400-19-6-3 | 0.24 | 0.57 | 0.21 | 0.22 | 9.46 |
| SGCC-400-19-6-4 | 0.29 | 0.61 | 0.26 | 0.26 | 8.52 |
| SGCC-400-19-6-5 | 0.25 | 0.71 | 0.25 | 0.25 | 0.41 |
| SGCC-400-19-6-6 | 0.23 | 0.60 | 0.23 | 0.23 | 0.22 |
| SGCC-400-19-6-7 | 0.22 | 0.51 | 0.18 | 0.18 | 18.75 |
| SGCC-400-19-6-8 | 0.20 | 0.50 | 0.22 | 0.22 | 10.60 |
| SGCC-400-19-6-9 | 0.17 | 0.47 | 0.16 | 0.17 | 1.87 |

C. The Roughness Parameters in Correlation With BPN

| Sample ID | Fractal dimension (3D) (From Full Depth) <no unit> | S_{al} ($s = 0.2000$) (From Top 1.0 mm) mm | Magnitude of 2D Fourier transform (From Top 1.0 mm) dBc |
|------------------|---|--|--|
| SGCC-200-12-4-1 | 2.690 | 2.569 | -34.799 |
| SGCC-200-12-4-2 | 2.749 | 2.234 | -41.688 |
| SGCC-200-12-4-3 | 2.535 | 3.025 | -38.466 |
| SGCC-200-12-4-4 | 2.530 | 2.649 | -41.774 |
| SGCC-200-12-4-5 | 2.598 | 2.272 | -45.378 |
| SGCC-200-12-4-6 | 2.565 | 3.802 | -47.337 |
| SGCC-200-12-4-7 | 2.763 | 2.088 | -33.390 |
| SGCC-200-12-4-8 | 2.574 | 2.567 | -39.350 |
| SGCC-200-12-4-9 | 2.779 | 1.949 | -35.850 |
| SGCC-200-12-4-10 | 2.627 | 3.655 | -29.030 |
| SGCC-200-12-5-1 | 2.499 | 3.058 | -39.502 |
| SGCC-200-12-5-2 | 2.824 | 1.963 | -47.349 |
| SGCC-200-12-5-3 | 2.521 | 3.212 | -30.350 |
| SGCC-200-12-5-4 | 2.653 | 1.867 | -41.842 |
| SGCC-200-12-5-5 | 2.516 | 3.664 | -30.436 |
| SGCC-200-12-5-6 | 2.518 | 3.009 | -50.679 |
| SGCC-200-12-5-7 | 2.451 | 2.871 | -24.132 |
| SGCC-200-12-5-8 | 2.610 | 2.520 | -15.812 |
| SGCC-200-12-5-9 | 2.609 | 2.146 | -45.481 |
| SGCC-200-12-5-10 | 2.654 | 2.105 | -34.674 |
| SGCC-200-12-6-1 | 2.000 | 2.725 | -40.429 |
| SGCC-200-12-6-2 | 2.616 | 2.121 | -50.010 |
| SGCC-200-12-6-3 | 2.797 | 1.571 | -29.512 |
| SGCC-200-12-6-4 | 2.599 | 2.523 | -34.107 |
| SGCC-200-12-6-5 | 2.773 | 2.374 | -19.859 |
| SGCC-200-12-6-6 | 2.571 | 3.253 | -28.072 |
| SGCC-200-12-6-7 | 2.727 | 4.267 | -24.024 |
| SGCC-200-12-6-8 | 2.581 | 2.664 | -37.137 |
| SGCC-200-12-6-9 | 2.632 | 1.511 | -18.978 |
| SGCC-400-12-4-1 | 2.590 | 2.940 | -38.646 |
| SGCC-400-12-4-2 | 2.680 | 5.253 | -32.732 |
| SGCC-400-12-4-3 | 2.587 | 4.737 | -41.386 |
| SGCC-400-12-4-4 | 2.617 | 2.412 | -43.436 |

| Sample ID | Fractal dimension (3D) (From Full Depth) <no unit> | S_{al} ($s = 0.2000$) (From Top 1.0 mm) mm | Magnitude of 2D Fourier transform (From Top 1.0 mm) dBc |
|------------------|---|--|--|
| SGCC-400-12-4-5 | 2.697 | 4.356 | -52.764 |
| SGCC-400-12-4-6 | 2.543 | 3.941 | -66.753 |
| SGCC-400-12-4-7 | 2.592 | 3.003 | -44.000 |
| SGCC-400-12-4-8 | 2.594 | 2.744 | -40.658 |
| SGCC-400-12-4-9 | 2.546 | 3.241 | -57.454 |
| SGCC-400-12-4-10 | 2.767 | 2.448 | -39.162 |
| SGCC-400-12-5-1 | 2.798 | 2.281 | -36.491 |
| SGCC-400-12-5-2 | 2.789 | 2.118 | -46.523 |
| SGCC-400-12-5-3 | 2.000 | 0.440 | -21.497 |
| SGCC-400-12-5-4 | 2.718 | 3.041 | -59.517 |
| SGCC-400-12-5-5 | 2.744 | 2.795 | -69.204 |
| SGCC-400-12-5-6 | 2.615 | 3.768 | -46.509 |
| SGCC-400-12-5-7 | 2.097 | 1.462 | -38.819 |
| SGCC-400-12-5-8 | 2.778 | 2.787 | -40.671 |
| SGCC-400-12-5-9 | 2.782 | 2.371 | -45.078 |
| SGCC-400-12-5-10 | 2.599 | 4.522 | -53.195 |
| SGCC-400-12-6-1 | 2.522 | 3.331 | -42.129 |
| SGCC-400-12-6-2 | 2.503 | 3.941 | -39.694 |
| SGCC-400-12-6-3 | 2.548 | 3.171 | -36.113 |
| SGCC-400-12-6-4 | 2.554 | 2.641 | -23.201 |
| SGCC-400-12-6-5 | 2.569 | 3.188 | -34.426 |
| SGCC-400-12-6-6 | 2.526 | 1.449 | -67.831 |
| SGCC-400-12-6-7 | 2.603 | 3.285 | -35.832 |
| SGCC-400-12-6-8 | 2.550 | 2.972 | -38.537 |
| SGCC-200-19-4-1 | 2.715 | 2.162 | -35.786 |
| SGCC-200-19-4-2 | 2.333 | 3.995 | -32.717 |
| SGCC-200-19-4-3 | 2.756 | 2.748 | -32.353 |
| SGCC-200-19-4-4 | 2.791 | 1.883 | -30.114 |
| SGCC-200-19-4-5 | 2.518 | 4.263 | -45.130 |
| SGCC-200-19-4-6 | 2.628 | 2.362 | -31.526 |
| SGCC-200-19-4-7 | 2.582 | 2.283 | -52.661 |
| SGCC-200-19-4-8 | 2.707 | 2.755 | -41.071 |
| SGCC-200-19-4-9 | 2.581 | 2.184 | -27.113 |
| SGCC-200-19-4-10 | 2.678 | 2.914 | -33.539 |
| SGCC-200-19-5-1 | 2.801 | 1.892 | -3.652 |
| SGCC-200-19-5-2 | 2.654 | 2.439 | -36.696 |
| SGCC-200-19-5-3 | 2.635 | 2.174 | -44.352 |

| Sample ID | Fractal dimension (3D) (From Full Depth) <no unit> | S_{al} ($s = 0.2000$) (From Top 1.0 mm) mm | Magnitude of 2D Fourier transform (From Top 1.0 mm) dBc |
|------------------|---|--|--|
| SGCC-200-19-5-4 | 2.656 | 1.878 | -37.043 |
| SGCC-200-19-5-5 | 2.720 | 2.389 | -45.051 |
| SGCC-200-19-5-6 | 2.771 | 1.915 | -32.673 |
| SGCC-200-19-5-7 | 2.790 | 1.948 | -22.820 |
| SGCC-200-19-5-8 | 2.636 | 2.143 | -25.370 |
| SGCC-200-19-5-9 | 2.604 | 2.414 | -41.373 |
| SGCC-200-19-5-10 | 2.640 | 1.919 | -45.849 |
| SGCC-200-19-6-1 | 2.604 | 1.576 | -21.825 |
| SGCC-200-19-6-2 | 2.732 | 1.677 | -37.119 |
| SGCC-200-19-6-3 | 2.124 | 2.632 | -47.465 |
| SGCC-200-19-6-4 | 2.542 | 3.822 | -34.491 |
| SGCC-200-19-6-5 | 2.804 | 1.841 | -45.523 |
| SGCC-200-19-6-6 | 2.776 | 2.239 | -49.079 |
| SGCC-200-19-6-7 | 2.760 | 2.149 | -31.149 |
| SGCC-200-19-6-8 | 2.588 | 1.732 | -24.865 |
| SGCC-200-19-6-9 | 2.602 | 1.708 | -26.446 |
| SGCC-200-19-6-10 | 2.581 | 1.956 | -25.011 |
| SGCC-400-19-4-1 | 2.684 | 4.176 | -61.983 |
| SGCC-400-19-4-2 | 2.533 | 3.851 | -49.666 |
| SGCC-400-19-4-3 | 2.566 | 3.141 | -28.771 |
| SGCC-400-19-4-4 | 2.754 | 2.307 | -39.344 |
| SGCC-400-19-4-5 | 2.725 | 3.713 | -39.366 |
| SGCC-400-19-4-6 | 2.539 | 2.756 | -21.719 |
| SGCC-400-19-4-7 | 2.757 | 2.542 | -59.443 |
| SGCC-400-19-4-8 | 2.684 | 3.794 | -35.336 |
| SGCC-400-19-5-1 | 2.585 | 2.346 | -60.977 |
| SGCC-400-19-5-2 | 2.560 | 4.115 | -31.013 |
| SGCC-400-19-5-3 | 2.734 | 3.941 | -30.761 |
| SGCC-400-19-5-4 | 2.768 | 2.736 | -58.018 |
| SGCC-400-19-5-5 | 2.764 | 3.275 | -57.377 |
| SGCC-400-19-5-6 | 2.724 | 4.094 | -56.726 |
| SGCC-400-19-5-7 | 2.588 | 3.049 | -56.796 |
| SGCC-400-19-5-8 | 2.594 | 2.598 | -39.644 |
| SGCC-400-19-5-9 | 2.602 | 3.052 | -27.771 |
| SGCC-400-19-5-10 | 2.730 | 3.615 | -43.017 |
| SGCC-400-19-6-1 | 2.697 | 1.508 | -59.540 |
| SGCC-400-19-6-2 | 2.575 | 1.878 | -48.536 |

| Sample ID | Fractal dimension (3D) (From Full Depth) <no unit> | S_{al} ($s = 0.2000$) (From Top 1.0 mm) mm | Magnitude of 2D Fourier transform (From Top 1.0 mm) dBc |
|-----------------|---|--|--|
| SGCC-400-19-6-3 | 2.621 | 1.612 | -49.485 |
| SGCC-400-19-6-4 | 2.585 | 1.962 | -52.428 |
| SGCC-400-19-6-5 | 2.640 | 2.267 | -18.680 |
| SGCC-400-19-6-6 | 2.576 | 1.487 | -52.661 |
| SGCC-400-19-6-7 | 2.597 | 2.043 | -33.792 |
| SGCC-400-19-6-8 | 2.709 | 1.249 | -53.170 |
| SGC-HMA-L-12-1 | 2.722 | 0.634 | -35.478 |
| SGC-HMA-L-12-2 | 2.740 | 0.538 | -26.099 |
| SGC-HMA-L-12-3 | 2.780 | 1.061 | -25.529 |
| SGC-HMA-L-12-4 | 2.565 | 0.518 | -43.048 |
| SGC-HMA-L-12-5 | 2.810 | 1.368 | -44.375 |
| SGC-HMA-L-12-6 | 2.401 | 0.375 | -34.858 |
| SGC-HMA-L-19-1 | 2.491 | 2.389 | -33.021 |
| SGC-HMA-L-19-2 | 2.356 | 1.319 | -16.402 |
| SGC-HMA-L-19-3 | 2.397 | 2.247 | -18.190 |
| SGC-HMA-L-19-4 | 2.417 | 0.574 | -9.451 |
| SGC-HMA-L-19-5 | 2.518 | 1.730 | -20.500 |
| RCC-200-12-1 | 2.553 | 3.151 | -68.874 |
| RCC-200-12-2 | 2.551 | 3.678 | -73.145 |
| RCC-200-12-3 | 2.539 | 3.914 | -64.731 |
| RCC-200-12-4 | 2.538 | 3.860 | -79.306 |
| RCC-200-12-5 | 2.529 | 4.060 | -59.779 |
| RCC-200-12-6 | 2.505 | 3.843 | -72.937 |
| RCC-200-12-7 | 2.659 | 2.839 | -79.907 |
| RCC-200-12-8 | 2.547 | 5.274 | -74.939 |
| RCC-200-12-9 | 2.540 | 2.760 | -64.056 |
| RCC-300-12-1 | 2.443 | 4.007 | -58.800 |
| RCC-300-12-2 | 2.398 | 6.302 | -68.163 |
| RCC-300-12-3 | 2.661 | 7.434 | -82.255 |
| RCC-300-12-4 | 2.544 | 3.822 | -73.401 |
| RCC-300-12-5 | 2.532 | 5.908 | -70.226 |
| RCC-300-12-6 | 2.555 | 3.079 | -64.834 |
| RCC-300-12-7 | 2.530 | 3.874 | -65.224 |
| RCC-300-12-8 | 2.515 | 6.190 | -73.806 |
| RCC-300-12-9 | 2.487 | 6.895 | -82.049 |
| RCC-400-12-1 | 2.521 | 3.524 | -68.541 |

| Sample ID | Fractal dimension (3D) (From Full Depth) <no unit> | S_{al} ($s = 0.2000$) (From Top 1.0 mm) mm | Magnitude of 2D Fourier transform (From Top 1.0 mm) dBc |
|---------------|---|--|--|
| RCC-400-12-2 | 2.521 | 3.332 | -73.895 |
| RCC-400-12-3 | 2.413 | 3.381 | -83.797 |
| RCC-400-12-4 | 2.408 | 3.397 | -65.768 |
| RCC-400-12-5 | 2.401 | 3.573 | -80.435 |
| RCC-400-12-6 | 2.378 | 3.232 | -60.074 |
| RCC-400-12-7 | 2.459 | 5.583 | -74.460 |
| RCC-400-12-8 | 2.498 | 3.874 | -86.861 |
| RCC-400-12-9 | 2.539 | 3.008 | -73.920 |
| RCC-400-12-10 | 2.533 | 3.048 | -68.740 |
| RCC-200-19-1 | 2.531 | 2.854 | -62.491 |
| RCC-200-19-2 | 2.563 | 2.771 | -67.089 |
| RCC-200-19-3 | 2.538 | 3.322 | -69.820 |
| RCC-200-19-4 | 2.477 | 5.201 | -76.846 |
| RCC-200-19-5 | 2.548 | 3.429 | -74.054 |
| RCC-200-19-6 | 2.535 | 3.052 | -76.947 |
| RCC-200-19-7 | 2.614 | 4.221 | -60.557 |
| RCC-200-19-8 | 2.482 | 3.117 | -74.370 |
| RCC-200-19-9 | 2.472 | 3.862 | -79.753 |
| RCC-300-19-1 | 2.354 | 1.966 | -79.746 |
| RCC-300-19-2 | 2.413 | 4.502 | -74.300 |
| RCC-300-19-3 | 2.447 | 5.162 | -66.004 |
| RCC-300-19-4 | 2.398 | 4.240 | -72.928 |
| RCC-300-19-5 | 2.464 | 6.462 | -88.344 |
| RCC-300-19-6 | 2.000 | 2.101 | -45.421 |
| RCC-300-19-7 | 2.376 | 6.728 | -70.590 |
| RCC-300-19-8 | 2.473 | 7.274 | -69.379 |
| RCC-400-19-1 | 2.425 | 3.378 | -73.492 |
| RCC-400-19-2 | 2.655 | 3.637 | -75.575 |
| RCC-400-19-3 | 2.407 | 4.372 | -62.609 |
| RCC-400-19-4 | 2.521 | 4.227 | -66.467 |
| RCC-400-19-5 | 2.511 | 3.200 | -67.435 |
| RCC-400-19-6 | 2.367 | 4.005 | -78.095 |
| RC-HMA-L-12-1 | 2.708 | 0.390 | -49.360 |
| RC-HMA-L-12-2 | 2.717 | 0.492 | -57.455 |
| RC-HMA-L-12-3 | 2.795 | 1.169 | -54.191 |
| RC-HMA-L-12-4 | 2.784 | 0.798 | -38.045 |
| RC-HMA-L-12-5 | 2.749 | 1.580 | -55.304 |

| Sample ID | Fractal dimension (3D) (From Full Depth) <no unit> | S_{al} ($s = 0.2000$) (From Top 1.0 mm) mm | Magnitude of 2D Fourier transform (From Top 1.0 mm) dBc |
|----------------|---|--|--|
| RC-HMA-L-12-6 | 2.752 | 0.845 | -52.657 |
| RC-HMA-L-12-7 | 2.394 | 0.720 | -59.132 |
| RC-HMA-L-12-8 | 2.639 | 0.797 | -52.550 |
| RC-HMA-L-12-9 | 2.686 | 0.701 | -56.775 |
| RC-HMA-L-12-10 | 2.657 | 0.471 | -56.631 |
| RC-HMA-L-12-11 | 2.597 | 0.520 | -46.412 |
| RC-HMA-L-19-1 | 2.479 | 0.600 | -40.258 |
| RC-HMA-L-19-2 | 2.223 | 1.197 | -51.227 |
| RC-HMA-L-19-3 | 2.507 | 0.471 | -38.631 |
| RC-HMA-L-19-4 | 2.552 | 0.924 | -49.992 |
| RC-HMA-L-19-5 | 2.664 | 0.818 | -63.224 |
| RC-HMA-L-19-6 | 2.592 | 0.627 | -47.946 |
| RC-HMA-L-19-7 | 2.570 | 0.522 | -53.538 |
| RC-HMA-L-19-8 | 2.544 | 0.654 | -45.561 |

CURRICULUM VITAE

PERSONAL INFORMATION

Surname, Name: Mahyar, Mahdi
Date and Place of Birth: 2 March 1982, Tabriz

EDUCATION

| Degree | Institution | Year of Graduation |
|-------------|--------------------------------|--------------------|
| MS | METU Civil Engineering, Turkey | 2012 |
| BS | IAU Civil Engineering, Iran | 2005 |
| High School | Abouzar High School, Tabriz | 1999 |

FOREIGN LANGUAGES

Advanced English, Fluent Turkish, Persian and Azerbaijani

PUBLICATIONS

1. Mahyar, M., Erdoğan, S.T., Tokyay, M. Extension of the chemical index model for estimating Alkali-Silica reaction mitigation efficiency to slags and natural pozzolans, (2018) *Construction and Building Materials*, 179, pp. 587-597.
2. Mahyar, M., Uçal, G.O., Tokyay, M. Hydration of alinite cement produced from soda waste sludge, (2018) *Construction and Building Materials*, 164, pp. 178-184.
3. Mahyar, M., Uçal, G.O., Tokyay, M., Yaman, I.Ö. Low-energy alinite cement from soda sludge waste, (2017) *American Concrete Institute, ACI Special Publication*, 2017-January (SP 320), pp. 24-31.
4. Mahyar, M., Şahin, M., Erdoğan, S.T. Mutual activation of blast furnace slag and a high-calcium fly ash rich in free lime and sulfates, (2016) *Construction and Building Materials*, 126, pp. 466-475.
5. Mahyar, M., Erdoğan, S.T. Phosphate-activated high-calcium fly ash acid-base cements, (2015) *Cement and Concrete Composites*, 63, pp. 96-103.